41/4-13-94 JS(2)

DOE/METC-94/1006
(DE94004072)

Fuel Cells
A Handbook
(Revision 3)

January 1994

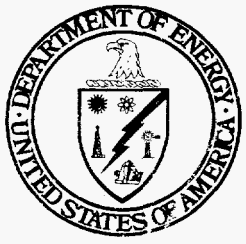

U.S. Department of Energy
Office of Fossil Energy
Morgantown Energy Technology Center
Morgantown, West Virginia

DISCLAIMER

DOE/METC-94/1006
(DE94004072)
Distribution Category UC-110

Fuel Cells
A Handbook
(Revision 3)

By
J.H. Hirschenhofer
D.B. Stauffer
R.R. Engleman

Gilbert/Commonwealth, Inc.
Reading, PA 19603
Under Contract No. DE-AC01-88FE61684

U.S. Department of Energy
Office of Fossil Energy
Morgantown Energy Technology Center
P.O. Box 880
Morgantown, West Virginia 26507-0880

January 1994

PREFACE

The past three decades have provided ever increasing opportunities for the development of fuel cell technology. Both the alkaline and polymer electrolyte fuel cells have demonstrated their capabilities in the Apollo, Gemini, and Space Shuttle manned space vehicle programs. The major effort is now focused on developing stationary power units. There are nearly a total of 50 MW of demonstrations being conducted or planned, and funded for on-site cogeneration and dispersed power generators by users in Japan, the U.S., and, more recently, Europe. Approximately 70 customers have purchased fuel cell demonstrators, and interest in the technology has been piqued in divergent parts of the world. Manufacturers are addressing fabrication and infrastructure issues by constructing semi-automatic fabrication facilities and forming companies to supply fuel cell units. They are strengthening their positions through international collaborations. The technology has progressed to where power plants have operated up to 13,000 hours. Actual prototype costs are known (from approximately $3,000/kW to $6,000/kW). Based on this, manufacturers are confident in projecting the commercial cost range for a complete power unit to be $1,000 to $1,500/kW, low enough to be competitive. The associated fuel cell stack cost would be $400/kW. Unit capacities available to users are being defined by manufacturers, and include 200 kW, 500 kW, 1,000 kW, 2 MW, 5 MW, 10 MW, and 20 MW. The early plants use natural gas as a fuel and, considering cogeneration, achieve up to 80 percent total fuel use. Net electrical efficiency of operating plants fueled by natural gas has reached over 40 percent; designs show up to 55 percent (HHV) is possible for the next natural gas units. Work is in progress for utilizing liquid fuels and coal to provide users with much needed information on other market expanding applications. More recently, a strong interest in using fuel cell propulsion for land transportation and submarine use is opening vast new user sectors.

Even with the activities mentioned above, there is still a lack of widespread awareness and appreciation of fuel cells within the energy sector. There are numerous opportunities where fuel cells could provide a feasible alternative to existing technologies. In order for fuel cells to displace existing technologies, the characteristics and benefits of fuel cells must be widely known before a rational decision can be made. Many avenues are available which disseminate public information on the various fuel cell technologies; among them are seminars, workshops, review meetings, and technical society meetings. In addition, various publications serve to document research and development activities on fuel cells. The purpose of this Fuel Cells Handbook is to present information describing fuel cells that is helpful to scientists, engineers, and technical managers who are not experienced in this technology, as well as to provide an update on the present technical status of the various types of fuel cells. Through this publication and related documents, it is hoped that a better appreciation of fuel cell technologies and their potential applications will be obtained.

In 1980 the Institute of Gas Technology published the "Handbook of Fuel Cell Performance" under the sponsorship of the U.S. Department of Energy. This document was revised as "Fuel

Cells, A Handbook" in 1988 by personnel of the Lawrence Berkeley Laboratory. Those publications serve as the genesis for this issue of the Handbook, which updates the developments in fuel cell technology since about 1988. Much of the text, terminology, and format in the earlier Handbooks has been retained where still pertinent to provide continuity among the versions. The focus of this issue is to introduce a series of algorithms which depict specific changes in fuel cell performance from references as a function of fuel, oxidant, thermodynamics, and other cell conditions. These algorithms were developed based on a review of technology progress and regression of fuel cell test data. The section on fuel cell systems was revised to provide guidance on the analysis of systems issues.

ACKNOWLEDGMENT

The authors of this version of the Fuel Cell Handbook would like to acknowledge the cooperation of the fuel cell community for their contributions to this Handbook. Many of our colleagues provided data, information, references, valuable suggestions, and constructive comments that were incorporated into the Handbook. In particular, we would like to acknowledge the contributions of the following individuals: S. Gottesfeld of Los Alamos National Laboratory, G. H. Kucera of Argonne National Laboratories, L. G. Marianowski of the Institute of Gas Technology, H. C. Maru of Energy Research Corporation, N. Q. Minh of Allied-Signal, and W. G. Parker and J. F. Pierre both of Westinghouse Electric Corporation.

The assistance of J. K. Fedeyko and T. R. Kunkelman of Gilbert/Commonwealth, Inc. at various stages of preparation of the manuscript is gratefully acknowledged.

The authors wish to thank Dr. Diane T. Hooie and Mr. William J. Huber of the U.S. Department of Energy, Morgantown Energy Technology Center, for their support and encouragement, and for providing the opportunity to write this Handbook.

This work was supported by the U.S. Department of Energy, Morgantown Energy Technology Center, Fuel Cells Branch, through the Assistant Secretary for Fossil Energy, U.S. Department of Energy under Contract Number DE-AC01-88FE61684.

CONTENTS

List of Figures

List of Figures

List of Figures

List of Tables

1. INTRODUCTION TO FUEL CELLS

1.1 Objective and Scope of the Fuel Cell Handbook

Fuel cells are electrochemical devices that convert the chemical energy of reaction directly into electrical energy. In a typical fuel cell, gaseous fuels are fed continuously to the anode (negative electrode) compartment and an oxidant (i.e., oxygen from air) is fed continuously to the cathode (positive electrode) compartment; the electrochemical reactions take place at the electrodes to produce an electric current. A fuel cell, although having similar components and several characteristics, differs from a typical battery in several respects. The battery is an energy storage device, that is, the maximum energy that is available is determined by the amount of chemical reactant stored within the battery itself. Thus, the battery will cease to produce electrical energy when the chemical reactants are consumed (i.e., discharged). In a secondary battery, the reactants are regenerated by recharging, which involves putting energy into the battery from an external source. The fuel cell, on the other hand, is an energy conversion device which theoretically has the capability of producing electrical energy for as long as the fuel and oxidant are supplied to the electrodes. In reality, degradation or malfunction of components limits the practical operating life of fuel cells.

A variety of fuel cells are in various stages of development. These are usually classified according to the type of electrolyte used in the cells and include: 1) polymer electrolyte fuel cell (PEFC), 2) alkaline fuel cell (AFC), 3) phosphoric acid fuel cell (PAFC), 4) molten carbonated fuel cell (MCFC) and 5) solid oxide fuel cell (SOFC). These fuel cells are listed in the approximate order of increasing operating temperature, ranging from ~80°C for PEFC, ~100°C for AFC, ~200°C for PAFC, ~650°C for MCFC and ~650 to 1000°C for SOFC. There have been numerous, complete natural gas to ac power, PAFC units demonstrated at customers' sites. Commercial price and life goals have yet to be achieved so that actual commercialization is still pending. MCFC technology is to the point that cells are being scaled to full size and full size stacks are beginning to be tested. SOFC and PEFC technologies are less developed with commercial cell sizes yet to be produced.

Fuel cells provide a new and exciting option for the efficient conversion of fossil fuels to electricity. Commercial development of fuel cell technology has been underway in the United States since the late 1960s with the U.S. Government playing a prominent role. Through the combined efforts of government, research institutes (i.e., the Electric Power Research Institute and the Gas Research Institute), and industry, fuel cell technology has advanced to near commercialization. Japanese and European countries are also active in fuel cell development. Further interest in the technology would be aided by making information on the technical status of fuel cells readily available to the fuel cell community and users. In the latter half of the 1970s, DOE supported a project to evaluate the technical status of PAFCs and MCFCs for stationary energy generation.

This study resulted in the publication of a fuel cell handbook (1) followed in 1988 by a major revision (2). These handbooks provided an assessment of fuel cell technology to about 1988. Rapid advances in the technology continue, thus an update of the technology status is necessary.

The objective of this publication is to update the technical status of fuel cell technologies. The basic formats and text of the previous fuel cell handbooks, which are still pertinent, are retained. The major emphasis has been placed on updating the technical advances in PAFC, MCFC, SOFC, and PEFC since about 1988. Attention was given to the development of fuel cell performance algorithms which can be used to estimate the performance change from a reference as a function of fuel, oxidant, thermodynamics, and other cell conditions. These algorithms were developed based on review and analysis of fuel cell test data in the previous handbooks and recently published data. The section on fuel cell systems was revised to provide an introduction to system issues.

1.2 Operating Principles

The basic physical structure or building block of a fuel cell consists of an electrolyte layer in contact with a porous anode and cathode on either side. A schematic representation of a fuel cell and the reactant/product gases and the ion conduction flow directions through the cell for PAFCs, PEFCs, MCFCs and SOFCs, is shown in Figure 1-1. Note that the ion specie and transport direction are different which influences the site of water production. These phenomena, in turn, cause significant system impact. The fuel and oxidant gases flow past the surface of the anode and cathode opposite the electrolyte, respectively, and generate electrical energy by the electrochemical oxidation of fuel, usually hydrogen, and the electrochemical reduction of oxygen. Appleby and Foulkes have noted that in theory, any substance capable of chemical oxidation that can be supplied continuously (as a fluid) can be burned galvanically as the fuel at the anode of a fuel cell. Similarly, the oxidant can be any fluid that can be reduced at a sufficient rate. Gaseous hydrogen has become the fuel of choice for most applications, because of its high reactivity when suitable catalysts are used and because of its flexibility to be produced from hydrocarbons or high energy density when stored cryogenically. Similarly, the most common oxidant is gaseous oxygen, which is readily and economically available from air for stationary, terrestrial applications (3). A three phase interface is established in the region of the porous electrode, the electrolyte, and the reactants. The nature of this interface plays a critical role in the electrochemical performance of a fuel cell, particularly in those fuel cells with liquid electrolytes (i.e., AFC, PAFC, MCFC). In such fuel cells, the reactant gases diffuse through a thin electrolyte film that wets portions of the porous electrode and react electrochemically on the electrode surface. If the porous electrode contains an excessive amount of electrolyte, the electrode may "flood" and restrict the transport of gaseous species in the electrolyte phase. The consequence is a reduction in the electrochemical performance of the porous electrode. Thus, a delicate balance must be maintained among the electrode, electrolyte, and gaseous phases in the porous electrode structure. Much of the recent effort in the development of fuel cell technology has been devoted to reducing the thickness of cell components while refining and improving the electrode structure and the electrolyte phase, with the aim of obtaining a higher and more stable electrochemical performance.

The functions of porous electrodes in fuel cells are: 1) to provide a *surface* site where gas/liquid ionization or deionization reactions can take place, 2) to *conduct* ions away from or into the three phase interface once they are formed (so an electrode must be made of materials that have good electrical conductance), and 3) to provide a physical *barrier* that separates the bulk gas phase and the electrolyte. A corollary of item 1 is that, in order to increase the rates of reactions,

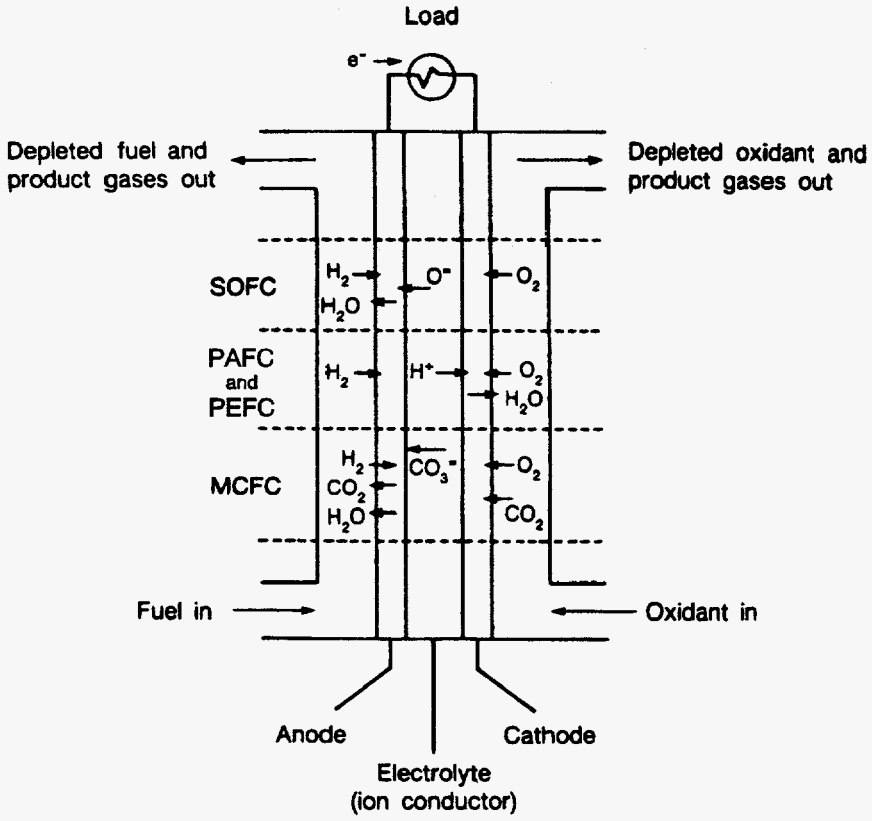

Figure 1-1 Schematic representation of a typical fuel cell showing the reactant/product gases and ion conduction flow paths for SOFCs, PAFCs, PEFCs, and MCFCs.

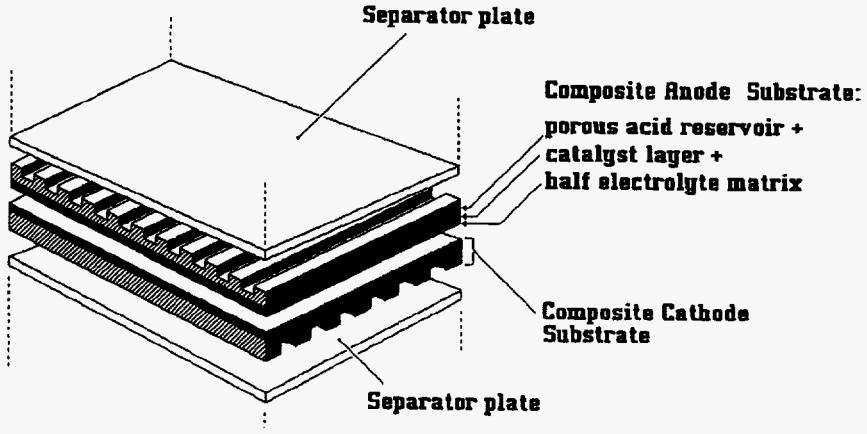

Figure 1-2 Expanded view of basic fuel cell structure which is a repeated unit in a fuel cell stack. *Source:* A. J. Appleby, F. R. Foulkes, *Fuel Cell Handbook*, Van Nostrand Reinhold, New York, NY, 1989.

the electrode material should be catalytic as well as conductive, porous rather than solid. The catalytic function of electrodes is more important in lower temperature fuel cells and less so in high temperature fuel cells since ionization reaction rates increase with temperature. It is also a corollary that the porous electrodes must be permeable to both electrolyte and gases, but not such that the media can be easily "flooded" by the electrolyte or "dried" by the gases in a one-sided manner.

The electrolyte not only transports dissolved reactants to the electrode, but it also conducts ionic charge between the electrodes and thereby completes the cell electric circuit, as illustrated in Figure 1-1. It also provides a physical barrier to separate the fuel and oxidant gas steams. In low temperature fuel cells (PEFC, AFC, PAFC), protons or hydroxyl ions are the major charge carriers in the electrolyte, whereas in the high temperature fuel cells, MCFC and SOFC, carbonate ions and oxygen ions are the charge carriers, respectively.

Additional components of a cell are best described by using a typical cell schematic, Figure 1-2. This figure depicts a state-of-the-art PAFC. As with batteries, individual fuel cells must be combined to produce appreciable amounts of electricity and so are joined by interconnects. Because of the configuration of a flat plate cell, Figure 1-2, the interconnect becomes a separator plate which has two functions: 1) to provide an electrical series connection between adjacent cells, and specifically for flat plate cells, 2) to provide a gas barrier that separates the fuel and oxidant of adjacent cells. The interconnect of the tubular solid oxide fuel cell is a special case and the reader is referred to Section 5 for its slightly altered function. However, all interconnects must be an electrical conductor and impermeable to gases. Other parts of the cell of importance are: 1) the structure for distributing the reactant gases across the electrode surface and which serve as mechanical support, shown as ribs in Figure 1-2, 2) electrolyte reservoirs for liquid electrolyte cells to replenish electrolyte lost over life, and 3) current collectors (not shown) which provide a path for the current between the electrodes and the separator of flat plate cells. Other arrangements of gas flow and current flow are used in fuel cell stack designs, and are mentioned in Sections 3 through 6 for the various type cells.

The physicochemical and thermomechanical properties of materials used in the cell components (i.e., electrodes, electrolyte, interconnect, current collector, etc.) determine the practical operating temperature and useful life of a fuel cell. Aqueous electrolytes are limited to temperatures of about 200°C or lower because of their high water vapor pressure and/or rapid degradation at higher temperatures. The operating temperature also plays an important role in dictating the type of fuel that can be utilized in a fuel cell. The low temperature fuel cells with aqueous electrolytes are, in most practical applications, restricted to hydrogen as a fuel. In high temperature fuel cells, CO and even CH_4 can be used because of the inherently rapid electrode kinetics and the lesser need for high electrocatalytic activity at high temperature. These aspects will be discussed in the following section.

1.2.1 Electrode Reactions

The typical electrochemical reactions that occur with different fuels and oxidants in practical fuel cells are summarized in Table 1-1. CO and CH_4 are shown in the table as undergoing anodic oxidation, but in actuality, direct oxidation may not occur. Instead, these reactants are potential fuels because they undergo chemical reaction with H_2O to produce H_2 which is the oxidizable fuel. In MCFCs, CO, and CH_4, when combined with H_2O in the proper environment, are sources of H_2 from water gas shift and steam reforming reactions, respectively. The direct oxidation of CO and CH_4 in high temperature SOFCs is feasible, but they are still not as easily oxidized as H_2. Low

temperature fuel cells (PAFC, PEFC, AFC) require noble metal electrocatalysts to achieve practical reaction rates at the anode and cathode, and hydrogen is the only acceptable fuel. With high temperature fuel cells (MCFC, SOFC), the requirements for electrocatalysis are relaxed, and the number of potential fuels is increased. Carbon monoxide "poisons" the noble metal anode electrocatalyst such as platinum (Pt) in low temperature fuel cells, but it serves as a potential source of H_2 in high temperature fuel cells where non-noble metal electrocatalysts such as nickel (Ni) are used.

The overall electrochemical reactions corresponding to the individual electrode reactions listed in Table 1-1 are given in Table 1-2, along with the appropriate form of the Nernst equation. The Nernst equation provides a relationship between the standard potential ($E°$) for the cell reaction and the equilibrium potential (E) at various temperatures and partial pressures (activities) of reactants and products. According to the Nernst equation, the equilibrium cell potential at a given temperature can be increased by operating at higher reactant pressures and improvements in fuel cell performance have, in fact, been observed at higher pressures (discussed in Section 2).

The electrochemical reactions of H_2 and O_2 in fuel cells produce H_2O. When a carbon containing fuel is involved in the anode reaction, CO_2 is also produced. In the case of the MCFC, CO_2 is required in the cathode reaction to maintain an invariant carbonate concentration in the electrolyte. Since CO_2 is produced at the anode and consumed at the cathode in MCFCs, and the concentrations in the anode and cathode feed streams are not necessarily equal, the Nernst equation in Table 1-2 includes the CO_2 partial pressure for both electrode reactions.

1.2.2 Transport Processes

The transport processes involving the mass transfer of reactants/products play a prominent role in the performance of porous electrodes in fuel cells. Transport processes involving heat transfer and thermal management are important in fuel cell systems, but these aspects will not be discussed here. The slow transport of reactant and product species through the porous electrode gives rise to the polarization discussed later (Section 1.3.2). A sequence of steps, involving both transport and rate processes, occurs when a reactant species undergoes electrochemical reaction in a porous electrode. One sequence suggested by Liebhafsky and Cairns (4) is presented in Table 1-3. With the exception of Steps 2 and 12, each of the other steps can be associated with a polarization that could contribute to an increase in the inefficiency of the electrode reaction. It is outside the scope of this presentation to describe each of the steps in Table 1-3. The details are found in Reference 4. The important point is that not all of the steps contribute significantly to the total polarization and that those steps can be disregarded. Thus, efforts to improve the performance of porous fuel cell electrodes can be directed at reducing the polarization associated with the remaining steps.

Transport processes involving diffusion, convection, and migration can take place in the gas phase in the pores of the electrodes or in the liquid (electrolyte) phase in the pores of the electrode. The relative contribution of these transport processes to the overall electrode polarization is affected by the porous electrode structure, electrolyte composition and temperature, and reactant gas composition and pressure.

The maximum rate of transport of reactant species to the electrode surface provides an upper limit to the rate of electrochemical reaction. Under these conditions a limiting current is reached. In a fuel cell with porous electrodes containing a liquid (electrolyte) layer, the diffusion of the reactant species through the electrolyte is usually the rate limiting transport process.

Table 1-1 Typical Electrochemical Reactions in Fuel Cells

Fuel Cell	Anode Reaction	Cathode Reaction
Proton Exchange	$H_2 \rightarrow 2H^+ + 2e^-$	$\frac{1}{2} O_2 + 2H^+ + 2e^- \rightarrow H_2O$
Alkaline	$H_2 + 2(OH)^- \rightarrow 2H_2O + 2e^-$	$\frac{1}{2} O_2 + H_2O + 2e^- \rightarrow 2(OH)^-$
Phosphoric Acid	$H_2 \rightarrow 2H^+ + 2e^-$	$\frac{1}{2} O_2 + 2H^+ + 2e^- \rightarrow H_2O$
Molten Carbonate	$H_2 + CO_3^= \rightarrow H_2O + CO_2 + 2e^-$ $CO + CO_3^= \rightarrow 2CO_2 + 2e^-$	$\frac{1}{2} O_2 + CO_2 + 2e^- \rightarrow CO_3^=$
Solid Oxide	$H_2 + O^= \rightarrow H_2O + 2e^-$ $CO + O^= \rightarrow CO_2 + 2e^-$ $CH_4 + 4O^= \rightarrow 2H_2O + CO_2 + 8e^-$	$\frac{1}{2} O_2 + 2e^- \rightarrow O^=$

CO - carbon monoxide
CO_2 - carbon dioxide
$CO_3^=$ - carbonate ion
e^- - electron
H^+ - hydrogen ion
H_2 - hydrogen
H_2O - water
O_2 - oxygen
OH^- - hydroxyl ion

Table 1-2 Fuel Cell Reactions and the Corresponding Nernst Equations

Cell Reactions[a]	Nernst Equation
$H_2 + \frac{1}{2}O_2 \rightarrow H_2O$	$E = E° + (RT/2F) \ln [P_{H_2}/P_{H_2O}] + (RT/2F) \ln [P_{O_2}^{1/2}]$
$H_2 + \frac{1}{2}O_2 + CO_2(c) \rightarrow H_2O + CO_2(a)$	$E = E° + (RT/2F) \ln [P_{H_2}/P_{H_2O}(P_{CO_2})_a] + (RT/2F) \ln [P_{O_2}^{1/2} (P_{CO_2})]_c$
$CO + \frac{1}{2}O_2 \rightarrow CO_2$	$E = E° + (RT/2F) \ln [P_{CO}/P_{CO_2}] + (RT/2F) \ln [P_{O_2}^{1/2}]$
$CH_4 + 2O_2 \rightarrow 2H_2O + CO_2$	$E = E° + (RT/8F) \ln [P_{CH_4}/P_{H_2O}^2 P_{CO_2}] + (RT/8F) \ln [P_{O_2}^2]$

(a) - anode
(c) - cathode
E - equilibrium potential
E° - standard potential
P - gas pressure
R - universal gas constant
T - temperature

[a] The cell reactions are obtained from the anode and cathode reactions listed in Table 1-1.

Table 1-3 Processes Involved in the Overall Electrochemical Reaction in Porous Fuel Cell Electrodes

Step	Process	Type
1	Transport of reactant to gas/electrolyte interface	Physical
2	Dissolution of reactant in electrolyte	Physical
3	Transport of reactant through electrolyte to electrode surface (double layer)	Physical
4	Pre-electrochemical homogeneous or heterogeneous chemical reaction	Chemical
5	Adsorption of electroactive species onto electrode	Chemical
6	Surface migration of adsorbed species	Physical
7	Electrochemical reaction involving electrically charged species	Electro-chemical
8	Post-electrochemical surface migration	Physical
9	Desorption of products	Chemical
10	Post-electrochemical reaction	Chemical
11	Transport of products away from electrode surface	Physical
12	Evolution of products from electrolyte	Physical
13	Transport of gaseous products from electrolyte/gas interface	Physical

Source: (Table 4.4-1) H.A. Liebhafsky and E.J. Cairns, *Fuel Cells and Fuel Batteries*, John Wiley and Sons, Inc., New York, NY, p. 107, 1968.

1.2.3 Porous Gas Electrodes

The current densities that are obtained from smooth electrodes are usually in the range of a single units mA/cm^2 or less because of rate limiting processes such as the available area of the reaction sites. Porous electrodes are commonly used in fuel cells to achieve much higher current densities. These high current densities are possible because the electrode has a high surface area which significantly increases the amount of reaction sites and the optimized electrode structure has favorable mass transport properties. In an idealized porous gas fuel cell electrode, high current densities at reasonable polarization are obtained when the liquid (electrolyte) layer on the electrode surface is sufficiently thin so that it does not significantly impede the transport of reactants to the electroactive sites, and a stable three phase (gas/electrolyte/electrode surface) interface is established. When an excessive amount of electrolyte is present in the porous electrode structure,

the concentration polarization increases to a large value and the electrode is considered to be "flooded".

The porous electrodes that are used in low temperature fuel cells consist of a composite structure that contains platinum (Pt) electrocatalyst on a high surface area carbon black and a PTFE (polytetrafluoroethylene) binder. Such electrodes for acid and alkaline fuel cells are described by Kordesch et al. (5). In these porous electrodes, PTFE is hydrophobic (acts as a wet proofing agent) and serves as the gas permeable phase, and carbon black is an electron conductor that provides a high surface area to support the electrocatalyst. Platinum serves as the electrocatalyst which promotes the rate of electrochemical reactions (ionization/deionization) for a given surface area. The carbon black also has a certain degree of hydrophobicity, depending on the surface properties of the material. The composite structure of PTFE and carbon establishes an extensive three phase interface in the porous electrode, which is the benchmark of PTFE bonded electrodes. Recently, some interesting results have been reported by Japanese workers on higher performance gas diffusion electrodes for acid fuel cells, see Section 3.1.2.

In MCFCs, which operate at relatively high temperature, there are no known materials that can serve to wet proof a porous structure against ingress by molten carbonates. Consequently, the technology used to obtain a stable three phase interface in MCFC porous electrodes is different from that used in PAFCs. In the MCFC, the stable interface is achieved in the electrodes by carefully tailoring the pore structures of the electrodes and the electrolyte matrix ($LiAlO_2$) so that the capillary forces establish a dynamic equilibrium in the different porous structures. Pigeaud et al. (6) provide a discussion of porous electrodes for MCFCs.

In an SOFC, there is no liquid electrolyte present that is susceptible to movement in the porous electrode structure and electrode flooding is not a problem. Consequently, the three phase interface that is necessary for efficient electrochemical reaction involves two solid phases (solid electrolyte/electrode) and a gas phase. A critical requirement of porous electrodes for SOFC is that they are sufficiently thin and porous to provide an extensive electrode/electrolyte interfacial region for electrochemical reaction.

1.3 Thermodynamics[a]

The common energy conversion devices (i.e., heat engines), which rely on the combustion of fossil fuels to produce electrical energy, have an intrinsic efficiency limitation imposed by the Carnot cycle. That is, the maximum efficiency (ε_c) is set by the high temperature (T_h) of the heat source and the low temperature (T_l) of the heat sink, i.e.,

$$\varepsilon_c = \frac{T_h - T_l}{T_h} \qquad (1\text{-}1)$$

Based on the Carnot cycle, the theoretical efficiency of a heat engine increases as the source temperature increases and the sink temperature decreases. If one takes for example $T_h = 1000°K$ and $T_l = 300°K$, $\varepsilon_C = 0.7$, i.e., 70% of the enthalpy of reaction is theoretically converted into useful work. Unfortunately, the maximum efficiency of practical heat engines based on the Carnot cycle is usually ≤40%. An attractive feature of fuel cells is that their efficiency is not limited by the

[a] See References 3, 7 and 8 for discussion on fuel cell thermodynamics.

Carnot cycle, and most of the chemical energy in the fuel may be converted to electricity, along with heat that is useful in some applications.

1.3.1 Reversible Thermodynamics

The maximum electrical work (W_{el}) obtainable in a fuel cell operating at constant temperature and pressure is given by the change in Gibbs free energy (ΔG) of the electrochemical reaction,

$$W_{el} = \Delta G = -nFE \tag{1-2}$$

where n is the number of electrons participating in the reaction, F is Faraday's constant (96,439 coulombs/g-mole electron) and E is the reversible potential of the cell. If we consider the case of all reactants and products being in the standard state, then,

$$\Delta G^\circ = -nFE^\circ \tag{1-3}$$

where the o superscript stands for standard state conditions (25°C and 1 atm).

The overall reactions given in Table 1-2 can be used to produce both electrical energy and heat. The maximum work available from a fuel source is related to the free energy of reaction in the case of a fuel cell, whereas the enthalpy of reaction is the pertinent quantity for a heat engine, i.e.,

$$\Delta G_r = \Delta H_r - T\Delta S_r \tag{1-4}$$

where the difference between ΔG_r and ΔH_r is proportional to the change in entropy (ΔS is the change in entropy, r depicts the state point of the reaction). This entropy change is manifested in changes in the degrees of freedom for the chemical system being considered. The maximum amount of electrical energy available is ΔG_r, as mentioned above, and the total energy available is ΔH_r. The amount of heat that is produced by a fuel cell operating reversibly is $T\Delta S_r$. Reactions in fuel cells that have negative entropy change generate heat, while those with positive entropy change may extract heat from their surroundings, if the irreversible generation of heat is smaller than the reversible absorption of heat.

The reversible potential of a fuel cell at temperature T is calculated from ΔG_T for the cell reaction at that temperature. This potential can be computed from the heat capacities (C_p) of the species involved as a function of T and using values of both ΔS° and ΔH° at one particular temperature, usually 298°K. Empirically, the heat capacity of a specie as a function of T can be expressed as:

$$C_p = a + bT + cT^2 \tag{1-5}$$

where a, b, and c are empirical constants. The difference in the heat capacities for the products and reactants involved in the stoichiometric reaction is given by:

$$\Delta C_p = \Delta a + \Delta bT + \Delta cT^2 \tag{1-6}$$

Since,

$$\Delta H_T = \Delta H^\circ_{298} + \int \Delta C_p dT \tag{1-7}$$

and, at constant pressure,

$$\Delta S_T = \Delta S^\circ_{298} + \int \frac{\Delta C_p}{T} dT \tag{1-8}$$

Then it follows that

$$\Delta H_T = \Delta H^\circ_{298} + \Delta\, a(T - 298) + 1/2\Delta\, b(T - 298)^2 + 1/3\Delta\, c(T - 298)^3 \tag{1-9}$$

and

$$\Delta S_T = \Delta S^\circ_{298} + \Delta\, a \ln\left(\frac{T}{298}\right) + \Delta\, b(T - 298) + 1/2\Delta\, c(T - 298)^2 \tag{1-10}$$

The coefficients a, b and c (see Appendix 9.1), as well as ΔS°_{298} and ΔH°_{298}, are available from standard reference tables, and may be used to calculate ΔH_T and ΔS_T. From these values it is then possible to calculate ΔG_T and E°_T.

For the general cell reaction,

$$aA + bB \rightarrow cC + dD \tag{1-11}$$

the free energy change can be expressed by the equation:

$$\Delta G = \Delta G^\circ + RT \ln \frac{[C]^c[D]^d}{[A]^a[B]^b} \tag{1-12}$$

When Equations 1-2 and 1-3 are substituted in Equation 1-12,

$$E = E^\circ + \frac{RT}{nF} \ln \frac{[A]^a[B]^b}{[C]^c[D]^d} \tag{1-13}$$

or

$$E = E^\circ + \frac{RT}{nF} \ln \frac{\Pi\,[\text{reactant activity}]}{\Pi\,[\text{product activity}]} \tag{1-14}$$

which is the general form of the Nernst equation. For the overall cell reaction, the cell potential increases with an increase in the activity of reactants and a decrease in the activity of products. Changes in temperature also influence the reversible cell potential, and the dependence of potential

on temperature varies with the cell reaction. Figure 1-3 illustrates the change in the reversible standard potential for the reactions:

$$H_2 + \tfrac{1}{2}O_2 \rightarrow H_2O \quad (1\text{-}15)$$

$$CO + \tfrac{1}{2}O_2 \rightarrow CO_2 \quad (1\text{-}16)$$

and,

$$CH_4 + 2O_2 \rightarrow 2H_2O + CO_2 \quad (1\text{-}17)$$

as a function of temperature. It is apparent from Figure 1-3 that the standard potentials for the oxidation of H_2 and CO show a marked decrease with an increase in temperature, whereas the corresponding potential for the oxidation of CH_4 is nearly invariant with temperature. The significance of these results is that the reversible cell voltage of high temperature fuel cells is usually lower than that of low temperature fuel cells. In practical fuel cells, the theoretical advantage in cell voltage for MCFC over SOFC is about 0.1 V and about 0.15 V for PAFC over MCFC, with comparable gas compositions. The actual difference in cell voltages between these fuel cells are less than the differences in theoretical voltages (9). This point will be discussed in the next section.

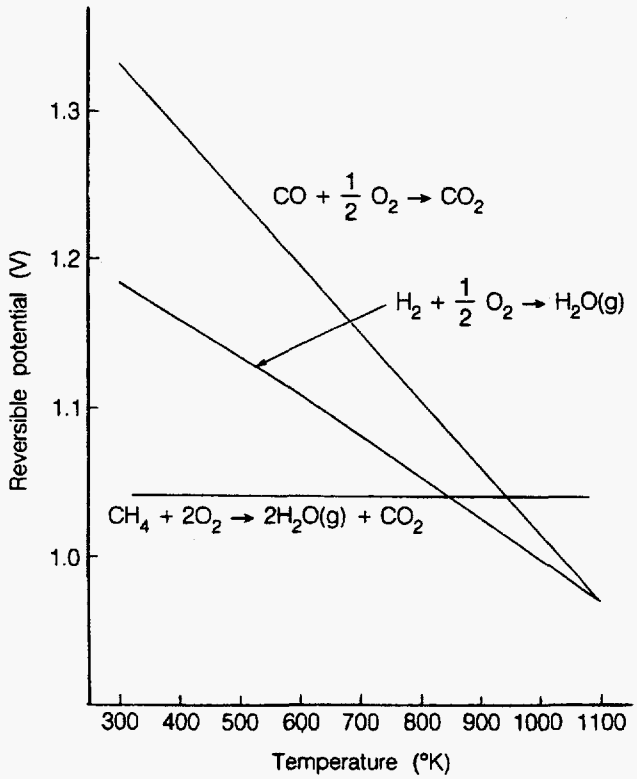

Figure 1-3 Reversible standard potential for fuel cell reactions as a function of temperature. *Source:* Reference (2).

1.3.2 Irreversible Thermodynamics

Useful amounts of work (electrical energy) are obtained from a fuel cell only when a reasonably large current is drawn, but the cell potential will be decreased from its equilibrium potential because of irreversible losses. There are several sources that contribute to irreversible losses in a practical fuel cell. The losses, which are often called polarization, overpotential or overvoltage, originate primarily from three sources: (i) ohmic polarization (η_{ohm}), (ii) concentration polarization (η_{conc}) and (iii) activation polarization (η_{act}). These losses result in a cell voltage (V) for a fuel cell that is less than its reversible potential.

Ohmic Polarization: The ohmic losses occur because of resistance to the flow of ions in the electrolyte and resistance to flow of electrons through the electrode materials. The dominant ohmic losses through the electrolyte phase are reduced by decreasing the electrode separation and enhancing the ionic conductivity of the electrolyte. Because both the electrolyte and fuel cell electrodes obey Ohm's law, the ohmic losses can be expressed by the equation,

$$\eta_{ohm} = iR \tag{1-18}$$

where i is the current flowing through the cell, and R is the total cell resistance, which includes electronic, ionic and contact resistances.

Concentration Polarization: As a reactant is rapidly consumed at the electrode by electrochemical reaction, concentration gradients will be established. Several processes may contribute to concentration polarization--slow diffusion in the gas phase in the electrode pores, solution/dissolution of reactants/products into/out of the electrolyte, or diffusion of reactants/products through the electrolyte to/from the electrochemical reaction site. At practical current densities, slow transport of reactants/products to/from the electrochemical reaction site is a major contributor to concentration polarization.

The rate of mass transport to an electrode surface in many cases can be described by Fick's first law of diffusion,

$$i = \frac{nFD\ (C_B - C_S)}{\delta} \tag{1-19}$$

where D is the diffusion coefficient of the reacting species, C_B is its bulk concentration, C_S is its surface concentration and δ is the thickness of the diffusion layer. The limiting current (i_L) is a measure of the maximum rate at which a reactant can be supplied to an electrode, and occurs when $C_S = 0$, i.e.,

$$i_L = \frac{nFDC_B}{\delta} \tag{1-20}$$

By appropriate manipulation of Equations 1-19 and 1-20 we arrive at:

$$\frac{C_S}{C_B} = 1 - \frac{i}{i_L} \tag{1-21}$$

The Nernst equation for the reactant species at equilibrium conditions, or when no current is flowing, is:

$$E\big|_{i=o} = E^\circ + \frac{RT}{nF} \ln C_B \tag{1-22}$$

When current is flowing, the surface concentration becomes less than the bulk concentration, and the Nernst equation becomes,

$$E = E^\circ + \frac{RT}{nF} \ln C_S \tag{1-23}$$

The potential difference (ΔE) produced by a concentration change at the electrode is called the concentration polarization:

$$\Delta E = \eta_{conc} = \frac{RT}{nF} \ln \frac{C_S}{C_B} \tag{1-24}$$

Upon substituting Equation 1-21 in 1-24, the concentration polarization is given by the equation:

$$\eta_{conc} = \frac{RT}{nF} \ln \left(1 - \frac{i}{i_L}\right) \tag{1-25}$$

In this analysis of concentration polarization, the activation polarization is assumed to be negligible. The charge transfer reaction has such a high exchange current density that the activation polarization is negligible in comparison with the concentration polarization.

Activation Polarization: Activation polarization is present when the rate of an electrochemical reaction at an electrode surface is associated with sluggish electrode kinetics. In other words, activation polarization is directly related to the rates of electrochemical reactions. There is a close similiarity between electrochemical and chemical reactions in that both involve an activation barrier that must be overcome by the reacting species. In the case of an electrochemical reaction with $\eta_{act} \geq$ 50-100 mV, η_{act} is described by the general form of the Tafel equation,

$$\eta_{act} = \frac{RT}{\alpha nF} \ln \frac{i}{i_o} \tag{1-26}$$

where α is the transfer coefficient and i_o is the exchange current density. The usual form of the Tafel equation is:

$$\eta_{act} = a + b \log i \tag{1-27}$$

where $a = (-2.3RT/\alpha nF) \log i_o$ and $b = 2.3RT/\alpha nF$. The term b is called the Tafel slope, and is obtained from the slope of a plot of η as a function of log i. The Tafel slope for an electrochemical reaction is about 100 mV/decade (log current density) at room temperature. Thus, a ten-fold increase in current density causes a 100 mV increase in the activation polarization. Conversely, if

the Tafel slope is only 50 mV/decade, then the same increase in current density produces a 50 mV increase in activation polarization. Clearly, there exists a strong incentive to develop electrocatalysts that yield a lower Tafel slope for electrochemical reactions.

The simplified description presented here did not consider the processes that give rise to activation polarization, except for attributing it to sluggish electrode kinetics. A detailed discussion of the subject is outside the scope of this presentation, but processes involving absorption of reactant species, transfer of electrons across the double layer, desorption of product species, and the nature of the electrode surface can all contribute to activation polarization.

Electrode Polarization: Activation and concentration polarizations can exist at both the positive (cathode) and negative (anode) electrodes in fuel cells. The total polarization at these electrodes is the sum of η_{act} and η_{conc}, or,

$$\eta_{anode} = \eta_{act,a} + \eta_{conc,a} \tag{1-28}$$

and,

$$\eta_{cathode} = \eta_{act,c} + \eta_{conc,c} \tag{1-29}$$

The effect of polarization is to shift the potential of the electrode ($E_{electrode}$) to a new value ($V_{electrode}$):

$$V_{electrode} = E_{electrode} \pm | \eta_{electrode} | \tag{1-30}$$

For the anode,

$$V_{anode} = E_{anode} + | \eta_{anode} | \tag{1-31}$$

and for the cathode,

$$V_{cathode} = E_{cathode} - | \eta_{cathode} | \tag{1-32}$$

The net result of current flow in a fuel cell is to increase the anode potential and to decrease the cathode potential, thereby reducing the cell voltage. Figure 1-4 illustrates the contribution to polarization of the two half cells for a PAFC. The reference point (zero polarization) is hydrogen. These polarization curves are typical of other types of fuel cells.

Cell Voltage: The cell voltage includes the contribution of the polarization and the anode and cathode potentials:

$$V_{cell} = V_{cathode} - V_{anode} - iR \tag{1-33}$$

When Equations 1-31 and 1-32 are substituted in Equation 1-33:

$$V_{cell} = E_{cathode} - | \eta_{cathode} | - (E_{anode} + | \eta_{anode} |) - iR \tag{1-34}$$

or

$$V_{cell} = \Delta E_e - | \eta_{cathode} | - | \eta_{anode} | - iR \tag{1-35}$$

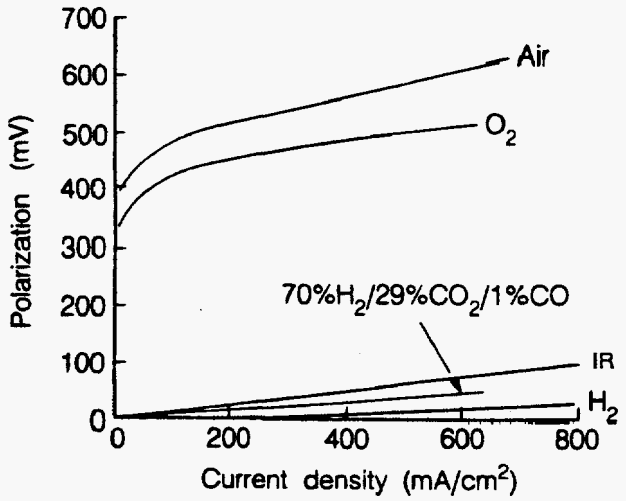

Figure 1-4 Contribution to polarization in PAFCs. Pt loading in anode and cathode is 0.5 mg/cm^2. 100% H_3PO_4, 180°C, 57°C dew-point, 1 atm.
Source: (Figure 2-1, page 2-1) J. A. S. Bett, H. R. Kunz, S. W. Smith and L. L. Van Dine, "Investigation of Alloy Catalysts and Redox Catalysts for Phosphoric Acid Electrochemical Systems," FCR-7157F, prepared by International Fuel Cells under Contract No. 9-X13-D6271-1 for Los Alamos National Laboratory, 1985.

where $\Delta E_e = E_{cathode} - E_{anode}$. Equation 1-35 shows that current flow in a fuel cell results in a decrease in the cell voltage because of losses by electrode and ohmic polarizations. The goal of fuel cell developers is to minimize the polarization so that V_{cell} approaches ΔE_e. This goal is approached by modifications to the fuel cell operating conditions (i.e., higher gas pressure, higher temperature, change in gas composition to lower the gas impurity concentration, etc.), improvement in electrode structures, better electrocatalysts, more conductive electrolyte, etc. However, for any fuel cell, trade-offs exist between achieving higher performance by operating at higher temperature or pressure and the problems associated with the stability/durability of cell components encountered at the more severe conditions.

Although, ohmic, concentration, and activation polarization are the classic fuel cell losses others exist as well in practical application. Two worthy of consideration are contact resistant losses and losses due to exchange currents.

Contact Resistance: Contact resistances at electrodes and separators account for losses due to spatial variation in material properties, fluxes, reaction rate densities, etc. Contact or terminal resistance is actually a form of ohmic resistance.

Exchange Current (of electrons *through the electrolyte rather than through the external load*): Exchange current is directly related to the chemical potential difference, so even at zero external load current there are electrons delivered to the cathode. Once oxygen ions are formed, they migrate through the electrolyte to the anode where they deionize to release an electron. The electron released migrates back to the cathode to continue the process or "exchange". With the ionization/deionization reactions proceeding at a low (but *non-zero* equilibrium) rate, the cell

voltage is diminished below that of reversible potential, even though there is no external current flowing. This form of loss, however, would become less significant once the external current is increased beyond a certain value. Moreover, the magnitude of the exchange current *actually decreases with an increase in external current* since the cell voltage, which drives the occurrence of exchange current in the first place, would drop further. This is the *only* form of losses that decreases with an increase in current output.

1.4 Types of Fuel Cells

Fuel cells can be classified by use of various categories, depending on the combination of type of fuel and oxidant, whether the fuel is processed outside (external reforming) or inside (internal reforming) of the fuel cell, the type of electrolyte, the temperature of operation, whether the reactants are fed to the cell by internal or external manifolds, etc. It is convenient (and has become standard practice) to primarily refer to fuel cells by the type of electrolyte used. This is logical because many other characteristics, particularly operating temperature, are limited by the electrolyte properties. A brief description of various electrolyte cells of current interest follows. A detailed discussion on each of these fuel cells may be found in References 3 and 10.

Polymer Electrolyte Fuel Cell: The electrolyte in this fuel cell is an ion exchange membrane (fluorinated sulfonic acid polymer or other similar polymers) which is an excellent proton conductor. The only liquid in this fuel cell is water, thus corrosion problems are minimal. Water management in the membrane is critical for efficient performance; the fuel cell must operate under conditions where the byproduct water does not evaporate faster than it is produced because the membrane must be hydrated. Because of the limitation on the operating temperature imposed by the polymer and problems with water balance, usually less than 120° C, a H_2-rich gas with little or no CO is used, and higher catalysts loadings (Pt in most cases) than those used in PAFCs are required in both the anode and cathode.

Alkaline Fuel Cell: The electrolyte in this fuel cell is concentrated (85 wt%) KOH in fuel cells operated at high temperature (~250° C), or less concentrated (35-50 wt%) KOH for lower temperature (< 120° C) operation. The electrolyte is retained in a matrix (usually asbestos), and a wide range of electrocatalysts can be used (e.g., Ni, Ag, metal oxides, spinels and noble metals).

Phosphoric Acid Fuel Cell: Concentrated phosphoric acid is used for the electrolyte in this fuel cell, which operates at 150-220° C. At lower temperatures, phosphoric acid is a poor ionic conductor and CO poisoning of the Pt electrocatalyst in the anode becomes more severe. The relative stability of concentrated phosphoric acid is high compared to other common acids, consequently the PAFC is capable of operating at the high end of the acid temperature range (100-220° C). In addition, the use of concentrated acid (~100%) minimizes the water vapor pressure so water management in the cell is not difficult. The matrix universally used to retain the acid is silicon carbide (3), and the electrocatalyst in both the anode and cathode is Pt.

Molten Carbonate Fuel Cell: The electrolyte in this fuel cell is usually a combination of alkali (Na, K) carbonates, which is retained in a ceramic matrix of $LiAlO_2$. The fuel cell operates at 600-700° C where the alkali carbonates form a highly conductive molten salt, with carbonate ions providing ionic conduction. At the high operating temperatures in MCFCs, Ni (anode) and nickel oxide (cathode) are adequate to promote reaction and noble metals are not required.

Solid Oxide Fuel Cell: The electrolyte in this fuel cell is a solid, nonporous metal oxide, usually Y_2O_3-stabilized ZrO_2. The cell operates at 650-1000° C where ionic conduction by oxygen ions takes place. Typically, the anode is Co-ZrO_2 or Ni-ZrO_2 cermet, and the cathode is Sr-doped $LaMnO_3$.

A more detailed discussion of these fuel cells is presented in Sections 3 through 6.

1.4.1 Characteristics

Fuel cells have many favorable characteristics for energy conversion devices; several of these general characteristics are:

- high energy conversion efficiency relatively independent of size or load
- modular design
- size flexibility
- very low environmental intrusion
- cogeneration capability
- siting ability
- fuel flexibility
- rapid load following capability

The general negative features of fuel cells for energy conversion include:

- sensitivity to certain fuel contaminants
- high market entry cost
- endurance/reliability has not been demonstrated

One of the main attractive features of fuel cell systems is their expected high fuel-to-electricity efficiency (40-60% based on lower heating value of the fuel), which is higher than that of many competing energy conversion systems. In addition, fuel cells operate at a constant temperature and the heat from the electrochemical reaction is available for cogeneration applications. Since fuel cells operate at near constant efficiency, independent of size, small fuel cells operate nearly as efficiently as large ones.[b] Thus, fuel cell power plants can be configured in a wide range of electrical output, ranging from watts to megawatts. Fuel cells are quiet and operate with virtually no gaseous or solid emissions, but they are sensitive to certain fuel contaminants which must be minimized in the fuel gas. Table 1-4 summarizes the impact of the major constituents within fuel gases on the various fuel cells. The reader is referred to Sections 3 through 6 for detail on trace contaminants. The two major impediments to the widespread use of fuel cells are: 1) high initial cost and 2) endurance operation; it is these two aspects which are the major focus of technological effort.

1.4.2 Advantages/Disadvantages

The fuel cell types addressed in this handbook have significantly different operating regimes. As a result their materials of construction, fabrication techniques, and system requirements differ.

---

[b] The fuel processor efficiency is size dependent, therefore, small fuel cell power plants using externally reformed hydrocarbon fuels would have a lower overall system efficiency.

These distinctions result in individual advantages and disadvantages which govern the potential of the various cells to be used for different applications.

Table 1-4 Summary of Major Fuel Constituents Impact on PAFC, MCFC, SOFC, and PEFC

Gas Species	PAFC	MCFC	SOFC	PEFC
H_2	fuel	fuel	fuel	fuel
CO	poison (>0.5%)	fuel	fuel	poison (>10 ppm)
CH_4	diluent	diluent	fuel	diluent
CO_2 & H_2O	diluent	diluent	diluent	diluent
S as (H_2S & COS)	poison (>50 ppm)	poison (>0.5 ppm)	poison (>1.0 ppm)	No studies to date (11)

The AFC was one of the first modern fuel cells to be developed, beginning in 1960. The application at that time was to provide on-board electric power for the Apollo space vehicle. Desirable attributes of the AFC include its excellent performance on hydrogen (H_2) and oxygen (O_2) compared to other candidate fuel cells due to its active O_2 electrode kinetics and its flexibility to use a wide range of electrocatalysts, an attribute which provides development flexibility. Once development was underway for space application, terrestrial applications began to be investigated. Developers recognized that pure hydrogen would be required in the fuel stream. This is because the carbon dioxide (CO_2) in any reformed fuel reacts with the potassium hydroxide (KOH) electrolyte to form a solid carbonate, destroying the electrolyte's ion mobility. Pure H_2 could be supplied to the anode by passing a reformed, H_2-rich fuel stream by a precious metal (palladium/silver) membrane. The H_2 molecule is able to pass through the membrane by absorption and mass transfer, and into the fuel cell anode. However, a significant pressure differential is required across the membrane and the membrane is prohibitive in cost. Even the small amount of CO_2 in ambient air, the source of O_2 for the reaction, would have to be scrubbed. Investigations soon showed that the scrubbing of the small amount of CO_2 within the air, coupled with the purification of the hydrogen, was not cost effective and that terrestrial application of the AFC could be limited to special applications at best.

The CO_2 in the reformed fuel gas stream and the air does not react with the electrolyte in an acid electrolyte cell, but is a diluent. This attribute and the relatively low temperature of the PAFC made it a prime, early candidate for terrestrial application. Although its cell performance is somewhat lower than the alkaline cell due to the cathode's slow oxygen reaction rate, and although the cell still requires hydrocarbon fuels to be reformed into an H_2-rich gas, the PAFC's system efficiency improved due to its higher temperature environment and less complex fuel conversion (no membrane and attendant pressure drop). The need for the process air scrubber is also eliminated. The rejected heat from the cell is high enough in temperature to heat water or air in a system operating at atmospheric pressure. Some steam is available in pressurized PAFCs, a key point in expanding cogeneration applications.

PAFC systems achieve about 37 to 42% electrical efficiency (based on the higher heating value (HHV) of natural gas). This is at the low end of the efficiency goal for fuel cell power plants. PAFCs use high cost precious metal catalysts such as platinum. The fuel has to be reformed

externally to the cell, and carbon monoxide (CO) has to be shifted by a water gas reaction to below 3 to 5 vol% at the inlet to the fuel cell anode or it poisons the catalyst. These limitations have prompted development of the alternate, higher temperature cells, MCFC and SOFC.

Many of the disadvantages of the lower temperature cells can be alleviated with the higher operating temperature MCFC (approximately 650° C). This temperature results in several benefits: the cell can be made of commonly available sheet metals that can be stamped for less costly fabrication, the cell reactions occur with nickel catalysts rather than with expensive precious metal catalysts, reforming can take place within the cell provided a reforming catalyst is added (results in a large efficiency gain), CO is a directly usable fuel, and the rejected cell heat is of sufficiently high temperature to drive a gas turbine and/or produce a high pressure steam for use in a steam turbine or for cogeneration.

The MCFC has some disadvantages, however: a source of CO_2 is required at the cathode to form the carbonate ion, the cell has a very low sulfur tolerance compared to the PAFC, and the higher temperatures promote material problems, particularly mechanical stability which impacts life.

The SOFC is the fuel cell with the longest, continuous development period, starting in the late 1950s, several year before the AFC. Since the electrolyte is a solid, the cell can be cast into flexible shapes, such as tubular, planar, or monolithic. The solid construction of the cell also alleviates any corrosion problems characterized by the liquid electrolyte cells and has the advantage of being impervious to gas cross-over from one electrode to the other. The absence of liquid also eliminates the problem of electrolyte movement or flooding in the electrodes. The kinetics of the cell are fast and CO is a directly useable fuel as it is in the MCFC. There is no requirement for CO_2 at the anode as with the MCFC. At the temperature of presently operating SOFCs (1000° C), fuel can be reformed within the cell with no additional reforming catalysts. The temperature of an SOFC is significantly higher than that of the MCFC. However, some of the rejected heat from an SOFC is needed for preheating the incoming process air.

The high temperature of the SOFC has its drawbacks. There are thermal expansion mismatches among materials and sealing between cells is difficult in the flat plate configurations. The high operating temperature places severe constraints on materials selection and results in difficult fabrication processes. The SOFC also exhibits a high electrical resistivity in the electrolyte which results in a lower cell performance than the MCFC by approximately 100 mV. Researchers would like to develop cells at a reduced temperature of 650° C, but the electrical resistivity of the solid electrolyte material presently used increases.

The PEFC, like the SOFC, has a solid electrolyte. As a result, this cell exhibits excellent resistance to gas cross-over. In contrast to the SOFC, the cell operates at a low 80° C. This results in a capability to bring the cell to its operating temperature quickly, but the rejected heat cannot be used for cogeneration or additional power purposes. Test results have shown that the cell can operate at very high current densities compared to the other cells.

Developers are using the advantages of the fuel cells to identify early applications of fuel cell power plants. It is the function of development to mitigate the disadvantages described to expand the application potential. Many research development issues are addressed for each of the cell types in Sections 3 through 6.

1.5 Applications

The advantages and disadvantages summarized in the previous section form the basis for selection of the candidate fuel cell types to respond to a variety of potential applications. The major potential applications for fuel cells are as on-board electric power for space vehicles and

other closed environments, as stationary electric or cogeneration power plants, and as motive power for vehicles.

1.5.1 Stationary Power Plants

There has been a dramatic increase within the past five years in installed and planned fuel cell demonstrations for terrestrial, stationary applications in the U.S. and abroad. These demonstrations provide guidance for early applications of fuel cell power plants. One interesting characteristic of fuel cells is the ability to be demonstrated at a small size, compared to competing technologies, without much of a performance penalty. This is advantageous because fuel cell power plants can be produced at a multi-kW size which will reduce the cost risk of establishing a commercial fuel cell industry. Demonstrations of larger plants will be delayed while the smaller plants are monitored and evaluated.

Fuel cell demonstrations now in progress include PAFCs, and SOFCs (12, 13). Firm plans for MCFCs demonstrations have been made for two 250 kW units and a 1.6 MW unit in the 1994 to 1996 time period (14, 15). There has been several production runs of PAFC plants for demonstration. In the U.S., there have been runs of 12.5 kW, 40 kW, and 200 kW units. The latest demonstration consists of fifty-six 200 kW plants which are being installed for 26 customers in eleven countries (16). Most of these 200 kW plants convert pipeline gas to ac grid quality power for a variety of on-site applications. Two are being installed to address the issue of using landfill gases (17, 18). In Japan, there have been several series of 50 kW and 100 kW PAFC plants (12). These demonstrations are primarily for gas utilities although some installations are for electric utilities. The largest fuel cell power plant operated to date, a PAFC 11 MW installation, has been a combined U.S./Jananese effort (19). Japanese gas companies are operating a 500 kW PAFC plant and are constructing a 1 MW PAFC plant to be started in 1995 (20). A Japanese electric utility is sponsoring a 5 MW PAFC plant (20). Two 25 kW SOFC plants are being demonstrated, one for the gas utility (cogeneration) and the other for an electric utility interested in operational aspects of the plant (21, 22). A 20 kW demonstration and a 100 kW SOFC demonstration are planned, in 1994 and 1995 by a U.S. electric utility and a U.S. gas company respectively (13).

On-site Cogeneration Power Plants

It is evolving that the first, near term (1997-1998), commercial fuel cell applications are expected to be on-site power plants in the 200 kW to 1 MW capacity range using PAFC plants, primarily for gas utilities at their customers' site. As a result, the customers can use the power plant rejected heat for cogeneration purposes. Demonstrations have shown that overall use of the fuel energy approaches 80% HHV for cogeneration applications (19). Demonstrations confirm that the rejected heat from the initial PAFC plants can be used for heating water, space heating, low pressure steam and possibly for absorption cooling. The MCFC plants, when ready, will be able to provide higher grade cogeneration heat expanding the application potential to the industrial sector. Special applications requiring dc power would benefit from cost and performance savings since the dc to ac inverter of the standard fuel cell power plant could be eliminated. Atmospheric PAFCs, MCFCs, and SOFCs have the attributes to compete for this market.

PEFCs have not been thought of as practical for stationary power plants that use reformed hydrocarbons for fuel because even small amounts of CO degrades performance. However, recent advances to selectively oxidize CO to CO_2 in the fuel steam (23) have caused reconsideration. As a result, two projects have been initiated to determine whether PEFC may be considered for

stationary power uses, one for utility power generation, the other at a refinery using hydrogen-rich off gases (24).

Dispersed Electric Generators

The next step in fuel cell applications is as dispersed generators for the electric utility industry. These plants would be run on pipeline gas and be larger than the on-site plants, probably in the 2 to 20 MW capacity range. Their electric efficiency is estimated to be from 35 to 55% based on the HHV of the fuel. A demonstration program is underway where U.S. municipal electric companies are sponsoring a 1.6 MW demonstration of a MCFC power plant (15). Startup is expected in 1995. An SOFC demonstration at the 50 kW size is being planned for an electric utility, but this is considered a precursor for larger size plants (13). A 5 MW PAFC dispersed plant is presently under construction in Japan for one of the Japanese electric utilities. It is expected to be started in 1994 (20). Atmospheric MCFCs and SOFCs and pressurized PAFCs are being considered for lower capacity level installations. Atmospheric SOFCs and internal reforming MCFCs and pressurized, external reforming MCFCs are the most promising candidates for the higher capacity level installations.

Since on-site and dispersed plants are the most likely first applications, certain high value installations have been identified to allow market penetration for the first units which are expected to be high cost. A consensus based on presentations at the 1992 Fuel Cell Seminar (e.g., 25) of these applications are:

- in environmentally restricted areas
- at substations as dispersed or distributed power units
- where low-Btu off-gases are available at low cost

Base Loaded Electric Power Plants

One of the most lucrative markets for fuel cells is the large (100 to 300 MW) base loaded stationary plants operating on coal. Studies showing the potential of high temperature fuel cells for plants of this size have been performed (26 - 28). These plants are expected to attain 50 to 55% efficiency based on the HHV of the fuel. The market for large stationary power plants will be difficult because of the coupling of a coal gasifier with fuel cells. Coal gasifiers produce a fuel gas product requiring cleaning to the stringent requirements of the fuel cells electrochemical environment and this is a difficult, costly process. The trend of environmental regulations has been for every more stringent cleanup. If this trend continues, other technologies will be subject to additional cost for cleanup which will improve the competitive position of plants based on the fuel cell approach. Fuel cell systems already exceed required emissions limits. U.S. developers have begun investigating the effect of coal gas on MCFCs and SOFCs (29, 30). A demonstration of a MCFC stack operating on a slip stream of an actual coal gasifier began in late 1993 (31). MCFCs and SOFCs coupled with coal gasifiers have the best attributes to compete for this market. Another related, early opportunity may be in repowering older, existing plants with high temperature fuel cells (32). The rejected heat from the fuel cell system can be used to produce steam for the existing plant's turbines.

1.5.2 Other Applications

Due of the modular nature of fuel cells, they are attractive for use in small portable units, ranging in size from 5 W or smaller to 100 W power levels; different power levels are attained by appropriate electrical connection of the fuel cells. The application of fuel cells in the space program (1 kW PEFC in the Gemini program and 1.5 kW AFC in the Apollo program) was demonstrated in the 1960s. More recently three 12 kW AFC units are being used in the Space Shuttle Orbiter. In these space applications, the fuel cells uses pure reactant gases.

Fuel cells of about 20 kW power level and greater are being considered for terrestrial transportation applications. The PAFC and PEFC, using reformed methanol for fuel, are both being evaluated for transportation use. A PEFC providing 125 kW power to a 20 passenger intracity transport bus is in the demonstration phase in Canada. There are at lease two other bus demonstrations in Europe, one using a 35 kW PEFC operating on liquid hydrogen and air, the other a 125 kW hybrid battery/75 kW AFC also operating on hydrogen and air. A discussion on fuel cells for electric vehicles is presented in References 33 and 34.

References

1. T.G. Benjamin, E.H. Camara and L.G. Marianowski, *Handbook of Fuel Cell Performance,* prepared by the Institute of Gas Technology for the U. S. Department of Energy under Contract No. EC-77-C-03-1545, May, 1980.
2. K. Kinoshita, F.R. McLarnon, E.J. Cairns, *Fuel Cells, A Handbook*, prepared by Lawrence Berkeley Laboratory for the U.S. Department of Energy under Contract DE-AC03-76SF00098, May, 1988.
3. A.J. Appleby, F.R. Foulkes, *Fuel Cell Handbook*, Van Norstand Reinhold, New York, NY, 1989.
4. H.A. Liebhafsky and E.J. Cairns, Fuel Cells and Fuel Batteries, John Wiley and Sons, Inc., New York, NY, p. 107, 1968.
5. K. Kordesch, J. Gsellmann, S. Jahangir and M. Schautz, in *Proceedings of the Symposium on Porous Electrodes: Theory and Practice,* Edited by H.C. Maru, T. Katan and M.G. Klein, The Electrochemical Society, Inc., Pennington, NJ, p. 163, 1984.
6. A. Pigeaud, H.C. Maru, L. Paetsch, J. Doyon and R. Bernard, in *Proceedings of the Symposium on Porous Electrodes: Theory and Practice,* Edited by H.C. Maru, T. Katan and M.G. Klein, The Electrochemical Society, Inc., Pennington, NJ, p. 234, 1984.
7. H.A. Liebhafsky, *J. Electrochem. Soc.,* **106,** 1069, 1959.
8. A.J. deBethune, *J. Electrochem. Soc.,* **107,** 937, 1960; *J. Electrochem. Soc.,* **108,** 608, 1961.
9. J.P. Ackerman, *Prog. Batteries & Solar Cells,* **5,** 13, 1984.
10. *Assessment of Research Needs for Advanced Fuel Cells,* Edited by S.S. Penner, DOE/ER/30060-T1, prepared by the DOE Advanced Fuel Cell Working Group for the United States Department of Energy under Contract No. De-AC01-84ER30060 November 1985; Energy **11,** 1 1986.
11. J.C. Amphlett, et. al., "Methanol, Diesel Oil and Ethanol as Liquid Sources of Hydrogen for PEM Fuel Cells" in the *28th Intersociety Energy Conversion Engineering Conference Proceedings*, American Chemcial Society, August, 1993.
12. J.H. Hirschenhofer, "International Data Book of Fuel Cell Activities, 1990", prepared for U.S. DOE/FE, 1990.

13. S.E. Veyo, "High Temperature Solid Oxide Fuel Cell - Customer Test Units", in *Agenda and Abstracts*, Joint Contractors Meeting, FE Fuel Cells and Coal-Fired Heat Engines Conference, U.S. DOE/METC, August 3-5, 1993.
14. R.R. Woods, "Overview of M-C Power's MCFC Power Generation System", in *Agenda and Abstracts*, Joint Contractors Meeting, FE Fuel Cells and Coal-Fired Heat Engines Conference, U.S. DOE/METC, August 3-5, 1993.
15. P.H. Eichenberger, T.P. O'Shea, "Update on the World's First 2-MW Carbonate Fuel Cell Demonstration", in *Fuel Cell Program and Abstracts*, 1992 Fuel Cell Seminar, Tucson, AZ, November 29-December 2, 1992.
16. W.H. Podolny, J.S. Schmitt, "Phosphoric Acid Fuel Cell Power Plants in Service - A Report", in *Fuel Cell Program and Abstracts*, 1992 Fuel Cell Seminar, Tucson, AZ, November 29-December 2, 1992.
17. G.J. Sandelli, "Demonstration of Fuel Cells to Recover Energy from Landfill Gas, Phase I Final Report: Conceptual Study" prepared for EPA by International Fuel Cells, Inc., EPA-00-R-92-007, January, 1992.
18. G.J. Sandelli, "Landfill Gas Treatment for Fuel Cell Applications", presented at 1992 Fuel Cell Seminar, Tucson, AZ, November 29-December 2, 1992.
19. K. Yokota, et. al., "GOI 11 MW FC Plant Operation Interim Report", in *Fuel Cell Program and Abstracts*, 1992 Fuel Cell Seminar, Tucson, AZ, November 29-December 2, 1992.
20. T. Koshimizu, K. Ito, T. Satomi, "Development of 5000 kW and 1000 kW PAFC Plants", JASME - ASME Joint Conference, ICOPE - 93, Tokyo, September, 1993.
21. S. Tekeuchi, et. al., "A 25 kW SOFC Generation System Verification Test", in *Fuel Cell Program and Abstracts*, 1992 Fuel Cell Seminar, Tucson, AZ, November 29-December 2, 1992.
22. K. Shinozaki, "Verification Test of a 25 kW Class SOFC Cogeneration System", in *Fuel Cell Program and Abstracts*, 1992 Fuel Cell Seminar, Tucson, AZ, November 29-December 2, 1992.
23. S. Gottesfeld, "Polymer Electrolyte Fuel Cells: Potential Transportation and Stationary Applications", Report 10, in *An EPRI/GRI Fuel Cell Workshop on Technology Research and Development*, Stonehart Associates, Madison, CT, 1993.
24. R.B.Fleming, et. al., "The Commercialization of Solid Polymer Fuel Cells", in *The International Fuel Cell Conference Proceedings*, NEDO, Makuhari, Japan, February 3-6, 1992.
25. T. Sigimoto, E. Gillis, L. Sjunnesson, "Fuel Cell Demonstrations World-Wide", presentation at the 1992 Fuel Cell Seminar, Tucson, AZ, November 29-December 2, 1992.
26. M. Farooque, "Development of Internal Reforming Carbonate Fuel Cell Stack Technology, Final Report", prepared for U.S. DOE/METC, DOE/MC/23274-2941, October, 1990.
27. W.L. Lundberg, "System Applications of Tubular Solid Oxide Fuel Cells", in *Proceedings of the 25th Intersociety Energy Conversion Engineering Conference*, American Institute of Chemical Engineers, New York, NY, August 12-17, 1990.
28. KTI, "Site-Specific Assessment of a 150-MW Coal Gasification Fuel Cell Power Plant", prepared for Electric Power Research Institute, EPRI EM-3162, November, 1983.
29. ERC, "Effects of Coal-Derived Trace Species on the Performance of Molten Carbonate Fuel Cells", topical report prepared for U.S. DOE/METC, DOE/MC/25009-T26, October, 1991.
30. N. Maskalick, "Contaminant Effects in Solid Oxide Fuel Cells", in *Agenda and Abstracts*, Joint Contractors Meeting, Fuel Cells and Coal-Fired Heat Engines Conference, U.S. DOE/METC, August 3-5, 1993.
31. D.M. Rastler, C. Keeler, C.V. Chang, "Demonstration of a Carbonate on Coal Derived Gas", Report 15, in *An EPRI/GRI Fuel Cell Workshop on Technology Research and Development*. Stonehart Associates, Madison, CT, 1993.

32. Westinghouse Electric Corporation, Bechtel Group, Inc., "Solid Oxide Fuel Cell Repowering of Highgrove Station Unit 1, Final Report", prepared for Southern California Edison Research Center, March, 1992.
33. *Power Sources for Electric Vehicles,* Edited by B.D. McNicol and D.A.J. Rand, Elsevier Science Publishers B.V., Amsterdam, The Netherlands, 1984.
34. A.C. Lloyd (SCAQMD) and P.G. Patil (U.S. DOE), "Impact of Fuel Cells on the Transportation Sector," in the *International Fuel Cell Conference Proceedings*, NEDO/MITI, Tokyo, Japan, pgs. 13-16, 1992.

2. FUEL CELL PERFORMANCE VARIABLES

The performance of fuel cells is affected by the operating variables (e.g., temperature, pressure, gas composition, reactant utilizations, current density) and other factors (impurities, cell life) that influence the reversible cell potential and the magnitude of the irreversible voltage losses described in Section 1. Any number of operating points can be selected for application of a fuel cell in a practical system as illustrated by Figure 2-1. The curve represents the characteristics of a fuel cell once its physical design is set. Changing the operating parameters, temperature and pressure, can have either a beneficial or detrimental impact on fuel cell performance. In practice, a compromise in the operating parameters is necessary to obtain optimum fuel cell performance and acceptable cell life. Application selections result in specific system requirements being defined such as power and voltage capacities. From this and through interrelated cycle studies the power, voltage, and current requirements of the fuel cell stack and individual cells are defined. Once this is known, it is a matter of selecting a cell operating point as shown by Figure 2-1 until the system requirements are satisfied (such as lowest cost, lightest unit, highest power density, etc.). For example, a design point at high current density will allow a smaller cell size at lower capital cost to be used for the stack, but a lower system efficiency results with attendant higher operating cost. This type of operating point would be typified by a space or vehicle application where lightweight is an important driver of cost effectiveness. Cells capable of high current density operation or of light weight would be of prime interest. Operating at a lower current density, but higher voltage (higher efficiency, lower operating cost) would be more suitable for stationary power plant operation. Operating at a higher pressure will increase cell performance, lowering cost. However, there will be a higher parasitic power to compress the reactants and the cell stack, pressure vessel, and piping will have to withstand the greater pressure load. This adds cost. It is evident that the selection of the design point interacts with the system design, see Section 7. The performance parts of Sections 3 through 6 address changes in cell performance as a function of major operating conditions to allow the reader to perform parametric analysis. Supporting data will be presented as well as the derived equations which resulted from an empirical analysis. The following discussion on performance operating variables is based on the descriptions in the previous fuel cell handbooks by Benjamin et al. (1) and Kinoshita (2).

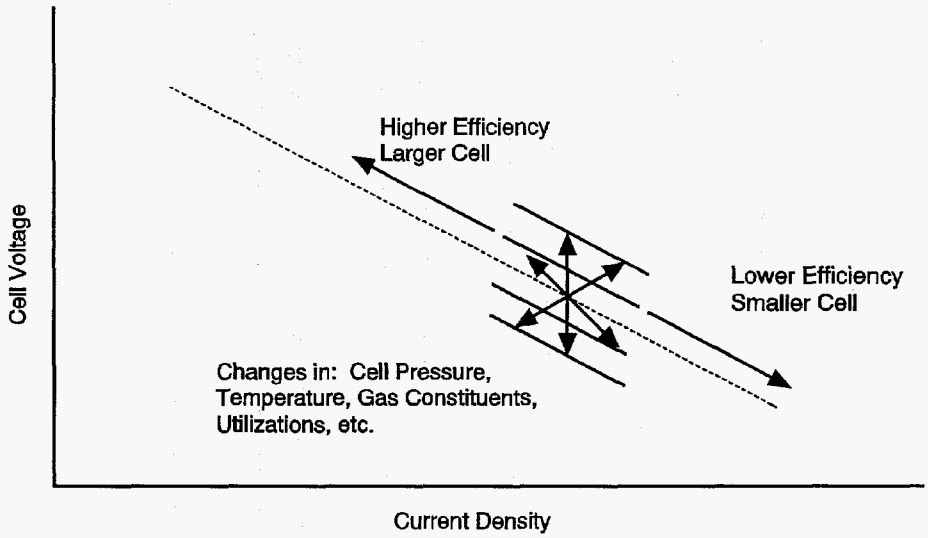

Figure 2-1 Flexibility of operating points according to cell parameters.

2.1 Temperature and Pressure

The effect of temperature and pressure on the reversible potential (E) of a fuel cell can be analyzed on the basis of changes in the Gibbs free energy with temperature and pressure. Differentiating Equation 1-4 with respect to temperature or pressure, and substituting into Equation 1-2, yields

$$\left(\frac{\partial E}{\partial T}\right)_P = \frac{\Delta S}{nF} \tag{2-1}$$

or

$$\left(\frac{\partial E}{\partial P}\right)_T = \frac{-\Delta V}{nF} \tag{2-2}$$

Because the entropy change for the H_2/O_2 reaction is negative, the reversible potential of H_2/O_2 fuel cell decreases with an increase in temperature by 0.84 mV/°C (reaction product is liquid water). For the same reaction, the volume change is negative, therefore, the reversible potential increases with an increase in pressure.

The practical effect of temperature on the voltage of fuel cells is illustrated schematically in Figure 2-2, which presents initial (i.e., early in life) performance data from typical operating cells and the dependence of the reversible potential of H_2/O_2 fuel cells on temperature (3). The cell voltages of AFCs, PEFCs, PAFCs and MCFCs show a strong dependence on temperature. The reversible potential decreases with increasing temperature, but the operating voltages of these fuel cells actually increase with an increase in operating temperature. PEFCs, however, exhibit a

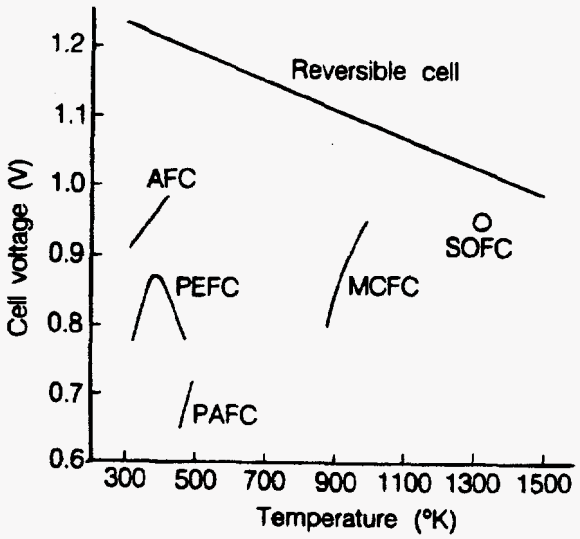

Figure 2-2 Dependence of the initial operating cell voltage of typical fuel cells on temperature. *Source*: Figure 1, p. 46) S.N. Simons, R.B. King and P.R. Prokopius, in *Symposium Proceedings Fuel Cells Technology Status and Applications*, Edited by E.H. Camara, Institute of Gas Technology, Chicago, IL, 45, 1982.

maximum in operating voltage[a] as can be seen in Figure 2-2. The operating temperature of present state-of-the-art SOFCs is limited to about 1000°C (1832°F) because the ohmic resistance of the solid electrolyte increases rapidly as the temperature decreases. Section 5 will describe efforts to develop reasonable performing SOFCs at temperatures of approximately 650°C. The other types of fuel cells typically operate at voltages considerably below the reversible cell voltage. The increase in performance is due to changes in the types of primary polarizations affecting the cell as temperature varies. An increase in the operating temperature is beneficial to fuel cell performance because of the increase in reaction rate, higher mass transfer rate, and usually lower cell resistance arising from the higher ionic conductivity of the electrolyte. In addition, the CO tolerance of electrocatalysts in low temperature fuel cells improves as the operating temperature increases. These factors all combine to reduce the polarization at higher temperatures. On the negative side, materials problems related to corrosion, electrode degradation, electrocatalyst sintering and recrystallization, and electrolyte loss by evaporation are all accelerated at higher temperatures.

An increase in operating pressure has several beneficial effects on fuel cell performance because the reactant partial pressure, gas solubility and mass transfer rates are higher. In addition, electrolyte loss by evaporation is reduced at higher operating pressures. Increased pressure also tends to increase system efficiencies. However, there are trade-offs such as thicker piping and additional expense for the compression process. Section 7 addresses system aspects of pressurization. The benefits of increased pressure must be balanced against hardware and materials problems, as well as power costs, imposed at higher operating pressure. In particular, higher pressures increase material problems in MCFCs (see Section 4.1), pressure differentials must be minimized to prevent reactant gas leakage through the electrolyte and seals, and high pressure favors carbon deposition and methane formation in the fuel gas.

---

[a] The cell voltage of PEFCs goes through a maximum as a function of temperature because of the difficulties with water management at higher temperature.

2.2 Reactant Utilization and Gas Composition

Both the reactant utilization and gas composition have a major impact on fuel cell efficiency. It is apparent from the discussion in Section 1 that fuel and oxidant gases containing a higher concentration of electrochemical reactants will produce a higher fuel cell voltage.

Utilization (U) refers to the fraction of the total fuel or oxidant introduced into a fuel cell that reacts electrochemically. In low temperature fuel cells, determining the fuel utilization is relatively straightforward when H_2 is the fuel because it is the only reactant that is involved in the electrochemical reaction,[b] i.e.,

$$U_f = \frac{H_{2,in} - H_{2,out}}{H_{2,in}} = \frac{H_{2,\text{ consumed}}}{H_{2,in}} \tag{2-3}$$

where $H_{2,in}$ and $H_{2,out}$ are the concentration of H_2 at the inlet and outlet of the fuel cell, respectively. However, hydrogen can be consumed by various other pathways, such as by chemical reaction (i.e., with O_2 and cell components) and loss via leakage out of the cell. These pathways increase the apparent utilization of hydrogen without contributing to the electrical energy produced by the fuel cell. A similar type of calculation is used to determine the oxidant utilization. For the cathode in MCFCs, two reactant gases, O_2 and CO_2, are utilized in the electrochemical reaction. The oxidant utilization should be based on the limiting reactant. Frequently O_2, which is readily available from make-up air, is present in excess and CO_2 is the limiting reactant.

A significant advantage of high temperature fuel cells such as MCFCs is their ability to use CO as a fuel. The anodic oxidation of CO in an operating MCFC is slow compared to the anodic oxidation of H_2, thus the direct oxidation of CO is not likely. However, the water gas shift reaction,

$$CO + H_2O = H_2 + CO_2 \tag{2-4}$$

reaches equilibrium rapidly in MCFCs at temperatures as low as 650°C (1200°F) to produce H_2. As H_2 is consumed, the reaction is driven to the right since both H_2O and CO_2 are produced in equal quantities in the anodic reaction. Because of the shift reaction, fuel utilization in MCFCs can exceed the value for H_2 utilization, based on the inlet H_2 concentration. For example, for a typical anode gas composition of 34% H_2/22% H_2O/13% CO/18% CO_2/12% N_2, a fuel utilization of 80% (i.e., equivalent to 110% H_2) can be achieved even though this would require 10% more H_2 (total of 37.6%) than is available in the original fuel. The high fuel utilization is possible because the shift reaction provides the necessary additional H_2 that is oxidized at the anode. In this case, the fuel utilization is given by:

$$U_f = \frac{H_{2,\text{ consumed}}}{H_{2,in} + CO_{in}} \tag{2-5}$$

where the H_2 consumed originates from the H_2 present at the fuel cell inlet ($H_{2,in}$) and any H_2 produced in the cell by the water gas shift reaction (CO_{in}).

Gas composition changes between the inlet and outlet of a fuel cell, caused by the electrochemical reaction, lead to reduced cell voltages. This voltage reduction arises because the

[b] Assumes no gas cross-over or leakage out of the cell.

cell voltage adjusts to the lowest electrode potential given by the Nernst equation for the various gas compositions at the exit of the anode and cathode chambers. Since electrodes are usually good electronic conductors and isopotential surfaces, the cell voltage may not exceed the minimum (local) value of the Nernst potential. In the case of a fuel cell with the flow of fuel and oxidant in the same direction (i.e., coflow), the minimum Nernst potential occurs at the cell outlet. When the gas flows are counterflow or crossflow, determining the location of the minimum potential is not straightforward.

The MCFC provides a good example to illustrate the influence of the extent of reactant utilization on the electrode potential. An analysis of the gas composition at the fuel cell outlet as a function of utilization at the anode (β) and cathode (γ) is presented in Appendix 9.2. The Nernst equation can be expressed in terms of the mole fraction of the gases (X_i) at the fuel cell outlet,

$$E = E^\circ + \frac{RT}{2F} \ln \frac{X_{H_2} X_{O_2}^{1/2} X_{CO_2,cathode} P^{1/2}}{X_{H_2O,anode} X_{CO_2,anode}} \qquad (2\text{-}6)$$

where P is the cell gas pressure. The second term on the right hand side of Equation 2-6, the so-called Nernst term, reflects the change in the reversible potential as a function of reactant utilization, gas composition, and pressure. Figure 2-3 illustrates the change in reversible cell potential calculated as a function of utilization using Equation 2-6. The reversible potential at 650°C (1200°F) and 1 atm pressure is plotted as a function of reactant utilization ($\beta = \gamma$) for inlet gas compositions of 80% H_2/20% CO_2 saturated with H_2O at 25°C (77°F) (fuel gas[c]) and 60% CO_2/30% O_2/10% inerts (oxidant gas); gas compositions and utilizations are listed in Table 2-1. The mole fractions of H_2 and CO in the fuel gas decrease as the utilization increases and the mole fractions of H_2O and CO_2 show the opposite trend. At the cathode the mole fractions of O_2 and CO_2 decrease with an increase in utilization because they are both consumed in the electrochemical reaction. The reversible cell potential plotted in Figure 2-3 is calculated from the equilibrium compositions for the water gas shift reaction at the cell outlet. An analysis of the data in the figure indicates that a change in the utilization from 20 to 80% will cause a decrease in the reversible potential of about 0.158 V, or roughly 0.0026 V/% utilization. These results show that MCFCs operating at high utilization will suffer a large voltage loss because of the magnitude of the Nernst term.

An analysis by Cairns and Liebhafsky (4) for a H_2/air fuel cell shows that a change in the gas composition that produces a 60 mV change in the reversible cell potential at near room temperature corresponds to a 300 mV change at 1200°C (2192°F). Thus, gas composition changes are more serious in high temperature fuel cells.

2.3 Current Density

Figure 2-4 is a depiction of the impact of current density on the performance of a fuel cell. The effects on performance of increasing current density were addressed in Section 1.3.2. That section described that activation, ohmic, and concentration losses occur as the current is changed. Figure 2-4 is a simplified depiction of how these losses affect the shape of the cell voltage-current characteristic. In summary, as current is initially drawn, sluggish kinetics (activation losses) cause

[c] Anode inlet composition is 64.5% H_2/6.4% CO_2/13% CO/16.1% H_2O after equilibration by water gas shift reaction.

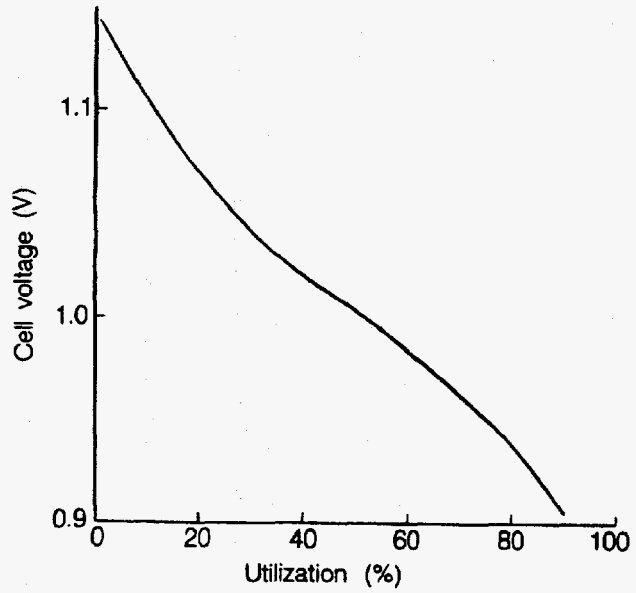

Figure 2-3 The variation in the reversible cell voltage as a function of reactant utilization (fuel and oxidant utilizations equal) in a MCFC at 650°C and 1 atm. Fuel gas: H_2/20% CO_2 saturated with H_2O at 25°C; oxidant gas: 60% CO_2/30% O_2/10% inert.

Table 2-1 Outlet Gas Composition as a Function of Utilization in MCFC at 650°C

Gas	Utilization[a] (%)				
	0	25	50	75	90
Anode[b]					
X_{H_2}	0.645	0.410	0.216	0.089	0.033
X_{CO_2}	0.064	0.139	0.262	0.375	0.436
X_{CO}	0.130	0.078	0.063	0.033	0.013
X_{H_2O}	0.161	0.378	0.458	0.502	0.519
Cathode[c]					
X_{CO_2}	0.600	0.581	0.545	0.461	0.316
X_{O_2}	0.300	0.290	0.273	0.231	0.158

[a] Same utilization for fuel and oxidant. Gas compositions are given in mole fractions.

[b] 80% H_2/20% CO_2 saturated with H_2O at 25°C. Fuel gas compositions are based on compositions for water-gas shift equilibrium.

[c] 30% O_2/60% CO_2/10% inert gas.

a decrease in cell voltage. At high current densities, there is an inability to diffuse enough reactants to the reaction sites (concentration losses) so that the cell experiences a sharp performance decrease through reactant starvation. There may also be an associated problem of diffusing the products of the cell reaction from the cell.

Ohmic losses predominate in the range of normal fuel cell operation. These losses can be expressed as iR losses where "i" is the current and "R" is the summation of internal resistances within the cell, Equation 1-18. As is readily evident from the equation, the ohmic loss is a direct function of current (current density and cell area) and thus the impact on voltage change is a linear function of current density.

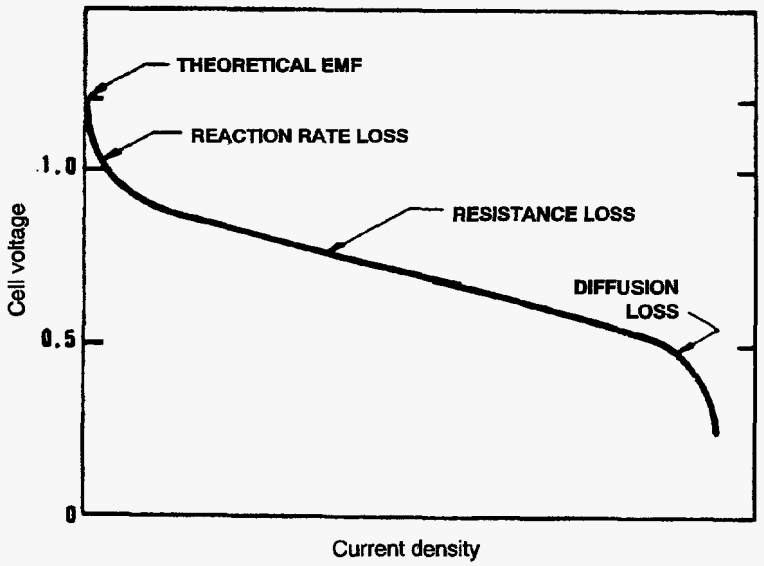

Figure 2-4 The voltage of a fuel cell decreases as the current is increased due to activation, concentration and ohmic losses.

It is interesting to observe that the resulting characteristic provides the fuel cell with a benefit compared to other energy conversion technologies. The fuel cell increases its efficiency as current is reduced from the designed, full load operating point. Other components within the fuel cell system operate at lower component efficiencies as the system's load is reduced. The combination of increased fuel cell efficiency and lower supporting component efficiencies usually results in a rather flat trace of total system efficiency as the load is reduced. Most competing energy conversion techniques experience a loss of efficiency as the design point load is reduced. This loss coupled, with the same supporting component losses of efficiency which the fuel cell system experiences, causes lower total efficiencies as the load is reduced. This gives the fuel cell system an operating cost advantage for applications where part load operation is important.

References

1. T. G. Benjamin, E. H. Camara and L. G. Marianowski, *Handbook of Fuel Cell Performance,* prepared by the Institute of Gas Technology for the U.S. Department Energy under Contract No. EC-77-C-03-1545, May 1980.

2. K. Kinoshita, F. R. McLarnon, E. J. Cairns, *Fuel Cells, A Handbook*, prepared by Lawrence Berkeley Laboratory for the U. S. Department of Energy under Contract DE-AC03-76F00098, May 1988.
3. S. N. Simons, R. B. King and P. R. Prokopius, in *Symposium Proceedings Fuel Cells Technology Status and Applications,* Edited by E. H. Camara, Institute of Gas Technology, Chicago, IL, 45, 1982.
4. E. J. Cairns and H. A. Liebhafsky, *Energy Conversion,* **9,** 63, 1969.

3. PHOSPHORIC ACID FUEL CELL

The phosphoric acid fuel cell (PAFC) is the fuel cell technology that is closest to commercialization. There are over 40 MW of demonstrators, worldwide, which have been tested, are being tested, or are being fabricated. Most of the plants are in the 50 to 200 kW capacity range, but large plants of 1 MW and 5 MW are being built. The largest plant operated to date achieved 11 MW of grid quality ac power (1, 2). Major efforts in the United States are concentrated on the development of PAFCs for stationary dispersed power plants and on-site cogeneration power plants. The major industrial participants are International Fuel Cells Corporation in the U.S. and Fuji Electric Corporation, Toshiba Corporation, and Mitsubishi Electric Corporation in Japan. In this chapter, the status of the cell components and the performance of PAFCs are discussed.

The electrochemical reactions occurring in PAFCs are:

$$H_2 \rightarrow 2H^+ + 2e^- \tag{3-1}$$

at the anode, and,

$$1/2O_2 + 2H^+ + 2e^- \rightarrow H_2O \tag{3-2}$$

at the cathode. The overall cell reaction is:

$$1/2O_2 + H_2 \rightarrow H_2O \tag{3-3}$$

The electrochemical reactions occur on highly dispersed electrocatalyst particles supported on carbon black. Platinum (Pt) or Pt alloys are used as the catalyst at both electrodes.

3.1 Cell Components

3.1.1 State-of-the-Art Components

The evolution from 1965 to the present day in the development of cell components for PAFCs is summarized in Table 3-1. In the mid-1960s, the conventional porous electrodes were polytetrafluoroethylene (PTFE)-bonded Pt black, and the loadings were about 9 mg Pt/cm^2. During the past two decades, Pt supported on carbon black has replaced Pt black in porous PTFE-bonded electrode structures as the electrocatalyst. A dramatic reduction in Pt loading has also occurred;

the loadings[a] are currently about 0.10 mg Pt/cm^2 in the anode and about 0.50 mg Pt/cm^2 in the cathode. The operating temperature, and correspondingly the acid concentration, of PAFCs has increased to achieve higher cell performance; temperatures of about 200°C (392°F) and acid concentrations of 100% H_3PO_4 are commonly used today. In addition, the operating pressure of PAFCs has surpassed 8 atm in the 11 MW electric utility demonstration plant.

Table 3-1 Evolution of Cell Component Technology for Phosphoric Acid Fuel Cells

Component	ca. 1965	ca. 1975	Current Status
Anode	• PTFE-bonded Pt black	• PTFE-bonded Pt/C	• PTFE-bonded Pt/C
		• Vulcan XC-72[a]	• Vulcan XC-72[a]
	• 9 mg/cm^2	• 0.25 mg Pt/cm^2	• 0.1 mg Pt/cm^2
Cathode	• PTFE-bonded Pt black	• PTFE-bonded Pt/C	• PTFE-bonded Pt/C
		• Vulcan XC-72[a]	• Vulcan XC-72[a]
	• 9 mg/cm^2	• 0.5 mg Pt/cm^2	• 0.5 mg Pt/cm^2
Electrode Support	• Ta mesh screen	• carbon paper	• carbon paper
Electrolyte Support	• glass fiber paper	• PTFE-bonded SiC	• PTFE-bonded SiC
Electrolyte	• 85% H_3PO_4	• 95% H_3PO_4	• 100% H_3PO_4

[a] Conductive oil furnace black, product of Cabot Corp. Typical properties: 002 d-spacing of 3.6 Å by X-ray diffusion, surface area of 220 m^2/g by nitrogen adsorption, and average particle size of 30 μm by electron microscopy.

One of the major breakthroughs in PAFC technology that occurred in the late 1960s was the development of carbon blacks and graphites for cell construction materials; these developments are reviewed by Appleby (3) and Kordesch (4). It was shown at that time that carbon black and graphite were sufficiently stable to replace the more expensive gold-plated tantalum cell hardware. The use of high surface area carbon blacks to support Pt permitted a dramatic reduction in Pt loading, without sacrificing electrode performance. It has been reported (3) that "without carbon, a reasonably inexpensive acid fuel cell would be impossible, since no other material combines the necessary properties of electronic conductivity, good corrosion resistance, low density, surface properties (especially in high area form) and, above all, low cost." However, carbon corrosion and Pt dissolution become problematic at cell voltages above ~0.8 V; consequently, low current densities with cell voltage above 0.8 and hot idle at open circuit potential are to be avoided.

[a] Assuming a cell voltage of 750 mV at 205 mA/cm^2 (approximate 11 MW design) and the current Pt loadings at the anode and cathode, ~54 g Pt is required per kilowatt of power generated.

The porous electrodes used in PAFCs are described extensively in the patent literature (5); see also the review by Kordesch (4). These electrodes contain a mixture of the electrocatalyst supported on carbon black and a polymeric binder, usually PTFE (about 30 to 50 wt%). The PTFE binds the carbon black particles together to form an integral (but porous) structure, which is supported on a porous carbon paper substrate. The carbon paper serves as a structural support for the electrocatalyst layer, as well as the current collector. A typical carbon paper used in PAFCs has an initial porosity of about 90%, which is reduced to about 60% by impregnation with 40 wt% PTFE. This wet proof carbon paper contains macropores of 3 to 50 μm diameter (median pore diameter of about 12.5 μm) and micropores with a median pore diameter of about 34 Å for gas permeability. The composite structure consisting of a carbon black/PTFE layer on carbon paper substrate forms a stable three phase interface in the fuel cell, with H_3PO_4 electrolyte on one side (electrocatalyst side) and the reactant gas environment on the other side of the carbon paper.

A bipolar plate serves to separate the individual cells and electrically connect them in series in a fuel cell stack (see Figure 1-2). In some designs, it also contains the gas channels for introducing the reactant gases to the porous electrodes and removing the products and inerts. Bipolar plates made from graphite resin mixtures that are carbonized at low temperature (~900°C/1652°F) are not suitable because of their rapid degradation in PAFC operating environments (6,7). However, the corrosion stability is improved by heat treatment to 2700°C (4892°F) (7), i.e., the corrosion current is reduced by two orders of magnitude at 0.8 V in 97% H_3PO_4 at 190°C (374°F) and 4.8 atm (70.5 psi). The all graphite bipolar plates are sufficiently corrosion resistant for a projected life of 40,000 hours in PAFCs, but they are still relatively costly to produce.

Several designs for the bipolar plate and ancillary stack components are being used by fuel cell developers, and these aspects are described in detail elsewhere (8-11). A typical PAFC stack contains cells connected in (electrical) series to obtain the practical voltage level desired for delivery to the load. In such an arrangement, individual cells are stacked with bipolar plates between the cells. The bipolar plates used in early PAFCs consisted of a single piece of graphite with gas channels machined on either side to direct the flow of fuel and oxidant gases in adjacent cells. Currently, both bipolar plates of the previous design and new designs consisting of several components are being considered. In the multi-component bipolar plates, a thin impervious plate serves to separate the reactant gases in adjacent cells in the stack, and separate porous plates with ribbed channels are used for directing gas flow. In a cell stack, the impervious plate is subdivided into two parts and each joins one of the porous plates. The porous structure, which allows rapid gas permeability, is also used for storing additional acid to replenish the supply lost by evaporation during the cell operating life.

In PAFC stacks, provisions must be included to remove the heat generated during cell operation. Heat is removed by either liquid (two phase water or a dielectric fluid) or gas (air) coolants which are routed through cooling channels located (usually about every fifth cell) in the cell stack. Liquid cooling requires complex manifolds and connections, but better heat removal is achieved than with air cooling. The advantage of gas cooling is its simplicity, reliability, and relatively low cost. The size of the cell is limited and the air cooling passages are much larger than the liquid cooling passages.

Improvements in the state-of-the-art of phosphoric acid cells are illustrated by Figure 3-1. The performance by the 10 ft^2 short stack, (f), results in a power density of nearly 310 W/cm^2.

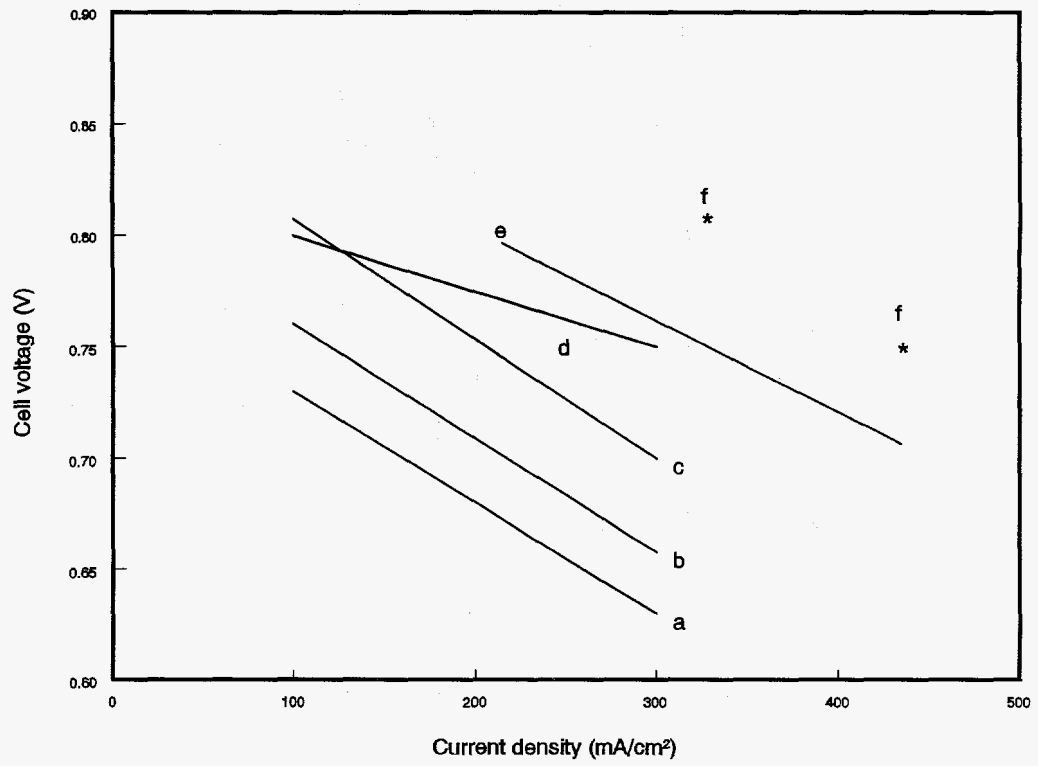

Figure 3-1 Improvement in the performance of H_2-rich fuel/air PAFCs.

(a) 1977 - 190°C, 3 atm, Pt loading of 0.75 mg/cm^2 on each electrode (12);
(b) 1981 - 190°C, 3.4 atm, cathode Pt loading of 0.5 mg/cm^2 (13);
(c) 1981 - 205°C, 6.3 atm, cathode Pt loading of 0.5 mg/cm^2 (13);
(d) 1984 - 205°C, 8 atm, electrocatalyst loading was not specified (14);
(e) 1992 - 205°C, 8 atm, 10 ft^2 short stack, 200 hrs, electrocatalyst loading not specified (15)
(f) 1992 - 205°C, 8 atm, subscale cells, electrocatalyst loading not specified (15)

3.1.2 Development Components

Phosphoric acid electrode/electrolyte technology has reached a level of maturity where developers and users commit resources to commercial capacity, multi-unit demonstrations and preprototype installations. Cell components are being manufactured at scale and in large quantities with confidence of meeting predicted performance. However, for the technology to achieve economic competitiveness with other energy technologies there is a need to further increase the power density of the cells, improve cell life, and reduce costs (16, 17), all of which are interrelated. Fuel cell developers continue to address these issues. A thorough description of development components is beyond the scope of this handbook. The interested reader is referred to full texts

such as the Fuel Cell Handbook (11) which provides a description of many research activities and is well referenced. However, a review of selected major works in progress will provide an indication of the developers' most recent and important quests to make PAFC successfully compete in future energy markets.

In 1992, the International Fuel Cells Corporation completed a government sponsored advanced water-cooled PAFC development project to improve the performance and lower the cost of their atmospheric and pressurized technology for on-site and utility applications (15). The project focused on five major activities: 1) produce a conceptual design of a large stack with a goal of 175 WSF (0.188 W/cm^2), 40,000 hour useful life, and a stack cost of less than $400/kW, 2) test pressurized Configuration "B" single cells developed in a previous program, but improved with proprietary design advances in substrates, electrolyte reservoir plates, catalysts, seals, and electrolyte matrix to demonstrate the 175 WSF (0.188 W/CM^2) power density goal, 3) test a pressurized short stack with subscale size, improved component cells and additional improvements in the integral separators and coolers to confirm the stack design, 4) test a pressurized short stack of improved full size cell components, nominal 10 ft^2 size (approximately 0.93 m^2), to demonstrate the 175 WSF (0.188 W/cm^2) power density goal, and 5) test an advanced atmospheric "on-site" power unit stack with the improved components.

A conceptual design of an improved technology stack operating at 120 psi (8.2 atm) and 405° F (207° C) was produced based on cell and stack development and tests. The stack would be composed of 355 10 ft^2 (approximately 1 m^2) cells and produce over 1 MW dc power in the same physical envelope as the 670 kW stack used in the 11 MW PAFC plant built for Tokyo Electric Power. The improvements made to the design were tested in single cells, and in subscale and full size short stacks. Table 3-2 summarizes the results. Single cells achieved an initial performance of 0.75 volts/cell at a current density of 400 ASF (431 mA/cm^2), 8.2 atm and 207° C condition which was 300 WSF (0.323 W/cm^2), well above the project goal. Several cells were operated to 600 ASF (645 mA/cm^2), achieving up to 0.66 volts/cell. The flat plate component designs were verified in a subscale stack prior to fabricating the full size short stack. The pressurized short stack of 10 ft^2 cells achieved a performance of 285 WSF (0.307 W/cm^2). Although the average cell performance, 0.71 volts/cell at 400 ASF (431 mA/cm^2) was not as high as the single cell tests, the performance was 65 percent over the project goal. Figure 3-2 presents single cell and stack performance data for pressurized operation. The stack was tested for over 3,000 hours. For reference purposes, Tokyo Electric Power Company's 11 MW power plant, operational in 1991, had an average cell performance of approximately 0.75 volts/cell at 190 mA/cm^2 or 0.142 W/cm^2 (18).

The atmospheric pressure on-site short stack consisting of 32 cells obtained an initial performance of 0.65 volts/cell at 200 ASF (215 mA/cm^2) or 0.139 W/cm^2. The performance degradation rate was less than 4 mV/1,000 hours during the 4,500 hour test. Single cells tested at atmospheric conditions achieved a 500 hour performance of approximately 0.75 volts/cell at 225 ASF (242 mA/cm^2) or 0.182 W/cm^2. The results from this program represent the highest performance of full size phosphoric acid cells and short stacks published to date.

Mitsubishi Electric Corporation is investigating alloyed catalysts, processes to produce thinner electrolytes, and increases in utilization of the catalyst layer (19). These improvements have resulted in an initial atmospheric performance of 0.65 mV at 300 mA/cm^2 or 0.195 W/cm^2 which is higher than the IFC performance mentioned above (presented in Table 3-2 for comparison). Note that this performance was obtained on small 100 cm^2 cells and has yet to be demonstrated with full-scale cells in stacks. Approaches to increase life are to use series fuel gas flow in the stack to

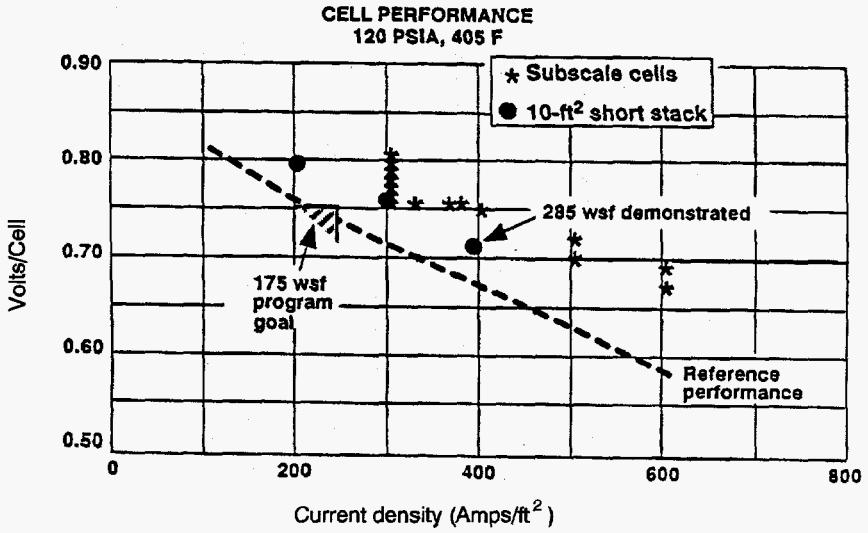

Figure 3-2 Advanced water-cooled PAFC performance.
Source: Reference 15.

alleviate corrosive conditions, provide well-balanced micro-pore size reservoirs to avoid electrolyte flooding, and use a high corrosion resistant carbon support for the cathode catalyst. These improvements have resulted in the lowest PAFC degradation rate publicly acknowledged, 2 mV/1,000 hours for 10,000 hours at 200 to 250 mA/cm^2 in a short stack with 3,600 cm^2 area cells.

Table 3-2 Advanced PAFC Performance

	Average Cell Voltage, V	Current Density mA/cm^2	Power Density W/cm^2
IFC Pressurized			
Project Goal			0.188
Single Cells	0.75	431	0.323
	to 0.66	645	
Full Size Short Stack	0.71	431	0.307
11 MW Reference	0.75	190	0.142
IFC Atmospheric			
Single Cells	0.75	242	0.182
Full Size Short Stack	0.65	215	0.139
Mitsubishi Electric Atmospheric			
Single Cells	0.65	300	0.195

Several important technology development efforts for which details have been published are catalysts improvements, advanced gas diffusion electrode development, and tests on materials which offer better carbon corrosion protection. The following text summarizes this work.

Transition metal (e.g., iron, cobalt) organic macrocycles[b] from the families of tetramethoxypheylporphyrins (TMPP), phthalocyanines (PC), tetraazaannulenes (TAA) and tetraphenylporphyrins (TPP) have been evaluated as O_2-reduction electrocatalysts in PAFCs. One major problem with these organic macrocycles is their limited chemical stability in hot concentrated phosphoric acid. However, after heat treatment of the organic macrocycle (i.e., CoTAA, CoPC, CoTMPP, FePC, FeTMPP) on carbon at about 500 to 800° C (932 to 1472° F), the pyrolyzed residue exhibits electrocatalytic activity, which in some instances is comparable to that of Pt, and has promising stability, at least up to about 100° C (212° F) (20). Another approach that has been successful for enhancing the electrocatalysis of O_2 reduction is to alloy Pt with transition metals such as Ti (21), Cr (22), V (23), Zr (23) and Ta (23). The enhancement in electrocatalytic activity has been explained by a correlation between the optimum nearest-neighbor distance of the elements in the alloy and the bond length in O_2 (24).

Conventional cathode catalysts comprise either platinum or platinum alloys supported on conducting carbon black at 10 wt% platinum. Present platinum loadings on the anode and cathode are 0.1 mg/cm^2 and 0.5 mg/cm^2, respectively (11, 15). It has been suggested by Ito et. al. that the amount of platinum may have been reduced to the extent that it might be cost effective to increase the amount of platinum loading on the cathode (25). However, a problem exists in that fuel cell stack developers have not experienced satisfactory performance improvements when increasing the platinum loading. Johnson Matthey Technology Centre (J-M) recently presented data which resulted in a performance improvement nearly in direct proportion to that expected based on the increase in platinum (26). Initial tests by J-M confirmed previous results that using platinum alloy catalysts, with a 10 wt% net platinum loading produces an improvement in performance. Platinum/nickel alloyed catalysts yielded a 49 wt% increase in specific activity over pure platinum. This translates into a 39 mV improvement in the air electrode performance at 200 mA/cm^2.

Johnson Matthey then determined that the platinum loading in the alloyed catalyst could be increased up to 30 wt% while retaining the same amount of platinum without any decrease in specific activity or performance. Note, that the amount of nickel, hence the total amount of alloyed catalyst, decreased. Next, J-M researchers increased the amount of platinum from 10 to 30 wt% while keeping the same amount of nickel catalyst loading. The total amount of alloyed catalyst increased in this case. Results showed an additional 36 wt% increase in specific activity which provided another 41 mV increase at 200 mA/cm^2. The ideal voltage increase would be 46 mV for this increase in platinum. Thus, the performance increase obtained experimentally was nearly in direct proportion to the theoretical amount expected. The type of carbon support did not seem to be a major factor based on using several typical supports during the tests.

The anode of a phosphoric acid fuel cell is sensitive to catalytic poisoning by even low amounts of contaminants. Yet, hydrogen-rich fuel gases, other than pure hydrogen, are produced with contaminants levels well in excess of the anode's tolerance limit. Of particular concern are CO, COS, and H_2S. The fuel stream in a current practice PAFC anode, operating at approximately 200° C (392° F), must contain 2 vol % or less of CO (11), less than 50 ppmv of COS plus H_2S, or less than 20 ppmv of H_2S (27). Current practice is to place COS and H_2S cleanup systems and CO shift converters prior to the cell to reduce the fuel stream contaminant levels to the required amounts. Giner, Inc. has performed experimental work to develop a contaminant tolerant anode

[b] See Reference 20 for literature survey.

catalyst with the purpose of reducing or eliminating the cleanup equipment (28). An anode catalyst, G87A-17-2, was identified which resulted in only a 24 mV loss from reference when exposed to a 75% H_2, 1% CO, 24% CO_2, 80 ppm H_2S gas mixture at 190°C (374°F), 85% fuel utilization, and 200 mA/cm^2. A baseline anode experienced a 36 mV loss from the reference at the same conditions. At 9.2 atm (120 psi) pressurization, the anode loss was only 19 mV at 190°C (374°F) and 17 mV at 210°C (410°F) (compared with pure H_2) with a gas of 71% H_2, 5% CO, 24% CO_2, and 200 ppm H_2S. Economic studies comparing the loss of the cell performance with the savings in cost of selected plant components showed no increase when the new anode catalyst was used with gas containing 1% CO/200 ppm H_2S. A $7/kW increase resulted with the 5% CO gas (compared to a 1% CO gas) at a 50 MW size. Some savings would result with the elimination of the low temperature shift converter. The real value for the catalyst may be its ability to tolerate excessive CO and H_2S concentrations during upsets and to simplify the system by the elimination of equipment.

As previously mentioned, state-of-the-art gas diffusion electrodes are configured to provide an electrolyte network and a gas network formed with the mixture of carbon black and PTFE. In the electrodes, carbon black agglomerates consisting of small primary particles, 0.02-0.04 μm, are mixed with much larger PTFE particles, ca. 0.3 μm. The carbon black surface may not be covered completely by the PTFE, due to the large size of conventional PTFE particles. The space in the agglomerates or that between the agglomerates and PTFE may act as gas networks at the initial stage of operation, but fill with electrolyte eventually because of the small contact angle of carbon black, uncovered with PTFE, to electrolyte ($<90°$), resulting in the degradation of cell performance. Attempts to solve this flooding problem by increasing the PTFE content have not been successful because of the offset of the performance resulting from the reduction of catalyst utilization. Higher performance and longer lifetime of electrodes are intrinsically at odds and there is a limitation of the improvement of the performance over life by the optimization of PTFE content in the current practice electrode structures. Watanabe et al. (29) have proposed a preparation method of an electrode working at 100% utilization of catalyst clusters, where the functions of gas diffusion electrodes are allotted completely to a hydrophilic, catalyzed carbon black and a wet-proofed carbon black. The former works as a fine electrolyte network and the latter works as a gas supplying network in a reaction layer. Higher utilization of catalyst clusters and longer life at the reaction layer are expected compared to state-of-the-art electrodes consisting of the uniform mixture of catalyzed carbon black and PTFE particles. The iR free electrode potentials for the reduction of oxygen and air at 200 mA/cm^2 on the advanced electrode are 10 mV higher than those of the conventional electrode.

As mentioned above, there is a trade-off between high power density and cell life performance. One of the major causes of declining cell performance over its life is that electrode flooding and drying, caused by the migration of phosphoric acid between the matrix and the electrodes, occurs during cell load cycling. Researchers at Fuji Electric have addressed two approaches to improve cell life performance while keeping power density high (30). In one, the wettability of the cathode and anode were optimized, and in the other a heat treatment was applied to the carbon support for the cathode catalyst. During tests, it was observed that a cell with a low cathode wettability and a high anode wettability was over 50 mV higher than a cell with the reverse wetting conditions after 40 start-stop cycles.

The use of carbon blacks with large surface areas to improve platinum dispersion on supports has been investigated as one way to increase the power density of a cell (31). However, some large surface area carbon blacks are fairly corrosive in hot potassium acid, resulting in a loss of catalytic activity. The corrosivity of the carbon support for a cathode catalyst affects both the rate of loss and of electrode flooding and, in turn, the life performance of a cell. Furnace black has been heat

treated at high temperatures by Fuji Electric to increase its resistance to corrosion. It was found that corrosivity can be increased and cell life performance improved by heat treating carbon supports at high temperatures, at least to around 3,000°C (5,432°F).

3.2 Performance

Cell performance for any fuel cell is a function of pressure, temperature, reactant gas composition and utilization. In addition, performance can be adversely affected by impurities in both the fuel and oxidant gases.

The sources of polarization in PAFCs (with cathode and anode Pt loadings of 0.5 mg Pt/cm^2, 180°C, 1 atm, 100% H_3PO_4) have been discussed in Section 2 and are illustrated as half cell performances in Figure 1-4. From Figure 1-4, it is clear that the major polarization occurs at the cathode, and furthermore, the polarization is greater with air (560 mV at 300 mA/cm^2) than with pure oxygen (480 mV at 300 mA/cm^2) because of dilution of the reactant. The anode exhibits very low polarization (~4 mV/100 mA/cm^2) on pure H_2, which increases when CO is present in the fuel gas. The ohmic (iR) loss in PAFCs is also relatively small, amounting to about 12 mV/100 mA/cm^2.

Typical PAFC's will generally operate in the range of 100 to 400 mA/cm^2 at 600 to 800 mV/cell. Voltage and power constraints arise from the increased corrosion of platinum and carbon components at cell potentials above approximately 800 mV.

3.2.1 Effect of Pressure

It is well known that an increase in the cell operating pressure enhances the performance of PAFCs (13, 32, 33). The theoretical change in voltage (ΔV_P) as a function of pressure (P) is expressed as,

$$\Delta V_P(mV) = \frac{3(2.3RT)}{2F} \log \frac{P_2}{P_1} \qquad (3\text{-}4)$$

where $\frac{3(2.3RT)}{2F}$ = 138 mV at 190°C (374°F). Experimental data (34) reported that the effect of pressure on cell performance at 190°C (374°F) and 323 mA/cm^2 is correlated by the equation:

$$\Delta V_P\ (mV) = 146 \log \frac{P_2}{P_1} \qquad (3\text{-}5)$$

where P_1 and P_2 are different cell pressures. The experimental data (34) also suggests that Equation 3-5 is a reasonable approximation for a temperature range of 177°C ≤ T ≤ 218°C (351°F ≤ T≤ 424°F) and a pressure range of 1 atm ≤ P ≤ 10 atm (14.7 psi ≤ P ≤ 147.0 psi). Data from Appleby (13) in Figure 3-1 indicate that the voltage gain observed by increasing the pressure from 3.4 atm (190°C) to 6.3 atm (205°C) is about 44 mV. According to Equation 3-5, the voltage gain calculated for this increase in pressure at 190° (374°F) is 39 mV[c] which is in reasonable agreement

[c] The difference in temperature between 190 and 205°C is disregarded so Equation 3-5 is assumed to be valid at both temperatures.

with experimental data in Figure 3-1. Measurements (32) of ΔV_P for an increase in pressure from 4.7 to 9.2 atm (69.1 to 135.2 psia) in a cell at 190° (374°F) show that ΔV_P is a function of current density, increasing from 35 mV at 100 mA/cm^2 to 42 mV at 400 mA/cm^2 (50% O_2 utilization with air oxidant, 85% H_2 utilization with pure H_2 fuel). From Equation 3-4, ΔV_p is 43 mV for an increase in pressure from 4.7 to 9.2 atm (69.1 to 135.2 psia) at 190° (374°F), which is very close to the experimental value obtained at 400 mA/cm^2. Other measurements (35) for the same increase in pressure from 4.7 to 9.2 atm (69.1 to 135.2 psia), but at a temperature of 210°C (410°F) show less agreement between the experimental data and Equation 3-4.

The improvement in cell performance at higher pressure and high current density can be attributed to a lower diffusion polarization at the cathode and an increase in the reversible cell potential. In addition, pressurization also decreases activation polarization at the cathode due to the increased oxygen and water partial pressures. If the partial pressure of water is allowed to increase, a lower acid concentration will result. This will increase ionic conductivity and bring about a higher exchange current density. The net outcome is a reduction in ohmic losses. It was reported (32) that an increase in pressure of a cell (100% H_3PO_4, 169°C (336°F) from 1 to 4.4 atm (14.7 to 64.7 psia) produces a reduction in acid concentration to 97%, and a decrease of about 0.001 ohm in the resistance of a small six cell stack (350 cm^2 electrode area).

3.2.2 Effect of Temperature

Figure 1-3 shows that the reversible cell potential for PAFCs consuming H_2 and O_2 decreases as the temperature increases by 0.27 mV/°C under standard conditions (product is water vapor). However, as discussed in Section 2, an increase in temperature has a beneficial effect on cell performance because activation polarization, mass transfer polarization and ohmic losses are reduced.

The kinetics for the reduction of oxygen on Pt improves[d] as the cell temperature increases. At a mid-range operating load (~250 mA/cm^2) load, the voltage gain (ΔV_T) with increasing temperature of pure H_2 and air is given by:

$$\Delta V_T \text{ (mV)} = 1.15 \, (T_2 - T_1) \, (°C) \qquad (3\text{-}6)$$

Data suggests that Equation 3-6 is reasonably valid for a temperature range of 180°C ≤ T ≤ 250°C (356°F ≤ T ≤ 482°F). It is apparent from this equation that each degree increase in cell temperature should produce a performance increase of 1.15 mV. Other data indicates that the coefficient for Equation 3-6 may be in the range of 0.55 to 0.75, rather than 1.15. Although temperature has only a minimal effect on the H_2 oxidation reaction at the anode, it is important in terms of anode poisoning. Figure 3-3 shows that increasing the cell temperature results in increased anode tolerance to CO poisoning. This increased tolerance is a result of reduced CO adsorption. A strong temperature effect is also seen for simulated coal gas (SCG in Fig. 3-3). Below 200°C (392°F) the cell voltage drop is significant. Experimental data suggests that the effect of contaminants is not additive, indicating that there is an interaction between CO and H_2S (36). Increasing temperature increases performance, but an elevated temperature also increases catalyst sintering, component corrosion and electrolyte degradation, evaporation and concentration.

[d] The anode shows no significant performance improvement from 140 to 180°C on pure H_2, but in the presence of CO, increasing the temperature results in a marked improvement in performance (see discussion in Section 3.2.4).

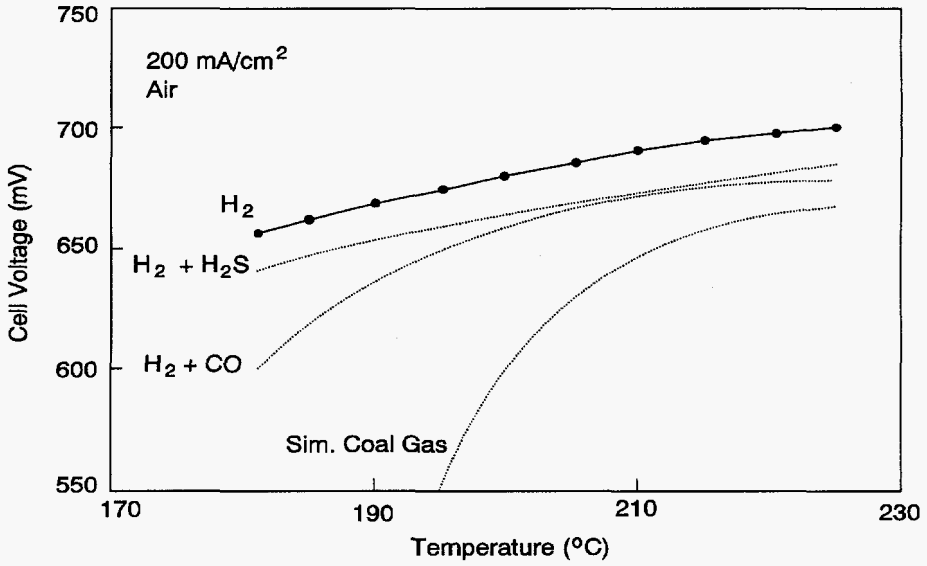

Figure 3-3 Effect of temperature: Ultra-high surface area Pt catalyst. Fuel: H_2, H_2 + 200 ppm H_2S and simulated coal gas.
Source: Ref. V. Jalan, J. Poirier, M. Desai, B. Morrisean, "Development of CO and H_2S Tolerant PAFC Anode Catalysts", Proceedings of the Second Annual Fuel Cell Contractors Review Meeting, 1990.

3.2.3 Effect of Reactant Gas Composition and Utilization

Increasing reactant gas utilization or decreasing inlet concentration results in decreased cell performance due to increased concentration polarization and Nernst losses. These effects are related to the partial pressures of reactant gases and are considered below.

Oxidant: The oxidant composition and utilization are parameters that affect the cathode performance, as evident in Figure 1-4. Air, which contains ~21% O_2, is the oxidant of choice for PAFCs. The use of air with ~21% O_2 instead of pure O_2 results in a decrease in the current density of about a factor of three at constant electrode potential. The polarization at the cathode increases with an increase in O_2 utilization. Experimental measurements (37) of the change of overpotential ($\Delta\eta_c$) at a PTFE-bonded porous electrode in 100% H_3PO_4 (191°C, atmospheric pressure) as a function of O_2 utilization is plotted in Figure 3-5 in accordance with Equation 3-7:

$$\Delta\eta_c = \eta_c \, \eta_{c,\infty} \tag{3-7}$$

where η_c and $\eta_{c,\infty}$ are the cathode polarizations at finite and infinite (i.e., high flow rate, close to 0% utilization) flow rates, respectively. The additional polarization that is attributed to O_2 utilization is reflected in the results, and the magnitude of this loss increases rapidly as the utilization increases. At a nominal O_2 utilization of 50% for prototype PAFC power plants, the additional polarization estimated from the results in Figure 3-4 is 19 mV. Based on experimental data (15, 37, 38), the voltage loss due to a change in oxidant utilization can be described by Equations 3-8 and 3-9:

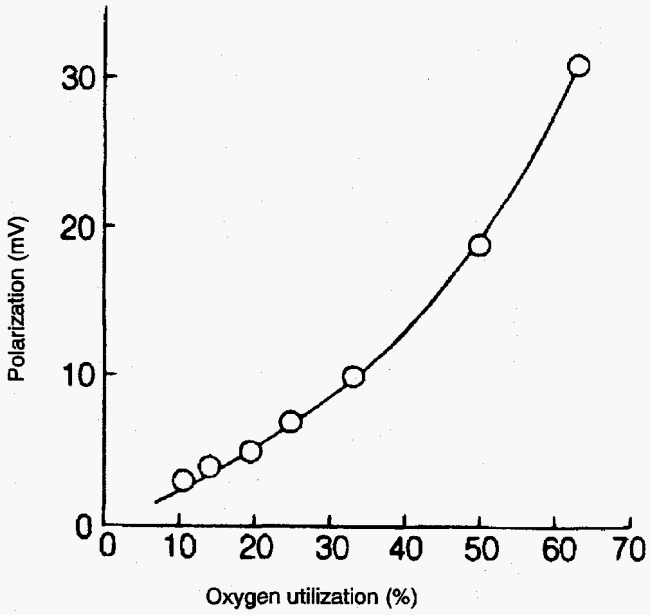

Figure 3-4 Polarization at cathode (0.52 mg Pt/cm^2) as a function of O_2 utilization, which is increased by decreasing the flow rate of the oxidant at atmospheric pressure. 100% H_3PO_4, 191°C, 300 mA/cm^2, 1 atm.
Source: Data taken from Table 5, Reference 37, Lu and France, 1982.

$$\Delta V_{Cathode}(mV) = 148 \log \frac{(\bar{P}_{02})_2}{(\bar{P}_{02})_1} \quad 0.04 \leq \frac{\bar{P}_{02}}{\bar{P}_{Total}} \leq 0.20 \tag{3-8}$$

$$\Delta V_{Cathode}(mV) = 96 \log \frac{(\bar{P}_{02})_2}{(\bar{P}_{02})_1} \quad 0.20 < \frac{\bar{P}_{02}}{\bar{P}_{Total}} < 1.00 \tag{3-9}$$

$\bar{P}_{02}$ is the average partial pressure of O_2 in the system. Using two equations provides a more accurate correlation to actual fuel cell operation. Equation (3-8) will generally be used for fuel cells using air as the oxidant and Equation 3-9 for fuel cells using an O_2-enriched oxidant.

Fuel: Hydrogen for PAFC power plants will typically be derived by conversion of a wide variety of primary fuels such as CH_4 (e.g., natural gas), petroleum products (e.g., naphtha), coal liquids (e.g., CH_3OH) or coal gases. Besides H_2, CO and CO_2 are also produced during conversion of these fuels (unreacted hydrocarbons are also present). These reformed fuels contain low levels of CO (after steam reforming and shift conversion reactions in the fuel processor) which cause anode poisoning in PAFCs. The CO_2 and unreacted hydrocarbons (e.g., CH_4) are electrochemically inert and act as diluents. Because the anode reaction is nearly reversible, the fuel composition and hydrogen utilization generally do not strongly influence cell performance. The voltage change due to a change in the partial pressure of hydrogen (which can result from a change in either the fuel composition or utilization) can be described by Equation 3-10 (15, 35, 36):

$$\Delta V_{Anode}(mV) = 55 \log \frac{(\bar{P}_{H2})_2}{(\bar{P}_{H2})_1} \quad (3\text{-}10)$$

where $\bar{P}_{H_2}$ is the average partial pressure of H_2 in the system. At 190°C (374°F), the presence of 10% CO_2 in H_2 should cause a voltage loss of about 2 mV. Thus, diluents in low concentrations are not expected to have a major effect on electrode performance; however, relative to the total anode polarization (i.e., 3 mV/100 mA/cm^2), the effects are large. It has been reported (15) that with pure H_2, the cell voltage at 215 mA/cm^2 remains nearly constant at H_2 utilizations up to 90%, and then it decreases sharply at H_2 utilizations above this value.

Low utilizations, particularly oxygen utilization, yields high performance. Low utilizations, however, result in poor fuel use. Optimization of this parameter is required. State-of-the-art utilizations used are on the order of 85% and 50% for the fuel and oxidant respectively.

3.2.4 Effect of Impurities

The concentration level of impurities entering the PAFC is very low relative to that of diluents or reactant gases, but their impact on the performance is significant. Some impurities (e.g., sulfur compounds) originate from the fuel gas entering the fuel processor and are carried into the fuel cell with the reformed fuel, whereas others (e.g., CO) are produced in the fuel processor.

Carbon Monoxide: The presence of CO in a H_2-rich fuel has a significant effect on the anode performance because CO poisons the electrocatalytic activity of Pt electrodes. The poisoning of Pt by CO is reported to arise from the dual site replacement of one H_2 molecule by two CO molecules on the Pt surface (39, 40). According to this model, the anodic oxidation current at a fixed overpotential, with (i_{CO}) and without (i_{H_2}) CO present, is given as a function of CO coverage (θ_{CO}) by Equation 3-11:

$$\frac{i_{CO}}{i_{H_2}} = (1 - \theta_{CO})^2 \quad (3\text{-}11)$$

For $[CO]/[H_2] = 0.025$, $\theta_{CO} = 0.31$ at 190°C (34), therefore, i_{CO} is about 50% of I_{H_2}.

As was discussed previously, both temperature and CO concentration have a major influence on the oxidation of H_2 on Pt in CO containing fuel gases. Benjamin et al. (34) derived Equation 3-12 for the voltage loss resulting from CO poisoning as a function of temperature.

$$\Delta V_{CO} = k(T) ([CO]_2 - [CO]_1) \quad (3\text{-}12)$$

Where k(T) is a constant that is a function of temperature and $[CO]_1$ and $[CO]_2$ are the percent CO in the fuel gas. The values of k(T) at various temperatures are listed in Table 3-3 (34). Using Equation 3-12 and the data in Table 3-3, it is apparent that for a given change in CO content, ΔV_{CO} is about 8.5 times larger at 163°C (325°F) than at 218°C (424°F). The correlation provided by Equation 3-12 was obtained at 269 mA/cm^2, thus, its use at significantly different current densities may not be appropriate. In addition, other more recent data (36) suggests a value for k(T) of -2.12 at a temperature of 190°C (374°F) rather than -3.54.

Table 3-3 Dependence of k(T) on Temperature

T (°C)	T (°F)	k(T)[a] (mV/%)
163	325	-11.1
177	351	-6.14
190	374	-3.54
204	399	-2.05
218	424	-1.30

[a] Based on electrode with 0.35 mg Pt/cm^2, and at 269 mA/cm^2.
Source: T.G. Benjamin, E.H. Camara and L.G. Marianowski, *Handbook of Fuel Cell Performance*, prepared by the Institute of Gas Technology for the United States Department of Energy under Contract No. EC-77-C-03-1545, 40, May 1980.

The data in Figure 3-5 illustrate the influence of H_2 partial pressure and CO content on the performance of Pt anodes (10% Pt supported on Vulcan XC-72, 0.5 mg Pt/cm^2) in 100% H_3PO_4 at 180°C (356°F) (10). Diluting the H_2 fuel gas with 30% CO_2 produces an additional polarization of about 11 mV at 300 mA/cm^2. The results show that the anode polarization with fuel gases of composition 70% H_2/(30-x)% CO_2/x% CO (x = 0, 0.3, 1, 3 and 5) increases considerably as the CO content increases to 5%.

Sulfur Containing Compounds: Hydrogen sulfide and carbonyl sulfide (COS) are impurities[e] in fuel gases from fuel processors and coal gasifiers in PAFC power plants. The concentration levels of H_2S in an operating PAFC (190 to 210°C (374 to 410°F), 9.2 atm (120 psig), 80% H_2 utilization <325 mA/cm^2) that can be tolerated by Pt anodes without suffering a destructive loss in performance are <50 ppm (H_2S + COS) or <20 ppm (H_2S) (41), and rapid cell failure occurs with fuel gas containing more than 50 ppm H_2S. Sulfur poisoning does not affect the cathode, and poisoned anodes can be re-activated by polarization at high potentials (i.e., operating cathode potentials). As was mentioned previously, there is a synergistic effect between H_2S and CO that can negatively impact cell performance. Figure 3-6 (36) shows the effect of H_2S concentration on ΔV with and without 10% CO present in H_2. The ΔV is referenced to performance on pure H_2 in the case of H_2S alone and to performance on H_2 with 10% CO for H_2S and CO. In both cases, at higher H_2S concentrations, the ΔV rises abruptly. This drop in performance occurs above 240 ppm for H_2S alone and above 160 ppm for H_2S with 10% CO.

Experimental studies by Chin and Howard (42) indicate that H_2S adsorbs on Pt and blocks the active sites for H_2 oxidation. The following electrochemical reactions, Equations 3-13, 3-14, 3-15 involving H_2S are postulated to occur on Pt electrodes:

$$Pt + HS^- \rightarrow Pt\text{-}HS_{ads} + e^- \quad (3\text{-}13)$$

$$Pt\text{-}H_2S_{ads} \rightarrow Pt\text{-}HS_{ads} + H^+ + e^- \quad (3\text{-}14)$$

and, $$Pt\text{-}HS_{ads} \rightarrow Pt\text{-}S_{ads} + H^+ + e^- \quad (3\text{-}15)$$

[e] Anode gases from coal gasifiers may contain total sulfur of 100 to 200 ppm.

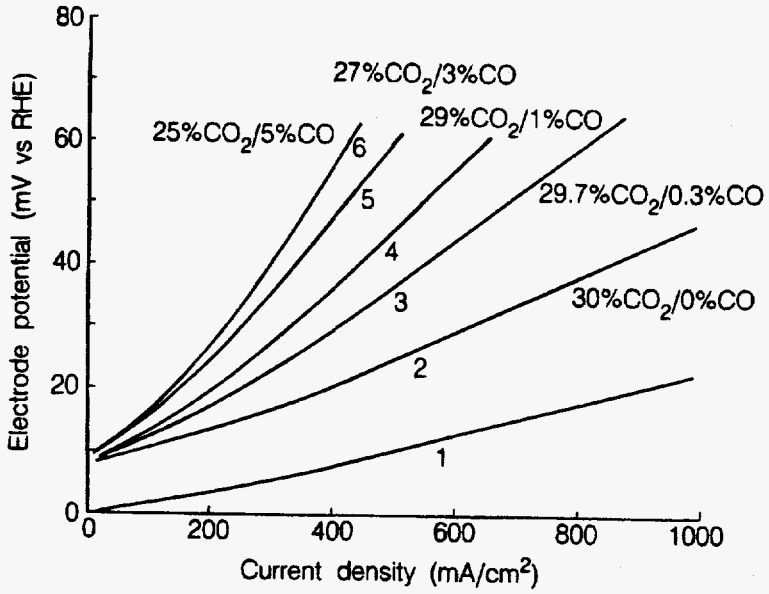

Figure 3-5 Influence of CO and fuel gas composition on the performance of Pt anodes in 100% H_3PO_4 at 180°C. 10% Pt supported on Vulcan XC-72, 0.5 mg Pt/cm^2. Dew point, 57°C. Curve 1, 100% H_2; Curves 2-6, 70% H_2 and CO_2/CO contents (mol%) specified. *Source*: (Page A-16) J.A.S. Bett, H.R. Kunz, S.W. Smith, and L.L. Van Dine, "Investigation of Alloy Catalysts and Redox Catalysts for Phosphoric Acid Electrochemical Systems," FCR-7157F, prepared by International Fuel Cells under Contract No. 9-X13-D6271-1 for Los Alamos National Laboratory, 1985.

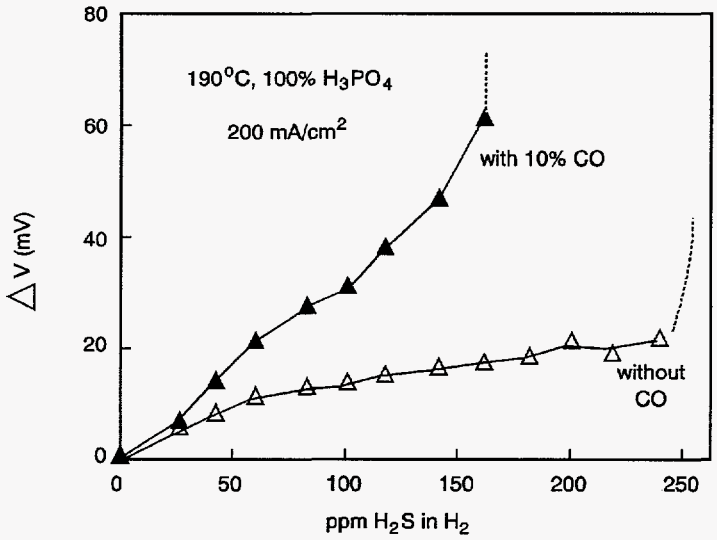

Figure 3-6 Effect of H_2S concentration: Ultra-high surface area Pt catalyst.
Source: V. Jalan, J. Poirier, M. Desai, B. Morrison, "Development of CO and H_2S Tolerant PAFC Anode Catalyst," Proceedings of the Second Annual Fuel Cell Contractors Review Meeting, 1990.

Elemental sulfur (see Equation 3-15) is only expected on Pt electrodes at high anodic potentials, and at sufficiently high potentials, sulfur is oxidized to SO_2. The extent of poisoning by H_2S increases with increasing H_2S concentration, electrode potential and exposure time. H_2S poisoning, however, decreases with increasing cell temperature.

Other Compounds: The effect of other compounds such as those containing nitrogen on PAFC performance has been adequately reviewed by Benjamin et al. (34). Molecular nitrogen acts as a diluent but other nitrogen compounds (e.g., NH_3, HCN, NO_X) may not be as innocuous. NH_3 in the fuel or oxidant gases reacts with H_3PO_4 to form a phosphate salt. $(NH_4)H_2PO_4$,

$$H_3PO_4 + NH_3 \rightarrow (NH_4)H_2PO_4 \qquad (3\text{-}16)$$

which results in a decrease in the rate of O_2 reduction. A concentration of less than 0.2 mol% $(NH_4)H_2PO_4$ must be maintained to avoid unacceptable performance losses (43). The effect of HCN and NO_X on fuel cell performance has not been clearly established.

3.2.5 Effects of Current Density

The voltage which can be obtained from a PAFC is reduced by ohmic, activation, and concentration losses which increase with increasing current density. The magnitude of this loss can be approximated by the following equations:

$$\Delta V_J\ (mV) = -0.53\ \Delta J \qquad \text{for } J = 100 - 200\ mA/cm^2 \qquad (3\text{-}18)$$
$$\Delta V_J\ (mV) = -0.39\ \Delta J \qquad \text{for } J = 200 - 650\ mA/cm^2 \qquad (3\text{-}19)$$

The coefficients in these equations have been derived from performance data for cells operating at 120 psia (8.2 atm), 405°F (207°F) (15), with fuel and oxidant utilizations of 85% and 70% respectively[f], an air fed cathode, and an anode inlet composition of 75% H_2, and 0.5% CO^2. Similarly, at atmospheric conditions, the magnitude of this loss can be approximated by:

$$\Delta V_J\ (mV) = -0.74\ \Delta J \qquad \text{for } J = 50 - 120\ mA/cm^2 \qquad (3\text{-}20)$$
$$\Delta V_J\ (mV) = -0.45\ \Delta J \qquad \text{for } J = 120 - 215\ mA/cm^2 \qquad (3\text{-}21)$$

The coefficients in the atmospheric condition equations have been derived from performance data for cells (44) operating at 14.7 psia (1 atm) and 400°F (204°C), fuel and oxidant utilizations of 80% and 60% respectively[f], an air fed cathode, and an anode inlet composition of 75% H_2 and 0.5% CO.

3.2.6 Effects of Cell Life

One of the primary areas of research is in extending cell life. The goal is to maintain the performance of the cell stack during a standard utility application (~40,000 hours). Current state-of-the-art PAFC's (45, 46, 47) show the following degradation over time:

$$\Delta V_{lifetime}\ (mV) = -3\ mV/1{,}000\ hours \qquad (3\text{-}22)$$

[f] Assumes graph operating conditions (not provided) are same as associated text of Ref. 15.

3.3 Summary of Equations for PAFC

The preceding sections provide parametric performance based on various referenced data at differing cell conditions. It is suggested that the following set of equations be used unless the reader prefers other data or rationale. Figure 3-7 is provided as reference PAFC performances at 8.2 atm and ambient pressure.

Parameter	Equation	Comments	
Pressure	$\Delta V_P\ (mV) = 146 \log \frac{P_2}{P_1}$	$1\ atm \le P \le 10\ atm$ $177°C \le T \le 218°C$	(3-5)
Temperature	$\Delta V_T\ (mV) = 1.15\ (T_2 - T_1)$	$180°C \le T \le 250°C$	(3-6)
Oxidant	$\Delta V_{cathode}\ (mV) = 148 \log \frac{(\bar{P}_{02})_2}{(\bar{P}_{02})_1}$	$0.04 \le \frac{\bar{P}_{02}}{\bar{P}_{Total}} \le 0.20$	(3-8)
	$\Delta V_{cathode}\ (mV) = 96 \log \frac{(\bar{P}_{02})_2}{(\bar{P}_{02})_1}$	$0.20 < \frac{\bar{P}_{02}}{\bar{P}_{Total}} < 1.0$	(3-9)
Fuel	$\Delta V_{anode}\ (mV) = 55 \log \frac{(\bar{P}_{H2})_2}{(\bar{P}_{H2})_1}$		(3-10)
CO Poisoning	$\Delta V_{CO}\ (mV) = -11.1\ ([CO]_2 - [CO]_1)$	$163°C$	(3-12)
	$\Delta V_{CO}\ (mV) = -6.14\ ([CO]_2 - [CO]_1)$	$177°C$	
	$\Delta V_{CO}\ (mV) = -3.54\ ([CO]_2 - [CO]_1)$	$190°C$	
	$\Delta V_{CO}\ (mV) = -2.05\ ([CO]_2 - [CO]_1)$	$204°C$	
	$\Delta V_{CO}\ (mV) = -1.30\ ([CO]_2 - [CO]_1)$	$218°C$	
Current Density	$\Delta V_J\ (mV) = -0.53\ \Delta J$ for $J = 100 - 200\ mA/cm^2$, $P = 8.2\ atm$		(3-18)
	$\Delta V_J\ (mV) = -0.39\ \Delta J$ for $J = 200 - 650\ mA/cm^2$, $P = 8.2\ atm$		(3-19)
	$\Delta V_J\ (mV) = -0.74\ \Delta J$ for $J = 50 - 120\ mA/cm^2$, $P = 1\ atm$		(3-20)
	$\Delta V_J\ (mV) = -0.45\ \Delta J$ for $J = 120 - 215\ mA/cm^2$, $P = 1\ atm$		(3-21)
Life Effects	$\Delta V_{lifetime}\ (mV) = -3mV/1{,}000\ hrs.$		(3-22)

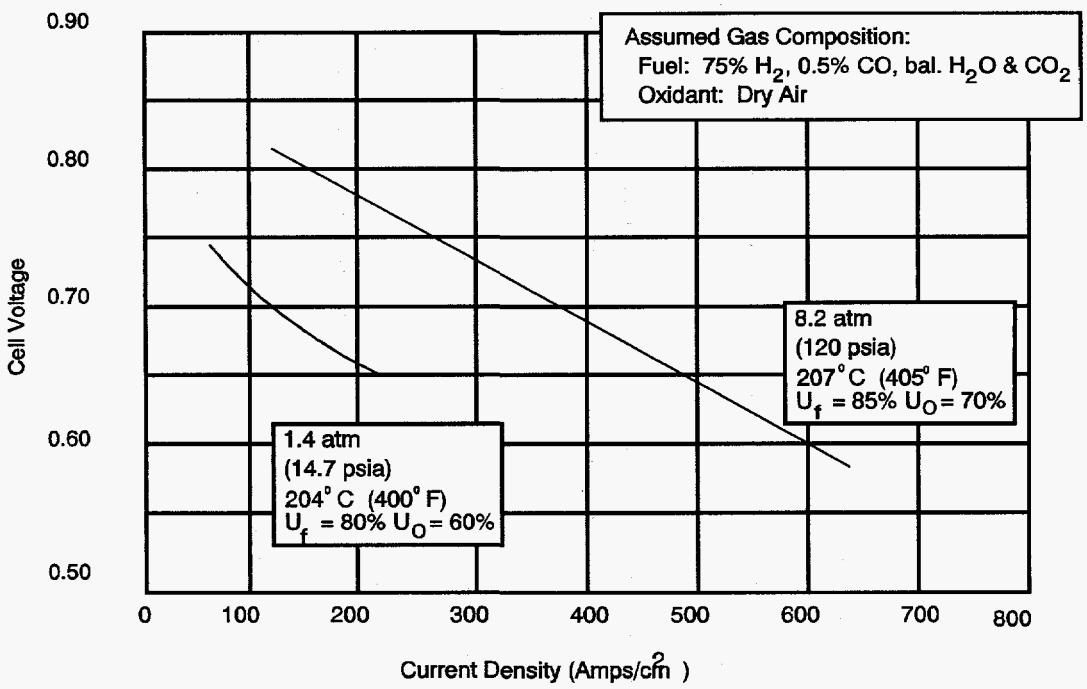

Figure 3-7 Reference performances at 8.2 atm and ambient pressure.
Source: Reference 15.

References

1. J. Hirschenhofer, "Latest Progress in Fuel Cell Technology," IEEE-Aerospace and Electronic Systems Magazine, 7, November 1992.
2. J. Hirschenhofer, "Status of Fuel Cell Commercialization Efforts," American Power Conference, Chicago, IL, April 1993.
3. J. Appleby, in *Proceedings of the Workshop on the Electrochemistry of Carbon*, Edited by S. Sarangapani, J. R. Akridge and B. Schumm, The Electrochemical Society, Inc., Pennington, NJ, p. 251, 1984.
4. K. V. Kordesch, "Survey of Carbon and Its Role in Phosphoric Acid Fuel Cells," BNL 51418, prepared for Brookhaven National Laboratory, December 1979.
5. K. Kinoshita, *Carbon: Electrochemical and Physicochemical Properties*, Wiley Interscience, New York, NY, 1988.
6. L. Christner, J. Ahmad and M. Farooque, in *Proceedings of the Symposium on Corrosion in Batteries and Fuel Cells and Corrosion in Solar Energy Systems,* Edited by C. J. Johnson and S. L. Pohlman, The Electrochemical Society, Inc., Pennington, NJ, p. 140, 1983.
7. P. W. T. Lu and L. L. France, in *Extended Abstracts*, Fall Meeting of The Electrochemical Society, Inc., Volume 84-2, Abstract No. 573, The Electrochemical Society, Inc., Pennington, NJ, p. 837, 1984.
8. M. Warshay, in *The Science and Technology of Coal and Coal Utilization,* Edited by B. R. Cooper and W. A. Ellingson, Plenum Press, New York, NY, p. 339, 1984.
9. P. R. Prokopius, M. Warshay, S. N. Simons and R. B. King, in *Proceedings of the 14th Intersociety Energy Conversion Engineering Conference,* Volume 2, American Chemical Society, Washington, D. C., p. 538, 1979.

10. S. N. Simons, R. B. King and P. R. Prokopius, in *Symposium Proceedings Fuel Cells Technology Status and Applications,* Edited by E. H. Camara, Institute of Gas Technology, Chicago, IL, p. 45, 1982.
11. A. J. Appleby, F. R. Foulkes, *Fuel Cell Handbook*, Van Nostrand Reinhold, New York, NY, 1989.
12. A. P. Fickett, in *Proceedings of the Symposium on Electrode Materials and Processes for Energy Conversion and Storage,* Edited by J. D. E. McIntyre, S. Srinivasan and F. G. Will, The Electrochemical Society, Inc. Pennington, NJ, p. 546, 1977.
13. A. J. Appleby, *J. Electroanal, Chem.,* **118,** 31, 1981.
14. J. Huff, "Status of Fuel Cell Technologies", in *Fuel Cell Seminar Abstracts*, 1986 National Fuel Cell Seminar, October 26-29, Tucson, AZ, 1986.
15. "Advanced Water-Cooled Phosphoric Acid Fuel Cell Development, Final Report," Report No. DE/MC/24221-3130, International Fuel Cells Corporation for U.S. DOE under Contract DE-AC21-88MC24221, South Windsor, CT, September 1992.
16. N. Giordano, E. Passalacqua, L. Pino, V. Alderucci, and P. L. Antonucci, "Catalyst and Electrochemistry in PAFC: A Unifying Approach," in *The International Fuel Cell Conference Proceedings*, NEDO/MITI, Tokyo, Japan, 1992.
17. B. Roland, J. Scholta, and H. Wendt, "Phosphoric Acid Fuel Cells - Materials Problems, Process Techniques and Limits of the Technology," in *The International Fuel Cell Conference Proceedings*, NEDO/MITI, Tokyo, Japan, 1992.
18. "Overview of 11 MW Fuel Cell Power Plant," Non-published information from Tokyo Electric Power Company, September 1989.
19. M. Matsumoto, K. Usami, "PAFC Commercialization and Recent Progress of Technology in Mitsubishi Electric," in *The International Fuel Cell Conference Proceedings*, NEDO/MITI, Tokyo, Japan, 1992.
20. J. A. S. Bett, H. R. Kunz, S. W. Smith and L. L. Van Dine, "Investigation of Alloy Catalysts and Redox Catalysts for Phosphoric Acid Electrochemical Systems," FCR-7157F, prepared by International Fuel Cells for Los Alamos National Laboratory under Contract No. 9-X13-D6271-1, 1985.
21. B. C. Beard and P. N. Ross, *J. Electrochem. Soc.,* **133,** 1839, 1986.
22. J. T. Glass, G. L. Cahen, G. E. Stoner and E. J. Taylor, *J. Electrochem. Soc.,* **134,** 58, 1987.
23. P. N. Ross, "Oxygen Reduction on Supported Pt Alloys and Intermetallic Compounds in Phosphoric Acid," Final Report, EM-1553, prepared under Contract 1200-5 for the Electric Power Research Institute, Palo Alto, CA, September 1980.
24. V. Jalan and J. Giner, in *DECHEMA Monographs,* Volume 102, Edited by J. W. Schultze, VCH Verlagsgesellschaft, Weinheim, West Germany, p. 315, 1986.
25. T. Ito, K. Kato, S. Kamitomai, M. Kamiya, "Organization of Platinum Loading Amount of Carbon-Supported Alloy Cathode for Advanced Phosphoric Acid Fuel Cell," in *Fuel Cell Seminar Abstracts*, 1990 Fuel Cell Seminar, Phoenix, AZ, November 25-28, 1990.
26. J. S. Buchanan, G. A. Hards, L. Keck, R. J. Potter, "Investigation into the Superior Oxygen Reduction Activity of Platinum Alloy Phosphoric Acid Fuel Cell Catalysts", in *Fuel Cell Seminar Abstracts*, Tucson, AZ, November 29-December 2, 1992.
27. K. Kinoshita, F. R. McLarnon, E. J. Cairns, *Fuel Cells, A Handbook*, prepared by Lawrence Berkeley Laboratory for the U.S. Department of Energy under Contract DE-AC03-76F00098, May 1988.
28. N. D. Kackley, S. A. McCatty, J. A. Kosek, "Improved Anode Catalysts for Coal Gas-Fueled Phosphoric Acid Fuel Cells," Final Report DOE/MC/25170-2861, prepared for U.S. Department of Energy under Contract DE-AC21-88MC25170, July 1990.
29. M. Watanabe, C. Shirmura, N. Hara, K. Tsurumi, "An Advanced Gas-Diffusion Electrode for Long-Life and High Performance PAFC," in *The International Fuel Cell Conference Proceedings*, NEDO/MITI, Tokyo, Japan, 1992.
30. M. Aoki, Y. Ueki, H. Enomoto, K. Harashima, "Some Approaches to Improve the Life Performance of Phosphoric Acid Fuel Cell," paper provided to the authors by Fuji Electric Corporate Research and Development, 1992, date of preparation unknown.

31. M. Watanabe, H. Sei, P. Stonehart, *Journal of Electroanalytical Chemistry*. **261**, 375, 1989.
32. M. Farooque, "Evaluation of Gas-Cooled Pressurized Phosphoric Acid Fuel Cells for Electric Utility Power Generation," Final Technical Report, NASA CR-168298 prepared by Energy Research Corp. under Contract No. DEN 3-201 for NASA Lewis Research Center, September 1983.
33. J. McBreen, W.E. O'Grady and R. Richter, *J. Electrochem. Soc.,* **131,** 1215, 1984.
34. T. G. Benjamin, E. H. Camara and L. G. Marianowski, *Handbook of Fuel Cell Performance,* prepared by the Institute of Gas Technology for the United States Department of Energy under Contract No. EC-77-C-03-1545, May 1980.
35. J. M. Feret, "Gas Cooled Fuel Cell Systems Technology Development," Final Report, NASA CR-175047, prepared by Westinghouse Electric Corp. under Contract No. DEN 3-290 for NASA Lewis Research Center, August 1985.
36. V. Jalan, J. Poirier, M. Desai, B. Morrisean, "Development of CO and H_2S Tolerant PAFC Anode Catalysts," in *Proceedings of the Second Annual Fuel Cell Contractors Review Meeting*, 1990.
37. P. W. T. Lu and L. L. France, in *Proceedings of the Symposium on Transport Processes in Electrochemical Systems,* R. S. Yeo, K. Katan and D. T. Chin, The Electrochemical Society, Inc., Pennington, NJ, p. 77, 1982.
38. P. N. Ross, "Anomalous Current Ratios in Phosphoric Acid Fuel Cell Cathodes," LBL-13955; submitted to *J. Electrochem. Soc.*, March 1986.
39. P. Ross and P. Stonehart, *Electrochim. Acta,* **21,** 441, 1976.
40. W. Vogel, J. Lundquist, P. Ross and P. Stonehart, *Electrochim. Acta,* **20,** 79, 1975.
41. H. R. Kunz, in *Proceedings of the Symposium on Electrode Materials and Processes for Energy Conversion and Storage,* Edited by J. D. E. McIntyre, S. Srinivasan and F. G. Will, The Electrochemical Society, Inc., Pennington, NJ, p. 607, 1977.
42. D. T. Chin and P. D. Howard, *J. Electrochem. Soc.,* **133,** 2447, 1986.
43. S. T. Szymanski, G. A. Gruver, M. Katz and H. R. Kunz, *J. Electrochem. Soc.*, **127,** 1440, 1980.
44. F. S. Kemp, IFC, "Status of Development of Water - Cooled Phosphoric Acid Fuel Cells", in *Proceedings of the Second Annual Fuel Cell Contractors Review Meeting*, U.S. DOE/METC, 1990.
45. N. Giordano, "Fuel Cells Activity at CNR, TAE Institute," CNR/TAE, Italy, 1992.
46. "Gas Cooled Fuel Cell Systems Technology Development," Westinghouse/DOE, WAES-TR-92-001, March, 1992.
47. K. Harasawa, I. Kanno, I. Masnda, "Fuel Cell R&D and Demonstration Programs at Electric Utilities in Japan," in *Fuel Cell Seminar Abstracts*, Tucson, AZ, November 29-December 2, 1992.

4. MOLTEN CARBONATE FUEL CELL

The MCFC is often referred to as a second generation fuel cell because it is expected to reach commercialization after PAFCs are available in the marketplace. Currently, three industrial corporations are actively pursuing the commercialization of MCFCs in the United States; these are Energy Research Corporation, International Fuel Cells Corporation, and M-C Power Corporation. Both Europe and Japan have at least three developers each pursuing the technology: these are Brandstofel Nederland (BCN), Deutsche Aerospace AG, Ansaldo (Italy), Hitachi, Ishikawajima-Harima Heavy Industries, and Mitsubishi Electric Corporation.

The electrochemical reactions occurring in MCFCs are:

$$H_2 + CO_3^{=} \rightarrow H_2O + CO_2 + 2e^- \tag{4-1}$$

at the anode, and

$$\tfrac{1}{2}O_2 + CO_2 + 2e^- \rightarrow CO_3^{=} \tag{4-2}$$

at the cathode. The overall cell reaction[a] is:

$$H_2 + \tfrac{1}{2}O_2 + CO_2\ (\text{cathode}) \rightarrow H_2O + CO_2\ (\text{anode}) \tag{4-3}$$

Besides the reaction involving H_2 and O_2 to produce H_2O, the equations shows a transfer of CO_2 from the cathode gas stream to the anode gas stream, with 1 mole CO_2 transferred along with two Faradays of charge or 2 gram moles of electrons. The reversible potential for a MCFC, taking into account the transfer of CO_2, is given by the equation:

$$E = E^\circ + \frac{RT}{2F} \ln \frac{P_{H_2} P_{O_2}^{1/2}}{P_{H_2O}} + \frac{RT}{2F} \ln \frac{P_{CO_{2,c}}}{P_{CO_{2,a}}} \tag{4-4}$$

where the subscripts a and c refer to the anode and cathode gas compartments, respectively. When the partial pressures of CO_2 are identical at the anode and cathode, and the electrolyte is invariant, the cell potential depends only on the partial pressures of H_2, O_2 and H_2O. Typically, the CO_2

[a] CO is not directly used by electrochemical oxidation, but produces additional H_2 when combined with water in the water gas shift reaction.

partial pressures are different in the two electrode compartments and the cell potential is affected accordingly, as shown in Equation 4-4.

It is usual practice in an MCFC system that the CO_2 generated at the anode be recycled to the cathode where it is consumed. This will require some type of device that will either (i) transfer the CO_2 from the anode exit gas to the cathode inlet gas ("CO_2 transfer device"), (ii) produce CO_2 by combustion of the anode exhaust gas, which is mixed with the cathode inlet gas, or (iii) supply CO_2 from an alternate source.

MCFCs differ in many respects from PAFCs because of their higher operating temperature (650 vs 200°C) and the nature of the electrolyte. The higher operating temperature of MCFCs provides the opportunity for achieving higher overall system efficiencies (potential for heat rates below 7,500 Btu/kWh) and greater flexibility in the use of available fuels.[b] On the other hand, the higher operating temperature places severe demands on the corrosion stability and life of cell components, particularly in the aggressive environment of the molten carbonate electrolyte. Another difference between PAFCs and MCFCs lies in the method used for electrolyte management in the respective cells. In a PAFC, PTFE serves as a binder and wet-proofing agent to maintain the integrity of the electrode structure and to establish a stable electrolyte/gas interface in the porous electrode. The phosphoric acid is retained in a matrix of PTFE and SiC between the anode and cathode. There are no materials available for use in MCFCs that are comparable to PTFE. Thus, a different approach is required to establish a stable electrolyte/gas interface in MCFC porous electrodes, and this is illustrated schematically in Figure 4-1. The MCFC relies on a balance in capillary pressures to establish the electrolyte interfacial boundaries in the porous electrodes (1-3). At thermodynamic equilibrium, the diameters of the largest flooded pores in the porous components are related by the equation:

$$\frac{\gamma_c \cos\,\theta_c}{D_c} = \frac{\gamma_e \cos\,\theta_e}{D_e} = \frac{\gamma_a \cos\,\theta_a}{D_a} \qquad (4\text{-}5)$$

where γ is the interfacial surface tension, θ is the contact angle of the electrolyte, D is the pore diameter, and the subscripts a, c and e refer to the anode, cathode and electrolyte matrix, respectively. By properly coordinating the pore diameters in the electrodes with those of the electrolyte matrix, which contains the smallest pores, the electrolyte distribution depicted in Figure 4-1 is established. This arrangement permits the electrolyte matrix to remain completely filled with molten carbonate, while the porous electrodes are partially filled, depending on their pore size distributions. According to the model illustrated in Figure 4-1 and described by Equation 4-5, the electrolyte content in each of the porous components will be determined by the equilibrium pore size (<D>) in that component; pores smaller than <D> will be filled with electrolyte, and pores larger than <D> will remain empty. A reasonable estimate of the volume distribution of electrolyte in the various cell components is obtained from the measured pore-volume-distribution curves and the above relationship for D (1,2).

Electrolyte management, that is, the control over the optimum distribution of molten carbonate electrolyte in the different cell components, is critical for achieving high performance and endurance with MCFCs. Various processes (i.e., consumption by corrosion reactions, potential driven migration, creepage of salt and salt vaporization) occur, all of which contribute to the redistribution of molten carbonate in MCFCs; these aspects are discussed by Maru et al. (4) and Kunz (5).

---

[b] *In situ* reforming of fuels in MCFCs is possible, and this is discussed later in the section.

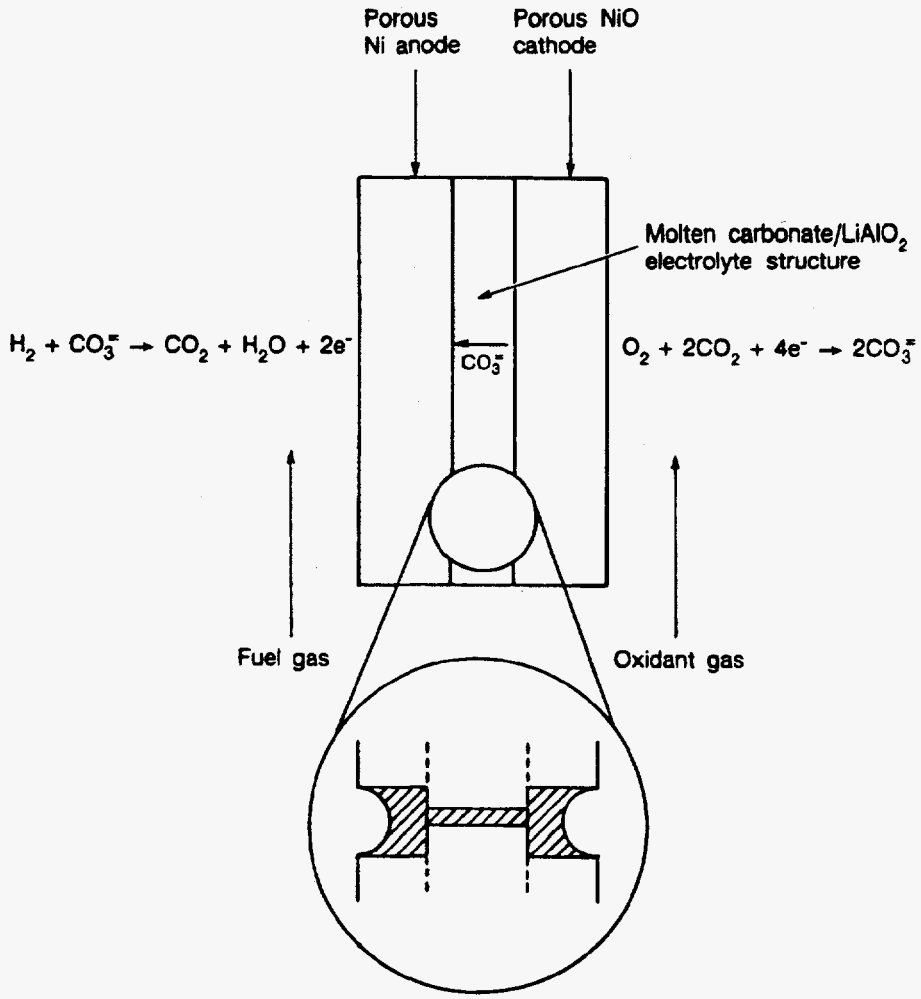

Figure 4-1 Schematic representation of a MCFC showing the dynamic equilibrium of molten carbonate in the porous cell elements. The porous electrodes are depicted with pores covered by a thin film of electrolyte.

4.1 Cell Components

4.1.1 State-of-the-Art

The data in Table 4-1 provide a chronology of the evolution in cell component technology for MCFCs. In the mid-1960s, the electrode materials were, in many cases, precious metals, but the technology soon evolved to the use of Ni-based alloys at the anode and oxides at the cathode. Since the mid-1970s, the materials for the electrodes and electrolyte structure (molten carbonate/$LiAlO_2$) have remained essentially unchanged. A major development in the 1980's has been the evolution in the technology for fabrication of electrolyte structures. Developments in cell components for MCFCs have been reviewed by Maru and co-workers (6, 7), Petri and Benjamin (8) and Selman (9). Over the past 20 years, the performance of single cells has improved from about 10 mW/cm^2 to

> 150 mW/cm^2. During the 1980s both the performance and endurance of MCFC stacks showed dramatic improvements. The data in Figure 4-2 illustrate the progress that has been made in the performance of single cells, and in the cell voltage at 160 A/ft^2 (172 mA/cm^2) of small stacks at 650°C, with low-Btu fuel [17% (H_2 + CO)] at 65 psia. Several MCFC stack developers have produced cell stacks with up to 1 m^2 cells. The tallest, full scale cell stack fabricated to date was built by ERC and has 246 cells of 5,600 cm^2 (6 ft^2) in area.

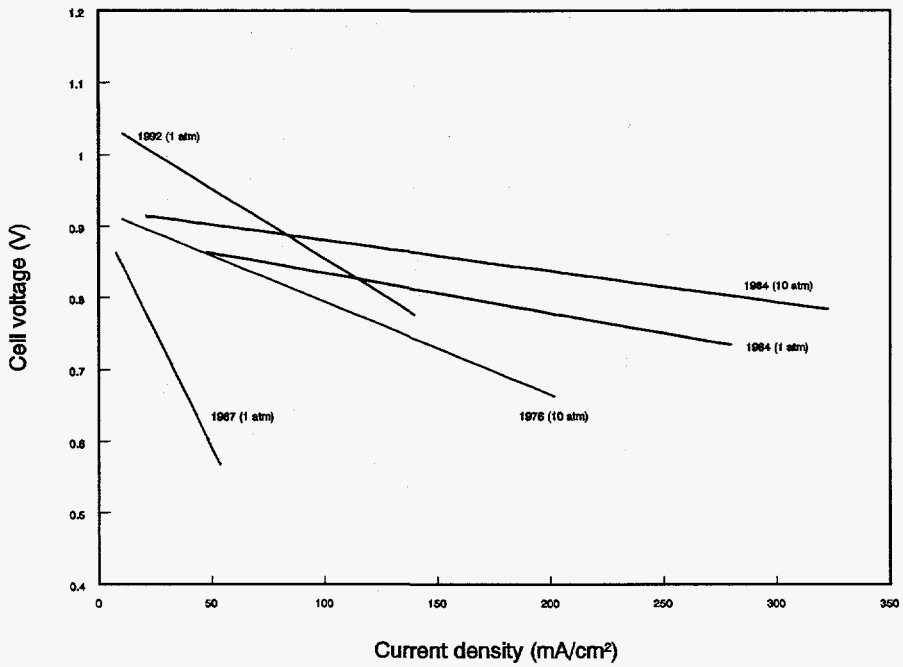

Figure 4-2 Progress in the generic performance of MCFCs on reformate gas and air.
Source: J.R. Huff, paper presented at the 1986 Fuel Cell Seminar, October 26-29, 1986, Tucson, AZ, M. Farooque, data from ERC testing, 1992.

The conventional process used to fabricate electrolyte structures until about 1980 involved hot pressing (about 5,000 psi) mixtures of $LiAlO_2$ and alkali carbonates (typically > 50 vol% in liquid state) at temperatures slightly below the melting point of the carbonate salts (e.g., 490°C for electrolyte containing 62 mol% Li_2CO_3-38 mol% K_2CO_3). These electrolyte structures (also called "electrolyte tiles") were relatively thick (1-2 mm) and difficult to produce in large sizes[c] because large tooling and presses were required. The electrolyte structures produced by hot pressing are often characterized by: 1) void spaces (<5% porosity), 2) poor uniformity of microstructure, 3) generally poor mechanical strength, and 4) high iR drop. To overcome these shortcomings of hot pressed electrolyte structures, alternative processes such as tape casting (7) and electrophoretic

[c] The largest electrolyte tile produced by hot pressing was about 1.5 m^2 in area (7).

Table 4-1 Evolution of Cell Component Technology for Molten Carbonate Fuel Cells

Component	ca. 1965	ca. 1975	Current Status
Anode	• Pt, Pd, or Ni	• Ni-10 wt% Cr	• Ni-10 wt% Cr • 3-6 μm pore size • 50-70% initial porosity • 0.5-1.5 mm thickness • 0.1-1 m^2/g
Cathode	• Ag_2O or lithiated NiO	• lithiated NiO	• lithiated NiO • 7-15 μm pore size • 70-80% initial porosity • 60-65% after lithiation and oxidation • 0.5-0.75 mm thickness • 0.5 m^2/g
Electrolyte Support	• MgO	• mixt. of α-, β- and γ-$LiAlO_2$ • 10-20 m^2/g	• γ-$LiAlO_2$ • 0.1-12 m^2/g • 0.5 mm thickness
Electrolyte[a]	• 52 Li-48 Na • 43.5 Li-31.5 Na-25 K • "paste"	• 62 Li-38 K • ~60-65 wt% • hot press "tile" • 1.8 mm thickness	• 62 Li-38 K • 50 Li-50 Na • 50 Li-50 K • ~50 wt% • tape cast • 0.5 mm thickness

[a] Mole percent of alkali carbonate salt

Specifications (current status) for the anode and cathode were obtained from: A. Pigeaud, H. C. Maru, L. Paetsch, J. Doyon and R. Bernard, in *Proceedings of the Symposium on Porous Electrodes: Theory and Practice*, Edited by H. C. Maru, T. Katan and M. G. Klein, The Electrochemical Society, Inc., Pennington, NJ, 1984, p. 234 and M. Farooque, "Development of Internal Reforming Carbonate Fuel Cell Technology, Final Report", DOE/MC/23274-2941, October, 3-17, 1990.

deposition(10) for fabricating thin electrolyte structures were developed. The greatest success to date with an alternative process has been reported with tape casting, which is a common processing technique used by the ceramics industry. This process involves dispersing the ceramic powder in a solvent,[d] which contains dissolved binders (usually an organic compound), plasticizers, and additives to yield the proper slip rheology. The slip is cast over a moving smooth substrate, and the desired thickness is established with a doctor blade device. After drying the slip, the "green" structure is assembled into the fuel cell where the organic binder is removed by thermal decomposition and the absorption of alkali carbonate into the ceramic structure occurs during cell start-up.

The tape casting and electrophoretic deposition processes are amenable to scale-up, and thin electrolyte structures (0.25-0.5 mm) can be produced. The ohmic resistance of an electrolyte structure,[e] and the resulting ohmic polarization, have a large influence on the operating voltage of MCFCs. ERC has stated that the electrolyte matrix encompasses 70% of the ohmic loss (12). At a current density of 160 mA/cm^2, the voltage drop (ΔV_{ohm}) of a 0.18 cm thick electrolyte structure, with a specific conductivity of ~ 0.3 $ohm^{-1}cm^{-1}$ at 650°C, was found to obey the relationship (10),

$$\Delta V_{ohm}\ (V) = 0.533t \qquad (4\text{-}6)$$

where t is the thickness in cm. Recent data confirms this result (12). Given this equation, it is apparent that a fuel cell with an electrolyte structure of 0.025 cm thickness would operate at a cell voltage that is 82 mV higher than that of an identical cell with an electrolyte structure of 0.18 cm thickness because of the lower ohmic loss. Thus, there is a strong incentive for making thinner electrolyte structures to obtain better cell performance.

The electrolyte composition affects the performance and endurance of MCFCs in several ways. Higher ionic conductivities, and hence lower ohmic polarization, are achieved with Li-rich electrolytes because of the relative high ionic conductivity of Li_2CO_3 compared to that of Na_2CO_3 and K_2CO_3. However, gas solubility and diffusivity are lower, and corrosion is more rapid, in Li_2CO_3.

The major problems with Ni-based anodes and NiO cathodes are structural stability and NiO dissolution, respectively (9). Sintering and mechanical deformation of the porous Ni-based anode under compressive load leads to severe performance decay by redistribution of electrolyte in a MCFC stack. The dissolution of NiO in molten carbonate electrolyte became evident when thin electrolyte structures were used. Despite the low solubility of NiO in carbonate electrolytes (~ 10 ppm), Ni ions diffuse in the electrolyte towards the anode and metallic Ni can precipitate in regions where a H_2 reducing environment is encountered. The precipitation of Ni provides a sink for Ni ions, and thus promotes the diffusion of dissolved Ni from the cathode. This phenomenon becomes worse at high CO_2 partial pressures (13, 14) because dissolution may involve the following mechanism,

$$NiO + CO_2 \rightarrow Ni^{2+} + CO^{=}_3 \qquad (4\text{-}7)$$

The dissolution of NiO has been correlated to the acid/base properties of the molten carbonate. The basicity of the molten carbonate is defined as equal to -log (activity of $O^{=}$) or -log a_{M_2O}, where

---

[d] An organic solvent is used because $LiAlO_2$ in the slip reacts with H_2O.

[e] Electrolyte structures containing 45 wt% $LiAlO_2$ and 55 wt% molten carbonate (62 mol% Li_2CO_3-38 mol% K_2CO_3) have a specific conductivity at 650°C of about 1/3 that of the pure carbonate phase (11).

a is the activity of the alkali metal oxide M_2O. Based on this definition, acidic oxides are associated with carbonates (e.g., K_2CO_3) that do not dissociate to M_2O, and basic oxides are formed with highly dissociated carbonate salts (e.g., Li_2CO_3). The solubility of NiO in binary carbonate melts, shows a clear dependence on the acidity/basicity of the melt (15, 16). In relatively acidic melts, NiO dissolution can be expressed by:

$$NiO \rightarrow Ni^{2+} + O^{=} \tag{4-8}$$

In basic melts, NiO reacts with $O^{=}$ to produce one of two forms of nickelate ions:

$$NiO + O^{=} \rightarrow NiO_2^{=} \tag{4-9}$$

or

$$2NiO + O^{=} + \tfrac{1}{2}O_2 \rightarrow 2NiO_2^{-} \tag{4-10}$$

A distinct minimum in NiO solubility is observed in plots of log (NiO solubility) versus basicity ($-\log a_{M_2O}$), which can be demarcated into two branches corresponding to acidic and basic dissolution. Acidic dissolution is represented by a straight line with a slope of +1, and a NiO solubility that decreases with an increase in a_{M_2O}. Basic dissolution is represented by a straight line with a slope corresponding to either -1 or -1/2, corresponding to Reactions 4-9 and 4-10, respectively. The CO_2 partial pressure is an important parameter in the dissolution of NiO in carbonate melts because the basicity is directly proportional to log P_{CO_2}. An MCFC usually operates with a molten carbonate electrolyte that is acidic.

The goal of 40,000 hours for the lifetime of MCFCs appears achievable with cell operation at atmospheric pressure, but at 10 atm cell pressure, only about 5,000 to 10,000 hours may be possible with currently available NiO cathodes (17). The solubility of NiO in molten carbonates is complicated by its dependence on several parameters: carbonate composition, H_2O partial pressure, CO_2 partial pressure, and temperature. For example, measurements of NiO dissolution by Kaun (18) indicate that the solubility is affected by changing the electrolyte composition; a lower solubility is obtained in a Li_2CO_3-K_2CO_3 electrolyte that contains less Li_2CO_3 (i.e., lower solubility in 38 mol% Li_2CO_3-62 mol% K_2CO_3 than in 62 mol% Li_2CO_3-38 mol% K_2CO_3 at 650°C). However, the solubility of Ni increases in the electrolyte with 38 mol% Li_2CO_3 when the temperature decreases, whereas the opposite trend is observed in the electrolyte with 62 mol% Li_2CO_3. Another study reported by Appleby (19) indicates that the solubility of Ni decreases from 9 to 2 ppm by increasing the Li concentration in Li_2CO_3-K_3CO_3 from 62 to 75 at%, and a lower solubility is obtained in 60 mol% Li_2CO_3-40 mol% Na_2CO_3 at 650°C. The total loss of Ni from the cathode by dissolution in 40,000 hours is expected to correspond to only about 10% of the total cathode thickness. However, ERC estimates a 30 to 40 percent loss of the baseline NiO cathode over 40,000 hours of operation (20). The loss of NiO from the cathode can be a critical problem if the possibility of a short circuit exists in the cell. The loss of NiO also facilitates compaction of the cathode. However, ERC endurance testing (7,000 to 10,000 hours) shows that the NiO loss is tolerable from the cathode performance point of view. The compaction of cathodes became evident in MCFC stacks once the anode creep was eliminated when strengthened by oxide dispersion (i.e., oxide dispersion strengthened or ODS anode).

The bipolar plates used in MCFC stacks are usually fabricated from thin ($\sim$15 mil) sheets of an alloy (e.g., Incoloy 825, 310S or 316L stainless steel) that are coated on one side (i.e., the side exposed to fuel gases in the anode compartment) with a Ni layer. The Ni layer is stable in the

reducing gas environment of the anode compartment, and it provides a conductive surface coating with low contact resistance. Approaches to circumvent the problems associated with gas leaks and corrosion of bipolar plates are described by Pigeaud et al. (21). Corrosion is largely overcome by application of a coating (about 50-μm thickness) at the vulnerable locations on the bipolar plate. For example, the wet-seal[f] area on the anode side is subject to a high chemical potential gradient because of the fuel gas inside the cell and the ambient environment (usually air) on the outside of the cell, which promotes corrosion (about two orders of magnitude greater than in the cathode wet-seal area (22)). A general discussion on corrosion in the wetseal area of MCFCs is presented by Donado et al. (23). A thin Al coating in the wetseal area of a bipolar plate provides corrosion protection by forming a protective layer of $LiAlO_2$ after reaction of Al with Li_2CO_3 (24). Such a protective layer would not be useful in areas of the bipolar plate that must permit electronic conduction because $LiAlO_2$ is an insulating material.

A dense and electronically insulating layer of $LiAlO_2$ is not suitable for providing corrosion resistance to the cell current collectors because these components must remain electrically conductive. The typical materials used for this application are 316 stainless steel and chromium plated stainless steels. However, materials with better corrosion resistance are required for long term operation of MCFCs. Research is underway to understand the corrosion processes of chromium in molten carbonate salts under both fuel gas and oxidizing gas environments (20, 25) and to identify improved alloys (26) for MCFCs. Stainless steels such as Type 310 and 446 have demonstrated better corrosion resistance than Type 316 in corrosion tests (26).

4.1.2 Development Components

MCFC cell components are limited by several technical problems (27), particularly those described in Section 4.1.1. A review of the literature from 1988 to the present shows that research efforts described in the previous issue of this handbook (28) essentially continue. It should be noted that MCFC component designs and operational approaches exist on an individual basis which would result in operation for 40,000 hour lifetime at atmospheric pressure and with natural gas fuel. The coupling of these improvements need to be proven to meet endurance goals; operation at pressure will definitely require changes. The studies described in the recent literature provide updated information on promising development of the electrodes, the electrolyte matrix, and the capability of the cell to tolerate trace constituents in the fuel supply. The objectives of these works are to increase the life of the cells, improve cell performance, lower cell component costs, and address the issues pertinent to coal operation. Descriptions of some of this work follow.

Anode: As stated in the Section 4.1.1 and Reference 29, present state-of-the-art anodes are made of a Ni/10%Cr alloy. The Cr was added to eliminate the problem of anode sintering. However, Ni/Cr anodes are susceptible to creep when placed under the torquing load required in the stack to minimize contact resistance between components. The Cr in the anode is also lithiated by the electrolyte, then it consumes carbonate. Developers are trying lesser amounts of Cr (8%) to reduce the loss of electrolyte, but some have found that reducing the Cr by 2 percentage points increased creep (30). Several developers have begun testing with Ni/Al alloy anodes which provide creep resistance with minimum electrolyte loss (30, 31, 32). The low creep rate with this alloy is attributed to the formation of $LiAlO_2$ dispersed in Ni (31).

---

[f] The area of contact between the outer edge of the bipolar plate and the electrolyte structure prevents gas from leaking out of the anode and cathode compartments. The gas seal is formed by compressing the contact area between the electrolyte structure and the bipolar plate so that the liquid film of molten carbonate at operating temperature does not allow gas to permeate through.

Even though the above work is providing a stable, non-sintering, creep resistant anode, electrodes made with Ni are relatively high in cost. Work is in progress to determine whether a cheaper material, particularly Cu, can be substituted for Ni to lower the cost while retaining stability. A complete substitution of Cu for Ni is not feasible since Cu would exhibit worse creep than Ni. It has been found that anodes made of a Cu - 50% Ni - 5% Al alloy will provide long term creep resistance (33). Another approach tested at IGT, showed that an "IGT" stabilized Cu anode had a lower percent creep than a 10% Cr - Ni anode. It's performance was about 40 to 50 mV lower than the standard cell at 160 mA/cm^2. An analysis hypothesized that the polarization difference could be reduced to 32 mV at most by pore structure optimization (34).

There is a need to provide better tolerance to sulfur poisoning gases in systems using MCFCs, especially when considering coal operation. The strong incentive for sulfur tolerant cells is to eliminate cleanup equipment which impacts system efficiency. This is especially true if low temperature cleanup is required since the system efficiency and capital cost suffer when the fuel gas temperature is first reduced, then increased to the cell temperature level. Tests are being conducted on ceramic anodes to alleviate the problems, including sulfur poisoning, being experienced with anodes (27). Anodes are being tested with undoped $LiFeO_2$ and $LiFeO_2$ doped with Mn and Nb. Preliminary test where several parameters were not strictly controlled showed that the alternative electrodes exhibited poor performance and would not operate over 80 mA/cm^2. At the present time, no alternative anodes have been identified. Instead, future work will focus on performing tests to better understand material behavior and to develop other alternative materials with emphasis on sulfur tolerance.

Cathode: An acceptable candidate material for cathodes must have adequate electrical conductivity, structural strength, and a low dissolution rate in molten alkali carbonates to avoid precipitation of metal in the electrolyte structure. Present state-of-the art cathodes are made of lithiated NiO (28, 29) which have acceptable conductivity and structural strength. However in early testing, the predecessor of International Fuel Cells Corporation found that the nickel dissolved, then precipitated and reformed as dendrites across the electrolyte matrix. This causes a loss of performance and eventual shorting of the cell, see Section 4.1.1. The dissolution of the cathode has turned out to be the primary life limiting constraint of MCFCs, particularly in pressurized operation (31). Developers are investigating several approaches to resolving the NiO dissolution problem: developing alternative materials for the cathodes, increasing in the matrix thickness, using additives in the electrolyte to increase its basicity, and increasing the fraction of Li in the baseline electrolyte.

Initial work on $LiFeO_2$ cathodes showed that electrodes made with this material were very stable chemically in the cathode environment; there was essentially no dissolution (27). However, these electrodes have poor performance relative to the state-of-the-art NiO cathode at atmospheric pressure due to the slow kinetics. The electrode shows promise at pressurized operation so it is still being investigated. Higher performance improvements are expected with Co-doped $LiFeO_2$; these cathodes will be tested in future work. It also has been shown that 5 mol% lithium doped NiO with a thickness of 0.02 cm provided a 43 mV overpotential (higher performance) at 160 mA/cm^2 compared to the state-of-the-art NiO cathode. It is assumed that further performance improvements could be made by reconfiguring the structure, such as decreasing the agglomerate size.

Life is shortened by a decrease in the electrolyte matrix thickness (35). Concurrently, an increase in matrix thickness brings about an increase in life. This is due to an increase in the Ni++ diffusion path which lowers the transport rate and shifts the Ni disposition zone. Developers found that an increase in electrolyte thickness from 0.5 mm to 1.0 mm, increased the time to short from 1,000 hr to 10,000 hr. Along with this, data showed that if the P_{CO_2} was reduced from 0.3 to 0.1,

then the Ni dissolution decreased by a third. U.S. developers concluded that a two-fold improvement in the time-to-short can be achieved using a 60% increase in matrix thickness and an additive of $CaCO_3$, see additives, next. However, this combined approach caused an approximately 20 mV reduction in performance at 160 mA/cm^2 (20).

Another idea for resolving the cathode dissolution problem is to formulate a milder cell environment. This leads to the approach of using additives in the electrolyte to increase its basicity. Small amounts of additives provide similar voltages to that measured without additives, but larger amounts adversely affect performance (36). Table 4-2 quantifies the limiting amounts of additives.

Table 4-2 Amount of Additives to Provide Optimum Performance

	62 MOL% Li_2CO_3/K_2CO_2	52 MOL% Li_2CO_3/NA_2CO_3
$CaCO_3$	0 - 15	0 - 5
$SrCO_3$	0 - 5	0 - 5
$BaCO_3$	0 - 10	0 - 5

Source: Reference 36

Another approach to having a milder cell environment is to increase the fraction of Li in the baseline electrolyte or change the electrolyte to Li/Na rather than the baseline 62/38 Li/K melt (20, 36, 37).

Electrolyte Structure: Ohmic losses contribute about 65 mV loss at the beginning of life and may increase to as much as 145 mV by 40,000 hours (12). The majority of the voltage loss is in the electrolyte and the cathode components. The electrolyte component offers the highest potential for reduction since 70% of the total cell ohmic loss occurs there. Two approaches have been investigated: increase the porosity of the electrolyte structure 5% which reduces the matrix resistance by 15% and change the melt to Li/Na from Li/K which can reduce the matrix resistivity by 40%. Work is continuing on the interaction of the electrolyte with the cathode components. At the present time, an electrolyte loss of 25% of the initial inventory can be projected with a low surface area cathode current collector and with the proper selection of material.

Another area for electrolyte structure improvement is the ability of the matrix to prevent gas crossover from one electrode to the other. ERC has produced an improved matrix fabrication process providing low temperature binder burnout. This process has resulted in frequently achieving a 1% allowable gas leakage, well below the goal of 2% (38).

Electrolyte Migration: Cell performance suffers because of leakage of the electrolyte from the cell. There is a tendency for the electrolyte to migrate from the positive end of the stack to the negative end of the stack. The leakage is through the gasket used to couple the external manifolds to the cell stack. The baseline gasket material presently used is of high porosity and provides a ready circuit for the electrolyte transfer. A new gasket design with a material having lower porosity plus end cell inventory capability offers the potential for reaching 40,000 hours, if only this mode of failure is considered (39). Stacks with internal manifolding do not require a gasket and do not experience this problem.

Coal Gas Trace Species: MCFCs to date have been operated on reformed or simulated natural gas and simulated coal gas. Testing is being conducted with simulated coal gas including the expected individual and multi-trace constituents to better understand coal operation (40). Table 4-3 shows the contaminants and their impact on MCFC operation. The table denotes the species of concern and what cleanup of the fuel gas is required to operate on coal gas. Confidence in operation with coal will require the use of an actual gasifier product. An ERC MCFC stack has been installed (Fall of 1993) using a slip stream of an actual coal gasifier to further clarify the issues of operation with trace gases (42).

Table 4-3 Qualitative Tolerance Levels for Individual Contaminants in Isothermal Bench-Scale Carbonate Fuel Cells

(Only 4 out of the 10 contaminants studied appear to have a significant effect)

CONTAMINANTS (typical ppm in raw coal gas)	REACTION MECHANISM	QUALITATIVE TOLERANCES	CONCLUSIONS
NO NOTICEABLE EFFECTS			
NH_3 (10,000) Cd (5) Hg (1) Sn (3)	$2NH_3 \rightarrow N_2 + 3H_2$ $Cd + H_2O \rightarrow CdO(s) + H_2$ (Hg Vapor Not Reactive) (Sn(l) Not Volatile)	~1 vol% NH_3 ~30 ppm Cd 35 ppm Hg No Vapor @ 650°C	No Effects No Cell Deposits No TGA Effects No Cell Deposits
MINOR EFFECTS			
Zn (100) Pb (15)	$Zn + H_2O \rightarrow ZnO(s) + H_2$ $Pb + H_2O \rightarrow PbS(s) + H_2$	<10 ppm Zn 1.0 ppm Pb sat'd vapor	No Cell Deposits at 75% Utilization Cell Deposits Possible in Presence of High H_2Se
SIGNIFICANT EFFECTS			
H_2S (15,000) HCl (500) H_2Se (5) As (10)	$xH_2S + Ni \rightarrow NiS_x + xH_2$ $2HCl + K_2CO_3 \rightarrow 2KCl(v) + H_2O/CO_2$ $xH_2Se + Ni \rightarrow NiSe_x + xH_2$ $AsH_3 + Ni \rightarrow NiAs(s) + 3/2H_2$	<0.5 ppm H_2S <0.1 ppm HCl <0.2 ppm H_2Se <0.05 ppm As	Recoverable Effect Long Term Effects Possible Recoverable Effect Cumulative Long Term Effect

Source: Reference 40, 41

4.2 Performance

The factors involved in choosing the operating condition for a MCFC are the same as those for the PAFC. These factors include stack size, heat transfer rate, voltage level, load requirement and cost. The performance curve is defined by cell pressure, temperature, gas composition and utilization. Typical MCFCs will generally operate in the range of 100 to 200 mA/cm^2 at 750 to 950 mV/cell.

Typical cathode performance curves obtained at 650°C with an oxidant composition (12.6% O_2/18.4% CO_2/69% N_2), which is anticipated for use in MCFCs, and a common baseline composition (33% O_2/67% CO_2) are presented in Figure 4-3 (17,43). The baseline composition contains the reactants, O_2 and CO_2, in the stoichiometric ratio that is needed in the electrochemical reaction at the cathode (Equation 4-2). With this gas composition, little or no diffusion limitations

occur in the cathode because the reactants are provided primarily by bulk flow. The other gas composition, which contains a substantial fraction of N_2, yields a cathode performance that is limited by gas phase diffusion from dilution by an inert gas.

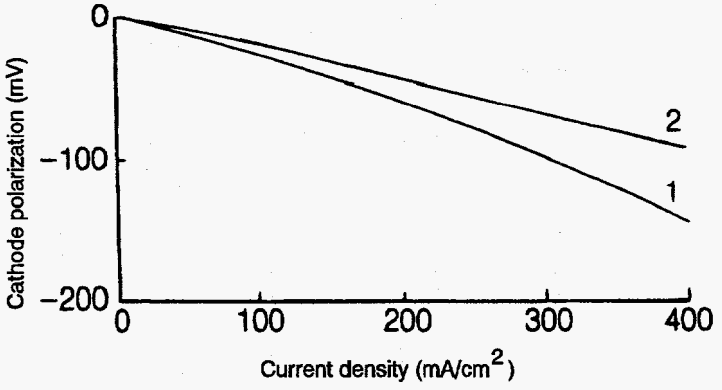

Figure 4-3 The effect of oxidant gas composition on cathode performance in MCFCs at 650°C. Curve 1, 12.6% O_2/18.4% CO_2/69.0% N_2; Curve 2, 33% O_2/67% CO_2.
Source: (Figure 3, p.2712) L. J. Bregoli and H. R. Kunz, *J. Electrochem. Soc.*, **129**, 2711, 1982.

In the 1980's the performance of MCFC stacks increased dramatically and, lately, cells as large as 1.0 m^2 are being tested in stacks. Most recently, the focus has been on achieving performance in a stack equivalent to single cells. Cells with an electrode area of 0.3 m^2 were routinely tested at ambient and above ambient pressures with improved electrolyte structures made by tape-casting processes (17). Several stacks have undergone endurance testing in the range of 7,000 to 10,000 hours. The voltage and power as a function of current density after 960 hours for a 1.0 m^2 stack consisting of 19 cells is shown in Figure 4-4. The data were obtained with the cell stack at 650°C and 1 atm.

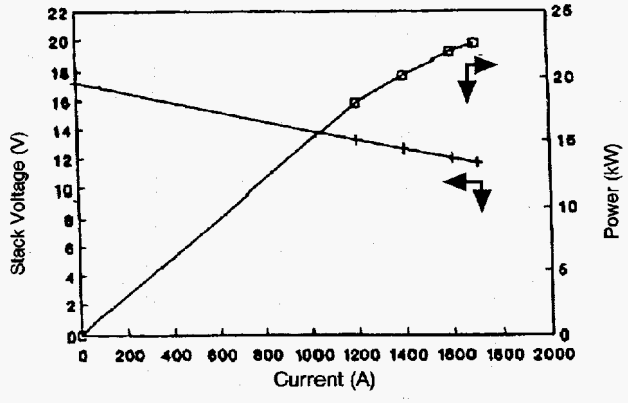

Figure 4-4 Voltage and power output of a 1.0/m^2 19 cell MCFC stack after 960 hours at 965°C and 1 atm. Fuel utilization was 75%.
Source: Benjamin et al, "Status of MCFC Technology at M-C Power-1992", 1992 Fuel Cell Seminar Program and Abstracts, 1992.

The remainder of this section will review the operating parameters which affect MCFC performance. Supporting data will be presented as well as the derived equations which result from this empirical analysis.

4.2.1 Effect of Pressure

The dependence of the reversible cell potential of MCFCs on pressure is evident from the Nernst equation. For a change in pressure from P_1 to P_2, the change in reversible potential (ΔV_p) is given by:

$$\Delta V_p = \frac{RT}{2F} \ln \frac{P_{1,a}}{P_{2,a}} + \frac{RT}{2F} \ln \frac{P_{2,c}^{3/2}}{P_{1,c}^{3/2}} \tag{4-11}$$

where the subscripts a and c refer to the anode and cathode, respectively. In a MCFC with the anode and cathode compartments at the same pressure (i.e., $P_1 = P_{1,a} = P_{1,c}$ and $P_2 = P_{2,a} = P_{2,c}$):

$$\Delta V_p = \frac{RT}{2F} \ln \frac{P_1}{P_2} + \frac{RT}{2F} \ln \frac{P_2^{3/2}}{P_1^{3/2}} = \frac{RT}{4F} \ln \frac{P_2}{P_1} \tag{4-12}$$

At 650°C,

$$\Delta V_p \text{ (mV)} = 20 \ln \frac{P_2}{P_1} = \left[46 \log \frac{P_2}{P_1} \right] \tag{4-13}$$

Thus, a ten-fold increase in cell pressure corresponds to an increase of 46 mV in the reversible cell potential at 650°C.

Increasing the operating pressure of MCFCs results in enhanced cell voltages because of the increase in the partial pressure of the reactants, increase in gas solubilities, and the increase in mass transport rates. Opposing the benefits of increased pressure are the effects of pressure on undesirable side reactions such as carbon deposition (Boudouard reaction):

$$2CO \rightarrow C + CO_2 \tag{4-14}$$

and methane formation (methanation),

$$CO + 3H_2 \rightarrow CH_4 + H_2O \tag{4-15}$$

In addition, decomposition of CH_4 to carbon and H_2 is possible,

$$CH_4 \rightarrow C + 2H_2 \tag{4-16}$$

but this reaction is suppressed at higher pressure. According to the Le Chatelier principle, an increase in pressure will favor carbon deposition by Equation 4-14[g] and methane formation by Equations 4-15 and 4-16. The water-gas shift reaction[h],

$$CO_2 + H_2 \rightleftharpoons CO + H_2O \qquad (4\text{-}17)$$

is not expected to be affected significantly by an increase in pressure because the number of moles of gaseous reactants and products in the reaction is identical. Carbon deposition in a MCFC is to be avoided because it can lead to plugging of the gas passages in the anode. Methane formation is detrimental to cell performance because the formation of each mole consumes three moles of H_2, which represents a considerable loss of reactant and would reduce the power plant efficiency.

The addition of H_2O and CO_2 to the fuel gas modifies the equilibrium gas composition so that the formation of CH_4 is minimized. Carbon deposition can be avoided by increasing the partial pressure of H_2O in the gas stream. The measurements (17) on 10 cm x 10 cm cells at 650°C using simulated gasified coal GF-1 (38% H_2/56% CO/6% CO_2) at 10 atm showed that only a small amount of CH_4 is formed. At open circuit, 1.4 vol% CH_4 (dry gas basis) was detected, and at fuel utilizations of 50 to 85%, 1.2 to 0.5% CH_4 was measured. The experiments with a high CO fuel gas (GF-1) at 10 atm and humidified at 163°C, showed no indication of carbon deposition in a subscale MCFC. These studies indicated that CH_4 formation and carbon deposition at the anodes in an MCFC operating on coal derived fuels can be controlled, and under these conditions, the side reactions would have little influence on power plant efficiency.

Figure 4-5 shows the effect of pressure (3, 5, and 10 atm) and oxidant composition (3.2% CO_2/23.2% O_2/66.3% N_2/7.3% H_2O and 18.2% CO_2/9.2% O_2/65.3% N_2/7.3% H_2O) on the performance of 70.5 cm^2 MCFCs at 650°C (46). The major difference in the results that occurs as the CO_2 pressure changes is the change in the open circuit potential, which increases with an increase in cell pressure and CO_2 content (see Equation 4-11). At 160 mA/cm^2, ΔV_p is -44 mV for a pressure change from 3 to 10 atm for both oxidant compositions.

Since ΔV_p is a function of the total gas pressure, the gas compositions in Figure 4-5 have little influence on ΔV_p. Based on these results the effect of cell voltage from a change in pressure can be expressed by the equation:

$$\Delta V_p\ (mV) = 84 \log \frac{P_2}{P_1} \qquad (4\text{-}18)$$

where P_1 and P_2 are different cell pressures. Another analysis by Benjamin et al (47) suggests that a coefficient less than 85 may be more applicable. The change in voltage as a function of pressure change was defined as:

$$\Delta V_p\ (mV) = 76.5 \log \frac{P_2}{P_1} \qquad (4\text{-}19)$$

---

[g] Data from translation of Russian literature (44) indicate the equilibrium constant is almost independent of pressure.

[h] Data from translation of Russian literature (45) indicate the equilibrium constant K is a function of pressure. In relative terms, if K (627°C) = 1 at 1 atm, it decreases to 0.74K at 500 atm and 0.60K at 1000 atm. At the operating pressures of the MCFC, the equilibrium constant can be considered invariant with pressure.

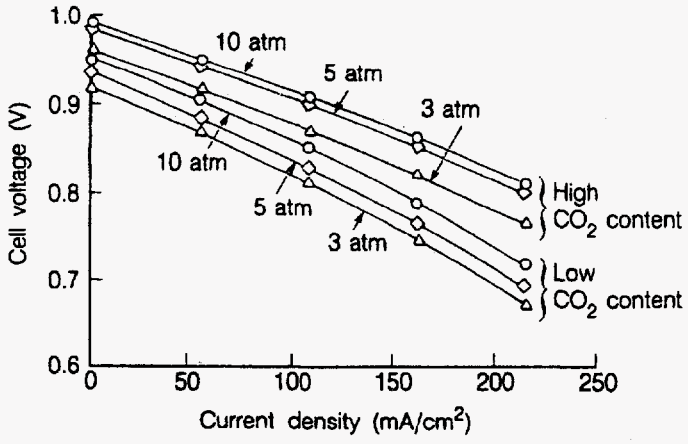

Figure 4-5 The influence of cell pressure on the performance of a 70.5 cm^2 MCFC at 650°C. Anode gas, not specified; cathode gases, 23.2% O_2/3.2% CO_2/66.3% N_2/7.3% H_2O and 9.2% O_2/18.2% CO_2/65.3% N_2/7.3% H_2O; 50% CO_2 utilization at 215 mA/cm^2. *Source:* (Figure 4, p. 395) H.R. Kunz and L.A. Murphy, in *Proceedings of the Symposium on Electrochemical Modeling of Battery, Fuel Cell, and Photoenergy Conversion Systems,* Edited by J. R. Selman and H. C. Maru, The Electrochemical Society, Inc., Pennington, NJ, 1986.

This equation was based on a load of 160 mA/cm^2 at a temperature of 650°C. It was also found to be valid for a wide range of fuels and for a pressure range of 1 atm $\leq$ P $\leq$ 10 atm. Recent results (48) verify the use of this coefficient. Figure 4-6 shows the influence of pressure change on voltage gain for three different stack sizes. These values are for a temperature of 650°C and a constant current density of 150 mA/cm^2 at a fuel utilization of 70%. The line which corresponds to a coefficient of 76.5 falls approximately in the middle of these values. Further improvements in cell performance will lead to changes in the logarithmic coefficient. Additional data (49, 50, 51) indicate that the coefficient may indeed be less than 76.5, but Equation 4-19 appears to be a good indication of the effects of pressure change on performance.

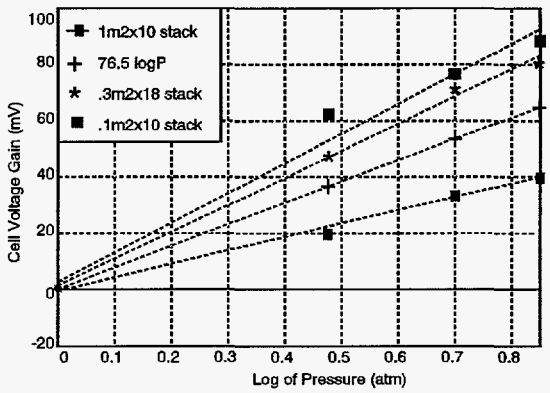

Figure 4-6 Influence of pressure on voltage gain.
Source: Research and Development on Fuel Cell Power Generation Technology FY1990 Annual Report, NEDO, April 1990.

4.2.2 Effect of Temperature

The influence of temperature on the reversible potential of MCFCs depends on several factors, one of which involves the equilibrium composition of the fuel gas.[i] The water gas shift reaction achieves rapid equilibrium[j] at the anode in MCFCs, and consequently CO serves as an indirect source of H_2. The equilibrium constant (K),

$$K = \frac{P_{CO}\ P_{H_2O}}{P_{H_2} P_{CO_2}} \tag{4-20}$$

increases with temperature (see Table 4-4 and Appendix 9.3), and the equilibrium composition changes with temperature and utilization to affect the cell voltage.

The influence of temperature on the voltage of MCFCs is illustrated by the following example. Consider a cell with an oxidant gas mixture of 30% O_2/60% CO_2/10% N_2, and a fuel gas mixture of 80% H_2/20% CO_2. When the fuel gas is saturated with H_2O vapor at 25°C, its composition becomes 77.5% H_2/19.4% CO_2/3.1% H_2O. After considering the equilibrium established by the water gas shift reaction (Equation 4-17), the equilibrium concentrations can be calculated (see also Appendix 9.2) using Equation 4-20 and the equilibrium constant; see for instance, Broers and Treijtel (55). The equilibrium concentrations are substituted into Equation 4-4 to determine E as a function of T.

Table 4-4 Equilibrium Composition of Fuel Gas and Reversible Cell Potential as a Function of Temperature

Parameter[a]	Temperature (°K)		
	800	900	1000
P_{H_2}	0.669	0.649	0.643
P_{CO_2}	0.088	0.068	0.053
P_{CO}	0.106	0.126	0.141
P_{H_2O}	0.137	0.157	0.172
E[b] (V)	1.155	1.143	1.133
K[c]	0.2474	0.4538	0.7273

[a] P is the partial pressure computed from the water gas shift equilibrium of inlet gas with composition 77.5% H_2/19.4% CO_2/3.1% H_2O at 1 atm.
[b] Cell potential calculated using Nernst equation and cathode gas composition of 30% O_2/60% Co_2/10% N_2.
[c] Equilibrium constant for water gas shift reaction from Reference 52.

---

[i] For a fixed gas composition of H_2, H_2O, CO, CO_2 and CH_4 there is a temperature, T_b, below which the exothermic Boudouard reaction is thermodynamically favored, and a temperature, T_m, above which carbon formation by the endothermic decomposition of CH_4 is thermodynamically favored; more extensive details on carbon deposition are found elsewhere (17, 52, 53 54).

[j] The dependence of equilibrium constant on temperature for carbon deposition, methanation and water gas shift reactions is presented in Appendix 9.3.

The results of these calculations are presented in Table 4-4. Inspection of the result shows a change in the equilibrium gas composition with temperature. The partial pressures of CO and H_2O increase at higher T because of the dependence of K on T. The result of the change in gas composition, and the decrease in E° with increasing T, is that E decreases with an increase in T. In an operating cell, the polarization is lower at higher temperatures, and the net result is that a higher cell voltage is obtained at elevated temperatures. The electrode potential measurements (9) in a 3 cm^2 cell[k] show that the polarization at the cathode is greater than at the anode, and that the polarization is reduced more significantly at the cathode with an increase in temperature. At a current density of 160 mA/cm^2, cathode polarization is reduced by about 160 mV when the temperature increases from 550 to 650°C, whereas the corresponding reduction in anode polarization is only about 9 mV (between 600 and 650°C, no significant difference in polarization is observed at the anode).

Baker et al. (56) investigated the effect of temperature (575 to 650°C) on the initial performance of small cells (8.5 cm^2). With steam reformed natural gas as the fuel and 30% CO_2/70% air as the oxidant, the cell voltage[l] at 200 mA/cm^2 decreased by 1.4 mV/°C for a reduction in temperature from 650 to 600°C, and 2.2 mV/°C for a decrease from 600 to 575°C. In the temperature range 650 to 700°C data analysis (51) indicates a relationship of 0.25 mV/°C. The following equations summarize these results.

$$\Delta V_T\ (mV) = 2.16\ (T_2 - T_1) \qquad 575°C \leq T < 600°C \qquad (4\text{-}21)$$

$$\Delta V_T\ (mV) = 1.40\ (T_2 - T_1) \qquad 600°C \leq T < 650°C \qquad (4\text{-}22)$$

$$\Delta V_T\ (mV) = 0.25\ (T_2 - T_1) \qquad 650°C < T \leq 700°C \qquad (4\text{-}23)$$

The two major contributors responsible for the change in cell voltage with temperature are the ohmic polarization and electrode polarization. It appears that in the temperature range of 575 to 650°C, about 1/3 of the total change in cell voltage with decreasing temperature is due to an increase in ohmic polarization, and the remainder from electrode polarization at the anode and cathode. Most MCFC stacks currently operate at an average temperature of 650°C. Most carbonates do not remain molten below 520°C and, as can be seen by the previous equations, cell performance is enhanced by increasing temperature. Beyond 650°C, however, there are diminishing gains with increased temperature. In addition, there is increased electrolyte loss from evaporation and increased material corrosion. An operating temperature of 650°C thus offers an optimization of high performance and stack life.

4.2.3 Effect of Reactant Gas Composition and Utilization

The voltage of MCFC's varies with the composition of the reactant gases. The effect of reactant gas partial pressure, however, is somewhat difficult to analyze. One reason involves the water gas shift reaction at the anode due to the presence of CO. The other reason is related to the consumption of both CO_2 and O_2 at the cathode. Data (48, 57, 58, 59) show that increasing the reactant gas utilization generally decreases cell performance.

---

[k] Electrolyte is 55 wt% carbonate eutectic (57 wt% Li_2CO_3, 31 wt% Na_2CO_3, 12 wt% K_2CO_3) and 45 wt% $LiA1O_2$, anode is Co + 10% Cr, cathode is NiO, fuel is 80% H_2/20% CO_2 and oxidant is 30% CO_2/70% air.

[l] Cell was operated at constant flow rate, thus the utilization changes with current density.

As reactant gases are consumed in an operating cell, the cell voltage decreases in response to the polarization (i.e., activation, concentration) and to the changing gas composition (see discussion in Section 2). These effects are related to the partial pressures of the reactant gases.

Oxidant: The electrochemical reaction at the cathode involves the consumption of two moles CO_2 per mole O_2 (see Equation 4-2), and this ratio provides the optimum cathode performance. The influence of the $[CO_2]/[O_2]$ ratio on cathode performance is illustrated in Figure 4-7 (42). As this ratio decreases, the cathode performance decreases, and a limiting current is discernible. In the limit, where no CO_2 is present in the oxidant feed, the equilibrium, involving the dissociation of carbonate ions becomes important.

$$CO_3^= \rightleftharpoons CO_2 + O^= \qquad (4\text{-}24)$$

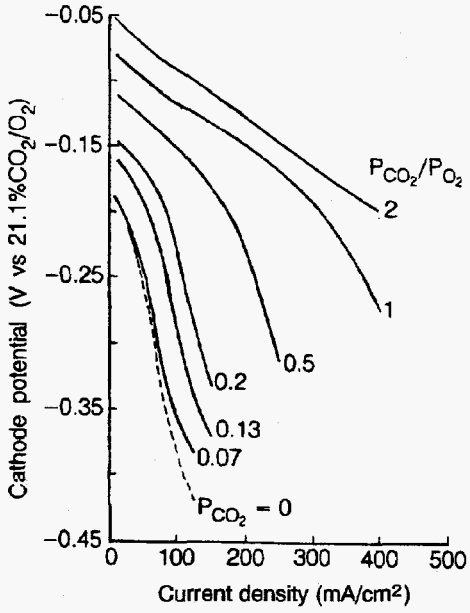

Figure 4-7 The effect of CO_2/O_2 ratio on cathode performance in a MCFC. Oxygen pressure is 0.15 atm.
Source: (Figure 5-10, p. 5-20) "Development of Improved Molten Carbonate Fuel Cell Technology," final report prepared by United Technologies Corp. for the Electric Power Research Institute under Contract #RP1085-4, July 1983.

Under these conditions the cathode performance shows the greatest polarization because of the composition changes that occur in the electrolyte. The change in the average cell voltage of a ten cell stack as a function of oxidant utilization is illustrated in Figure 4-8. In this stack, the average cell voltage at 172 mA/cm^2 decreases by about 30 mV for a 30 percentage points increase

in oxidant (20 to 50%) utilization. Based on this additional data (48, 57, 58), the voltage loss due to a change in oxidant utilization can be described by the following equations:

$$\Delta V_{cathode}\ (mV) = 250 \log \frac{\left[\bar{P}_{CO_2}\ \bar{P}_{O_2}^{\frac{1}{2}}\right]_2}{\left[\bar{P}_{CO_2}\ \bar{P}_{O_2}^{\frac{1}{2}}\right]_1} \qquad \text{for } 0.04 \leq \left[\bar{P}_{CO_2}\ \bar{P}_{O_2}^{\frac{1}{2}}\right] \leq 0.11 \qquad (4\text{-}25)$$

$$\Delta V_{cathode}\ (mV) = 99 \log \frac{\left[\bar{P}_{CO_2}\ \bar{P}_{O_2}^{\frac{1}{2}}\right]_2}{\left[\bar{P}_{CO_2}\ \bar{P}_{O_2}^{\frac{1}{2}}\right]_1} \qquad \text{for } 0.11 < \left[\bar{P}_{CO_2}\ \bar{P}_{O_2}^{\frac{1}{2}}\right] \leq 0.38 \qquad (4\text{-}26)$$

where the $\bar{P}_{CO_2}$ and $\bar{P}_{O_2}$ are the average partial pressures of CO_2 and O_2 in the system.

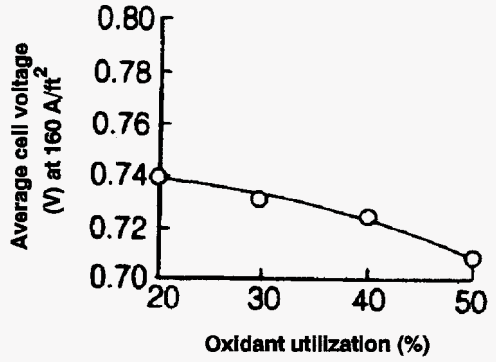

Figure 4-8 Influence of reactant gas utilization on the average cell voltage of a MCFC stack. *Source:* (Figure 4-21, p. 4-24) J. M. King, A. P. Meyer, C. A. Reiser and C. R. Schroll, "Molten Carbonate Fuel Cell System Verification and Scale-up," EM-4129, final report prepared by United Technologies Corp. for the Electric Power Research Institute, Research Project 1273-1, July 1985.

Fuel: The data in Table 4-5 from Lu and Selman (60) illustrate the dependence of the anode potential on the composition of five typical fuel gases and two chemical equilibria occurring in the anode compartment.[m] The calculations show the gas compositions and open circuit anode potentials obtained after equilibria by the water gas shift and CH_4 steam reforming reactions are considered. The open circuit anode potential calculated for the gas compositions after equilibration, and experimentally measured, are presented in Table 4-5. The equilibrium gas compositions obtained by the shift and steam reforming reactions clearly show that, in general, the H_2 and CO_2 contents in the dry gas decrease, and CH_4 and CO are present in the equilibrated gases. The anode potential varies as a function of the $[H_2]/[H_2O][CO_2]$ ratio; a higher potential is obtained when this ratio is higher. The results show that the measured potentials are in good agreement with

[m] No gas phase equilibrium exists between O_2 and CO_2 in the oxidant gas which could alter the composition or cathode potential.

the values calculated, assuming simultaneous equilibria of the shift and the steam reforming reactions reach equilibrium rapidly in the anode compartments of MCFCs.

Table 4-5 Influence of Fuel Gas Composition on Reversible Anode Potential at 650°C

Typical Fuel Gas[a]	Gas Composition (mole fraction) H_2	H_2O	CO	CO_2	CH_4	N_2	$-E^b$ (mV)
Dry gas							
High Btu (53°C)	0.80	-	-	0.20	-	-	1116±3[c]
Intermed. Btu (71°C)	0.74	-	-	0.26	-	-	1071±2[c]
Low Btu 1 (71°C)	0.213	-	0.193	0.104	0.011	0.479	1062±3[c]
Low Btu 2 (60°C)	0.402	-	-	0.399	-	0.199	1030±[c]
Very low Btu (60°C)	0.202	-	-	0.196	-	0.602	1040±[c]
Shift equilibrium							
High Btu (53°C)	0.591	0.237	0.096	0.076	-	-	1122[d]
Intermed. Btu (71°C)	0.439	0.385	0.065	0.112	-	-	1075[d]
Low Btu 1 (71°C)	0.215	0.250	0.062	0.141	0.008	0.326	1054[d]
Low Btu 2 (60°C)	0.231	0.288	0.093	0.228	-	0.160	1032[d]
Very low Btu (60°C)	0.128	0.230	0.035	0.123	-	0.484	1042[d]
Shift and Steam Steam-reforming							
High Btu (53°C)	0.555	0.267	0.082	0.077	0.020	-	1113[d]
Intermed. Btu (71°C)	0.428	0.394	0.062	0.112	0.005	-	1073[d]
Low Btu 1 (71°C)	0.230	0.241	0.067	0.138	0.001	0.322	1059[d]
Low Btu 2 (60°C)	0.227	0.290	0.092	0.229	0.001	0.161	1031[d]
Very low Btu (60°C)	0.127	0.230	0.035	0.123	0.0001	0.485	1042[d]

[a] Temperature in parenthesis is the humidification temperature
[b] Anode potential with respect to 33% O_2/67% CO_2 reference electrode
[c] Measured anode potential
[d] Calculated anode potential, taking into account the equilibrated gas composition

Source: (Table 1, p. 385) S. H. Lu and J. R. Shelman, in *Proceedings of the Symposium on Molten Carbonate Fuel Cell Technology,* Edited by J. R. Selman and T. D. Claar, The Electrochemical Society, Inc., Pennington, NJ, 1984.

Considering the Nernst equation further, an analysis shows that the maximum cell potential, for a given fuel gas composition, is obtained when $[CO_2]/[O_2] = 2$. Furthermore, the addition of inert gases to the cathode, for a given $[CO_2]/[O_2]$ ratio, causes a decrease in the reversible potential. On the other hand, the addition of inert gases to the anode increases the reversible potential, for a given $[H_2]/[H_2O][CO_2]$ ratio and oxidant composition. This latter result occurs because two moles of products are diluted for every mole of H_2 reactant. However, the addition of inert gases to either gas stream in an operating cell can lead to an increase in concentration polarization.

Figure 4-9 depicts an average voltage loss for the stack of about 30 mV for a 30% increase in fuel utilization (30 to 60%). This and other data (59) suggests that the voltage loss due to a change in fuel utilization can be described by the following equation:

$$\Delta V_{anode}\ (mV) = 173 \log \frac{\left(\bar{P}_{H_2}/\bar{P}_{CO_2}\bar{P}_{H_2O}\right)_2}{\left(\bar{P}_{H_2}/\bar{P}_{CO_2}\bar{P}_{H_2O}\right)_1} \qquad (4\text{-}27)$$

where $\bar{P}_{H_2}$, $\bar{P}_{CO_2}$, and $\bar{P}_{H_2O}$ are the average partial pressures of H_2, CO_2 and O_2 in the system.

The above discussion implies that MCFCs should be operated at low reactant gas utilizations to maintain voltage levels, but doing this means inefficient fuel use. As with other fuel cell types, a compromise must be made to optimize overall performance. Typical utilizations are 75 to 85% of the fuel and 50% for the oxidant.

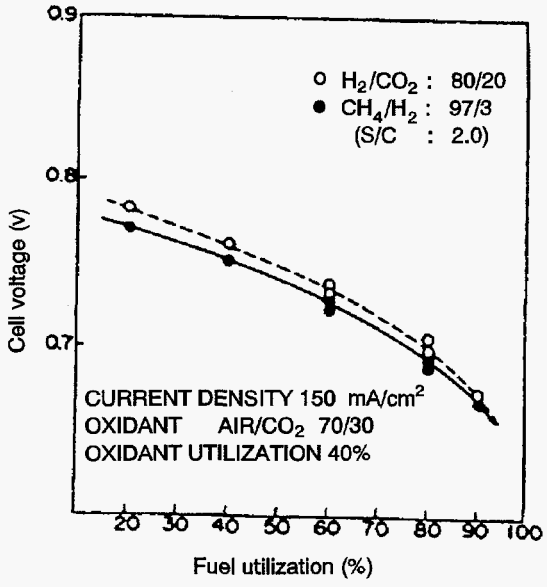

Figure 4-9 Dependence of cell voltage on fuel utilization.
Source: T. Tanaka et.al., "Research on On-Site Internal-Reforming Molten Carbonate Fuel Cell", 1989 International Gas Research Conference, Pg 252, 1989.

4.2.4 Effect of Impurities

Gasified coal is expected to be the major source of fuel gas for MCFCs, but because coal contains many contaminants in a wide range of concentrations, fuel derived from this source also contains a considerable amount of contaminants.[n] A critical concern with these contaminants is the concentration levels that can be tolerated by MCFCs without suffering significant degradation in performance or reduction in cell life. A list of some possible effects of contaminants from coal derived fuel gases on MCFCs is summarized in Table 4-6 (61).

Table 4-6 Contaminants from Coal Derived Fuel Gas and Their Potential Effect on MCFCs

Class	Contaminant	Potential Effect
Particulates	Coal fines, ash	• Plugging of gas passages
Sulfur compounds	H_2S, COS, CS_2, C_4H_4S	• Voltage losses • Reaction with electrolyte via SO_2
Halides	HCl, HF, HBr, $SnCl_2$	• Corrosion • Reaction with electrolyte
Nitrogen compounds	NH_3, HCN, N_2	• Reaction with electrolyte via NO_x
Trace metals	As, Pb, Hg, Cd, Sn Zn, H_2Se, H_2Te, AsH_3	• Deposits on electrode • Reaction with electrolyte
Hydrocarbons	C_6H_6, $C_{10}H_8$, $C_{14}H_{10}$	• Carbon deposition

Source: (Table 1, p. 299) G. L. Anderson and P. C. Garrigan, in *Proceedings of the Symposium on Molten Carbonate Fuel Cell Technology,* Edited by J. R. Selman and T. D. Claar, The Electrochemical Society, Inc., Pennington, NJ (1984).

The typical fuel gas composition and contaminants from an air blown gasifier, which enter the MCFC at 650°C after hot gas cleanup, and the tolerance level of MCFCs to these contaminants are listed in Table 4-7 (51, 62, 63). It is apparent from this example that a wide spectrum of contaminants is present in coal derived fuel gas. The removal of these contaminants can add considerably to the efficiency. A review of various options for gas cleanup is presented by Anderson and Garrigan (61) and Jalan et al. (64).

Sulfur: It is now well established that sulfur compounds in low ppm (parts per million) concentrations in fuel gas are detrimental to MCFCs (65-69). The tolerance of MCFCs to sulfur compounds (65) is strongly dependent on temperature, pressure, gas composition, cell components and system operation (i.e., recycle, venting, gas cleanup). The principal sulfur compound that has an adverse affect on cell performance is H_2S. At atmospheric pressure and high gas utilization (~75%, < 10 ppm H_2S (tolerance level depends on anode gas composition and partial pressure of H_2) in the fuel can be tolerated at the anode, and < 1 ppm SO_2 is acceptable in the oxidant (65).

[n] Table 9.2 for contaminant levels found in fuel gases from various coal gasification processes.

These concentration limits increase when the temperature increases, but they decrease at increasing pressures.

Table 4-7 Typical Gas Composition and Contaminants from Air Blown Coal Gasifier After Hot Gas Cleanup, and Tolerance Limit of MCFCs to Contaminants

Fuel Gas[a] (mol%)	Contaminants[b,c]	Content[b,c]	Remarks[b]	Tolerance[c,d] Limit
19.2 CO	Particulates	<0.5 mg/l	also includes ZnO from H_2S cleanup stage	<0.1 g/l for large particulates >0.3 μm
13.3 H_2	NH_3	2600 ppm		<10,000ppm
2.6 CH_4	AsH_3	<5 ppm		< 1 ppm
6.1 CO_2	H_2S	<10 ppm	After first-stage cleanup	<0.5 ppm
12.9 H_2O	HCl	500 ppm	Also includes other halides	<10 ppm
45.8 N_2	Trace Metals	<2 ppm <2 ppm <2 ppm <2 ppm	Pb Cd Hg Sn	<1 ppm 30+ ppm 35+ ppm NA
	Zn	<50 ppm	From H_2S hot cleanup	<20 ppm
	Tar	4000 ppm	Formed during desulfurization cleanup stage	<2000 ppm[e]

[a]Humidified fuel gas enters MCFC at 650°C
[b](Table 1, p. 177) A. Pigeaud, in *Proceedings of the Sixth Annual Contractors Meeting on Contaminant Control in Coal-Derived Gas Streams*, DOE/METC-86/6042, Edited by K.E. Markel and D.C. Cicero, U.S. Department of Energy, Morgantown, WV, July, 1986.
[c]M.C. Williams and D.A. Berry, "Overview of the DOE-Funded Fuel Cell Contaminants R&D Program", 1990 Fuel Cell Seminar Program and Abstracts, 1990.
[d]A. Pigeaud, Progress Report prepared by Energy Research Corporation for the U.S. Department of Energy, Morgantown, WV under Contract No. DE-AC21-84MC21154, June 1987.
[e]Benzene

The mechanisms by which H_2S affects cell performance has been investigated extensively (66-69). The adverse affects of H_2S occur because of:

- chemisorption on Ni surfaces to block active electrochemical sites
- poisoning of catalytic reaction sites for the water gas shift reaction
- oxidation to SO_2 in a combustion reaction, and subsequent reaction with carbonate ions in the electrolyte.

The adverse effect of H_2S on the performance of MCFCs is illustrated in Figure 4-10. The cell voltage of a 10 cm x 10 cm cell at 650°C decreases when 5 ppm H_2S is added to the fuel gas (10% H_2/5% CO_2/10% H_2O/75% He), and current is drawn from the cell. The measurements indicate that low concentrations of H_2S do not affect the open circuit potential, but they have a major impact on the cell voltage as the current density is progressively increased. The decrease in cell voltage is not permanent;[o] when fuel gas without H_2S is introduced into the cell, the cell voltage returns to the level for a cell with clean fuel. These results can be explained by the chemical and electrochemical reactions that occur involving H_2S and $S^=$. A nickel anode at anodic potentials reacts with H_2S to form nickel sulfide:

$$H_2S + CO_2^= \rightarrow H_2O + CO_2 + S^= \quad (4\text{-}28)$$

followed by,

$$Ni + xS^= \rightarrow NiS_x + 2xe^- \quad (4\text{-}29)$$

When the sulfided anode returns to open circuit, the NiS_x is reduced by H_2:

$$NiS_x + xH_2 \rightarrow Ni + xH_2S \quad (4\text{-}30)$$

Similarly when a fuel gas without H_2S is introduced to a sulfided anode, reduction of NiS_x to Ni can also occur. Detailed discussions on the effect of H_2S on cell performance is presented by Vogel and co-workers (66, 67) and Remick (68, 69).

The rapid equilibration of the water gas shift reaction in the anode compartment provides an indirect source of H_2 by the reaction of CO and H_2O. If H_2S poisons the active sites for the shift reaction, this equilibrium might not be established in the cell, and a lower H_2 content than predicted would be expected. Fortunately, the evidence (68, 69) indicates that the shift reaction is not significantly poisoned by H_2S. In fact, Cr used in stabilized-Ni anodes appears to act as a sulfur tolerant catalyst for the water gas shift reaction (69).

The CO_2 required for the cathode reaction is expected to be supplied by recycling the anode gas exhaust (after combustion of the residual H_2) to the cathode. Therefore, any sulfur in the anode effluent will be present at the cathode inlet unless provisions are made for sulfur removal. In the absence of a sulfur removal scheme, sulfur enters the cathode inlet as SO_2, which reacts quantitatively (equilibrium constant is 10^{15} to 10^{17}) with carbonate ions to produce alkali sulfates. these sulfate ions are transported through the electrolyte structure to the anode during cell operation. At the anode, $SO_4^=$ is reduced to $S^=$, thus increasing the concentration of $S^=$ there.

[o]The effects of H_2S on cell voltage is reversible if H_2S concentrations are present at levels below that required to form nicket sulfide.

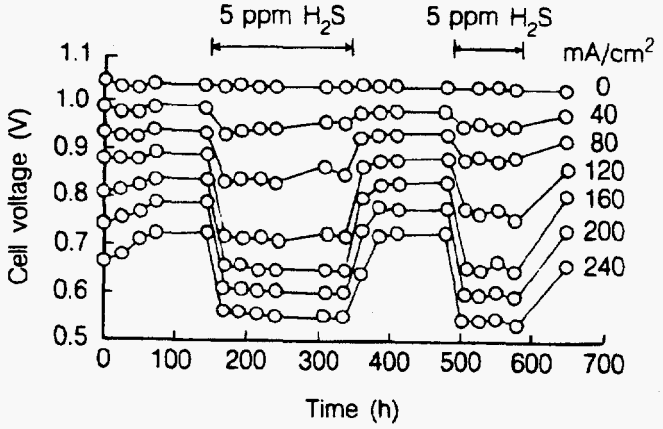

Figure 4-10 Influence of 5 ppm H_2S on the performance of a bench scale MCFC (10 cm x 10 cm) at 650°C, fuel gas (10% H_2/5% CO_2/10% H_2O/75% He) at 25% H_2 utilization. *Source:* (Figure 4, p 443) R.J. Remick, in Proceedings of the Fourth Annual Contractors Meeting on Containment Control in Hot Coal-Derived Gas Streams, DOE/METC-85/3, Edited by K.E. Markel, U.S. Department of Energy, Morgantown, WV, May 1984.

Based on the present understanding of the effect of sulfur on MCFCs, and with the available cell components, it is projected that long term operation (40,000 hr) of MCFCs may require fuel gases with sulfur[p] levels of the order 0.01 ppm or less, unless the system is purged of sulfur at periodic intervals or sulfur is scrubbed from the cell burner loop (67). Sulfur tolerance would be approximately 0.5 ppm (see Table 4-3) in the latter case. Considerable effort has been devoted to develop low cost techniques for sulfur removal, and research and development are continuing (70, 71).

Halides: Halogen containing compounds are destructive to MCFCs because they can lead to severe corrosion of cathode hardware. Thermodynamic calculations (72) show that HCl and HF react with molten carbonates (Li_2CO_3 and K_2CO_3) to form CO_2, H_2O and the respective alkali halides. Furthermore, the rate of electrolyte loss in the cell is expected to increase because of the high vapor pressure of LiCl and KCl. The concentration of Cl^- species in coal derived fuels is typically in the range 1 to 500 ppm. It has been suggested (73) that the level of HCl should be kept below 1 ppm in the fuel gas, perhaps below the level of 0.5 ppm (41), but the tolerable level for long term operation has not been established.

***Nitrogen Compounds*:** Compounds such as NH_3 and HCN do not appear to be harmful to MCFCs (61, 74). However, if NO_x is produced by combustion of the anode effluent in the cell burner loop, it could react irreversibly with the electrolyte in the cathode compartment to form nitrate salts. The projection by Gillis (75) for the NH_3 tolerance level of MCFCs was 0.1 ppm (see Table 4-6), but Table 4-3 indicates that the level could be increased to 1 vol% (41).

---

[p] Both COS and CS_2 appear to be equivalent to H_2S in their effect on MCFCs (67).

Solid Particulates: These contaminants can originate from a variety of sources, and their presence is a major concern because they can block gas passages and/or the anode surface. Carbon deposition, and conditions which can be used to control its formation, has been discussed earlier in this section. Solid particles such as ZnO, which is used for sulfur removal, can be entrained in the fuel gas leaving the desulfurizer. The results by Pigeaud (63) indicate that the tolerance limit of MCFCs to particulates larger than 3 μm diameter is <0.1 g/l.

Other Compounds: Experimental studies indicate that 1 ppm As from gaseous AsH_3 in fuel gas does not affect cell performance, but when the level is increased to 9 ppm As, the cell voltage drops rapidly by about 120 mV at 160 mA/cm^2 (62). Trace metals, such as Pb, Cd, Hg and Sn in the fuel gas, are of concern because they can deposit on the electrode surface or react with the electrolyte (12). Table 4-3 addresses limits of these trace metals.

4.2.5 Effects of Current Density

The voltage output from an MCFC is reduced by ohmic, activation, and concentration losses which increase with increasing current density. The major loss over the range of current densities of interest is the linear iR loss. The magnitude of this loss (iR) can be described by the following equations (57, 76, 77):

$$\Delta V_J(mV) = -1.21\Delta J \qquad \text{for } 50 \leq J \leq 150 \qquad (4\text{-}31)$$

$$\Delta V_J(mV) = -1.76\Delta J \qquad \text{for } 150 \leq J \leq 200 \qquad (4\text{-}32)$$

where J is the current density (mA/cm^2) at which the cell is operating.

4.2.6 Effects of Cell Life

Endurance of the cell stack is a critical issue in the commercialization of MCFCs. Adequate cell performance must be maintained over the desired length of service, quoted by one MCFC developer as 2mV/1000 hours over a cell stack lifetime of 40,000 hours (38). Current state-of-the-art MCFCs (48, 57, 59, 78, 79) depict an average degradation over time of:

$$\Delta V_{lifetime}(mV) = -5mV/1000 \text{ hours} \qquad (4\text{-}33)$$

4.2.7 Internal Reforming

In a conventional fuel cell system, a carbonaceous fuel is fed to a fuel processor where it is steam reformed to produce H_2 (as well as other products, CO and CO_2, for example), which is then introduced into the fuel cell and electrochemically oxidized. The internal reforming molten carbonate fuel cell, however, eliminates the need for a separate fuel processor for reforming carbonaceous fuels. This concept appears practical in high temperature fuel cells where the steam reforming reaction[r] can be sustained with catalysts. By closely coupling the reforming reaction and

[r] Steam reforming of CH_4 is typically performed at 750 to 900°C, thus at the lower operating temperature of MCFCs a high activity catalyst is required. Methanol is also a suitable fuel for internal reforming and it does not require an additional catalyst because the Ni-based anode is sufficiently active.

the electrochemical oxidation reaction within the fuel cell, the concept of the internal reforming MCFC is realized. The internal reforming MCFC eliminates the need for the external fuel processor with its ancillary equipment. It was recognized early that the internal reforming MCFC approach provides a highly efficient, simple, reliable and cost effective alternative to the conventional MCFC system (80). Development to date in the U.S. and Japan continues to support this expectation (76, 81).

There are two alternate approaches to internal reforming molten carbonate cells: indirect internal reforming (IIR) and direct internal reforming (DIR). In the first approach, the reformer section is separated, but adjacent to the fuel cell anode. This cell takes advantage of the close coupled thermal benefit where the exothermic heat of the cell reaction can be used for the endothermic reforming reaction. Another advantage is that the reformer and the cell environments don't have a direct physical effect on each other. A disadvantage is that the conversion of methane to hydrogen is not promoted as well as in the direct approach. In the DIR cell, hydrogen consumption reduces its partial pressure, thus driving the methane reforming reaction, Equation 4-28, to the right. Figure 4-11 depicts one developer's approach where IIR and DIR have been combined.

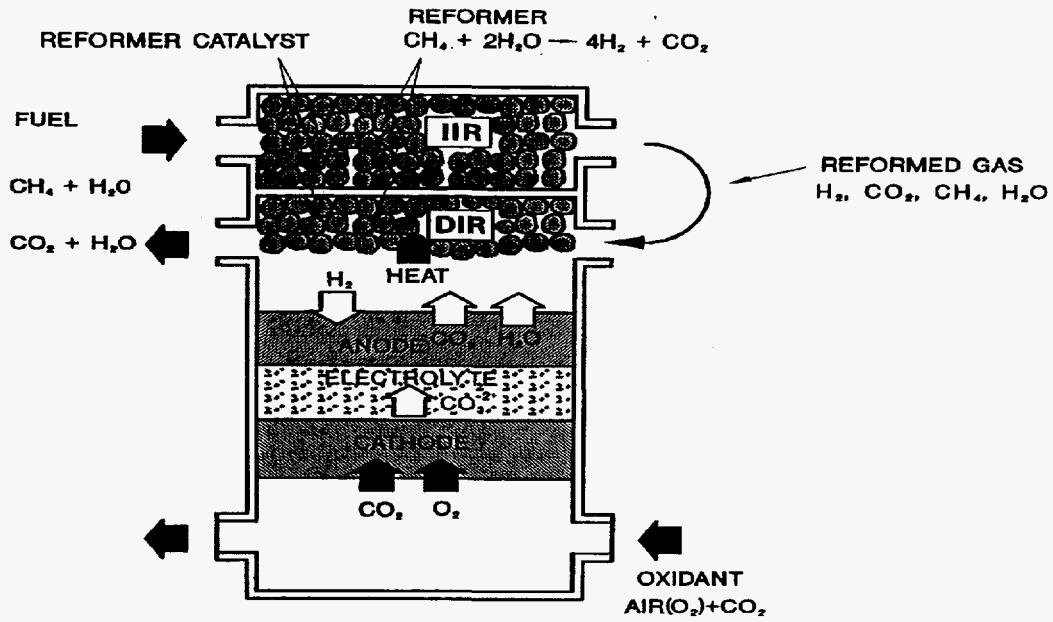

Figure 4-11 Operating concept for the IIR/DIR molten carbonate fuel cell design.
Source: M. Farooque, "Development of Internal Reforming Carbonate Fuel Cell Stack Technology", Final Report, DOE/MC/23274-2941, October, 1991.

Methane is a common fuel utilized in internal reforming MCFCs, where the steam reforming reaction:

$$CH_4 + H_2O \rightarrow CO + 3H_2 \qquad (4\text{-}28)$$

occurs simultaneously with the electrochemical oxidation of hydrogen (see Reaction 4-1) in the anode compartment. The steam reforming reaction is endothermic, with $\Delta H_{650°C}$ = 53.87 kcal/mol

(80), whereas the overall fuel cell reaction is exothermic. In an internal reforming MCFC, the heat required for Reaction 4-28 is supplied by the heat from the fuel cell reaction, thus eliminating the need for external heat exchange which is required by a conventional fuel processor. In addition, the product steam from Reaction 4-1 can be used to enhance the reforming reaction and the water gas shift reaction (Reaction 4-17) to produce additional H_2. The forward direction of Reaction 4-28 is favored by high temperature and low pressure, and thus an internal reforming MCFC is best suited to operate near atmospheric pressure.

A supported Ni catalyst (e.g., Ni supported on MgO or $LiAlO_2$) provides sufficient catalytic activity to sustain the steam reforming reaction at 650°C to produce sufficient H_2 to meet the needs of the fuel cell. The interrelationship between the conversion of CH_4 to H_2 and its utilization in an internal reforming MCFC at 650°C is illustrated in Figure 4-12. At open circuit, about 83% of the CH_4 was converted to H_2, which corresponds closely to the equilibrium concentration at 650°C. When current is drawn from the cell, H_2 is consumed and H_2O is produced, and the conversion of CH_4 increases and approaches 100% at fuel utilizations greater than about 50%. Thus, by appropriate thermal management and adjustment of H_2 utilization with the rate of CH_4 reforming, a similar performance can be obtained in internal reforming MCFC stacks with natural gas and with synthesized reformate gas containing H_2 and CO_2, Figure 4-13. Currently, the concept of internal reforming has been successfully demonstrated for 10,000 hours in 2 to 3 kW stacks and for 250 hours in a 100 kW stack (82). The performance of the 2 kW stack over time can be seen in Figure 4-14 (57).

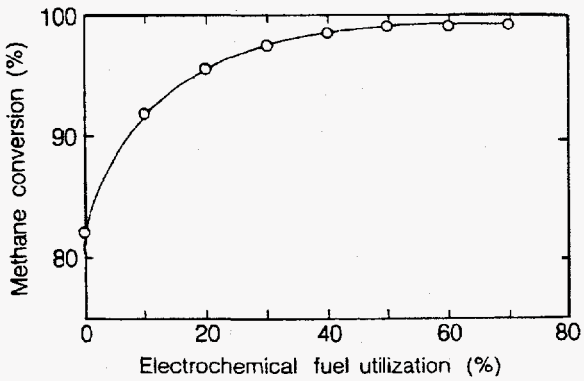

Figure 4-12 Relationship between CH_4 conversion and fuel utilization in an internal reforming MCFC at 650°C and 1 atm. Steam/carbon ratio = 2.5, hydrogen/carbon ratio = 0.1. *Source:* (Figure 3, p. 269) H.C. Maru and B.S. Baker, *Prog. Batteries & Solar Cells*, **5**, 264, 1984.

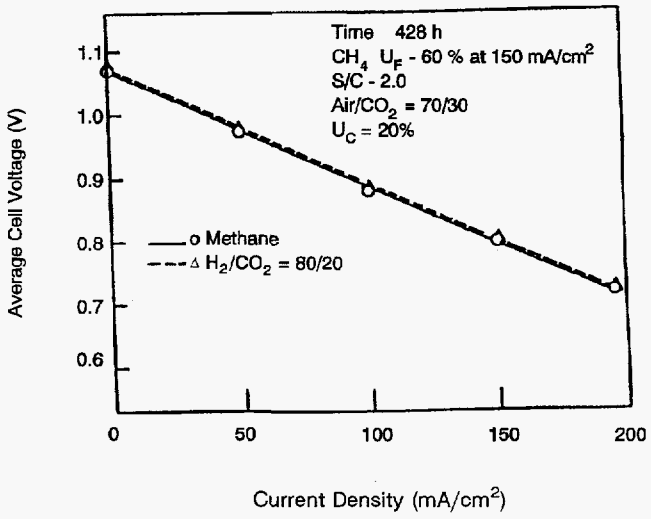

Figure 4-13 Voltage current characteristics of a 3kW, five cell DIR stack with 5,016 cm^2 cells operating on 80/20% H_2/CO_2 and methane.
Source: T. Tanaka, et. al., "Development of Internal Reforming Molten Carbonate Fuel Cell Technology", in *Proceedings of the 25th IECEC*, Vol. 3, American Institute of Chemical Engineers, New York, NY, 1990.

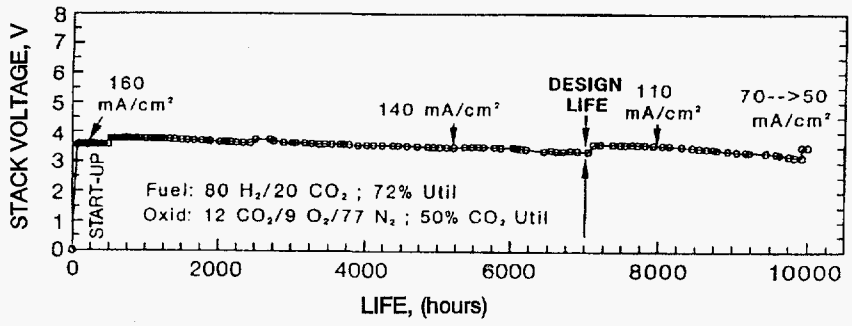

Figure 4-14 Performance data of a 0.37m^2 2 kW internally reformed MCFC stack at 650°C and 1 atm.
Source: M. Farooque, Data from ERC testing, 1992.

4.3 SUMMARY OF EQUATIONS FOR MCFC

The preceding sections provide parametric performance based on various referenced data at different operating conditions. It is suggested that the following set of equations could be used for performance adjustments unless the reader prefers other data or correlations. Figure 4-15 is provided as reference MCFC performance.

Parameter	Equation	Comments	
Pressure	$\Delta V_p(mV) = 76.5 \log \frac{P_2}{P_1}$	$1 \text{ atm} \le P \le 10 \text{ atm}$	(4-19)
Temperature	$\Delta V_T(mV) = 2.16(T_2 - T_1)$	$575°C \le T < 600°C$	(4-21)
	$\Delta V_T(mV) = 1.40(T_2 - T_1)$	$600°C \le T \le 650°C$	(4-22)
	$\Delta V_T(mV) = 0.25(T_2 - T_1)$	$650°C < T \le 700°C$	(4-23)
Oxidant	$\Delta V_{cathode}(mV) = 250 \log \frac{(\bar{P}_{CO_2} \bar{P}^{1/2}_{O_2})_2}{(P_{CO_2} P^{1/2}_{O_2})_1}$	$0.04 \le (\bar{P}_{CO_2} \bar{P}^{1/2}_{O_2}) \le 0.11$	(4-25)
	$\Delta V_{cathode}(mV) = 99 \log \frac{(\bar{P}_{CO_2} \bar{P}^{1/2}_{O_2})_2}{(\bar{P}_{CO_2} \bar{P}^{1/2}_{O_2})_1}$	$0.11 \le (\bar{P}_{CO_2} \bar{P}^{1/2}_{O_2}) \le 0.38$	(4-26)
Fuel	$\Delta V_{anode}(mV) = 173 \log \frac{(\bar{P}_{H_2}/\bar{P}_{CO_2} \bar{P}^{1/2}_{H_2O})_2}{(\bar{P}_{H_2}/\bar{P}_{CO_2} \bar{P}^{1/2}_{O_2})_1}$		(4-27)
Current Density	$\Delta V_J(mV) = -1.21 \Delta J$	$50 \le J \le 150 mA/cm^2$	(4-31)
	$\Delta V_J(mV) = -1.76 \Delta J$	$150 < J \le 200 mA/cm^2$	(4-32)
Life Effects	$\Delta V_{lifetime}(mV) = -5mV/1000 \text{ hours}$		(4-33)

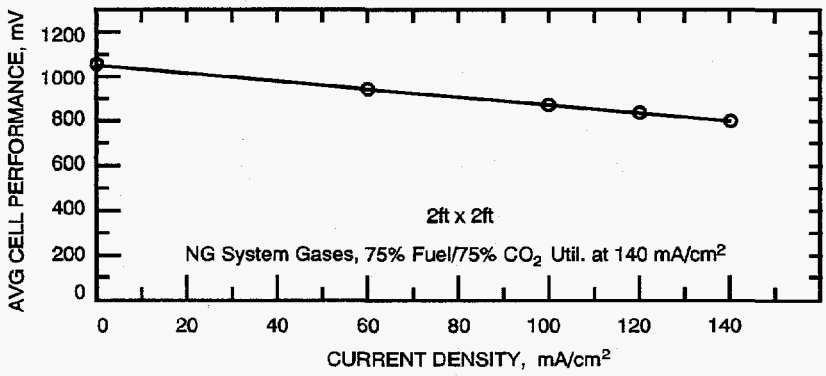

Figure 4-15 Average cell voltage of a $0.37m^2$ 2 kW internally reformed MCFC stack at 650°C and 1 atm. Fuel (100% cell), oxidant (12% CO_2/9% O_2/77% N_2).
Source: M. Farooque, Data from ERC testing, 1992.

References

1. H. C. Maru and L. G. Marianowski, *Extended Abstracts,* Abstract #31, Fall Meeting of the Electrochemical Society, October 17-22, 1976, Las Vegas, NV, p. 82, 1976.
2. J. Mitteldorf and G. Wilemski, *J. Electrochem. Soc.,* **131,** 1784, 1984.
3. R. H. Arendt, *J. Electrochem. Soc.,* **129,** 942, 1982.
4. H. C. Maru, A. Pigeaud, R. Chamberlin and G. Wilemski, in *Proceedings of the Symposium on Electrochemical Modeling of Battery, Fuel Cell, and Photoenergy Conversion Systems,* Edited by J. R. Selman and H. C. Maru, The Electrochemical Society, Inc., Pennington, NJ, p. 398, 1986.
5. H. R. Kunz, *J. Electrochem. Soc.,* **134,** 105, 1987.
6. A. Pigeaud, H. C. Maru, L. Paetsch, J. Doyon and R. Bernard, in *Proceedings of the Symposium on Porous Electrodes: Theory and Practices,* Edited by H. C. Maru, T. Katan and M. G. Klein, The Electrochemical Society, Inc., Pennington, NJ, p. 234, 1984.
7. H. C. Maru, L. Paetsch and A. Pigeaud, in *Proceedings of the Symposium on Molten Carbonate Fuel Cell Technology,* Edited by R. J. Selman and T. D. Claar, The Electrochemical Society, Inc., Pennington, NJ, p. 20, 1984.
8. R. J. Petri and T. G. Benjamin, in *Proceedings of the 21st Intersociety Energy Conversion Engineering Conference,* Volume 2, American Chemical Society, Washington, DC, p. 1156, 1986.
9. R. J. Selman, *Energy,* **11,** 153, 1986.
10. C. E. Baumgartner, V. J. DeCarlo, P. G. Glugla and J. J. Grimaldi, *J. Electrochem. Soc.,* **132,** 57, 1985.
11. P. G. Glugla and V. J. DeCarlo, *J. Electrochem. Soc.,* **129,** 1745, 1982.
12. C. Yuh, M. Farooque, and R. Johnsen, ERC, "Understanding of Carbonate Fuel Cell Resistances in MCFCs", in *Proceedings of the Fourth Annual Fuel Cells Contractors Review Meeting*, U.S. DOE/METC, Pgs. 53 - 57, July, 1992.
13. C. Baumgartner, *J. Electrochem. Soc.,* **131,** 1850, 1984.
14. W. M. Vogel, L. J. Bregoli, H. R. Kunz and S. W. Smith, in *Proceedings of the Symposium on Molten Carbonate Fuel Cell Technology,* Edited by R. J. Selman and T. D. Claar, The Electrochemical Society, Inc., Pennington, NJ, p. 443, 1984.
15. M. L. Orfield and D. A. Shores, in *Corrosion 86,* Paper No. 88, National Association of Corrosion Engineers, Houston, TX, 1986.
16. D. A. Shores, in *Proceedings of the 22nd Intersociety Energy Conversion Engineering Conference,* Volume 2, American Institute of Aeronautics & Astronautics, New York, NY, p. 1023, 1987.
17. "Development of Improved Molten Carbonate Fuel Cell Technology," Final Report prepared by United Technologies Corp. for the Electric Power Research Institute, Palo Alto, CA, under Contract #RP1085-4, July 1983.
18. T. D. Kaun, in *Proceedings of the Fourth International Symposium on Molten Salts,* Edited by M. Blander, D. S. Newman, M. L. Saboungi, G. Mamantov and K. Johnson, The Electrochemical Society, Inc., Pennington, NJ, p. 489, 1984.
19. A. J. Appleby, "Advanced Fuel Cells and Their Future Market," to be published in *Energy Conservation Strategies,* Progress Series, Edited by W. E. Murphy and L. H. Fletcher, American Society of Aeronautics and Astronautics, New York, NY.
20. M. Farooque, ERC, "Development on Internal Reforming Carbonate Fuel Cell Technology, Final Report", prepared for U.S. DOE/METC, DOE/MC/23274-2941, Pgs. 3 - 18, October, 1990.
21. A. Pigeaud, A. J. Skok, P. S. Patel, and H. C. Maru, *Thin Solid Films,* **83,** 1449, 1981.

22. R. A. Donado, L. G. Marianowski, H. C. Maru and J. R. Selman, *J. Electrochem. Soc.,* **131,** 2541, 1984.
23. R. A. Donado, L. G. Marianowski, H. C. Maru and J. R. Selman, *J. Electrochem. Soc.,* **131,** 2535, 1984.
24. R. B. Swaroop, J. W. Sim and K. Kinoshita, *J. Electrochem. Soc.,* **125,** 1799, 1978.
25. H. S. Hsu and J. H. DeVan, *J. Electrochem. Soc.,* **133,** 2077, 1986.
26. D. A. Shores and P. Singh, in *Proceedings of the Symposium on Molten Carbonate Fuel Cell Technology,* Edited by R. J. Selman and T. D. Claar, The Electrochemical Society, Inc., Pennington, NJ, p. 271, 1984.
27. G. Kucera, K. Myles, A. Brown, M. Roche, D. Chu, and E. Indacochea, "ANL's Research and Development of Alternate Components for MCFCs", *in Proceedings of the Fourth Annual Fuel Cells Contractors Review Meeting*, U.S. DOE/METC, July, 1992, Pgs. 31 - 41.
28. K. Kinoshita, F. McLarnon, and E. Cairns, *Fuel Cells, A Handbook*, prepared by Lawrence Berkeley Laboratory for the U.S. Department of Energy under Contract DE-AC-3-76F00098, May 1988.
29. N. Minh, "High Temperature Fuel Cells", in *CHEMTECH*, journal published by the American Chemical Society, Vol. 21, No. 1, January, Pgs. 32-37, 1991.
30. Y. Yamamasu, T. Kakihara, E. Kasai, and T. Morita, IHI, "Component Development and Durability Test of MCFC", in *The International Fuel Cell Conference Proceedings*, NEDO/MITI, Tokyo, Japan, Pgs. 161-164, 1992.
31. H. Urushibata and T. Murahashi, MELCO, "Life Issues of Molten Carbonate Fuel Cell", in *The International Fuel Cell Conference Proceedings*, NEDO/MITI, Tokyo, Japan, Pgs. 223-226, 1992.
32. S. Takashima, K. Ohtsuka, T. Kara, M. Takeuchi, Y. Fukui, and H. Fujimura, Hitachi, "MCFC Stack Technology at Hitachi", in *The International Fuel Cell Conference Proceedings*, NEDO/MITI, Tokyo, Japan, Pgs. 265-268, 1992.
33. K. Hoshino and T. Kohno, Central Research Institute, Mitsubishi Material Co., "Development of Copper Base Anodes for Molten Carbonate Fuel Cells", in *The International Fuel Cell Conference Proceedings*, NEDO/MITI, Tokyo, Japan, Pgs. 169-172, 1992.
34. E. T. Ong, R. A. Donado, K. E. Hrdina, IGT, "Copper-Based Anode", in *Fuel Cell Program and Abstracts*, 1990 Fuel Cell Seminar, November 25-28, 1990, Phoenix, AR, pg. 314-317.
35. Y. Mugikura, Y. Izaki, T. Watanabe, H. Kinoshita, E. Kouda, T. Abe, Central Research Institute of Electric Power Industry, and H. Urushibata, S. Yoshioka, H. Maeda, and T. Murahashi, MELCO, "Evaluation of MCFC Performance at Elevated Pressure:, *in The International Fuel Cell Conference Proceedings*, NEDO/MITI, Tokyo, Japan, Pgs. 215-218, 1992.
36. K. Tanimoto, Y. Miyazaki, M. Yanagida, S. Tanase, T. Kojima, N. Ohtori, H. Okuyama, and T. Kodama, Government Industrial Research Institute, Osaka, "Cell Performance of Molten Carbonate Fuel Cell with Alkali and Alkaline Earth Carbonate Mixtures:, in *The International Fuel Cell Conference Proceedings*, NEDO/MITI, Tokyo, Japan, Pgs. 185-188, 1992.
37. K. Ota, S. Mitsushima, K Kato, and N. Kamiya, Yokahama National University, "Solubilities of Metal Oxides in Molten Carbonate:, in Proceedings of the Second Symposium on Molten Carbonate Fuel Cell Technology, Volume 90 - 16, The Electrochemical Society, Inc. Pennington, NJ, Pgs. 318-327, 1990.
38. M. Farooque, ERC, "Development on Internal Reforming Carbonate Fuel Cell Technology, Final Report", prepared for U.S. DOE/METC, DOE/MC/23274-2941, October, 1990, Pgs. 3-6 - 3-11, 1990.

39. M. Farooque, ERC, "Development on Internal Reforming Carbonate Fuel Cell Technology, Final Report:, prepared for U.S. DOE/METC, DOE/MC/23274-2941, October, 1990, Pgs. 4-19 - 4-29.
40. A. Pigeaud, ERC, and G. Wilemski, Physical Sciences, "Effects of Coal-Derived Trace Species on the Performance of Carbonate Fuel Cells", *in Proceedings of the Fourth Annual Fuel Cells Contractors Review Meeting*, U.S. DOE/METC, Pgs. 42-45, July, 1992.
41. "Effects of Coal-Derived Trace Species on the Performance of Molten Carbonate Fuel Cells", Topical Report prepared by Energy Research Corporation for US DOE/METC, DOE/MC/25009-T26, October, 1991.
42. D. Rastler, EPRI, G. Devore, Destec Engineering, R. Castle, Haldor Topsoe, and C. Chi, ERC, "Demonstration of a Carbonate Fuel Cell Stack on Coal-Derived Gas", *in Fuel Cell Seminar Abstracts*, Tucson, AR, November 29-December 2, 1992 Pgs. 186-190, 1992.
43. L. J. Bregoli and H. R. Kunz, *J. Electrochem. Soc.*, **129,** 2711, 1982.
44. M. G. Gonikberg, *Chemical Equilibria and Reaction Rates at High Pressures,* Translated from Russian by M. Artment, Edited by S. Monson, published for the National Science Foundation, Washington, D.C., by the Israel Program for Scientific Translations Jerusalem, Israel, p. 58., 1963
45. M. G. Gonikberg, *Chemical Equilibria and Reaction Rates at High Pressures,* Translated from Russian by M. Artment, Edited by S. Monson, published for the National Science Foundation, Washington, DC, by the Israel Program for Scientific Translations, Jerusalem, Israel, p. 133, 1963.
46. H. R. Kunz and L. A. Murphy, in *Proceedings of the Symposium on Electrochemical Modeling of Battery, Fuel Cell, and Photoenergy Conversion Systems,* Edited by J. R. Selman and H. C. Maru, The Electrochemical Society, Inc., Pennington, NJ, p. 379, 1986.
47. T. G. Benjamin, E. H. Camara and L. G. Marianowski, *Handbook of Fuel Cell Performance,* prepared by the Institute of Gas Technology for the United States Department of Energy under Contract No. EC-77-C-03-1545, May, 1980.
48. Research and Development on Fuel Cell Power Generation Technology FY1990 Annual Report, NEDO, April, 1991.
49. M. Hosalaetal, "IHI Large Site Molten Carbonate Fuel Cell Advancements", *Fuel Cell Program and Abstracts* 1990 Fuel Cell Seminar, Phoenix, AR, November 25-28, 1990.
50. W. H. Johnson, "Molten Carbonate Fuel Cell Technology Improvement", Quarterly Technical Progress Report No. 23 for the Period Ending May, 1990, prepared for US DOE/METC, DOE/MC/23270-2923, September, 1990.
51. D. B. Stauffer et al, "An Aspen/SP MCFC Performance User Block", G/C Reports No. 2906, July 1991.
52. J. R. Rostrup-Nielsen, in *Catalysis Science and Technology,* Edited by J. R. Anderson and M. Boudart, Springer-Verlag, Berlin, German Democratic Republic, p. 1, 1984.
53. H. A. Leibhafsky and E. J. Cairns, *Fuel Cells and Fuel Batteries,* John Wiley and Sons, Inc., New York, NY, p. 654, 1968.
54. T. D. Tawari, E. Pigeaud and H. C. Maru, in *Proceedings of the Fifth Annual Contractors Meeting on Contaminant Control in Coal-Derived Gas Streams,* DOE/METC-85/6025, Edited by D. C. Cicero and K. E. Markel, U.S. Department of Energy, Morgantown, WV, p. 425, January, 1986.
55. G. H. J. Broers and B. W. Triejtel, *Advanced Energy Conversion,* **5,** 365, 1965.
56. B. Baker, S. Gionfriddo, A. Leonida, H. Maru and P. Patel, "Internal Reforming Natural Gas Fueled Carbonate Fuel Cell Stack," Final Report prepared by Energy Research Corporation for the Gas Research Institute, Chicago, IL, under Contract No. 5081-244-0545, March, 1984.

57. M. Farooque, Data from ERC testing, 1992.
58. S. Kaneko et al, "Research on On-Site Internal Reforming Molten Carbonate Fuel Cell", 1989 International Gas Research Conference, 1989.
59. M. Farooque, "Development of Internal Reforming Carbonate Fuel Cell Stack Technology", Final Report, DOE/MC/23274-2941, October, 1991.
60. S. H. Lu and J. R. Selman, in *Proceedings of the Symposium on Molten Carbonate Fuel Cell Technology,* Edited by R. J. Selman and T. D. Claar, The Electrochemical Society, Inc., Pennington, NJ, p. 372, 1984.
61. G. L. Anderson and P. C. Garrigan, in *Proceedings of the Symposium on Molten Carbonate Fuel Cell Technology,* Edited by R. J. Selman and T. D. Claar, The Electrochemical Society, Inc., Pennington, NJ, p. 297, 1984.
62. A. Pigeaud, in *Proceedings of the Sixth Annual Contractors Meeting on Containment Control in Coal-Derived Gas Streams,* DOE/METC-86/6042, Edited by K. E. Markel and D. C. Cicero, U.S. Department of Energy, Morgantown, WV, p. 176, July, 1986.
63. A. Pigeaud, "Study of the Effects of Soot, Particulate and Other Contaminants on Molten Carbonate Fuel Cells Fueled by Coal Gas," Progress Report prepared by Energy Research Corporation for U.S. Department of Energy, Morgantown, WV, under Contract No. DE-AC21-84MC21154, June, 1987.
64. V. Jalan, M. Desai and C. Brooks, in *Proceedings of the Symposium on Molten Carbonate Fuel Cell Technology,* Edited by R. J. Selman and T. D. Claar, The Electrochemical Society, Inc., Pennington, NJ, p. 506, 1984.
65. L. J. Marianowski, *Prog. Batteries & Solar Cells,* **5,** 283, 1984.
66. W. V. Vogel and S. W. Smith, *J. Electrochem. Soc.,* **129,** 1441, 1982.
67. S. W. Smith, H. R. Kunz, W. M. Vogel and S. J. Szymanski, in *Proceedings of the Symposium on Molten Carbonate Fuel Cell Technology,* Edited by R. J. Selman and T. D. Claar, The Electrochemical Society, Inc., Pennington, NJ, p. 246, 1984.
68. R. J. Remick and E. H. Camara, paper presented at the Fall Meeting for The Electrochemical Society, Inc., New Orleans, LA, October 7-12, 1984.
69. R. J. Remick, in *Proceedings of the Fourth Annual Contractors Meeting on Contaminant Control in Hot Coal-Derived Gas Streams,* DOE/METC-85/3, Edited by K. E. Markel, U.S. Department of Energy, Morgantown, WV, p. 440, May, 1984.
70. P. S. Patel, S. M. Rich and H. C. Maru, in *Proceedings of the Fourth Annual Contractors Meeting on Contaminant Control in Hot Coal-Derived Gas Streams,* DOE/METC-85/3, Edited by K. E. Markel, U.S. Department of Energy, Morgantown, WV, p. 425, May, 1984.
71. G. L. Anderson, F. O. Berry, G. D. Harmon, R. M. Laurens and R. Biljetina, in *Proceedings of the Fifth Annual Contractors Meeting on Contaminant Control in Coal-Derived Gas Streams,* DOE/METC-85/6025, Edited by D. C. Cicero and K. E. Markel, U.S. Department of Energy, Morgantown, WV, p. 87, January 1986.
72. T. P. Magee, H. R. Kunz, M. Krasij and H. A. Cole, "The Effects of Halides on the Performance of Coal Gas-Fueled Molten Carbonate Fuel Cell," Semi-Annual Report, October 1986 - March 1987, prepared by International Fuel Cells for the U.S. Department of Energy, Morgantown, WV, under Contract No. DE-AC21-86MC23136, May, 1987.
73. G. N. Krishnan, B. J. Wood, G. T. Tong and M. A. Quinlan, in *Proceedings of the Fifth Annual Contractors Meeting on Contaminant Control in Coal-Derived Gas Streams,* DOE/METC-85/6025, Edited by D. C. Cicero and K. E. Markel, U.S. Department of Energy, Morgantown, WV, p. 448, January 1986.

74. M. C. Williams and D. A. Berry", "Overview of the DOE-Funded Fuel Cell Contaminants R&D Program", Fuel Cell Seminar Program and Abstracts, 1990 Fuel Cell Seminar, Phoenix, AR, November 25-28, 1990.
75. E. A. Gillis, *Chem. Eng. Prog.,* **88,** October, 1980.
76. T. Tanaka, et. al., "Development of Internal Reforming Molten Carbonate Fuel Cell Technology", in *Proceedings of the 25th IECEC*, American Institute of Chemical Engineers, New York, NY, August, 1990.
77. M. Miyazaki, T. Okada, H. Ide, S. Matsumoto, T. Shinoki, J. Ohtsuki, "Development of an Indirect Internal Reforming Molten Carbonate Fuel Cell Stack", in the 27th Intersociety Energy Conversion Engineering Conference Proceedings, San Diego, CA, Aug. 3-7, 1992, pg. 290, 1992.
78. W. H. Johnson, "International Fuel Cells MCFC Technical Accomplishment", in *Proceedings of the Second Annual Fuel Cells Contractor's Review Meeting*, US DOE/METC, May 1990.
79. T. Benjamin, G. Rezniko, R. Donelson, D. Burmeister," IMHEX^R MCFC Stack Scale-Up", in the *Proceedings of the 27th Intersociety Energy Conversion Engineering Conference*, Vol. 3, San Diego, CA, Aug. 3-7, 1992, pg. 290, 1992.
80. H.C. Maru and B.S. Baker, *Prog. Batteries & Solar Cells*, **5**, 264, 1984.
81. M. Faroogue, G. Steinfield, and H. Maru, "Comparative Assessment of Coal-Fueled Carbonate Fuel Cell and Competing Technologies", in *Proceedings of the 25th IECEC*, Vol. 3, American Institute of Chemical Engineers, New York, NY, 1990.
82. M. Faroogue, "MCFC Power Plant System Verification", presentation at *FE Fuel Cells and Coal-Fired Heat Engines Conference*, US DOE/METC, August 3-5, 1993.

5. SOLID OXIDE FUEL CELL

Solid oxide fuel cells[a] (SOFCs) have emerged as a serious alternative high temperature technology contender. An inspection of its attributes shows why. Of primary importance, is that there is no liquid electrolyte with its attendant material corrosion and electrolyte management problems. The operating temperature of >600° C allows internal reforming, promotes rapid kinetics with nonprecious materials, and produces high quality byproduct heat for cogeneration or for use in a bottoming cycle, similar to the MCFC. However, the high temperature of the SOFC places stringent requirements on its materials. The development of suitable materials and the fabrication of ceramic structures are presently the key technical challenges facing SOFCs (1).

The solid state character of all SOFC components means that, in principle, there is no restriction on the cell configuration. Instead, it is possible to shape the cell according to criteria such as overcoming design or application issues. Cells are being developed in several configurations as shown on Figure 5-1. One of these approaches, the tubular cell, has undergone development at Westinghouse Electric Corporation since the late 1950s. During recent years, Westinghouse developed the tubular concept to the status where it is now being demonstrated at user sites in a complete, operating fuel cell power unit of nominal 25 kW (40 kW max) capacity. The flat plate and the monolithic designs are at a much earlier development status typified by subscale, single cell and short stack development (up to 40 cells). Companies pursuing these concepts in the U.S. are Allied-Signal Aerospace Company, Ceramatec, Inc., Technology Management, Inc., and Ztek, Inc. There are at least seven companies in Japan, eight in Europe, and one in Australia developing SOFCs.

The electrochemical reactions (Figure 5-2) occurring in SOFCs utilizing H_2 and O_2 are based on Equations 5-1 and 5-2;

$$H_2 + O^{=} \rightarrow H_2O + 2e^{-} \qquad (5\text{-}1)$$

at the anode, and

$$\tfrac{1}{2}O_2 + 2e \rightarrow O^{=} \qquad (5\text{-}2)$$

at the cathode. The overall cell reaction is

$$H_2 + \tfrac{1}{2}O_2 \rightarrow H_2O \qquad (5\text{-}3)$$

[a] A broader, more generic name for fuel cells operating at the temperatures described in this section would be "ceramic" fuel cells. The electrolyte of these cells are made primarily from solid ceramic material to survive the high temperature environment. The electrolyte of present SOFCs are oxygen ion conducting. Ceramic cells could also be proton conducting.

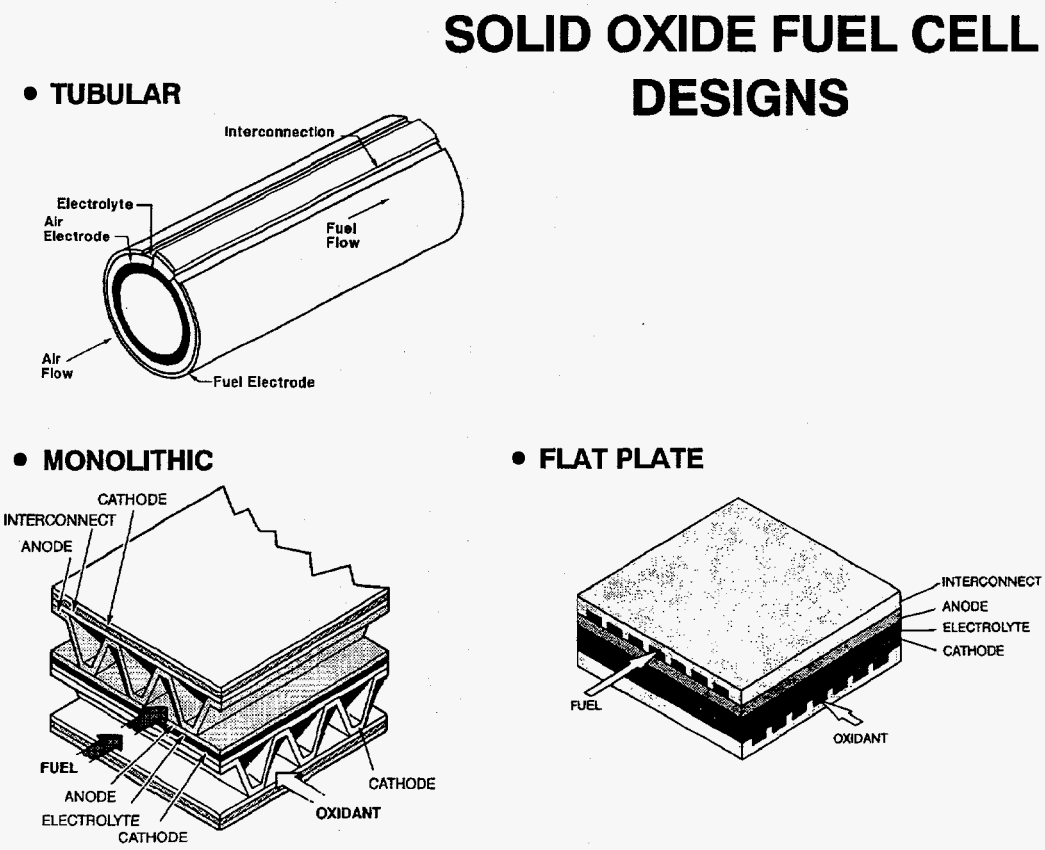

Figure 5-1 Solid oxide fuel cell designs at the cathode.

The corresponding Nernst equation (Equation 5-4) for Reaction 5-3 is:

$$E = E^{\circ} + \frac{RT}{2F} \ln \frac{P_{H_2} P_{O_2}^{1/2}}{P_{H_2O}} \qquad (5\text{-}4)$$

Carbon monoxide (CO) and hydrocarbons such as methane (CH_4) can be used as fuels in SOFCs. It is also feasible that the water gas shift involving CO ($CO + H_2O \rightarrow H_2 + CO_2$) and the steam reforming of CH_4 ($CH_4 + H_2O \rightarrow 3H_2 + CO$) occur at the high temperature environment of SOFCs to produce H_2 that is easily oxidized at the anode. The direct oxidation of CO in fuel cells is well established. It appears that the reforming of CH_4 to hydrogen predominates in the present SOFCs. SOFC designs for the direct oxidation of CH_4 has not been thoroughly investigated in SOFCs in the past (2,3) nor lately (no significant work was found). For reasons of simplicity in this handbook, the reaction of CO is considered as a water gas shift rather than an oxidation. Similarly, the favored reaction of H_2 production from steam reforming is retained. Hydrogen produced by the water gas shift and the reforming of methane is included in the amount of hydrogen subject to reaction in Equations 5-1, 5-3, and 5-4.

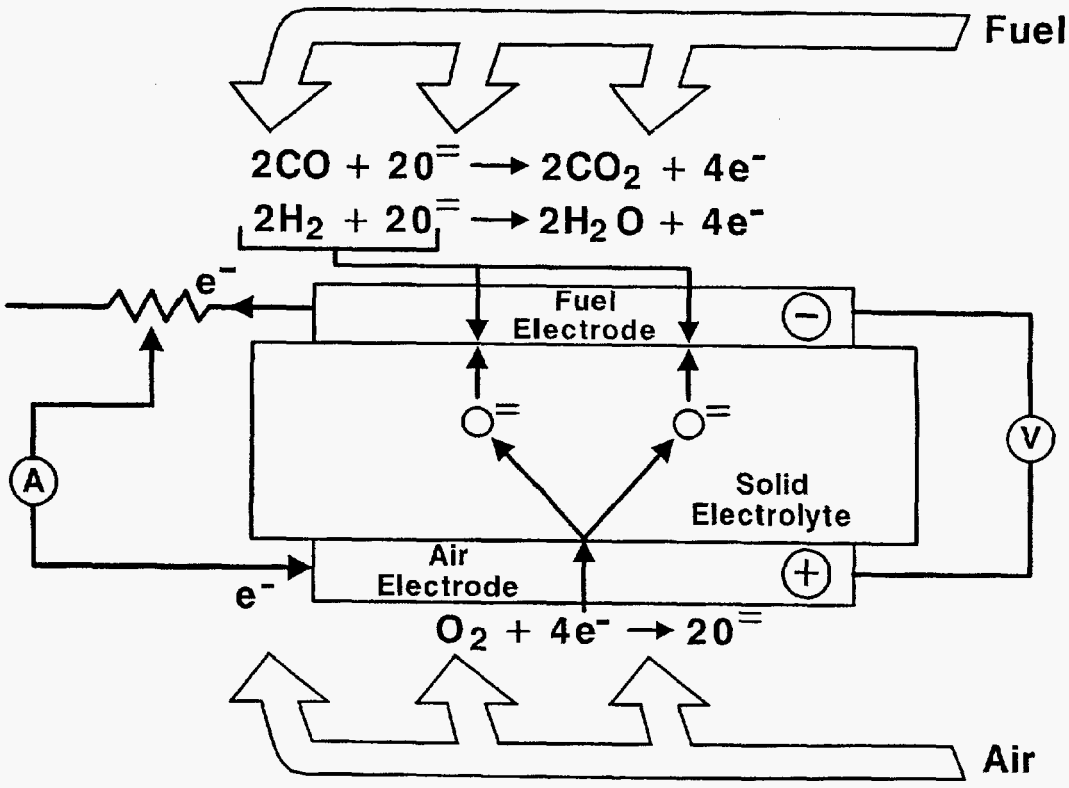

Figure 5-2 Solid oxide fuel cell operating principles.
Source: Westinghouse Electric Corporation, Science and Technology Center.

5.1 Cell Components

5.1.1 State-of-the-Art

Table 5-1 provides a brief description of the materials currently used in the various cell components of the more developed tubular SOFC, and those that were considered earlier. Because of the high operating temperatures of present SOFCs (approximately 1,000°C), the materials used in the cell components are limited by: (1) chemical stability in oxidizing and/or reducing environments, (2) chemical stability of contacting materials, (3) conductivity and (4) thermomechanical compatibility. These limitations have prompted investigations of developing cells with compositions of oxide and metals which operate at intermediate temperatures in the range of 650°C (see Section 5.1.2). A more detailed description on the current status of the cell components for SOFCs is presented by Minh (1, 4) and Appleby (5).

Present SOFC designs make use of thin film wall concepts where films of electrode, electrolyte, and interconnect material are deposited one on another and sintered forming a cell structure. The fabrication techniques differ according to the type of cell configuration and developer. For example, an "electrochemical vapor deposition" (EVD) technique has been developed which produces thin layers of refractory oxides that are suitable for the electrolyte and cell interconnection in the Westinghouse tubular SOFC design (6). In this technique, the appropriate metal chloride vapor is introduced on one side of the porous support tube surface, and

Table 5-1 Evolution of Cell Component Technology for Tubular Solid Oxide Fuel Cells

Component	ca. 1965	ca. 1975	Current Status[b]
Anode	• porous Pt	• Ni/ZrO_2 cermet[b]	• Ni/ZrO_2 cermet[c] (30 mol% Ni) • deposit slurry • 12.5×10^{-6} cm/cm °C • ~150 μm thickness • 20-40% porosity
Cathode	• porous Pt	• stabilized ZrO_2 impregnated with praesodymium oxide and covered with SnO doped Im_2O_3	• Sr doped lanthanum manganite (10 mol% Sr) • deposit slurry, sinter • ~1 mm thickness • 12×10^{-6} cm/cm °C expansion from room temperature to 1,000°C[d] • 20-40% porosity
Electrolyte	• yttria stabilized ZrO_2 • 0.5-mm thickness	• yttria stabilized ZrO_2	• yttria stabilized ZrO_2 (8 mol% Y) • EVD[d] • 10.5×10^{-6} cm/cm °C expansion from room temperature to 1,000°C[d] • ~40-μm thickness
Cell Interconnect	• Pt	• Mn doped cobalt chromite	• Mg doped lanthanum chromite (10 mol% Mg) • EVD • ~40 μm thickness
Support Tube[e]	• yttria stabilized ZrO_2	• yttria stabilized ZrO_2	• calcia stabilized ZrO_2 (15 mol% CaO) • 34-35% porosity • 12.8 mm inner diameter • 1-2 mm wall thickness

[b] Specifications for Westinghouse SOFC

[c] Y_2O_3 stabilized ZrO_2

[d] EVD = electrochemical vapor deposition

[e] The support tube has recently been eliminated in the Westinghouse tubular cell design. The cathode is now extruded and is thicker than before to compensate for the elimination of the support tube.

H_2/H_2O is introduced on the other side. The gas environments on both sides of the support tube act to form two galvanic couples, as demonstrated in Equations 5-5 and 5-6.

$$MeCl_y + \tfrac{1}{2}yO^{=} \rightarrow MeO_{y/2} + \tfrac{1}{2}yCl_2 + ye^{-} \quad (5\text{-}5)$$

$$H_2O + 2e^{-} \rightarrow H_2 + O^{=} \quad (5\text{-}6)$$

The net result is the formation of a dense and uniform metal oxide layer in which the deposition rate is controlled by the diffusion rate of ionic species and the concentration of electronic charge carriers. This procedure is used to fabricate the solid electrolyte (yttria stabilized zirconia) and the interconnection (Mg doped lanthanum chromite).

The anode consists of metallic Ni and a Y_2O_3 stabilized ZrO_2 skeleton, the latter which serves to inhibit sintering of the metal particles and to provide a thermal expansion coefficient comparable to those of the other cell materials. The anode structure is fabricated with a porosity of 20 to 40% to facilitate mass transport of reactant and product gases. The Sr doped lanthanum manganite ($La_{1-x}Sr_xMnO_3$, x = 0.10-0.15) that is most commonly used for the cathode material is a p-type conductor. Similar to the anode, the cathode is a porous structure that must permit rapid mass transport of reactant and product gases. The cell interconnection material (Mg doped lanthanum chromite, $LaCr_{1-x}Mg_xO_3$, x = 0.02-0.10), however, must be impervious to fuel and oxidant gases and must possess good electronic conductivity. In addition, the cell interconnection is exposed to both the cathode and anode environments, thus it must be chemically stable under O_2 partial pressures of about ~1 to 10^{-18} atm at 1000°C (1832°F).

The solid oxide electrolyte must be free of porosity that permits gas to permeate from one side of the electrolyte layer to the other, and it should be thin to minimize ohmic loss. In addition, the electrolyte must have a transport number for $O^{=}$ of as close to unity as possible, and a transport number for electronic condition of as close to zero as possible. Zirconia-based electrolytes are suitable for SOFCs because they exhibit pure anionic conductivity over a wide range of O_2 partial pressures (1 to 10^{-20} atm). The other cell components should permit only electronic conduction,[f] and interdiffusion of ionic species in these components at 1000°C (1832°F) should not have a major effect on their electronic conductivity. Other severe restrictions placed on the cell components are that they must be stable to the gaseous environments in the cell and they must be capable of withstanding thermal cycling. The materials listed in Table 5-1 appear to have the properties for meeting these requirements.

The resistivities of typical cell components at 1000°C (1832°F) under fuel cell gaseous environments are (7): 10 ohm cm (ionic) for the electrolyte (8-10 mol% Y_2O_3 doped ZrO_2), 0.5 ohm cm (electronic) for the cell interconnection (Mg doped $LaCrO_3$), 0.01 ohm cm (electronic) for the cathode (Sr doped $LaMnO_3$) and 0.001 ohm cm (electronic) for the anode (Ni/ZrO_2 cermet[g]). It is apparent that the solid oxide electrolyte is the least conductive of the cell components, followed by the cell interconnection. Furthermore, an operating temperature of about 1000°C (1832°F) is necessary if the ionic conductivity of the solid electrolyte (i.e., 0.02 $ohm^{-1}cm^{-1}$ at 800°C (1472°F) and 0.1 $ohm^{-1}cm^{-1}$ at 1000°C (1832°F)) is to be within even an order of magnitude of that of aqueous electrolytes. The solid electrolyte in SOFCs must be only about

---

[f] Mixed conducting (i.e, electronic and ionic) materials for anodes may be advantageous if H_2 oxidation can occur over the entire surface of the electrode to enhance current production, instead of only in the region of the three phase interface (gas/solid electrolyte/electrode). Similarly, mixed conductors may also be advantageous for cathodes.

[g] The cermet becomes an electronic conductor at Ni contents of >30 vol% (8).

25-50 μm thick if its ohmic loss at 1000°C (1832°F) is to be comparable to that of the electrolyte in PAFCs (9). Fortunately, thin electrolyte structures of about 40 μm thickness can be fabricated by EVD, as well as by tape casting and other ceramic processing techniques.

The successful operation of SOFCs requires individual cell components that are thermally compatible so stable interfaces are established at 1000°C (1832°F), i.e., thermal expansion coefficients for cell components must be closely matched to minimize or reduce stresses arising from differential thermal expansion between components. Fortunately, the support tube, solid electrolyte and cathodes that are listed in Table 5-1 have reasonably close thermal expansion coefficients [i.e., $\sim 10^{-5}$cm/cm°C from room temperature to 1000°C (1832°F).] An anode made of 100 mol% nickel would have excellent electrical conductivity. However, the thermal expansion coefficient of 100 mol% nickel would be 50% greater than the ceramic electrolyte, cathode, or support tube causing a thermal mismatch. This thermal mismatch has been resolved by mixing cermet powders with Ni or NiO. The trade-off of the amount of Ni (to achieve high conductivity) and amount of ceramic (to better match the other component thermal coefficients of expansion) is Ni/YSZ: 30/70, by volume (1). The conductivity of the compromise material is significantly lower than pure nickel so other means of addressing the thermal mismatch are being pursued to allow an increase in the amount of anode nickel, see Section 5.1.3.

A configuration for electrically connecting tubular cells to form a stack is illustrated in the section describing the sealless tubular configuration (Figure 5-6). The cells are connected in a series-parallel array by nickel felt strips which are exposed to the reducing fuel gas. In this arrangement the nickel felt strips and cell interconnections extend the length of the support tube. Since the current flows in the peripheral direction of the thin electrodes, a relatively large ohmic loss exists which places an upper limit on the tube diameter.

5.1.2 Cell Configuration Options

As with the other cell types, it is necessary to stack SOFCs to increase the voltage and power being produced. Because there are no liquid components, the SOFC can be cast into flexible shapes, Figure 5-1. As a result, the cell configurations can respond to other design prerequisites. This feature has resulted in three major configuration and variations of them. The major configurations are: tubular (Westinghouse and Mitsubishi Heavy Industries (MHI)), flat plate (Ceramatec and MHI), and monolithic (Allied-Signal). Variations of the flat plate configuration are: circular disk with center manifolding (Fuji Electric, Technology Management, Inc., and Ztek), train cell stacking (National Chemical Laboratory for Industry, Japan) and the Heat Exchanger Integrated Stack (Sulzer).

In the early 1960s, experimental SOFCs with a planar geometry were evaluated, but this geometry presented a problem for building cell stacks because of difficulties with fabricating large flat, thin cells an obtaining adequate gas seals[h]. A tubular configuration (i.e., cylindrical design) was adopted for SOFCs which appeared to alleviate the problems with gas seals and thin layer structure fabrication. An early tubular design is illustrated in the schematic representation of the cross section of a SOFC stack in Figure 5-3. Overlapping components (i.e., electrodes, electrolyte, cell interconnection) in thin layers (10-50 μm) are deposited on a porous support tube of calcia-stabilized zirconia; fabrication of the fuel cell stack is described by Isenberg (3) and Sverdrup et al. (9). In this tubular design, individual fuel cells are arranged in bands along the support tube and are connected in series by a ceramic interconnect material. Another variation of an early

[h] Recently, the monolith and the planar structures using bipolar current collection have received more consideration for SOFCs due to new gas sealing and fabrication techniques.

tubular design is referred to as a "bell and spigot" configuration (see Figure 5-4), which consists of short, cylindrical electrolyte segments shaped so that they can be fitted one into the other and connected to form a long tube by bell-and-spigot joints (10, 11). A variation of this design which was less complex used a series of cones which were interconnected. The sealless tubular design, however, is the most advanced among the several SOFC configuration concepts.

Sealless Tubular Configuration: The most developed solid oxide fuel cell is the Westinghouse tubular cell. This approach results in minimizing seal problems between adjacent cells. A schematic representation of the cross section of the present Westinghouse tubular design[i] for a SOFC and its gas manifold are presented in Figures 5-5 and 5-6, respectively. In this design, the cathode is formed by extrusion. Then, the electrolyte and the cell interconnection are deposited by EVD on the cathode, which provides a mechanically strong structure for the thin cell components. The anode is sequentially formed on the electrolyte layer by slurry deposition. A major advantage of this design over earlier designs is that relatively large single tubular cells can be constructed in which the successive active layers can be deposited without chemical or material interference with previously deposited layers. The support tube is closed at one end. The tubular approach with one closed end minimizes or eliminates gas seals between cells. The manifolding of the oxidant and fuel gases for this tubular cell is illustrated in Figure 5-6. The oxidant gas is introduced via a central Al_2O_3 injector tube, and the fuel gas is supplied to the exterior of the closed-end tube. In this arrangement, the Al_2O_3 tube extends to the proximity of the closed end of the tube and the oxidant flows back past the cathode surface to the open end. The fuel gas flows past the anode on the exterior of the cell, and in a parallel direction (coflow) to the oxidant gas. The spent gases are exhausted into a common plenum where the remaining active gases react and the generated heat serves to preheat the incoming oxidant stream. One attractive feature of this arrangement is that it eliminates the need for leak-free gas manifolding of the fuel and oxidant streams. However, the sealless tubular design results in a relatively long current path around the circumference of the cell to the interconnect, limiting performance, Figure 5-7. The support tube also limits cell performance by restricting the flow of oxygen to the cathode/electrolyte interface (1). Lately, Westinghouse has been successful with reducing the thickness of the support tube, then eliminating it all together (4, 12). As the porous support tube thickness was reduced, the thickness of the air electrode was increased. Concurrent to the tube reduction effort, Westinghouse increased the length of the cell active area from 30 to 100 cm. The elimination of the support tube and the increase in cell length resulted in a six-fold increase in cell power output. Figure 5-1 depicts a section of the new configuration.

Bipolar (Flat Plate) Configuration: A bipolar structure, which is the common configuration for cell stacks in PAFCs and MCFCs, permits a simple series electrical connection between cells without the need for external cell interconnections such as those used with the tubular configuration shown in Figure 5-7. Perpendicular current collection in a cell stack with a bipolar design should have a lower ohmic polarization than the tubular configuration, and overall stack performance should be improved. However, gas leaks in a SOFC of bipolar configuration with compressive seals are difficult to prevent, and thermal stresses at the interfaces between dissimilar materials must be accommodated to prevent mechanical degradation of cell components. Planar electrodes and solid electrolyte structures were proposed for use in high temperature fuel cells and electrolysis cells by Hsu and co-workers (13, 14) in the mid-1970's. Later, Hsu (15, 16) developed bipolar structures

[i] The present tubular design is about 50 cm length and 1.27 cm diameter. These cells produce about 35 W each, thus about 28 cells are required to generate 1 kW.

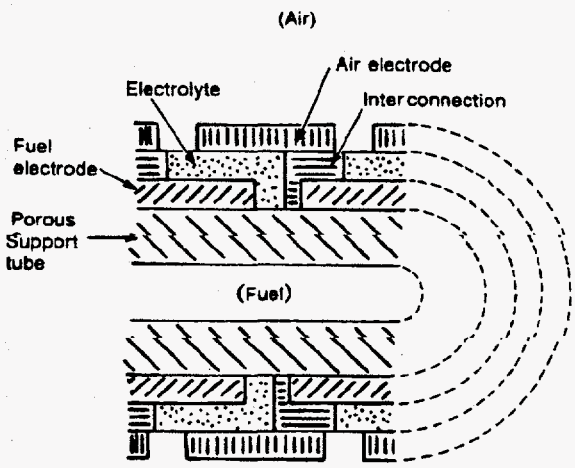

Figure 5-3 Schematic representation of the cross section (in the axial direction of the support tube) of an early tubular configuration for SOFCs.
Source: (Figure 2, p. 256) E.F. Sverdup, C.J. Warde and A.D. GLasser, in *From Electrocatalysis to Fuel Cells*, Edited by G. Sandstede, University of Washington Press, Seattle, WA, 1972.

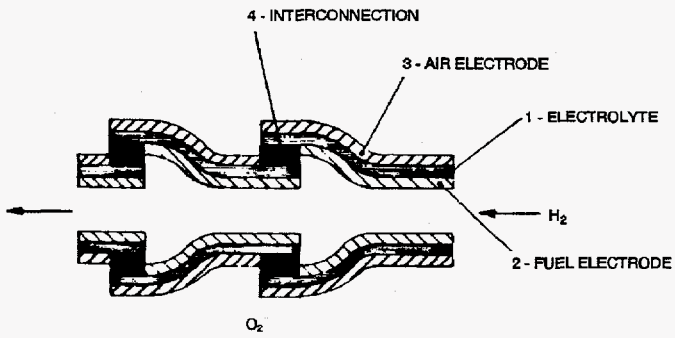

Figure 5-4 Schematic representation of the cross section (in the axial direction of the series-connected cells) of an early "bell and spigot" configuration for SOFCs.
Source: (Figure 24, p. 332) *Fuel Cells*, DOE/METC-86/0241, Technology Status Report, Morgantown Energy Technology Center, Morgantown, WV, 1986.

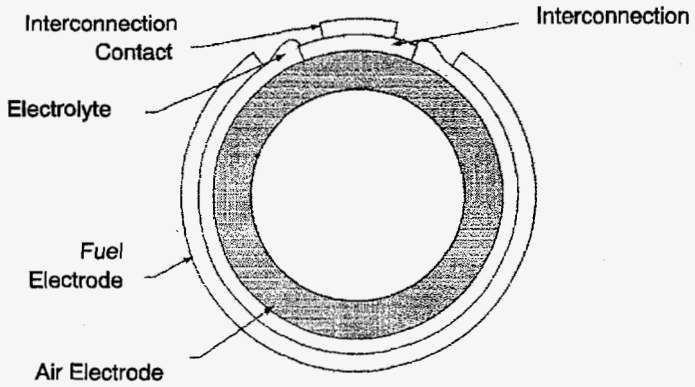

Figure 5-5 Schematic representation of the cross section of present tubular configuration for SOFCs.
Source: Westinghouse Electric Corporation Science and Technology Center

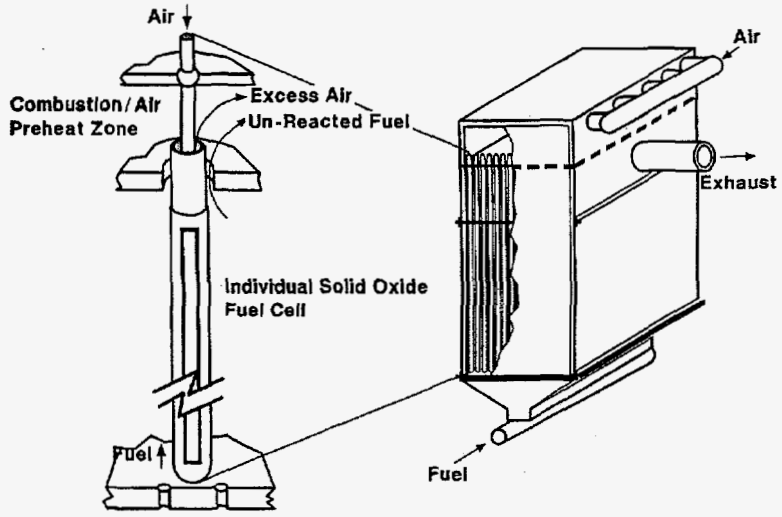

Figure 5-6 Schematic representation of the gas-manifold design for a tubular SOFC.
Source: Westinghouse Electric Corporation Science and Technology Center

for SOFCs which are reported to have the following attractive features: 1) high power density, 2) structural ruggedness, 3) concealed electrodes, 4) ease of heat removal, and 5) low-stress assembly.

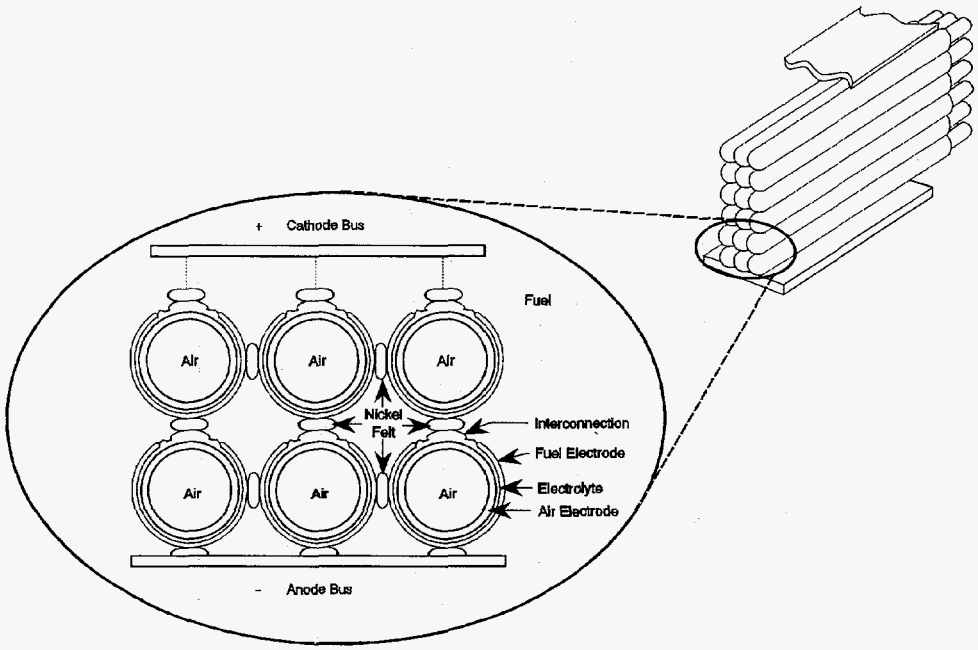

Figure 5-7 Cell-to-cell connections among tubular SOFCs.
Source: Westinghouse Electric Science and Technology Center

Solid electrolyte structures of yttria-stabilized ZrO_2 of up to 10 cm diameter and 0.25 mm thickness with better than 0.025 mm flatness have been fabricated (16). The interconnect, having ribs on both sides, forms gas flow channels and serves as a bipolar gas separator contacting the anode and cathode of adjoining cells. The flat plate design offers improved power density relative to the tubular and segmented cell-in-series designs but requires high temperature gas seals at the edges of the plates. Compressive seals have been proposed; however, the unforgiving nature of a compressive seal can lead to a nonuniform stress distribution on the ceramic and cracking of the layers. Further, seals may limit the height of a cell stack. There is a higher probability for mismatches in tolerances (creating unacceptable stress levels) in taller stacks. Fabrication and assembly appear to be simpler for the flat plate design as compared with the other designs. The electrolyte and interconnect layers are made by tape casting. The electrodes are applied by the slurry method, by screen printing, or by plasma spraying. Fuel cell stacks are formed by stacking up layers much like other fuel cell technologies (4). Tests of single cells and two cell stacks of SOFCs with a planar configuration (5 cm diameter) have demonstrated power densities up to 0.12 W/cm^2. One major technical difficulty with these structures is their brittleness in tension; the tensile strength is only about 20% of their compressive strength. However, the two cell stack was able to withstand five thermal cycles without suffering detectible physical damage, and adequate gas sealing between cells was reported. Developers at Tokyo Gas have reported a 400 cm^2 and a ten cell stack of small 5 cm x 5 cm cells (17). The successful demonstration of larger multicell stacks has yet to be performed.

Monolithic Configuration: The monolith configuration is a more complex design of the bipolar configuration for SOFCs. A schematic representation of a cross section of the monolith structure proposed for SOFCs is presented in Figure 5-8, and details of its fabrication are described by Fee and co-workers (18, 19) and Mihn et al (1). The structure resembles the corrugated assembly used

in cardboard boxes. The small channels are formed from thin (25 to 100 μm) layers of the active cell components, and these channels serve for passage of the fuel and oxidant streams. In this design the anode, cathode and solid electrolyte, which have the compositions listed in Table 5-1, are tapecast or tape calendered into thin layer structures. The complete assembly is then heat treated in air to produce the SOFC monolith. The principal challenge of this technology is to match the thermal properties (i.e., thermal expansion, shrinkage rates) of the individual materials so that they can be heat treated (i.e., controlled heating to ~400°C (752°F) to burn out the organic binder, plasticizer and dispersant, and further heating to between 1200 and 1600°C (2192 to 2912°F) to sinter the ceramic materials together, followed by cool down to room temperature, to form the appropriate monolith structure. The residual thermal stresses that develop because of the differences in thermal expansion of the individual layer components can lead to mechanical failure of the monolith structure. This problem has been analyzed by Majumdar et al. (20).

Of particular concern is the ability to cofire the $LaCrO_3$ interconnect at temperatures below 1400°C in an oxidizing atmosphere. The interconnect densifies to 90 to 100% theoretical if fired alone in air. However, the material does not densify when fired in contact with the electrodes. At present the most promising approach is to use very thin anode and cathode layers. The electrode pore volume is filled with chromate which densifies and this allows the interconnect to densify (21).

Another challenge is to manifold the fuel and oxidant gases. A coflow or counterflow pattern for the gases can be adapted to the monolith structure as shown in Figure 5-8. A cross flow pattern for the gases requires only a simple manifold, but the monolith structure for this manifold is more complex.

The bipolar configuration for the monolith SOFC uses perpendicular current collection. This minimizes the iR losses inherent in the arrangement of tubular SOFCs shown in Figure 5-5. In addition, the honeycomb configuration provides a strong self-supporting structure which eliminates the need for a porous support. The scale-up of the monolith structure from single cells to bipolar SOFC stacks has the potential to significantly improve the specific energy and specific power of the SOFC.

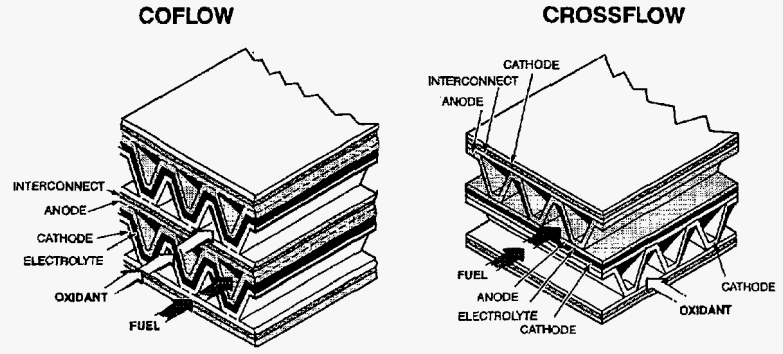

Figure 5-8 Schematic representation of coflow and crossflow cross sections of the monolith SOFC configurations.
Source: Allied-Signal Aerospace Company

Small SOFCs with the monolith structure (9 cm^2 active area) have been fabricated and tested at 1000°C. Current densities as high as 2.5 A/cm^2 have been achieved on hydrogen and air, and an array consisting of two cells in series has operated for more than 600 hours at 250 mA/cm^2 and

~0.7 V. These cells were also operated with hydrocarbon fuels (e.g., natural gas, CH_4, C_3H_8, C_8H_{18}, C_2H_5OH, and simulated diesel fuel) that were mixed with H_2O, and the performance was similar to that obtained with hydrogen. Furthermore, the presence of about 5 ppm sulfur in the natural gas had no detrimental effect on cell performance.

The cell performance obtained to date indicates that the interfacial resistance is the limiting factor. In particular, the interfacial resistance at the fuel electrode/electrolyte interface needs to be reduced further by optimizing the distribution of Ni. The successful scale-up of the small arrays into larger stacks (i.e., larger area and greater number of cells in series connection) has progressed to fabricating 12 cell crossflow stacks of 25 cm^2 cell area.

5.1.3 Development Components

Materials and design approaches have been developed so that SOFC technology, particularly the Westinghouse tubular cell configuration, is technically feasible. However, the application of the materials used in the non-restrained tubular cell to the restrained alternative planar configurations results in excessive mechanical stresses. Moreover, the present approaches exhibit lower than desired performance (higher operating costs) and difficult designs and fabrication (higher capital costs). The major issue for improving SOFC technology is to develop materials which sustain good performance while withstanding the high operating temperature presently used (1,000° C) or develop alternate cells with mixtures of ceramics and metals which operate at an intermediate temperature of 650° C. A consensus of related critical issues are: 1) the present materials and relevant designs used in the SOFC must operate at high temperature to obtain performance due to their intrinsic high resistivity, 2) there are high mechanical stresses arising from differential thermal expansion coefficients of adjacent component materials, 3) there are interfacial reactions among adjacent components caused by the high sintering temperatures needed to obtain high density which alter component design integrity, and 4) high temperatures are required in the fabrication of ceramic components which adds production complexity, hence cost. Raw material costs are $7/kW to $15/kW but manufacturing drives this to $700/kW for the stack (4, 22, 23). Research, as summarized below, is being performed to address these and other issues to bring SOFC technology into the competitive range.

Two approaches are being pursued to alleviate the many materials and design concerns. They are: 1) research is proceeding to address material and design improvements which allow operation within the high temperature environment (1,000° C) of the existing state-of-the-art components and 2) proponents contend that the cell operating temperature and, perhaps, the associated fabricating temperatures can be lowered to reduce manufacturing cost while maintaining performance. If the operating temperature can be lowered enough (600 to 800° C), metals could be substituted for ceramics, especially in the cathode and interconnect. There would be more material selection with lower temperature operation and metal processing is less expensive than ceramic processing (22).

a) High Temperature Cell Development (Present Operating Temperature, 1,000° C)

Development work for cells operating at 1,000° C is focused on increasing the mechanical toughness of the cell materials to alleviate the impact of thermal mismatch and to develop techniques which will decrease interfacial changes of the various material layers during thin film cell fabrication. Interfacial issues among cell components include diffusion, volatization, and segregation of trace constituents. For example, there is evidence that $La_2Zr_2O_7$ and $SrZrO_3$ form at the cathode/electrolyte interface and that Sr and Mn ions diffuse across the interface at temperatures as low as 800° C for up to 400 hours (24).

Approaches to resolving the mismatch caused by different component materials' thermal expansion coefficient include: increasing the fracture toughness of the electrolyte, controlling the electrolyte processing faults, varying the component thickness, and adding minor constituents to alter the anode properties.

The electrolyte of choice at present is yittria, fully stabilized ZrO_2. Researchers are investigating partially stabilized ZrO_2 and adding Al_2O_3 to fully yittria stabilized ZrO_2 to strengthen the electrolyte matrix. Yamamoto et. al (25) have investigated the tetragonal phase (TZP) of zirconia to strengthen the electrolyte structure so that it can be made thinner to obtain lower resistivity. This increased strength is needed for self-supporting planar cells. An increase in bending strength of 1200 MPa was observed in the TZP material compared to 300 MPa for cubic zirconia stabilized with > 7.5 mol% Y_2O_3. The TZP was stabilized by taking advantage of fine particle technology and minor doping of Y_2O_3. Resistivity increased slightly.

To reduce cracking during cool-down, model work has shown that the use of fairly thin electrolytes (approximately 0.5 to 3 mils and anode/electrolyte/cathode thickness ratios of 2:1:1) reduce the possibilities of cracking for monolithic cells (26).

It has been observed that solid oxide fuel cell voltage losses are dominated by ohmic polarization and that the most significant contribution to the ohmic polarization is the interfacial resistance between the anode and the electrolyte (27). This interfacial resistance is dependant on nickel distribution in the anode. A process has been developed, PMSS (Pyrolysis of metallic soap slurry), where NiO particles are surrounded by thin films or fine precipitates of yittria stabilized zirconia (YSZ) to improve nickel dispersion to strengthen adhesion of the anode to the YSZ electrolyte. This may help relieve the mismatch in thermal expansion between the anode and the electrolyte.

Researchers have surmised that there would be a reduction in interfacial activity among adjacent components if the interconnect could be sintered to a high density at temperature below 1550° C (26, 28, 29). Either chemical or physical sintering aids could be used. One approach is to use synthesized submicrometer, active powders. The use of these powders causes a depleting or enriching of the rare earth substitution cation with La or Y on one component while holding Cr concentrations constant on the other. This, in turn, alters the sintering temperature. Results show that high densities might be achievable at temperatures of 1400° C and below (29).

Alternative fabrication methods to sintering and electrochemical vapor deposition (EVD), which is proving difficult to scale-up, are receiving more attention. These methods include plasma spraying, chemical vapor deposition (CVD), and reaction processes. There are many development projects being conducted in fabrication techniques. Examples of some of the work follow.

Investigations are being conducted to determine whether jet vapor deposition (JVD) could be substituted for EVD, which is expensive and is proving difficult to scale larger in size. JVD is a thin film technique in which sonic gas jets in a low vacuum fast flow serve as deposition sources. Results showed the YSZ films can be made dense and pinhole free; they seal highly porous electrode surfaces and are gas tight. Conductivity needs to be improved, which should be obtainable. The ultimate goal will be to fabricate thin film SOFCs, both electrolyte and the electrodes, in an unbroken sequence of JVD steps. This would also allow the use of alternate metal cathode, such as Ag thin films (23).

Due to number of conditions which can be set independently, plasma spray techniques may make it attractive to fabricate dense, gas tight, or porous layers with conditions where one layer's application does not affect the preceding layer (30). The Electrotechnical Laboratory in Japan has demonstrated applying a YSZ on a substrate using a laser plasma spray approach. The sprayed material maintained identical crystalline structure during the process. Since a high melting point

material was coated on a low melting point material, this method offers the potential for multilayer coating (31).

b) Intermediate Temperature Cell Development (~650°C Operating Temperature)

The YSZ electrolyte suffers a significant decrease in conductivity if operated at temperatures in the range of 600 to 800°C. The product of conductivity and thickness could be maintained, however, if the electrolyte structure is reduced in thickness when lowering the temperature. Researchers are investigating fabricating thin film YSZ structure using sol gel processes, plasma enhanced chemical vapor deposition, and by simple tape calendaring (22, 32, 33). Others are synthesizing selected perovskite powders expected to possess low activation energy for ionic conduction and an intrinsically high population of ionic charge carriers for electrolyte application. This research is associated with an extensive investigation of the effect of lattice structure on ionic conductivity. The identification of these materials would allow lower temperature operation. The general material area of perovskites has been chosen as having good conductivity and are chemically stable, but the development of the exact chemical composition and preparation technique remains to be completed (34).

Other alternative material research includes investigating materials which exhibit polarizable (easily weakened) metal oxygen bonds; open, layered structures for greater ion mobility; and lower coordination numbers for the mobile ions. These are important criteria for high conductivity (35). This approach to electrolyte development is to try to stabilize a very conductive oxide by compound formation or by solid solution formation with more stable oxides. Conductivity of 10^{-1}/ohm cm have been obtained with Zn doped $La_{1-x}Bi_xA1O_3$ compared to 1.8×10^{-2}/ohm cm for YSZ at 700°C (36).

The problem in the quest for a metal separator which operates at the 600 to 800°C temperature is that it becomes oxidized. One solution is to place a coating which forms CrO_3 which maintains a high conductivity. Problems with thermal mismatch must still be solved (37).

It is possible that cell performance obtained in the 1000°C cells can be maintained at lower temperature operation if mixed electronic and ionic conduction materials are selected for the electrodes, instead of relying on materials with just electronic conduction. There are several benefits to mixed conduction. The most important is that oxygen reduction can occur at any point on the cathode rather than only at the three phase interface. Several organizations are investigating mixed conduction materials for the cathode and anode which have thermal expansion coefficients matched to YSZ electrolyte and good conductivity. For example, lanthanum strontium ferrite, lanthanum strontium cobaltites, p-type semi-conductors, and n-type semi-conductors are better electrocatalysts than the state-of-the-art lanthanum strontium manganite, because these are mixed conductors (38). The content of the first two materials must be altered to obtain a good thermal expansion match to the YSZ electrolyte (22).

5.2 Performance [j]

The thermodynamic efficiency of SOFCs at open circuit voltage is lower than that of MCFCs and PAFCs which utilize H_2 and O_2 because of the lower ΔG^k at higher temperatures (see discussion in Section 2). However, as mentioned in Section 2, the higher operating temperature of SOFCs is beneficial in reducing polarization.

The voltage losses in SOFCs is governed by ohmic losses in the cell components. The contribution to ohmic polarization (iR) in a tubular cell[l] is reported (7) to originate 65% from cathode, 25% from the anode, 9% from the electrolyte, and 1% from the interconnect, when these components have thicknesses (mm) of 0.7, 0.1, 0.04 and 0.04, respectively, and specific resistivities (ohm cm) at 1000°C of 0.013, 0.001, 10, and 0.5, respectively. The cathode iR dominates the total ohmic loss despite the higher specific resistivities of the electrolyte and cell interconnection because of the short conduction path through these components and the long current path (i.e., 1.1 cm) in the plane of the cathode. The current path in the anode is about 0.8 cm and its resistivity is about an order of magnitude lower than that of the cathode, so for typical thickness of these electrodes (see above) the iR loss in the cathode is about 2.5 times greater than that in the anode.

5.2.1 Effect of Pressure

It is expected that SOFCs, like PAFCs and MCFCs, would show an enhanced performance by increasing cell pressure. Operating SOFCs, however, at elevated pressures has largely been unexplored. Although specific experimental data has not been published, it has been suggested (40) that the following equation approximates the effect of pressure on cell performance at 1,000°C (1832°F):

$$\Delta V_p(mV) = 59 \log \frac{P_2}{P_1} \qquad (5\text{-}7)$$

where P_1 and P_2 are different cell pressures. The above correlation was based on the assumption that overpotentials are predominately affected by gas pressures and that these overpotentials decrease with increased pressure.

5.2.2 Effect of Temperature

The dependence of SOFC performance on temperature is illustrated in Figure 5-9 for a two cell stack using air (low utilization) and a fuel of 67% H_2/22% CO/11% H_2O (low utilization). The sharp decrease in cell voltage as a function of current density at 800°C (1472°F) is a

---

[j] This section provides practical information which may be used for estimating the relative performance of SOFCs based on various operating parameters at this time. The user should be cautioned that the amount of data available from tests of SOFCs, especially parametric, is limited compared to PAFCs and MCFCs. In addition, the SOFCs being developed have unique designs, are constructed of varying materials, and are fabricated by differing techniques. SOFCs, particularly the flat plate types, will undergo considerable development in materials, design, and fabrication techniques. As SOFC technology progresses, it will mature towards more standardized cells as has happened with PAFCs and MCFCs which are closer to conformity. The process is expected to result in an evolution of the performance trends depicted here.

[k] ΔG decreases from 54.617 kcal/mole at 27°C to 43.3 kcal/mole at 927°C, whereas ΔH is nearly constant over this temperature range (39).

[l] A uniform current distribution through the electrolyte is assumed.

manifestation of the high ohmic polarization (i.e., low ionic conductivity) of the solid electrolyte at this temperature. The ohmic polarization decreases as the operating temperature increases

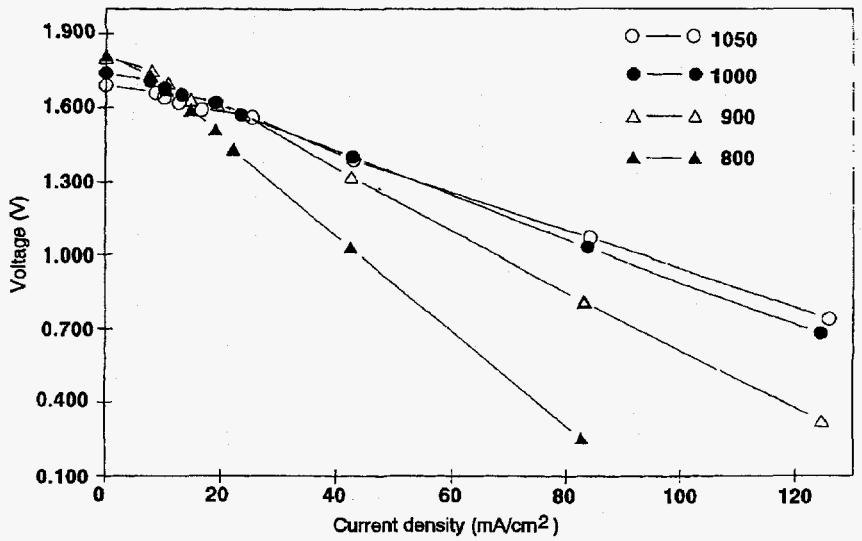

Figure 5-9 Two cell stack performance with 67% H_2 + 22% CO + 11% H_2O/air
Source: Allied-Signal Aerospace Company, 1992.

to 1050°C (1922°F), and correspondingly, the current density at a given cell voltage increases. The data in Figure 5-9 show a larger decrease in cell voltage with decreasing temperature between 800 and 900°C (1472 to 1652°F) than that between 900 and 1000°C (1652 to 1832°F), at constant current density. This and other data suggest that the voltage gain with respect to temperature is a strong function of temperature and current density. One reference (40) postulates the voltage gain as:

$$\Delta V_T(mV) = 1.3(T_2 - T_1)(°C) \tag{5-8}$$

for a cell operating at 1,000°C, 160 mA/cm^2, and a fuel composition of 67% H_2/22% CO/11% H_2O. In light of the strong functionality with respect to current density, it might be more appropriate to describe the voltage gain with the following relationship:

$$\Delta V_T(mV) = K(T_2 - T_1)(°C) * J \tag{5-9}$$

where J is the current density in mA/cm.

The following values of K have been deduced from several references which utilized a fuel composition of 67% H_2/22% CO/11% H_2O, and an air oxidant.

K	Temperature (°C)	Ref.
0.008	~1,000	40
0.006	1,000 - 1,050	44
0.014	900 - 1,000	
0.068	800 - 900	
0.003	900 - 1,000	41
0.009	800 - 900	

As can be seen there is a reasonably large range in the value of K between these references. As the SOFC technology matures these differences may reconcile to a more cohesive set of values. In the interim, the following single average combination of the above K values may help the reader if no specific information is available.

$$\Delta V_T(mV) = 0.008(T_2 - T_1)(°C) * J(mA/cm^2) \quad (5\text{-}10)$$

$$\Delta V_T(mV) = 0.04(T_2 - T_1)(°C) * J(mA/cm^2) \quad (5\text{-}11)$$

Equations 5-10 and 5-11 are for a fuel comprised of 67% H_2/22% CO/11% H_2O. Experiments using different fuel combinations, such as 80% H_2/20% CO_2 (42) and 97% H_2/3% H_2O (43, 44), suggest that these correlations may not be valid for other fuels. Figure 5-10 presents a set of performance curves for a fuel of 97% H_2/3% H_2O at various temperatures. Voltage actually increases with decreasing temperature for current densities below approximately 65 mA/cm^2. Other data (43) shows that this inverse relationship can extend to current densities as high as 200 mA/cm^2.

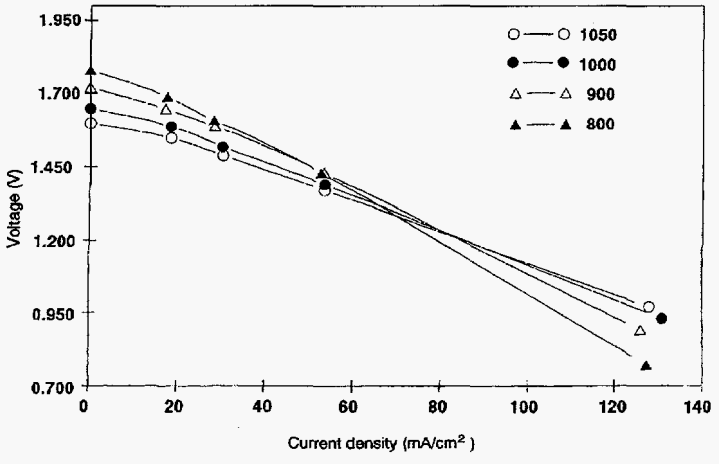

Figure 5-10 Two cell stack performance with 97% H_2 and 3% H_2O/air.
Source: Allied-Signal Aerospace Company, 1992.

5.2.3 Effect of Reactant Gas Composition and Utilization

Since SOFCs operate at high temperature, they are capable of internally reforming fuel gases (i.e., CH_4 and other light hydrocarbons) without the use of a specific reforming catalyst (i.e., anode itself is sufficient), and this attractive feature of high temperature operation of SOFCs has recently been experimentally verified. Another important aspect of SOFCs is that recycle of CO_2 from the spent fuel stream to the inlet oxidant, as required by MCFCs, is not necessary because SOFCs utilize only O_2 at the cathode.

Oxidant: The performance of SOFCs, like that of other fuel cells, improves with pure O_2 rather than air as the oxidant. With a fuel of 67% H_2/22% CO/11% H_2O at 85% utilization, the cell voltage at 1000°C shows an improvement with pure O_2 over that obtained with air (see Figure 5-11). In the figure, the experimental data are extrapolated by a dashed line to the theoretical Nernst potential for the inlet gas compositions. At a target current density of 160 mA/cm^2 for the tubular SOFC operating on the above mentioned fuel gas, a difference in cell voltage of about 55 mV is obtained. The difference in cell voltage with pure O_2 and air increases as the current density increases, which suggests that concentration polarization plays a role during O_2 reduction in air.

Based on the Nernst equation, the theoretical voltage gain due to a change in oxidant utilization at T = 1000°C is:

$$\Delta V_{Cathode} = 63 \log \frac{(\bar{P}_{O_2})_2}{(P_{O_2})_1} \tag{5-12}$$

where $\bar{P}_{O_2}$ is the average partial pressure of O_2 in the system. Data (40) suggest that a more accurate depiction of voltage gain is described by :

$$\Delta V_{Cathode} = 92 \log \frac{(\bar{P}_{O_2})_2}{(\bar{P}_{O_2})_1} \tag{5-13}$$

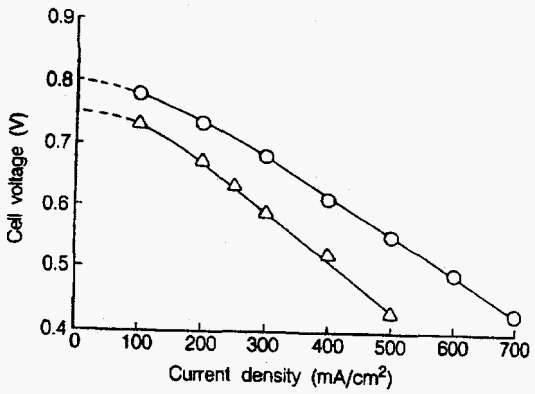

Figure 5-11 Cell performance at 1000°C with pure oxygen (O) and air (Δ), both at 25% utilization. Fuel (67% H_2/22% CO/11%H_2O) utilization is 85%.
Source: C. Zeh, private communication (last edition of Handbook), April 29, 1987.

Fuel: The influence of fuel gas composition on the theoretical open circuit potential of SOFCs is illustrated in Figure 5-12, following the discussion by Sverdrup, et al. (9). The oxygen/carbon (O/C) atom ratio and hydrogen/carbon (H/C) atom ratio, which define the fuel composition, are plotted as a function of the theoretical open circuit potential at 1000° C. If hydrogen is absent from the fuel gas, H/C = 0. For pure CO, O/C = 1, and for pure CO_2, O/C = 2. The data in the figure show that the theoretical potential decreases from above 1 V to about 0.6 V as the amount of O_2 increases and the fuel gas composition changes from CO to CO_2. The presence of hydrogen in the fuel produces two results: (a) the potential is higher, and (b) the O/C ratio corresponding to complete oxidation extends to higher values. These effects occur because the equilibrium composition obtained by the water gas shift reaction in gases containing hydrogen (H_2O) and carbon (CO) produces H_2, but this reaction is not favored at higher temperatures (see Appendix 9.3). In addition, the theoretical potential for the H_2/O_2 reaction exceeds that for the CO/O_2 reaction (see Figure 1-3) at temperatures about 800° C, consequently, the addition of hydrogen to the fuel gas will yield a higher open circuit potential in SOFCs. Based on the Nernst equation, the theoretical voltage gain due to a change in fuel utilization at T = 1000° C is:

$$\Delta V_{Anode} = 126 \log \frac{(\bar{P}_{H_2}/\bar{P}_{H_2O})_2}{(\bar{P}_{H_2}/\bar{P}_{H_2O})_1} \qquad (5\text{-}14)$$

where $\bar{P}_{H_2}$ and $\bar{P}_{H_2O}$ are the average partial pressures of H_2 and H_2O in the system.

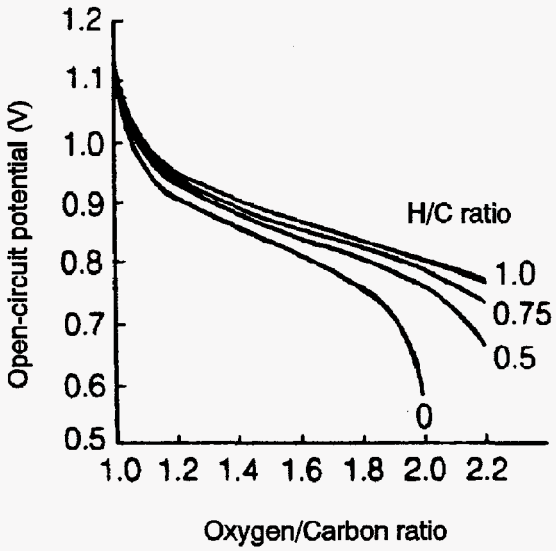

Figure 5-12 Influence of gas composition of the theoretical open-circuit potential of SOFC at 1000° C.
Source: (Figure 3, p. 258) E.F. Sverdrup, C.J. Warde and A.D. Glasser, in *From Electrocatalysis to Fuel Cells*, Edited by G. Sandstede, University of Washington Press, Seattle, WA, 1972.

The fuel gas composition also has a major effect on the cell voltage of SOFCs. The performance data (45) obtained from a 15 cell stack (1.7 cm^2 active electrode area per cell) of the tubular configuration (see Figure 5-1) at 1000°C illustrate the effect of fuel gas composition. With air as the oxidant and fuels of composition 97% H_2/3% H_2O, 97% CO/3% H_2O, and 1.5% H_2/3% CO/75.5% CO_2/20% H_2O, the current densities achieved at 80% voltage efficiency were ~220, ~170 and ~100 mA/cm^2, respectively. The reasonably close agreement in the current densities obtained with fuels of composition 97% H_2/3% H_2O and 97% CO/3% H_2O indicates that CO is a useful fuel for SOFCs. However, with fuel gases that have only a low concentration of H_2 and CO (i.e., 1.5% H_2/3% CO/75.5% CO_2/20% H_2O), concentration polarization becomes significant and the performance is lower.

The reference fuel gas that is currently utilized in experimental SOFCs has a composition 67% H_2/22% CO/11% H_2O. With this fuel (85% utilization) and air as the oxidant (25% utilization), individual cells (~1.5 cm diameter, 30 cm length and ~110 cm^2 active surface area) have delivered a peak power of 22 W (46). The change in the cell voltage with fuel utilization for a SOFC that operates on this reference fuel and pure O_2 or air as oxidant (25% utilization) is shown in Figure 5-13 (41). The cell voltage decreases with an increase in the fuel utilization at constant current density. Insufficient data are available in the figure to determine whether the temperature has a significant effect on the change in cell voltage with utilization. However, the data does suggest that a larger voltage decrease occurs at 1000°C than at 800 or 900°C. Based on this and other data (40, 47) the voltage gain at T = 1000°C and with air is defined by Equation 5-15:

$$\Delta V_{Anode} = 172 \log \frac{(\bar{P}_{H_2}/\bar{P}_{H_2O})_2}{(\bar{P}_{H_2}/\bar{P}_{H_2O})_1} \qquad (5\text{-}15)$$

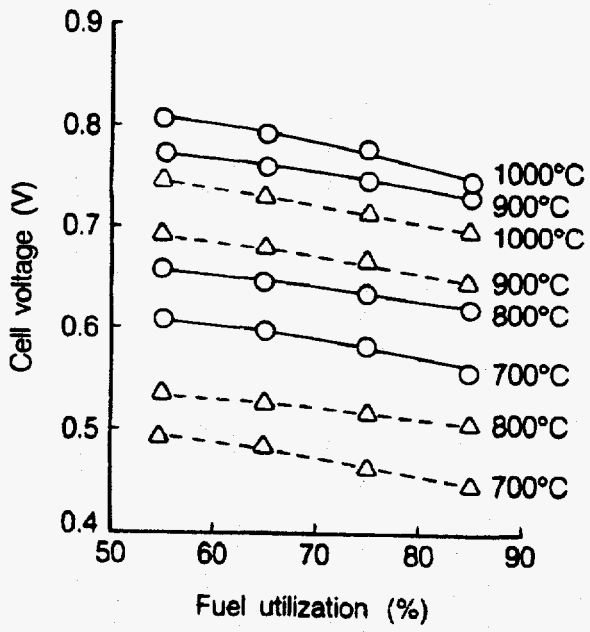

Figure 5-13 Variation in cell voltage as a function of fuel utilization and temperature. Oxidant (0 - pure O_2; Δ - air) utilization is 25%. Currently density is 160 mA/cm^2 at 800, 900 and 1000°C and 79 mA/cm^2 at 700°C.
Source: C. Zeh, private communication (last edition of Handbook), April 29, 1987.

5.2.4 Effect of Impurities

Hydrogen sulfide (H_2S), hydrogen chloride (HCl) and ammonia (NH_3) are impurities typically found in coal gas. Each of these substances are potentially harmful to the performance of SOFC's. Recent experiments (47) have used a simulated oxygen-blown coal gas containing 37.2% CO/34.1% H_2/0.3% CH_4 /14.4% CO_2/13.2% H_2O/0.8% N_2. These experiments have shown no degradation due to the presence of 5,000 ppm NH_3. An impurity level of 1 ppm HCl has also shown no detectable degradation. H_2S levels of 1 ppm result in an immediate performance drop, but this loss soon stabilizes into a normal linear degradation. Figure 5-14 shows the performance of the experimental cell over time. Additional experiments have shown that removing H_2S from the fuel stream returns the cell to nearly its original level. It has also been found that maintaining an impurity level of 5,000 ppm NH_3 and 1 ppm HCl, but decreasing the H_2S level to 0.1 ppm, eliminates any detrimental effect due to the presence of sulfur, even though, as mentioned above, 1 ppm H_2S causes virtually no degradation.

In addition, silicon (Si), which can also be found in coal gas, has been studied (47) as a contaminant. It is believed to accumulate on the fuel electrode in the form of silica (SiO_2). The deposition of the Si throughout the cell has been found to be enhanced by high (~50%) H_2O content in the fuel. Si is transported by the following reaction:

$$SiO_2\,(S) + 2H_2O\,(g) \rightarrow Si(OH)_4\,(g) \qquad (5\text{-}15)$$

As the CH_4 component of the fuel reforms to CO and H_2, H_2O is consumed. This favors the reversal of Equation 5-15 which allows SiO_2 to be deposited downstream, possibly on exposed nickel surfaces. Oxygen-blown coal gas, however, only has an H_2O content of ~13% and this is not expected to allow for significant Si transport.

5.2.5 Effects of Current Density

The voltage level of a SOFC is reduced by ohmic, activation, and concentration losses which increase with increasing current density. The magnitude of this loss is described by the following equation which was developed from information in the literature (21, 44, 48, 49, 50, 51):

$$\Delta V_j(mV) = -0.73\Delta J \qquad (T = 1{,}000^\circ C) \qquad (5\text{-}16)$$

where J is the current density (mA/cm^2) at which the cell is operating.

5.2.6 Effects of Cell Life

The endurance of the cell stack is of primary concern for SOFCs. As SOFC technology has continued to approach commercialization, research in this area has increased and improvements made, Figure 5-15. Current data (48, 49, 52, 53, 54) for a number of stack sizes depicts an average degradation of individual cells of:

$$\Delta V_{lifetime}\,(mV) = -7mV/1000\ hours \qquad (5\text{-}17)$$

Westinghouse's state-of-the-art SOFCs have been tested up to 40,000 hrs (53).

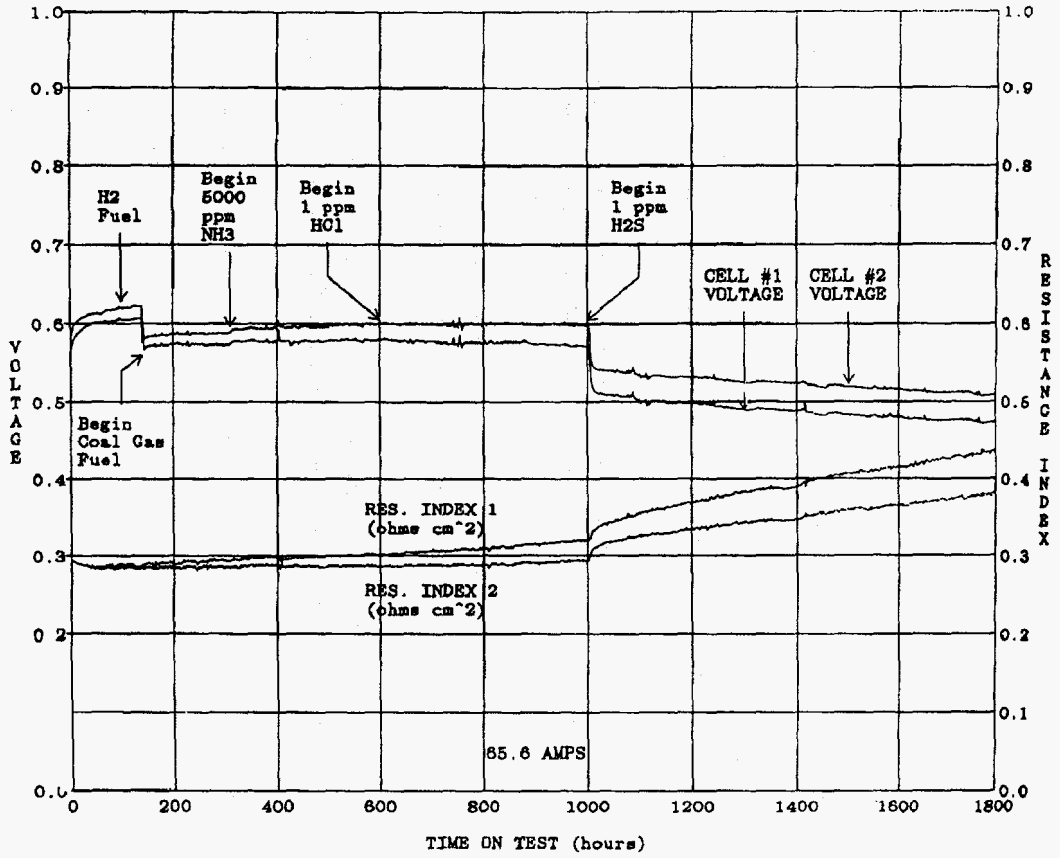

Figure 5-14 SOFC performance at 1000°C and 350 mA/cm², 85% fuel utilization and 25% air utilization. Fuel = simulated air-blown coal gas containing 5000 ppm NH_3, 1 ppm HCl and 1 ppm H_2S.
Source: (47)

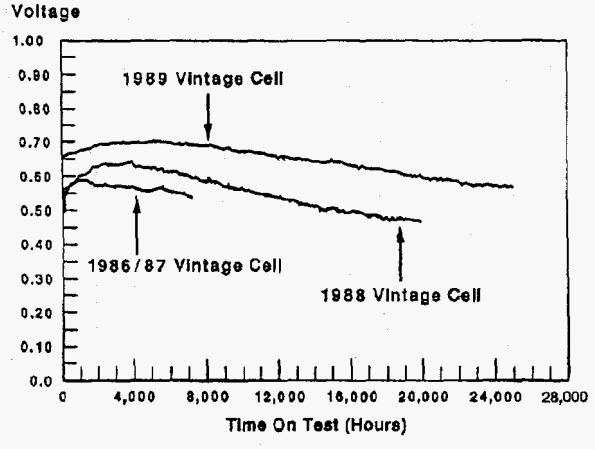

Figure 5-15 Cell degradation improvements.
Source: (53)

5.3 Summary of Equations for SOFC [j]

The preceding sections provide parametric performance based on various referenced data at different operating conditions. It is suggested that the following set of equations could be used for performance adjustments unless the reader prefers other data or correlations.

Parameter	Equation	Comments	
Pressure	$\Delta V_p(mV) = 59 \log \frac{P_2}{P_1}$	$1 \text{ atm} \le P \le 10 \text{ atm}$	(5-7)
Temperature[m]	$\Delta V_T(mV) = 0.008(T_2 - T_1)(°C) * J$	$900°C \le T < 1050°C$	(5-10)
	$\Delta V_T(mV) = 0.04(T_2 - T_1)(°C) * J$	$800°C < T \le 900°C$	(5-11)
Oxidant	$\Delta V_{Cathode}(mV) = 92 \log \frac{(\bar{P}_{O_2})_2}{(\bar{P}_{O_2})_1}$	$0.16 \le \frac{\bar{P}_{O_2}}{\bar{P}_{Total}} \le 0.20$	(5-13)
Fuel	$\Delta V_{Anode}(mV) = 172 \log \frac{(\bar{P}_{H_2}/\bar{P}_{H_2O})_2}{(\bar{P}_{H_2}/\bar{P}_{H_2O})_1}$	$0.9 \le \bar{P}_{H_2}/\bar{P}_{H_2O} \le 6.9$ T=1000° C, with air	(5-15)
Current Density	$\Delta V_J(mV) = 0.73\Delta J$	$50 < J < 400 \text{ mA/cm}^2$ P = 1 atm., T = 1,000°C	(5-16)
Life Effects	$\Delta V_{lifetime}(mV) = -7mV/1{,}000 \text{ hours}$		(5-17)

References

1. N.Q. Minh, "Ceramic Fuel Cells", *J. Am. Ceram. Soc.*, **76**[3]563-88, 1993.
2. T.H. Edsell and S.N. Flengas, *J. Electrochem. Soc.*, **118**, 1890 (1971).
3. A.O. Isenberg, in *Proceedings of the Symposium on Electrode Materials and Processes for Energy Conversion and Storage*, Edited by J.D.E. McIntyre, S. Srinivasan and F.G. Will, The Electrochemical Society, Inc., Pennington, NJ, 1977, p. 682.
4. N. Q. Minh, "High-Temperature Fuel Cells, Part 2: The Solid Oxide Cell," *ChemTech,* Vol. 21, February, 1991.
5. A. J. Appleby, F. R. Foulkes, *Fuel Cell Handbook*, Van Nostrand Reinhold, New York, NY, 1989.
6. A.O. Isenberg, in *Proceedings of the Symposium on Electrode Materials and Processes for Energy Conversion and Storage,* Edited by J.D.E. McIntyre, S. Srinivasan and F.G. Will, The Electrochemical Society, Inc., Pennington, NJ, 1977, p. 572.
7. D.C. Fee, S.A. Zwick and J.P. Ackerman, in *Proceedings of the Conference on High Temperature Solid Oxide Electrolytes*, held at Brookhaven National Laboratory, August 16-17, 1983, BNL 51728, compiled by F.J. Salzano, October 1983, p. 29.

---

[j] See Footnote j on page 5-15.

[m] where J = mA/cm^2, for fuel composition of 67% H_2/22% CO/11% H_2O

8. D.W. Dees, T.D. Claar, T.E. Easler, D.C. Fee and F.C. Mrazek, *J. Electrochem. Soc.*, **134**, 2141, 1987.
9. E.F. Sverdrup, C.J. Warde and A.D. Glasser, in *From Electrocatalysis to Fuel Cells*, Edited by G. Sandstede, University of Washington Press, Seattle, WA, 1972, p. 255.
10. D.H. Archer, L. Elikan, and R.L. Zahradnik, in *Hydrocarbon Fuel Cell Technology*, Edited by B.S. Baker, Academic Press, New York, NY, 1965, p. 51.
11. D.H. Archer, J.J. Alles, W.A. English, L. Elikan, E.F. Sverdrup, and R.L. Zahradnik, in *Fuel Cell Systems, Advances in Chemistry Series 47*, Edited by R.F. Gould, American Chemical Society, Washington, DC, 1965, p. 332.
12. E.R. Ray, "Westinghouse Tubular SOFC Technology", in *Fuel Cell Program and Abstracts,* in 1992 Fuel Cell Seminar, Tucson, AZ, November 29-December 2, 1992.
13. M.S.S. Hsu, W.E. Morrow and J.B. Goodenough, in *Proceedings of the 10th Intersociety Energy Conversion Engineering Conference*, The Institute of Electrical and Electronics Engineering, Inc., New York, NY, 1975, p. 555.
14. M.S.S. Hsu and T.B. Reed, in *Proceedings of the 11th Intersociety Energy Conversion Engineering Conference*, American Institute of Chemical Engineers, New York, NY, 1976, p. 1.
15. M. Hsu, "Zirconia Fuel Cell Power System" in 1985 *Fuel Cell Seminar Abstracts*, 1985 Fuel Cell Seminar, Tucson, AZ, May 19-22, 1985.
16. M. Hsu, "Zirconia Fuel Cell Power System Planar Stack Development" in *Fuel Cell Abstracts*, 1986 Fuel Cell Seminar, Tucson, AZ, October 26-29, 1986.
17. Y. Jatsuzaki, et al., "High Power Density SOFC Development at Tokyo Gas", in *Fuel Cell Program and Abstracts*, 1992 Fuel Cell Seminar, Tucson, Arizona, November 29-December 2, 1992.
18. D.C. Fee, paper presented "Characterization of Monolithic Fuel Cell Components," in *Fuel Cell Abstracts*, 1986 Fuel Cell Seminar, Tucson, AZ, October 26-29, 1986.
19. D.C. Fee, in *Proceedings of the 21th Intersociety Energy Conversion Engineering Conference*, American Chemical Society, Washington, D.C., 1986, p. 1634.
20. S. Majumdar, T. Claar and B. Flandermeyer, *J. Amer. Ceram. Soc.*, **69**, 628, 1986.
21. N. Minh et al, "Monolithic Solid Oxide Fuel Cell Development: Recent Technical Progress," Allied-Signal, in *Fuel Cell Seminar Program and Abstracts*, 1992 Fuel Cell Seminar, 1992.
22. K. Krist, "Gas Research Institute's Fundamental Research on Intermediate-Temperature Planar Solid Oxide Fuel Cells", in *Fuel Cell Program and Abstracts*, 1992 Fuel Cell Seminar, Tucson, AZ, November 29-December 2, 1992.
23. B.L. Halpern, J.W. Golz, Y. Di, "Jet Vapor Deposition of Thin Films for Solid Oxide and Other Fuel Cell Applications", in *Proceedings of the Fourth Annual Fuel Cells Contractors Review Meeting*, U.S. DOE/METC, July, 1992.
24. H.U. Anderson, M.M. Nasrallah, "Characterization of Oxides for Electrical Delivery Systems", in *An EPRI/GRI Fuel Cell Workshop on Fuel Cell Technology Research and Development*, New Orleans, LA, April 13-14, 1993.
25. O. Yamamoto, et al., "Zirconia Based Solid Ion Conductors", in *The International Fuel Cell Conference Proceedings*, NEDO/MITI, Tokyo, Japan, 1992.
26. M. Krumpelt, et al., "Supporting Research for MSOFC Development", in *Proceedings of the Fourth Annual Fuel Cells Contractors Review Meeting*, U.S. DOE/METC, July, 1992.
27. Y. Matsuzaki, et al., "High Power Density SOFC Development at Tokyo Gas", in *Fuel Cell Program and Abstracts*, 1992 Fuel Cell Seminar, Tucson, AZ, November 29-December 2, 1992.

28. C. Bagger, "Improved Production Methods for YSZ Electrolyte and Ni-YSZ Anode for SOFC", in *Fuel Cell Program and Abstracts*, 1992 Fuel Cell Seminar, Tucson, AZ, November 29-December 2, 1992.
29. J.L. Bates, "Alternative Materials for Solid Oxide Fuel Cells: Factors Affecting Air-Sintering of Chromite Interconnections", in *Proceedings of the Fourth Annual Fuel Cells Contractors Review Meeting*, U.S. DOE/METC, July, 1992.
30. A.R. Nicoll, G. Barbezat, A. Salito, "The Potential of Plasma Spraying for the Deposition of Coatings on SOFC Components", in *The International Fuel Cell Conference Proceedings*, NEDO/MITI, Tokyo, Japan, 1992.
31. F. Uchiyama, et al., "ETL Multi-Layer Spray Coating for SOFC Component", in *The International Fuel Cell Conference Proceedings*, NEDO/MITI, Tokyo, Japan, 1992.
32. C. Tanner, et al., "Fabrication and Characterization of Ceria-Based Electrolytes", in *An EPRI/GRI Fuel Cell Workshop on Fuel Cell Technology Research and Development*, New Orleans, LA, April 13-14, 1993.
33. N.Q. Minh, C.R. Horne, R.A. Gibson, "A Novel and Cost-Effective Fabrication Method for Reduced-Temperature Solid Oxide Fuel Cell Applications", in *An EPRI/GRI Fuel Cell Workshop on Fuel Cell Technology Research and Development*, New Orleans, LA, April 13-14, 1993.
34. A.F. Sammells, "Perovskite Solid Electrolytes for SOFC", in *Proceedings of the Fourth Annual Fuel Cells Contractors Review Meeting*, U.S. DOE/METC, July, 1992.
35. I. Bloom, et al., "Electrolyte Development for Intermediate Temperature, Solid Oxide Fuel Cells", in *Fuel Cell Program and Abstracts*, 1992 Fuel Cell Seminar, Tucson, AZ, November 29-December 2, 1992.
36. I. Bloom, M. Krumpelt, "Intermediate Temperature Electrolytes for SOFC", in *Proceedings of the Fourth Annual Fuel Cells Contractors Review Meeting*, U.S. DOE/METC, July, 1992.
37. H. Tsuneizumi, et al., "Development of Solid Oxide Fuel Cell with Metallic Separator", in *The International Fuel Cell Conference Proceedings*, NEDO/MITI, Tokyo, Japan, 1992.
38. P. Han, et al., "Novel Oxide Fuel Cells Operating at 600 - 800°C", in *An EPRI/GRI Fuel Cell Workshop on Fuel Cell Technology Research and Development*, New Orleans, LA, April 13-14, 1993.
39. J.T. Brown, Energy, **11**, 209, 1986.
40. H. Ide et al, "Natural Gas Reformed Fuel Cell Power Generation Systems - A Comparison of Three System Efficiencies," in *Proceedings of the 24th Intersociety Energy Conversion Engineering Conference*, The Institute of Electrical and Electronics Engineers, Washington, D.C., 1989.
41. C. Zeh, private communication, last edition of Handbook, April 29, 1987.
42. A. Sammells, "Perovskite Electrolytes for SOFC," in *Proceedings of the Third Annual Fuel Cells Contractors Review Meeting*, U.S. DOE/METC, pg. 152, June, 1991.
43. A. Khandkar & S. Elangovan, "Planar SOFC Development Status," in *Proceedings of the Second Annual Fuel Cells Contractors Review Meeting*, U.S. DOE/METC, pg. 152, May, 1990.
44. Data from Allied-Signal Aerospace Company, 1992.
45. C. J. Warde, A. O. Isenberg, J. T. Brown "High-Temperature Solid-Electrolyte Fuel-Cells-Status and Programs at Westinghouse," in *Program and Abstracts*, ERDA/EPRI Fuel Cell Seminar, Palo Alto, CA, June 29-30 to July 1, 1976.
46. W.J. Dollard and J.T. Brown, "Overview of the Westinghouse Solid Oxide Fuel Cell Program," in *Fuel Cell Abstracts*, 1986 Fuel Cell Seminar, Tucson, AZ, Oct 26-29, 1986.
47. N. Maskalick, "Contaminant Effects in Solid Oxide Fuel Cells," Proceedings of the Fourth Annual Fuel Cells Contractors Review Meeting, U.S. DOE/METC, July, 1992.

48. Y. Yoshida et al, "Development of Solid Oxide Fuel Cell," paper provided by Mitsubishi Heavy Industries Ltd.
49. A. Khandkar et al, "Planar SOFC Technology Status and Overview," Ceramatec, Inc., in *Fuel Cell Seminar Program and Abstracts*, 1992 Fuel Cell Seminar, Tucson, AZ, November 29-December 2, 1992.
50. "Research and Development on Fuel Cell Power Generation Technology," FY 1990 Annual Report, NEDO, April, 1991.
51. T. Nakanishi, "Substrate Type, Planar Solid Oxide Fuel Cell," Fuji Electric, in *Fuel Cell Seminar Program and Abstracts*, 1992 Fuel Cell Seminar, Tucson, AZ, November 29-December 2, 1992.
52. Y. Akiyama et al, "Development of a Planar Solid Oxide Fuel Cell at Sanyo," in *Fuel Cell Seminar Program and Abstracts*, 1992 Fuel Cell Seminar, Tucson, AZ, November 29-December 2, 1992.
53. E. Ray, "High Temperature Tubular Solid Oxide Fuel Cell Development," Proceedings of the Fourth Annual Fuel Cells Contractors Review Meeting, U.S. DOE/METC, July, 1992.
54. E. Erdle et al, "Status of Planar SOFC Development of Dornier," in *Fuel Cell Seminar Program and Abstracts*, 1992 Fuel Cell Seminar, Tucson, AZ, November 29-December 2, 1992.

6. ALTERNATIVE FUEL CELL TECHNOLOGIES

The discussion in Sections 3, 4 and 5 focused on the three major fuel cell systems (i.e., PAFC, MCFC, and SOFC) currently being considered for stationary power applications. The other fuel cell systems, PEFC and AFC, have been demonstrated primarily in vehicular power applications, both terrestrial (motive) and space (on-board). Excellent overviews of the PEFC (1) and AFC (2,3) technologies are available. In this section, the status of PEFCs and AFCs will be reviewed.

6.1 Polymer Electrolyte Fuel Cell

The use of organic cation exchange membrane polymers in fuel cells was originally conceived by William T. Grubbs (4) in 1959. The desired function of the ion membrane was originally to provide an ion conductive gas barrier. Strong acids were used to provide a contact between the adjacent membrane and catalytic surfaces. During further development, it was recognized that the cell functioned well without adding acid. As a result, present PEFCs do not use any electrolyte other than the hydrated membrane itself (5). The basic cell consists of a proton conducting membrane, such as a perfluorosulphonic acid polymer, sandwiched between two Pt impregnated porous electrodes. The back of the electrodes are made hydrophobic by coating with an appropriate compound, such as Teflon^{R}. This wet proof coating provides a path for gas diffusion to the catalyst layer.

The electrochemical reactions of the PEFC are similar to those of the PAFC: H_2 at the anode provides a proton, freeing an electron in the process which must pass through an external circuit to reach the cathode. The proton, which remains solvated with a certain number of water molecules, diffuses through the membrane to the cathode to react with O_2 and the returning electron (6). Water is produced at the cathode.

Due to the intrinsic construction materials, low temperature operation, approximately 80° C, is possible. The cell is also able to sustain operation at very high current densities. These attributes lead to a fast start capability and the ability to make a compact, light cell (6). Other attributes are that there is no corrosive fluid spillage hazard and there is lower sensitivity to orientation. As a result, the PEFC is particularly suited for vehicular power application. This application means that the fuel of choice for terrestrial applications will probably be methanol (7), although hydrogen storage on-board in the form of pressurized gas is being considered. Space applications will use hydrogen. The cell is also being considered for stationary power application, but to a lesser degree. Fuels being considered for early, stationary power units are natural gas and hydrogen-rich off-gases.

The low operating temperature, 80° C, results in both advantages and disadvantages. Low temperature operating capability is advantageous because the cell can start from ambient conditions quickly, especially when pure H_2 fuel is available. It is a disadvantage in that Pt catalysts are

required to promote the electrochemical reaction. Only a few ppm of CO can be tolerated with the Pt catalysis at 80°C. Reformed hydrocarbons contain about one percent of CO. If the PEFC is to use a reformed hydrocarbon fuel, such as methanol or natural gas, then a mechanism to reduce the level of CO in the fuel gas is needed. The low temperature of operation also means that little if any heat is available from the fuel cell for any endothermic reforming process (8, 9).

There is a distinction in the PEFC in that water is produced in the liquid state, not steam. One of the critical issues of polymer cells is the necessity to maintain a high water content in the electrolyte to obtain acceptable ion conductivity. The ionic conductivity of the electrolyte is higher when water content is high. The water content in the cell is determined by the balance of water or its transport during the reactive mode of operation. Contributions to the water transport are the water drag through the cell, back diffusion from the cathode, and the diffusion of any water in the fuel stream through the anode. The water transport is a function of the cell current and the characteristics of the membrane and the electrodes. Water drag refers to the amount of water which is pulled by osmotic action[a] along with the proton (10). Between 1 and 2.5 molecules are dragged with each proton (11). As a result, the ion exchanged can be envisioned as a hydrated proton, $H(H_2O)_n^+$. The water drag increases at high current density and, therefore, the water balance could become of greater concern. However, back diffusion of water from the cathode to the anode through the thin membrane results in a net water transport of nearly zero during operation (11,12). A detail modeling of the reactions and water balance are beyond the scope of this handbook. References (13) and (14) are sources for further information on PEFC modeling.

Without control, an imbalance will occur between water production and evaporation within the cell. The imbalance between production and evaporation rates of water can result in either flooding of the electrodes or membrane dehydration, both of which are detrimental to performance. As inferred previously, the membrane operates most efficiently and offers a low resistance to current flow in a fully saturated state. The adherence of the membrane to the electrode will be adversely affected if dehydration occurs. Intimate contact between the electrodes and the electrolyte membrane is important since there is no free liquid electrolyte to form a conducting bridge. If more water is exhausted than produced, then it is important to humidify the incoming anode gas. But if there is too much humidification, the electrode floods, thus causing problems with diffusing the gas to the electrode. A smaller current, larger reactant flow, lower humidity, higher temperature, or lower pressure will result in a water deficit. A higher current, smaller reactant flow, higher humidity, lower temperature, or higher pressure will lead to a water surplus. There have been attempts to control the water in the cell by using external wicking connected to the membrane to either drain or supply water by capillary action. However, the favored practice is to control the cell water content by humidifying the incoming reactant gases (13). Ballard Power Systems of Canada has demonstrated stack designs and automated systems which manage water balances successfully.

Both temperature and pressure of operation have a significant influence on cell performance and the impact of these parameters will be described later. Present cells operate at 80°C, nominally, 0.285 MPa (30 psig) (6), and a range of 0.10 to 1.0 MPa (10 to 100 psig). However, with the appropriate current collectors and supporting structure, polymer electrolyte fuel cells and electrolysis cells should be capable of operating at pressures up to 3000 psi and differential pressures up to 500 psi (15).

---

[a]There is a question on whether there is actually a net transfer of water across the membrane. For example, Srvinivasan at Texas A&M notes that the proton transfer across the membrane may be by a "hopping" mechanism within the lattice of the membrane which is called the "Grothus conduction". If so, there would be no drag on the water molecules.

6.1.1 State-of-the-Art Components

There has been an increased interest in polymer electrolyte fuel cells only within the last five years. As a result, the cells are not as developed as PAFCs, MCFCs, or SOFCs. Development has reached the point where motive power applications appear achievable at an acceptable cost with a hybrid fuel cell/battery system (16). Noticeable accomplishments in the technology have been that Ballard Power Systems has achieved an operating life of 3,000 hrs. with a 35 cell stack (17) which is Ballard's standard commercial unit. This unit achieves up to 5 kW. The unit has been used as a basic block for a 120 kW motive powered 10 m (32 ft.) transit bus demonstration. Another company, Energy Partners in the U.S., has built a unit for providing traction power to an automobile achieving 15 kW with three 60 cell (780 cm^2/cell) stacks (18). Developers have obtained a maximum power density of at least 2 W/cm^2 and current densities up to approximately 6 A/cm^2 have been reported for single cells operating on pure oxygen. With air operation, there is a limit of less than 2 A/cm^2 at a cell voltage of 0.5 or below. This is attributed to the formation of a nitrogen barrier at the back of the cathode which causes a mass transport limit (19). Stacks of cells have operated to approximately 2 A/cm^2. In the descriptions which follow, Ballard Power Systems fuel cells are considered representative of the state-of-the-art due to the company's discernible position in the transportation and stationary fuel cell application fields.

As stated earlier, a polymer electrolyte fuel cell consists of a proton conducting membrane such as a perfluorosulfonic acid polymer, sandwiched between two Pt impregnated porous electrodes which have been made hydrophobic by coating with an appropriate compound. Manufacturing details of the Ballard Power Systems cell and stack design are proprietary (20). However, the literature does provide some information on the cell and stack design. An example schematic of a manufacturer's cell is shown in Figure 6-1 (21).

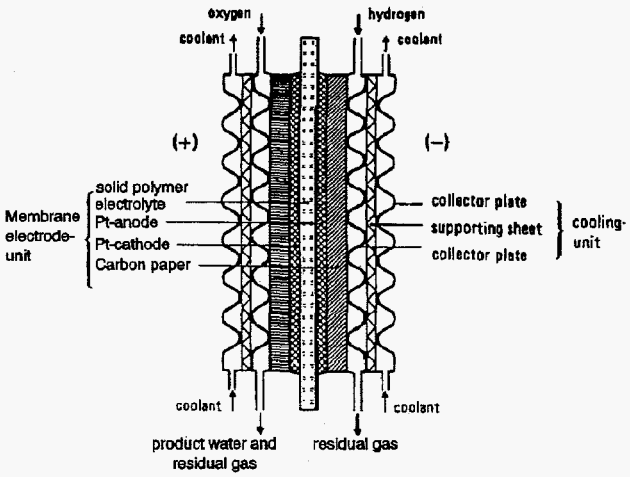

Figure 6-1 PEFC schematic.
Source: Reference (21).

The standard electrolyte material presently used in PEFCs is a fully fluorinated Teflon^R based material produced by E.I. DuPont de Nemours for space application in the mid-1960s. The DuPont electrolytes have the generic brand name, Nafion^R and the specific type used most often in present PEFCs is membrane No. 117 (22). The Nafion membranes, which are fully fluorinated polymers, exhibit exceptionally high chemical and thermal stability, i.e., stable against chemical attack in strong

bases, strong oxidizing and reducing acids, H_2O_2, CI_2, H_2 and O_2 at temperatures up to 125° C (23). A Teflon[R] like structure serves as a backbone of the membrane with side chains terminating in sulfonic acid functional groups (16). DuPont fluorinated electrolytes exhibited a substantial improvement in life over previous electrolytes when introduced, achieving over 50,000 hours. Recently, the Dow Chemical Company has produced an electrolyte membrane, the XUS 13204.10, which exhibits somewhat lower electrical resistance and permits increased current densities than the Nafion[R] membrane particularly when used in thinner form (20). The use of this membrane is not standard; it will be described in more detail with other technology development components.

The present electrodes are cast as thin films each of which contains 10% Pt on carbon supports weighing 4 mg/cm^2. The state-of-the-art electrodes are bonded to the membrane.

The current collectors, which are placed adjacent to the back of the electrodes are a thin piece of hydrophobic carbon felt paper (21). This paper can also provide some rigidity for the cell. The bipolar separator plate is configured with graphite material (20). Cooling is accomplished by using a heat transfer fluid, usually water, which is pumped through integrated coolers within the stack. The temperature rise across the cell is kept to less than 10° C. Water cooling and humidification are in series and thus, there is a need for high quality water. The cooling unit of a cell can be integrated to supply reactants to the membrane/electrode unit, remove reaction products from the cell, and seal off the various media against each other and the outside, Figure 6-1 (21). The conducting parts of the frames are titanium, non-conducting parts are polysulfone (24).

Reformed hydrocarbon fuels contain at least 1% CO. Yet even small amounts of in the gas stream will preferentially adsorbed on the Pt catalysts surface and block access of the H_2 to the catalyst sites. Tests indicate that approximately 10 ppm of CO in the gas stream begin to impact cell performance (7, 25). Ballard Power Systems has demonstrated stable operation on reformed natural gas fuel by converting the CO to CO_2 using a selective oxidation combined with the reforming process.

A number of technical and cost issues facing polymer electrolyte fuel cells at the present stage of development have been recognized by managers and researchers (7, 16, 26, 27, 28). These issues concern the cell membrane, cathode performance, and cell heating limits.

The membranes used in the present cells are expensive and available only in limited ranges of thickness and specific ionic conductivity. There is a need to lower the cost of the present membranes and to investigate lower cost membranes which continue to exhibit low resistivity. This is particularly important for transportation applications where high current density operation is needed. Cheaper membranes promote lower cost PEFCs and thinner membranes with lower resistivities could contribute to power density improvements (28). It is estimated that the cost of perfluorosulfonate membrane could fall ten-fold, making them cost effective, if the market increased significantly.

There is some question of whether higher utilization of the catalyst is needed even though new research has resulted in the loadings being reduced to less than 1 mg/cm^2. Some researchers cite a need for higher utilization of catalysts (19). Others state that because only 10% of the cell materials cost is tied up in catalyst, even with a loading of 1 mg/cm^2, it is cost effective to concentrate on the design of an effective membrane and electrode assembly at this time (26). Others believe that Pt alloy, alternate catalysts (29), and/or CO tolerant catalysts should be developed which provide comparable performance as Pt (19).

Performance of the cathode when operating on air at high current densities needs improving. At higher current densities there is a limiting gas permeability and/or ionic conductivity within the catalysts layer. A nitrogen blanket forming on the gas supply side of the cathode is suspected of additional limitations (7). There is a need to develop a cathode which lessens the impact of the

nitrogen blanket, increases the pressurization of the cell, or increases the ionic conductivity of the cathode catalyst.

There are local heating problems which limit stack operation with air to a current density of approximately 2 A/cm^2. Single cells have shown the capability to operate at higher current densities on pure O_2. It may be possible to increase current density, and hence, power density, with better cooling.

6.1.2 Development Components

Because the developmental status of the PEFCs is at an earlier stage than the fuel cells described previously, the difference between state-of-the-art and developmental components is less distinguishable. However, there is ongoing research to improve the performance of the cell and lower its cost. This research closely, but not completely, parallels the issues mentioned previously. The principle areas of development are improving cell membranes, handling of the CO in the fuel stream, electrode design refinements, and extension of the PEFC technology to directly convert methanol in the cell.

The Dow Chemical Company has developed, the XUS 13204.10 membrane, which when incorporated in a PEFC, has been reported to achieve higher performance than that obtained with Nafion membranes, Figure 6-2. The Dow membrane, also a perfluorinated-sulfonic acid, has a lower equivalent weight than Nafion and is prepared with shorter anion-anion distances. It has more sulfonic acid groups per CF_2 than Nafion (19). Because of these characteristics, the membrane has a slight increase in conductivity and water retention capability. Most of the improvement in performance can be attributed to the Dow membrane being supplied at a thickness of 2 mils where the Nafion membrane is supplied at 7 mils thickness. DuPont is now producing a membrane of 2 mils thick and it is achieving the same performance as the top curve in Figure 6-2 (30).

Both the Nafion 117 and the Dow XUS 13204.10 membranes are, at present, expensive and available only in limited ranges of thickness and specific ionic conductivity. There is a need to investigate alternative membranes. Two approaches which have been suggested are the partially fluorinated membranes and possibility of using simultaneous radiation grafting of styrene on FEP (fluoro-ethylene-propylene) films by sulfonation (28). Endurance testing proved steady performance for high grafted membranes over periods of more than 300 hours at a cell temperature of 60° C. Low grafted membranes and the commercial Morgane CDS showed considerable decay of cell power during the same time period. At a cell temperature of 80° C all membranes suffered from a fast degradation. Alternate combinations of base and grafted polymers will have to be explored for the higher temperature operation.

Methods have demonstrated the capability to reduce CO in a methanol reformed gas (anode fuel supply stream) from 1% to approximately 10 ppm by a selective oxidation process based on a Pt/alumina catalyst. But the performance of the anode catalyst, though satisfactory, is impacted even by this low amount of CO. Scientist at Los Alamos National Laboratory has demonstrated an approach to remediate this problem by bleeding a small amount of air or O_2 into the anode compartment. Figure 6-3 shows that a performance equivalent to that obtained on pure hydrogen can be achieved with this approach. It is assumed that this approach would also be applicable to a reformed natural gas fuel which incorporates a water gas shift to obtain CO levels of 1% into the fuel cell. This approach results in a loss of fuel which should not exceed 4%, provided that the reformed fuel gas can be limited to 1% CO (7). Another approach is to develop a CO tolerant anode catalyst. Reportedly, stacks have been produced with these catalysts (6) but no results were

reported and an effective replacement to Pt catalyst has not been identified (7). At this time, Pt catalyst will have to be used requiring an associated system efficiency penalty.

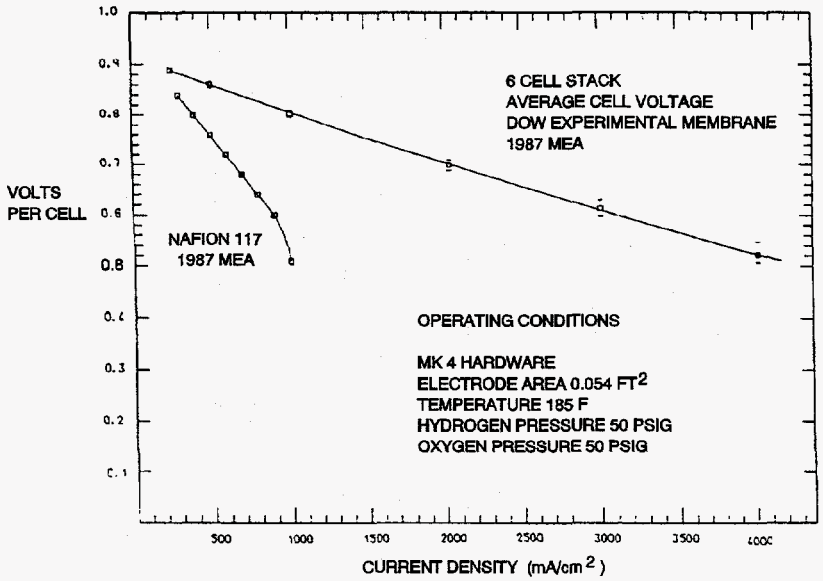

Figure 6-2 Multi-cell stack performance on Dow membrane.
Source: Reference (31).

Water transport can be controlled by the hydrophobic agent, FEP, in the gas diffusion layer of the anode. Experiments have been conducted to determine the impact of the hydrophobic component in the diffusion layer. Results show that as FEP is decreased, the water transport is increased. As water transport is increased, the ionic resistance is decreased. However, gas diffusion decreases as water transport increases. The final results of this analysis is that there is a need to control the amount of FEP to provide a water transport (H_2O/H^+) which balances lower ionic resistance with an acceptable amount of gas diffusion (10).

Previously, cells were made with an unimpregnated electrode/Nafion electrolyte interface. Later, the proton conductor was impregnated into the active layer of the electrode. This allowed reduced loadings to 0.4 mg/cm^2 while obtaining high power density (15). The standard "Prototech" electrodes contained 10% Pt on carbon supports. New electrodes have been fabricated at Texas A&M with 20 to 40% Pt on carbon while maintaining 0.4 mg/cm^2 loading. Scientist at Texas A&M have found that sputtering a thin layer of Pt (0.05 mg/cm^2) on the front surface of the electrodes improves performance (19).

A more recent approach has been developed to fabricate Pt/C catalyst layers of high performance with loadings as low as 0.1 mg Pt/cm^2 (32). The electrode structure was improved by increasing the contact area between the electrolyte and the Pt clusters. The contact area was increased by 1) the supported catalyst and the ionomeric additive being cast together to form the catalyst layer to ensure that the thickness of the catalyst layer coincides with the depth of the ionomer and 2) the contact area between the additive and the catalyst has been increased by completely eliminating the Teflon component and by improving the dispersion of the ionomer

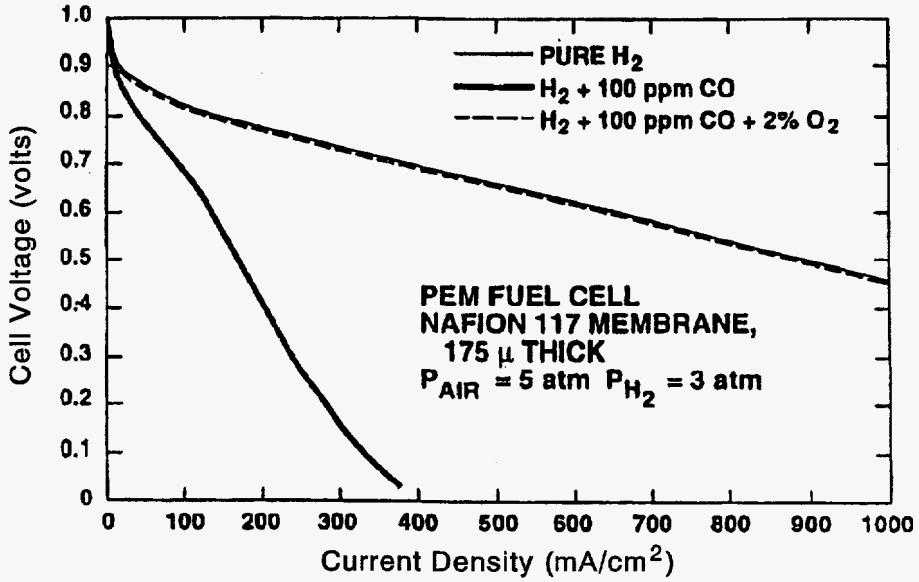

Figure 6-3 Effect on PEFC performances of bleeding oxygen into the anode compartment. *Source*: Reference (7).

throughout the catalyst layer. This is done by blending the solubilized ionomer and the platinized carbon into a homogeneous "ink" from which the thin film catalyst layer of the electrode is cast. Lately, the tetrabutyl ammonium (TBA) form of Nafion^R has been used for preparation of the catalyst layer. It is thermoplastic. The catalyst layer is then coated onto a Teflon blank. This assembly is hot pressed onto the electrolyte membrane. After removal from the press and cooling, the Teflon blank is pulled away leaving a thin film adhered to the membrane. Alternately, the catalyst layer can be applied directly to the membrane. A separate, telfonized carbon cloth serves as the hydropholic backing. The two part construction of the electrode catalyst layer and backing, is performed separately with the properties that best suit the function of each region. The advantages of this fabrication approach is that a thinner catalyst layer of 2 to 3 microns and a very uniform mix of catalyst and ionomer is produced. For example, loadings of 0.17 to 0.13 mg/Pt/cm^2 have been fabricated. The cell generated 3 A/cm^2 at voltage higher than 0.4 on pressurized O_2 and 0.65 V at 1 A/cm^2 on pressurized air (32, 33).

Stable performance was demonstrated to 4,000 hours with Nafion membrane cells having 0.13 mg Pt/cm^2 and cell conditions of 2.4/5.1 atm, H_2/air, and 80°C (4,000 hr. performance was 0.5 V at 600 mA/cm^2). These results mean that the previously worrisome problem of water management is not severe, particularly after thinner membranes of somewhat lower equivalent weight have become available. Some losses may be caused by slow anode catalysts deactivation, but it has been concluded that the Pt catalysts ripening phenomenon does not contribute significantly to the long term performance losses observed in PEFCs (7).

There is considerable interest in extending PEFC technology to the direct methanol and formaldehyde electro-oxidation (34, 35). This requires Pt-based bi-metallic catalysts. Tests have been conducted with gas diffusion type Vulcan XC-72/Toray support electrodes with Pt-Sn (0.5 mg/cm^2, 8% Sn) and Pt-Ru (0.5 mg/cm^2, 50% Ru). The electrodes have Teflon^R content of 20% in the catalyst layer.

6.1.3 Performance

A summary of the performance levels achieved with PEFCs since the mid-1960s is presented in Figure 6-4 (36). Because of the changes in the operating conditions involving pressure, temperature, reactant gases, etc., a wide range of performance levels can be obtained. The performance of the PEFC in the U.S. Gemini Space Program was 37 mA/cm^2 at 0.78 V in a 32 cell stack that typically operated at 50°C and 2 atm (1). Current technology yields performance levels which are vastly superior. Recent unpublished results from Los Alamos National Laboratory show that a performance of 0.78 V at about 200 mA/cm^2 (3 atm H_2 and 5 atm air) can be obtained at 80°C in PEFCs containing a Nafion membrane and electrodes with a Pt loading of 0.4 mg/cm^2. Further details on the recent developments in the performance of PEFCs with Nafion membranes are presented by Watkins et al. (37).

Both temperature and pressure have a significant influence on PEFC performance. The effect of an increase in temperature is a lowering of the internal resistance of the cell, mainly by a decrease in the ohmic resistance of the electrolyte. In addition, mass transport limitations are also reduced at higher temperatures. The overall result is an improvement in cell performance. Experimental data (38, 39, 40) suggests a voltage gain in the range of 1.1 mV to 2.5 mV for each degree (°C) of temperature increase. Improving the cell performance through an increase in temperature is limited by the high vapor pressure of water in the ion exchange membrane which is susceptible to dehydration and loss of ionic conductivity.

The influence of O_2 pressure on the performance of a PEFC at 93°C is illustrated in Figure 6-5 (41). An increase in the O_2 pressure from 30 to 135 psig (3 to 10.2 atm) produces an increase of 42 mV in the cell voltage at 215 mA/cm^2. According to the Nernst equation, the increase in the reversible cathode potential that is expected for this increase in O_2 pressure is about 12 mV, which is considerably less than the measured value. When the temperature of the cell is increased to 104°C, the cell voltage increases by 0.054 V for the same increase in O_2 pressure. Additional data suggests an even greater pressure effect. A PEFC at 50°C and 500 mA/cm^2 (38) exhibited a voltage gain of 83 mV for an increase in pressure from 1 to 5 atm. Another PEFC at 80°C and 431 mA/cm^2 (39) showed a voltage gain of 22 mV for a small pressure increase from 2.4 to 3.4 atm. These results demonstrate that an increase in the pressure of O_2 results in a significant reduction in the polarization at the cathode.

Currently, the major focus of R&D on PEFC technology is to develop a fuel cell system for terrestrial transportation applications, which require the development of low cost cell components. Reformed methanol is expected to be a major fuel source for PEFCs in transportation applications. Because the operating temperature of PEFCs is much lower than that of PAFCs, poisoning of the anode electrocatalyst by CO from steam reformed methanol is a concern. The performances achieved with a proprietary anode in a PEFC with four different concentrations of CO in the fuel gas are shown in Figure 6-6. The graph also shows that at higher current densities the poisoning effect of CO is increased. At these higher current densities, the presence of CO in the fuel causes the cell voltage to become unstable and cycle over a wide range. Additional data (42) has suggested that the CO tolerance of a Pt electrocatalyst can be enhanced by either increasing the temperature or the pressure. As mentioned in Section 6.1.2, developers have designed systems to operate with reformed fuels containing CO, but these system "fixes" reduce efficiency.

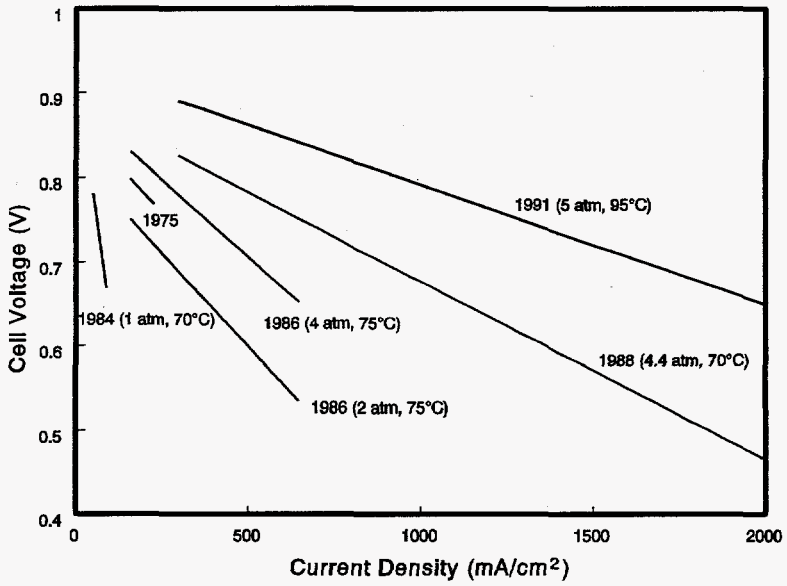

Figure 6-4 Evolutionary changes in the generic performance of PEFCs (a) H_2/O_2, (b) reformate fuel/air, (c) H_2/air.
Source: Reference (13, 36, 38).

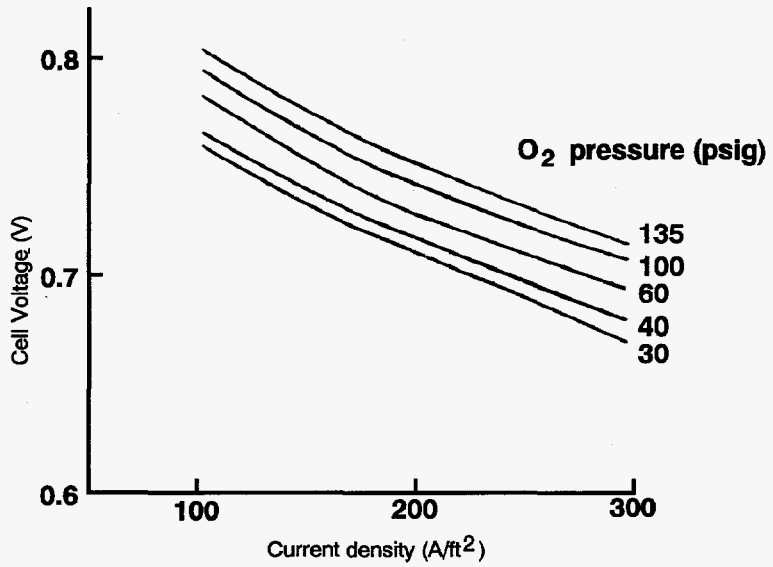

Figure 6-5 Influence of O_2 pressure on the performance of PEFCs at 93° C. Electrode loadings of 2 mg/cm^2 Pt. Oxidant: 30 to 135 psig O_2; fuel: 30 psig H_2.
Source: (Figure 29, p. 49) A. LaConti, G. Smarz and F. Sribnik, "New Membrane-Catalyst for Solid Polymer Electrolyte Systems," final report prepared by Electro-Chem Products, Hamilton Standard for Los Alamos National Laboratory under Contract No. 9-X53-D6272-1, 1985.

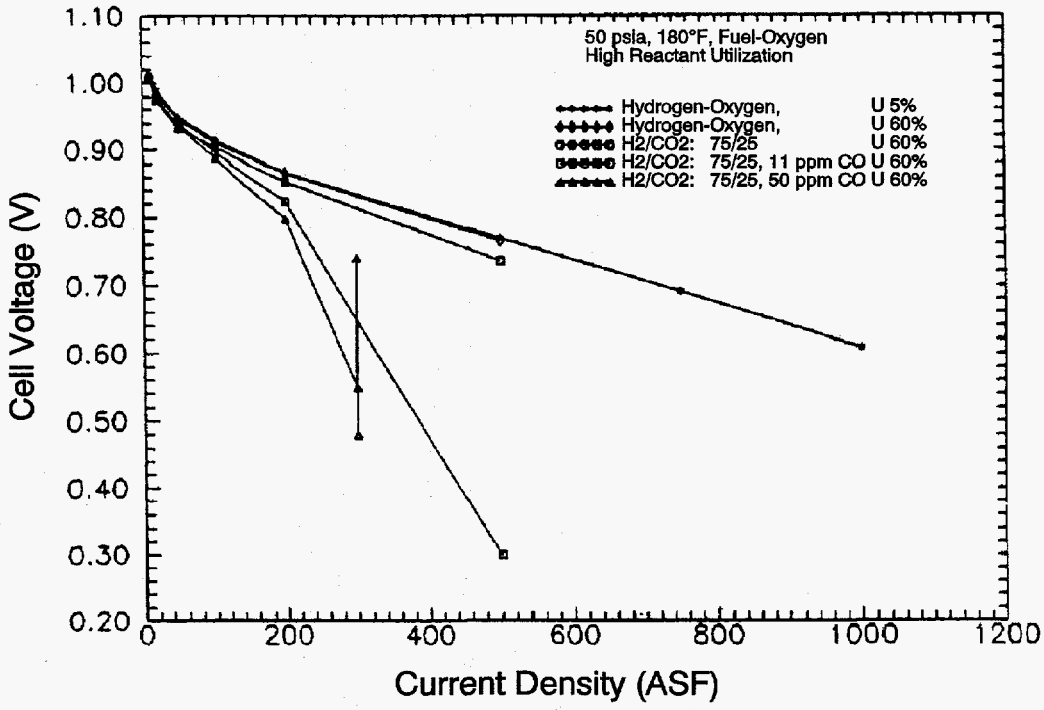

Figure 6-6 Cell performance with carbon monoxide in reformed fuel.
Source: Reference (41).

6.2 Alkaline Fuel Cell

Oxygen reduction kinetics are more rapid in alkaline electrolytes than in acid electrolytes, and the use of non-noble metal electrocatalysts in AFCs is feasible. However, a major disadvantage of AFCs is that alkaline electrolytes (i.e., NaOH, KOH) do not reject CO_2. The consequence of this property is that AFCs are currently restricted to specialized applications where pure H_2 and O_2 are utilized.

The AFC used in the U.S. Apollo Space Program was based, in large part, on the technology originally developed by F.T. Bacon (43) in the 1930s. The fuel cell developed by Bacon operated at 200 to 240°C with 45% KOH, and the pressure was maintained at 40 to 55 atm to prevent the electrolyte from boiling. The anode consisted of a dual-porosity Ni electrode (two layer structure with porous Ni of 16 μm maximum pore diameter on the electrolyte side and 30 μm power diameter on the gas side), and the cathode consisted of a porous structure of lithiated NiO. The three phase boundary in the porous electrodes was maintained by a differential gas pressure across the electrode since a wetproofing agent was not available at that time, i.e., PTFE as a wetproofing material did not exist, and it would not be stable in the high temperature alkaline solution (44).

The AFCs for the U.S. Apollo Space Program (fuel cell module: 57 cm diameter, 112 cm high, ~110 kg, 1.42 kW at 27-31 V, 0.6 kW average power) utilized pure H_2 and O_2 and concentrated electrolyte (85% KOH) to permit cell operation at a lower pressure (~60 psia reactant gas pressure) without electrolyte boiling. With this concentrated electrolyte, the cell performance is not as high as in the less concentrated electrolyte, consequently the operating temperature was increased to 260°C. The typical performance of this AFC was 0.85 V at 150 mA/cm^2, which

compared favorably to the performance of the Bacon cell operating at about 10 times higher pressure. The alkaline fuel cells in the Space Shuttle Orbiter (fuel cell module: 35 cm higher, 38 cm wide, 101 cm long, 91 kg, 12 kW at 27.5 V, 7 kW average power) operate in the same pressure range as for the Apollo program but at a lower temperature (80 to 90°C) and a higher current density (470 mA/cm^2 at 0.86 V). The electrodes contain high loadings of noble metals (anode: 10 mg (80% Pt-20% Pd)/cm^2 on an Ag plated Ni screen, cathode: 20 mg (90% Au-10% Pt)/cm^2 on a Ag-plated Ni screen) that are bonded with PTFE to achieve high performance at the lower temperature of 80 to 90°C. A wide variety of materials (e.g., potassium titanate, ceria, asbestos, zirconium phosphate gel) have been used in the microporous separators for AFCs. A brief survey of the advanced technology components in AFCs for space applications is given by Sheibley and Martin (45).

The AFCs for remote applications (i.e., space, undersea, military) are not strongly constrained by cost. On the other hand, the consumer and industrial markets require the development of low cost components if the AFC is to successfully compete with alternative technologies. Much of the recent interest in AFCs for mobile and stationary terrestrial applications has addressed the development of low cost cell components. In this regard, carbon based porous electrodes play a prominent role, and the following discussion focuses on their application in AFCs.

The performance of AFCs since 1960 has undergone many changes, as evident in the performance data in Figure 6-7 (36). The early AFCs were operated at relatively high temperatures and pressures to meet the requirements for space applications, as discussed above. More recently, a major focus of the technology is for terrestrial applications where low cost components operating at near ambient temperature and pressure with air as the oxidant are desirable. This shift in the fuel cell operating parameters has resulted in the lower performance shown in Figure 6-7.

The kinetics of O_2 reduction in alkaline electrolytes are more favorable than in H_3PO_4. Consider a Pt cathode (0.25 mg/cm^2) in 30% KOH at 70°C and in 96% H_3PO_4 at 165°C. The cathode potentials (vs RHE) at 100 mA/cm^2 in these two electrolytes are 0.868 and 0.730 mV, respectively, according to data reported by Appleby (Figure 2.15-1 in Reference 46). Various explanations have been advanced for the higher O_2 reduction rates in alkaline electrolytes (47); these explanations are outside the scope of the present discussions. The practical consequence of the higher performance of Pt cathodes in alkaline electrolytes is that AFCs are capable of higher efficiencies than PAFCs at a given current density, or higher power densities at the same efficiency. It is estimated (44) that the efficiency of AFCs on pure H_2 is about 60% and that of PAFCs is about 50%, based on the HHV of H_2.

The performance of catalyzed (0.5-2.0 mg noble metal/cm^2) carbon-based[b] porous electrodes for H_2 oxidation and O_2 reduction in 9 N KOH at 55-60°C is presented in Figure 6-8. These results were obtained in the 1960s (48) using technology that is similar to that employed in fabricating electrodes for PAFCs. The performance of the electrodes shows a dependence on the reactant gas concentration, with a higher polarization evident at lower concentrations. The performance of AFCs with carbon-based electrodes has not changed dramatically since these early results were obtained. The performance of a single cell with supported noble metal electrocatalysts (0.5 mg Pt-Rh/cm^2 anode, 0.5 mg Pt/cm^2 cathode) in 12 N KOH at 65°C is shown in Figure 6-9 (49). These results reported in 1986 are comparable to those obtained in 1965. The iR free electrode potentials (vs RHE) at 100 mA/cm^2 in Figure 6-9 are 0.9 V with O_2 and 0.85 V with air. One major difference between the early cathodes and the cathodes in current use is the limiting current for O_2 reduction from air has been improved (i.e., 100-200 mA/cm^2 vs >250 mA/cm^2).

---

[b] Vulcan XC-72 (furnace black) or acetylene black (thermal black) is commonly used.

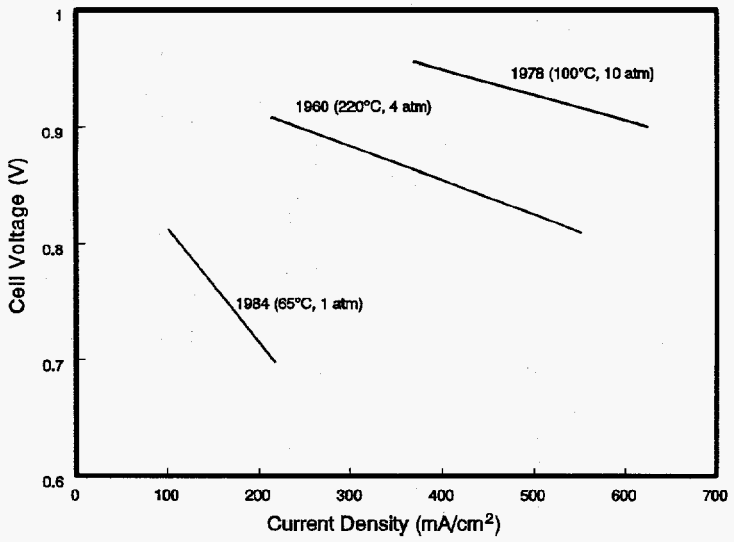

Figure 6-7 Evolutionary changes in the performance of AFCs. Solid line is H_2/O_2 dashed line is H_2/air.
Source: Reference (36).

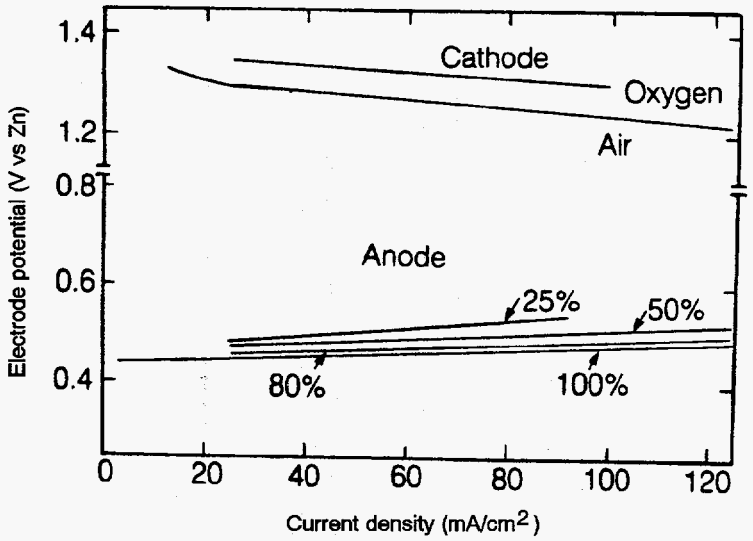

Figure 6-8 iR free electrode performance with oxygen, air, and various H_2 containing gases in 9 N KOH at 55 to 60°C. Catalyzed (noble metal loading of 0.5 to 2.0 mg/cm^2) carbon-based porous electrode.
Source: (Figure 9, p. 170) M.B. Clark, W.G. Darland and K.V. Kordesch, *Electro-Chem. Tech.*, **3**, 166, 1965. Reference (48).

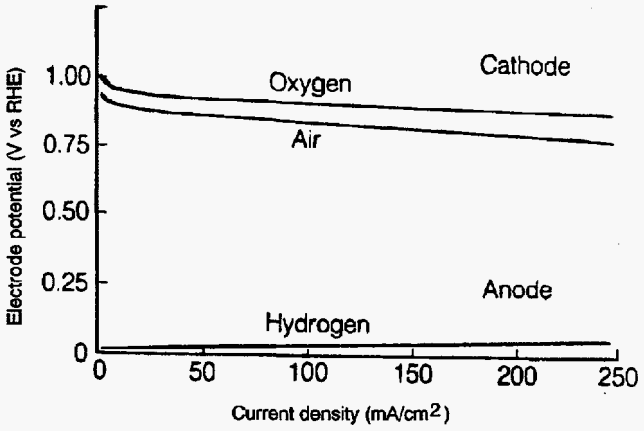

Figure 6-9 iR free electrode performance in 12 N KOH at 65°C. Catalyzed (0.5 mg Pt/cm^2-cathode, 0.5 mg Pt-Rh/cm^2-anode) carbon-based porous electrodes.
Source: (Figure 22, p. 322) K. Tomantschger, F. McClusky, L. Oporto, A. Reid, and K. Kordesch, *J. Power Sources*, **18**, 317, 1986. Reference (49).

The improvement in the air performance of catalyzed carbon based cathodes with an increase in cell temperature is illustrated in Figure 6-10. As expected, the electrode potential at a given current density decreased at lower temperatures, and the decrease is more significant at higher current densities. In the temperature range of 60 to 90°C, the cathode performance increases by about 0.5 mV/°C at 50 to 150 mA/cm^2. Early data by Clark et al. (48) indicated a temperature coefficient for AFCs at 50-70°C of about 3 mV/°C at 50 mA/cm^2, and cells with higher polarization had higher temperature coefficients under load. Later measurements by McBreen et al. (50) on H^2/air single cells (289 cm^2 active area, carbon based Pd anode and Pt cathode) with 50% KOH showed that the temperature coefficient above 60°C was considerably lower than that obtained at lower temperatures (see Figure 6-11). At 100 mA/cm^2, the temperature coefficient is about 0.7 mV/°C above 63°C and about 4 mV/°C below 63°C.

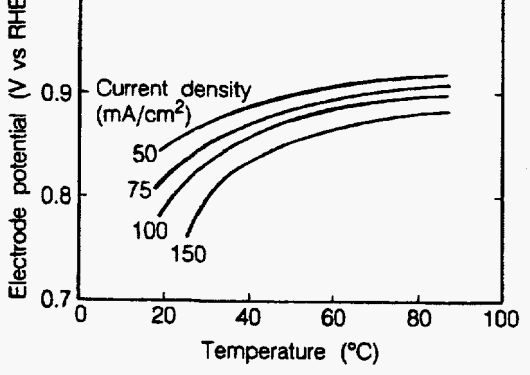

Figure 6-10 Influence of temperature on O_2 (air) reduction in 12 N KOH. Catalyzed (0.5 mg Pt/cm^2 cathode) carbon-based porous electrodes.
Source: (Figure 10, p. 324), K. Tomantschger, F. McClusky, L. Oporto, A. Reid, and K. Kordesch, *J. Power Sources*, **18**, 317, 1986.

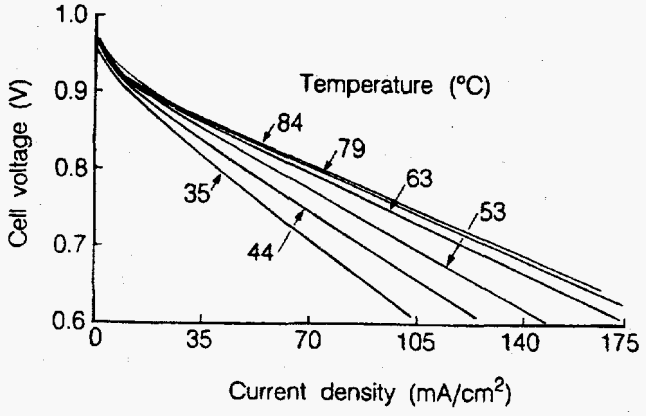

Figure 6-11 Influence of temperature on the cell voltage of an AFC (289 cm^2 active area, carbon-based Pd anode and Pt cathode) with 50% KOH.
Source: (Figure 6, p. 889) J. McBreen, G. Kissel, K.V. Kordesch, F. Kulesa, E.J. Taylor, E. Gannon and S. Srinivasan, in *Proceedings of the 15th Intersociety Energy Conversion Engineering Conference*, Volume 2, American Institute of Aeronautics and Astronautics, New York, NY, 1980.

AFCs suffer a drastic performance loss with fuels containing CO_2 from reformed fuels, and from the presence of CO_2 in air (approximately 350 ppm CO_2 in ambient air). The negative impact of CO_2 arises from its reaction with OH^-;

$$CO_2 + 2OH^- \rightarrow CO_3^= + H_2O \qquad (6\text{-}1)$$

which produces the following effects: 1) reduces the OH^- concentration and interferes with kinetics, 2) causes an increase in the electrolyte viscosity resulting in lower diffusion coefficients and lower limiting currents, 3) causes the eventual precipitation of carbonate salts in the pores of the porous electrode, 4) reduces the oxygen solubility, and 5) reduces the electrolyte conductivity. The influence of CO_2 on air cathodes (0.2 mg Pt/cm^2 supported on carbon black) in 6 N KOH at 50°C can be ascertained by analysis of the performance data presented in Figure 6-12 (51). The air electrodes were operated continuously at 32 mA/cm^2, and periodically current-voltage performance curves were measured. The air performance in both CO_2 free air and CO_2 containing air show evidence of degradation with time. However, with CO_2 free air the performance remains nearly constant with 2000 to 3000 hour operation. Another method to illustrate the influence of CO_2 on air performance is obtained by analysis of the electrode potential at a constant current density as a function of time. Data obtained from Figures 6-12a and 6-12b for the electrode potential at 100 mA/cm^2 as a function of time are plotted in Figure 6-12c. At short times, the potential of the air electrode in both CO_2 free air and CO_2 containing air are comparable. However, at longer times a higher performance is clearly evident for the air electrode in CO_2 free air. Higher concentrations of KOH are also detrimental to the life of O_2 electrodes operating with CO_2 containing air, but operating the electrode at higher temperature is beneficial because it increases the solubility of CO_3 in the electrolyte. Modifying the operating conditions can prolong electrode life, but it is clear from the results in Figure 6-12 that the life expectancy of air cathodes is lowered by the presence of CO_2. Extensive studies by Kordesch et al. (51) indicate that the operational life of air electrodes (PTFE-bonded carbon electrodes on porous nickel substrates) with CO_2 containing air in 9 N KOH

at 65°C ranges from 1600 to 3400 hours at a current density of 65 mA/cm^2. The life of these electrodes with CO_2 free air tested under similar conditions ranged from 4000 to 5500 hours. It has been reported (44) that a lifetime of 15,000 hours has been achieved with AFCs, and failure at this time is by attack of the cell frames.

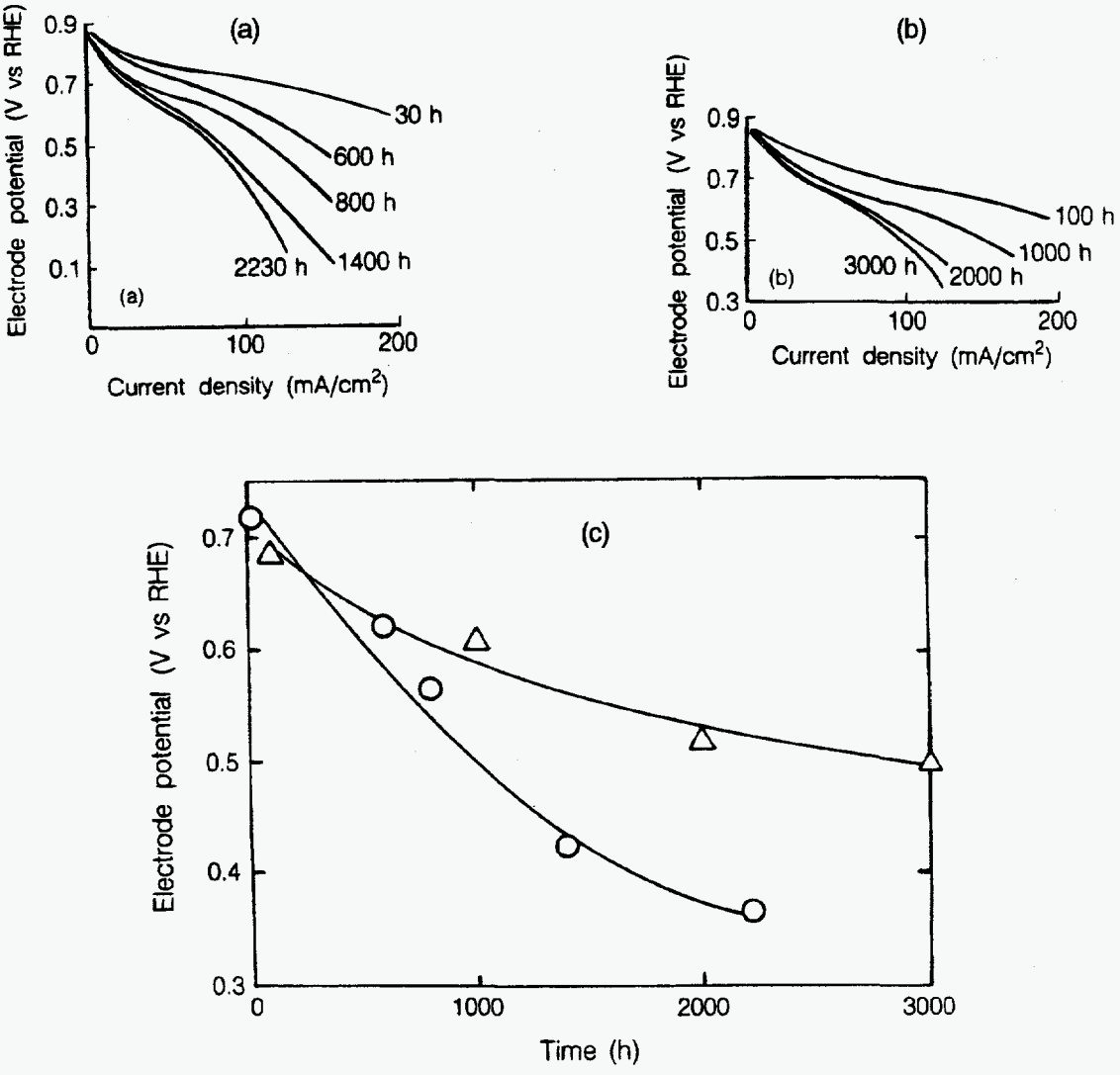

Figure 6-12 Influence of CO_2 on the air performance of supported Pt cathodes (0.2 mg/cm^2 supported on carbon black) in 6 N KOH at 50°C. (a) CO_2 containing air, (b) CO_2 free air. Current-voltage curves were measured periodically for electrodes continuously operated at 32 mA/cm^2, (c) Variation in electrode potential as a function of time at 100 mA/cm^2 with (O) CO_2 containing air and (Δ) CO_2 free air.

Source: (Figures 1 and 2, p. 381) K. Kordesch, J. Gsellmann and B. Kraetschmer, in *Power Sources 9*, Edited by J. Thompson, Academic Press, New York, NY, 1983.

References

1. A.J. Appleby and E.B. Yeager, *Energy*, **11**, 137, 1986.
2. A.J. Appleby, F. R. Foulkes, *Fuel Cell Handbook*, Van Nostrand Reinhold, NY, NY, 1989.
3. E.J. Taylor and S. Srinivasan, in *Power Sources for Electric Vehicles*, Edited by B.D. McNicol and D.A.J. Rand, Elsevier Science Publishers B.V., Amsterdam, The Netherlands, p. 839, 1984.
4. W.T. Grubb, *Proceedings of the 11th Annual Battery Research and Development Conference*, PSC Publications Committee, Red Bank, NJ, p. 5, 1957; U.S. Patent No. 2,913,511, 1959.
5. H. Grune, *in 1992 Fuel Cell Seminar Program and Abstracts*, The Fuel Cell Seminar Organizing Committee, November 29 - December 2, 1992 Tucson, Arizona, p. 161, 1992.
6. J. C. Amphlett, M. Farahani, R. F. Mann, B. A. Peppley and P. R. Roberge, in *Proceedings 26th Intersociety Energy Conversion Engineering Conference*, August 4-9, 1991 Volume 3, Conversion Technologies/Electrochemical Conversion, American Nuclear Society, La Grange, Illinois, p. 624, 1991.
7. S. Gottesfeld, "Polymer Electrolyte Fuel Cells: Potential Transportation and Stationary Applications," No. 10, in *An EPRI/GRI Fuel Cell Workshop on Technology Research and Development*, Stonehart Associates, Madison, Connecticut, 1993.
8. M. Krumpelt and K. M. Myles, No. 8, in *An EPRI/GRI Fuel Cell Workshop on Technology Research and Development*, April 13-14, 1993, Stonehart Associates, Madison, Connecticut, 1993.
9. M. Krumpelt, R. Kumar, J. Miller, and C. Christianson, in *1992 Fuel Cell Seminar Program and Abstracts*, The Fuel Cell Seminar Organizing Committee, November 29 - December 2, 1992 Tucson, Arizona, p. 35, 1992.
10. N. Giordano et. al., in *Proceedings 26th Intersociety Energy Conversion Engineering Conference*, August 4-9, 1991, Volume 3, Conversion Technologies/Electrochemical Conversion, American Nuclear Society, La Grange, Illinois, p. 624, 1991.
11. T. A. Zawodzinski et. al., J. of Electrochemical Society 140, 1042, 1993.
12. T. E. Springer et. al., J. of Electrochemical Society 138, 2335, 1991.
13. D. M. Bernardi, *J. Electrochem. Soc.*, **137**, 3344, 1990.
14. T. E. Springer, M. S. Wilson, and S. Gottesfeld, "Modeling and Experimental Diagnostics in Polymer Electrolyte Fuel Cells", submitted to J. Electrochem. Soc., LA-UR-93-1469 Los Alamos National Laboratory, New Mexico, 1993.
15. T.G. Coker, A.B. LaConti and L.J. Nuttall, in *Proceedings of the Symposium on Membranes and Ionic and Electronic Conducting Polymers*, Edited by E.G. Yeager, B. Schumm, K. Mauritz, K. Abbey, D. Blankenship and J. Akridge, The Electrochemical Society, Inc., Pennington, NJ, p. 191, 1983.
16. "Information Sheet", prepared by U.S. Department of Energy, Office of Propulsion Systems, Proton Exchange Membrane Fuel Cell Program, DE93000009, November 1992.
17. R.B. Fleming, K.W. Dircks, K.B. Prater, E.G. Pow, B.N. Gorbell, "The Commercialization of Solid Polymer Fuel Cells", in *The International Fuel Cell Conference Proceedings*, New Energy and Industrial Technology Development Organization, February 3-6, 1992, Makuhari, Japan, 393, 1992.
18. J.M. Ewan and C-k. Yu, "The Green Car™; A Fuel Cell Powered Automobile", in *The International Fuel Cell Conference Proceedings*, New Energy and Industrial Technology Development Organization, February 3-6, 1992, Makuhari, Japan, 409, 1992.
19. S. Srinivasan, O.A. Velev, A Parthasarathy, D.J. Manko, and A.J. Appleby, Journal of Power Sources, **36**, 299, 1991.

20. N.E. Vanderborgh, M.C. Kimble, J.R. Huff, and J.C. Hedstrom, in *27th Intersociety Energy Conversion Engineering Conference Proceedings, Volume 3*, Conversion Technologies/Electrochemical Conversions, San Diego, CA August 3-7, 1992, published by Society of Automotive Engineers, Inc., Warrendale, PA, 407, 1992.
21. K. Strasser, in *26th Intersociety Energy Conversion Engineering Conference Proceedings, Volume 3, Conversion Technologies/Electrochemical Conversion*, Boston, Massachusetts, August 4-9, 1991, published by Society of Automotive Engineers, Inc., Warrendale, PA, 631 1991.
22. Ballard, J. of Power Sources, **29** 239-250, 1990.
23. W.G.F. Grot, G.E. Munn and P.N. Walmsley, paper presented at the 141st National Meeting of the Electrochemical Society, Inc., Houston, TX, May 7-11, 1972; Abstract No. 154.
24. V. Peinecke, K. Ledjeff, and A. Heinzel, in *1992 Fuel Cell Seminar Program and Abstracts*, Tucson, Arizona, November 29 - December 2, 1992, sponsored by Fuel Cell Seminar Organizing Committee, 171, 1992.
25. "Investigation of Design and Manufacturing Methods for Low-Cost Fabrication of High Efficiency, High Power Density PEM Fuel Cell Power Plant" prepared by International Fuel Cells, Final Report FCR-11320A, June 10, 1991.
26. K. Sikairi, K. Tsurumi, S. Kawaguchi, M. Watanabe, and P. Stonehart, in *1992 Fuel Cell Seminar Program and Abstracts*, Tucson, AZ, November 29 - December 2, 1992, sponsored by Fuel Cell Organizing Committee, 153, 1992.
27 S. Srinivasan, O.A. Velev, A. Parthasarathy, A.C. Ferriera, S. Mukerjee, M. Wakizoe, Y. W. Rho, Y. T. Kho, and A.J. Appleby, in *1992 Fuel Cell Seminar Program and Abstracts*, Tucson, Arizona November 29 - December 2, 1992, sponsored by Fuel Cell Organizing Committee, 619, 1992.
28. F.N. Buchi, B. Gupta, M. Rouilly, P.C. Hauser, A. Chapiro, and G.G. Scherer, *27th Intersociety Energy Conversion Engineering Conference Proceedings, Volume 3*, Conversion Technologies/Electrochemical Conversions, San Diego, CA, August 3-7, 1992, published by Society of Automotive Engineers, Inc., Warrendale, PA, 419 , 1992.
29. D.M. MacArthur and T. Malinski, in *1992 Fuel Cell Seminar Program and Abstracts*, Tucson, AZ, November 29 - December 2, 1992, sponsored by Fuel Cell Organizing Committee, 165, 1992.
30. T. A. Zawodzinski, T. A. Springer, F. Uribe, and S. Gottesfeld, "Characterization of Polymer Electrolytes for Fuel Cell Applications", Solid State Tonics 60, Pages 199-211, North-Holland, 1993.
31. K. Prater, "The Renaissance of the Solid Polymer Fuel Cell", Ballard Power Systems, Inc., Journal of Power Sources, **29**, 1990.
32. M.S. Wilson, T.E. Springer, T.A. Zawodzinski and S. Gottesfeld, in *26th Intersociety Energy Conversion Engineering Conference Proceedings, Volume 3*, Conversion Technologies/Electrochemical Conversion, Boston, Massachusetts, August 4-9, 1991, published by Society of Automotive Engineers, Inc., Warrendale, PA, 636, 1991.
33. C. Derouin, T. Springer, F. Uribe, J. Valerio, M. Wilson, T. Zawodzinski and S. Gottesfeld, in *1992 Fuel Cell Seminar Program and Abstracts*, Tucson AZ, November 29 - December 2, 1992, sponsored by Fuel Cell Organizing Committee, 615, 1992.
34. P.D. Naylor, P.J. Mitchell and P.L. Adcock, in *1992 Fuel Cell Seminar Program and Abstracts*, Tucson, AZ, November 29 - December 2, 1992, sponsored by Fuel Cell Organizing Committee, 575, 1992.

35. S.R. Narayanan, E. Vamos, H. Frank, S. Surampudi and G. Halpert, in *1992 Fuel Cell Seminar Program and Abstracts*, Tucson, AZ, November 29 - December 2, 1992, sponsored by Fuel Cell Organizing Committee, 233, 1992.
36. J. Huff, paper presented at the 1986 J. R. Huff, "Status of Fuel Cell Technologies", Fuel Cell Seminar Abstracts. Fuel Cell Seminar, October 26-29, 1986, Tucson, AZ.
37. D. Watkins, K. Dircks, E. Epp and A. Harkness, *Proceedings of the 32nd International Power Sources Symposium*, The Electrochemical Society, Inc., Pennington, NJ, p. 590, 1986.
38. J. Srmivason, et al., "High Energy Efficiency and High Power Density Proton Exchange Membrane Fuel Cells - Electrode Kmetics and Mass Transport, Journal of Power Sources, **36**, 1991.
39. J.C. Amphlett, et al., "The Operation of a Solid Polymer Fuel Cell: A Parametric Model," Royal Military College of Canada.
40. K. Ledjeff, et al., "Low Cost Membrane Fuel Cell for Low Power Applications", Fraunhofer-Institute for Solar Energy Systems, Program and Abstracts, 1992 Fuel Cell Seminar.
41. A. LaConti, G. Smarz and F. Sribnik, "New Membrane-Catalyst for Solid Polymer Electrolyte Systems," Final Report prepared by Electro-Chem Products, Hamilton Standard for Los Alamos National Laboratory under Contract No. 9-X53-D6272-1, 1986.
42. "Investigation of Design and Manufacturing Methods for Low-Cost Fabrication of High Efficiency, High Power Density PEM Fuel Cell Power Plant," IFC/LANL, Final Report FCR-11320A, 1991.
43. F.T. Bacon, *Electrochim. Acta*, **14**, 569, 1969.
44. J. O'M Bockris and A.J. Appleby, *Energy*, **11**, 95, 1986.
45. D.W. Sheibley and R.A. Martin, *Prog. Batteries Solar Cells*, **6**, 155, 1987.
46. A.J. Appleby, *Energy*, **11**, 13, 1986.
47. K.F. Blurton and E. McMullin, *Energy Conversion*, **9**, 141, 1969.
48. M.B. Clark, W.G. Darland and K.V. Kordesch, *Electrochem. Tech.*, **3**, 166, 1965.
49. K. Tomantschger, F. McClusky, L. Oporto, A. Reid and K. Kordesch, *J. Power Sources*, **18**, 317, 1986.
50. J. McBreen, G. Kissel, K.V. Kordesch, F. Kulesa, E.J. Taylor, E. Gannon and S. Srinivasan, in *Proceedings of the 15th Intersociety Energy Conversion Engineering Conference*, Volume 2, American Institute of Aeronautics and Astronautics, New York, NY, p. 886, 1980.
51. K. Kordesch, J. Gsellmann and B. Kraetschmer, in *Power Sources 9*, Edited by J. Thompson, Academic Press, New York, NY, p. 379, 1983.

7. FUEL CELL SYSTEMS

A fuel cell power system embodies more than just the fuel cell stack. In a rudimentary form, fuel cell power systems consist of a fuel processor, fuel cell power section, power conditioner, and potentially a cogeneration or bottoming cycle in order to utilize the rejected heat. A simple schematic of these basic systems and their interconnections is presented by Figure 7-1.

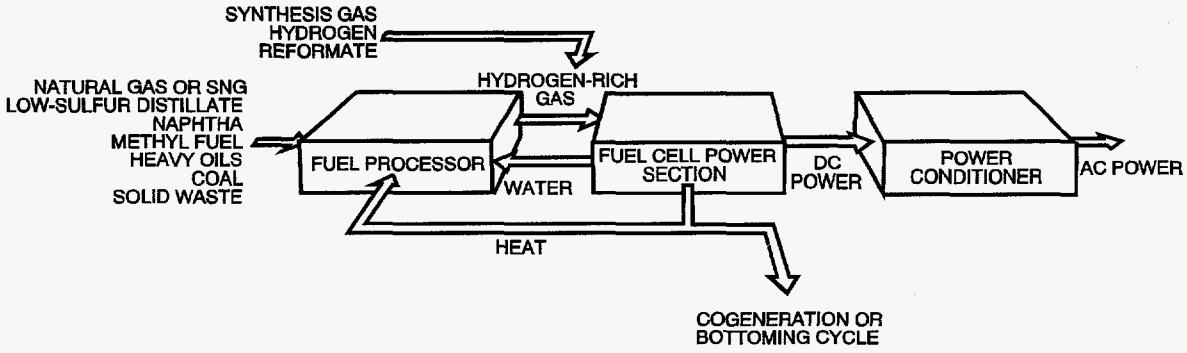

Figure 7-1 A rudimentary fuel cell power system schematic.

The cell and stacks comprising the power sections have been discussed extensively in the previous sections of this handbook. Section 7.1 addresses fuel processors, the power conditioner and rejected heat utilization. System optimization issues are addressed in Section 7.2.

7.1 SYSTEM PROCESSES

The design of a fuel cell system involves more than the optimization of the fuel cell section with respect to efficiency or economics. It involves the minimization of the cost of electricity (or product as in a cogeneration system) within the constraints of the desired application. For most applications, this requires that the fundamental processes be integrated into an efficient plant with low capital costs. Often these objectives are conflicting, so compromises, or design decisions must be made. In addition, project specific objectives, such as the desired fuel, emission levels, potential uses of rejected heat (electricity, steam or heat), the desired output levels, volume or weight criteria (volume/kW or weight/kW), and tolerance for risk all influence the design of the fuel cell power system.

A detailed discussion of all the trade-offs and considerations of system design is outside the scope of this handbook. Nevertheless, a brief discussion of various system options is presented.

7.1.1 Fuel Processors

Fuel processing depends on both the raw fuel and the fuel cell technology. The fuel cell technology determines what constituents are desirable and acceptable in the processed fuel, (see Table 1-4). For example, fuel sent to a PAFC needs to be H_2-rich and have less than 5% CO, while both the MCFC and SOFC fuel cells are capable of utilizing CO through the water gas shift reaction that occurs within the fuel cell. In addition, SOFCs and internal reforming MCFCs are also capable of utilizing methane (CH_4) within the cell whereas PAFCs are not. Contamination limits are also fuel cell technology specific and therefore help to determine the specific cleanup processes that are required.

Since the components and design of a fuel processing subsection depend on the raw fuel type, the following discussion is organized by the raw fuel being processed. For the purpose of this discussion, the cleanup and fuel preparation processes such as water gas shift are considered to be part of the fuel processing section.

Hydrogen Processing: When hydrogen is supplied directly to the fuel cell, as may be the case in transportation systems powered by either PEFC or AFC, the fuel processing section is not much more than a delivery system. However, in most power plant applications, hydrogen needs to be generated from other fuels and processed to meet the various system requirements.

Natural Gas Processing: Natural gas contains sulfur containing odorants (mercaptans, disulfides, or commercial odorants) for leak detection. Since neither fuel cells nor reformer catalysts are sulfur tolerant, the sulfur must be removed. This is usually accomplished with a zinc oxide sulfur polisher and the possible use of a hydrodesulfurizer, if required. The zinc oxide polisher is able to remove the mercaptans and disulfides. However, some commercial odorants such as Pennwalt's Pennodorant 1013 or 1063, contain THT (tetrahydrothiophene), more commonly known as thiophane, and require the addition of a hydrodesulfurizer before the zinc oxide catalyst bed. The hydrodesulfurizer will, in the presence of hydrogen convert the thiophane into H_2S which is easily removed by the zinc oxide polisher. The required hydrogen is supplied by recycling a small amount of reformed natural gas. Although a zinc oxide reactor can operate over a wide range of temperatures, a minimum bed volume is achieved at temperatures between 350 to 400°C (660 to 750°F).

Natural gas is usually converted to H_2 and CO in a steam reforming reactor. Steam reforming reactors yield the highest percentage of hydrogen of any reformer type. The basic steam reforming reactions for methane and a generic hydrocarbon are:

$$CH_4 + H_2O \rightleftharpoons CO + 3H_2 \tag{7-1}$$

$$C_nH_m + nH_2O \rightleftharpoons nCO + (m/2 + n)H_2 \tag{7-2}$$

$$CO + H_2O \rightleftharpoons CO_2 + H_2 \tag{7-3}$$

In addition to natural gas, steam reformers can be used on light hydrocarbons such as butane and propane. In fact, with a special catalyst, steam reformers can also reform naphtha.

Steam reforming reactions are highly endothermic and need a significant heat source. Often the residual fuel exiting the fuel cell is burned to supply this requirement. Fuels are typically reformed at temperatures of 760 to 980°C (1400 to 1800°F).

A typical steam reformed natural gas product is presented in Table 7-1.

Table 7-1 Typical Steam Reformed Natural Gas Product

Mole Percent	Reformer Effluent	Shifted Reformate
H_2	46.3	52.9
CO	7.1	0.5
CO_2	6.4	13.1
CH_4	2.4	2.4
N_2	0.8	0.8
H_2O	37.0	30.4
Total	100.0	100.0

A partial oxidation reformer can also be used for converting gaseous fuels, but do not produce as much hydrogen as the steam reformers. For example, a methane fed partial oxidation reformer would only produce about 75% of the hydrogen (after shifting) that was produced by a steam reformer. Therefore, partial oxidation reformers are typically used only on liquid fuels. Partial oxidation reformers rank second after steam reformers with respect to their hydrogen yield. For illustration, the overall partial oxidation reaction for methane is:

$$CH_4 + 1/2O_2 \rightleftharpoons CO + 2H_2 \qquad (7\text{-}4)$$

When natural gas is utilized in a PAFC system the reformate must be water gas shifted because of the high CO levels in the raw reformate gas. A PAFC stack can tolerate about 1-2% CO before having an adverse affect on the cell performance due to catalyst poisoning. The shift conversion is often performed in two or more stages when CO levels are high. A first high temperature stage allows high reaction rates, while a low temperature converter allows for a higher conversion. Excess steam is also utilized to enhance the CO conversion. A single stage shift reactor is capable of converting 80 to 95% of the CO (2). The water gas shift reaction is mildly exothermic, so multiple stage systems must have interstage heat exchangers. Feed temperatures of high and low temperature shift convertors range from approximately 260-370°C (500-700°F) and 200-260°C (400-500°F), respectively. Hydrogen formation is enhanced by low temperatures, but is unaffected by pressure.

Liquid Fuel Processing: Liquid fuels such as distillate, naphtha, diesel oil, and heavy fuel oil can be reformed in partial oxidation reformers. All commercial partial oxidation reactors employ noncatalytic partial oxidation of the feed stream by oxygen in the presence of steam with flame temperatures of approximately 1300 to 1500°C (2370 to 2730°F) (2).

For illustration, the overall partial oxidation reaction for pentane is:

$$C_5H_{12} + 5/2O_2 \rightleftharpoons 5CO + 6H_2 \qquad (7\text{-}5)$$

The overall reaction is exothermic, and largely independent of pressure. The process is usually performed at 20 - 40 atm in order to yield smaller equipment (2). A typical fuel composition for a fuel oil fed partial oxidation reformer is presented in Table 7-2.

Table 7-2 Typical Steam Reformed Fuel Oil Product (2)

Mole Percent (dry, basis)	Reformer Effluent
H_2	48.0
CO	46.1
CO_2	4.3
CH_4	0.4
N_2	0.3
H_2S	0.9
Total	100.0

Coal Processing: Numerous coal gasification systems are available today. However, they can be reasonably classified as one of three basic types: 1) Moving-bed, 2) Fluidized-bed, and 3) Entrained-bed. All three of these types utilize steam, and air or oxygen to partially oxidize coal into a gas product. The moving-bed gasifiers produce a low temperature (425 - 650°C; 800 - 1200°F) gas containing devolatilization products such as methane, and ethane, and a hydrocarbon liquid stream containing naphtha, tars, oils and phenolics. Entrained-bed gasifiers produce a gas product at high temperature (>1260°C; > 2300°F) which essentially eliminates the devolatilization products from the gas stream and the generation of liquid hydrocarbons. In fact, the entrained-bed gas product is comprised almost entirely of hydrogen, carbon monoxide and carbon dioxide. The fluidized-bed gasifier product gas falls somewhere in between these two other reactor types in composition and temperature (925 - 1040°C; 1700 - 1900°F).

The heat required for gasification is essentially supplied by the partial oxidation of the coal. Overall, the gasification reactions are exothermic, so waste heat boilers are often utilized at the gasifier effluent. The temperature, and therefore composition, of the product gas is dependent upon the amount of oxidant and steam, and the design of the reactor that each gasification process utilizes.

Gasifiers typically produce contaminants which need to be removed before entering the fuel cell anode. These contaminants include: H_2S, COS, NH_3, HCN, particulates, and tars, oils and phenols. (See Table 4-3 for the MCFC contaminant list.) The contaminant levels are dependent upon both the fuel composition and the gasifier employed. There are two families of cleanup that can be utilized to remove the sulfur impurities: hot and cold gas cleanup systems. The cold gas cleanup technology is commercial, has been proven over many years, and provides the system designer with several choices. The hot gas cleanup technology is still developmental and would likely need to be joined with other low temperature cleanup systems to remove the non-sulfur

impurities in a fuel cell system. For example, tars, oils, phenols, and ammonia could all be removed in a low temperature water quench followed by gas reheat.

A typical cold gas cleanup process on an entrained bed gasifier would include the following subprocesses: Heat exchange (steam generation, and regenerative heat exchange), particulate removal (cyclones and particulate scrubbers), COS hydrolysis reactor, ammonia scrubber, acid gas (H_2S) scrubbers (Sulfinol, SELEXOL), sulfur recovery (Claus and SCOT processes), and sulfur polishers (zinc oxide beds). All of these cleanup systems increase system complexity and cost, while decreasing efficiency and reliability. In addition, many of these systems have specific temperature requirements which necessitate the addition of several heat exchangers or direct contact coolers.

For example, a COS hydrolysis reactor needs to operate at about 180°C (350°F), the ammonia and acid scrubbers need to be in the vicinity of 40°C (100°F), while the zinc oxide polishers need to be about 370°C (700°F). Thus, gasification systems with cold gas cleanup often become a maze of heat exchange and cleanup systems.

Typical fuel compositions for several oxygen blown coal gasification products are presented in Table 7-3.

Table 7-3 Typical Coal Gas Compositions for Selected Gasifier Type-Fueled by Illinois No. 6 Bituminous Coal (4)

Mole Percent (dry, basis)	Lurgi	Koppers-Totzek	Shell
Gasifier Type	Moving-Bed	Fluidized-Bed	Entrained-Bed
Ar	trace	-	1.1
CH_4	3.3	-	-
C_2H_4	0.1	-	-
C_2H_6	0.2	-	-
CO	5.8	43.4	60.3
CO_2	11.8	6.1	1.6
COS	trace	0.1	0.1
H_2	16.1	18.7	30.0
H_2O	61.8	30.2	2.0
H_2S	0.5	0.6	1.2
N_2	0.1	0.9	3.6
NH_3 + HCN	0.3	-	0.1
Total	100.0	100.0	100.0

Other Solid Fuel Processing: Solid fuel other than coal can also be utilized in fuel cell systems. For example, biomass and RDF (Refuse-Derived-Fuels) can be integrated into a fuel cell system as long as the gas product is processed to meet the requirements of the fuel cell. The resulting systems would be very similar to the coal gas system with appropriate gasifying and cleanup systems. However, since biomass gas products can be very low in sulfur, the acid cleanup systems may simply consist of large sulfur polishers.

7.1.2 Power Conditioners

Power conditioning for a fuel cell power plant includes power consolidation, current control, ac to dc inversion, (unless the application is dc) and stepping the voltage up through a transformer. In a systems analysis, the important aspect of power conditioning is the efficiency of the power conversion and incorporation of the small power loss into the cycle efficiency. Power conditioning efficiencies are typically on the order of 94 (1) to 97%.

7.1.3 Rejected Heat Utilization

Rejected heat, that is, heat not utilized in the fuel processing and fuel cell subsystems, can be utilized to provide hot water, steam, or additional electricity. The utilization of the rejected heat depends upon the needs of the end user as well as the specifics of the process. The higher temperature fuel cells, (i.e., MCFC and SOFC), are capable of generating significant quantities of high pressure superheated steam because of the high temperature of the rejected heat. In a large fuel cell power system, on the order of 100 to 200 MW or more, production of electricity via a steam turbine bottoming cycle may be advantageous. In pressurized fuel cell systems, it may also be advantageous to utilize a gas expander before the steam generation. Possible areas for rejected heat utilization equipment include: at the gasifier effluent, before the cold gas cleanup, around the fuel cell, and in the fuel cell or burner exhaust.

7.2 SYSTEM OPTIMIZATIONS

The design, optimization and integration of a fuel cell power system is very complicated. Many possible design options and trade-offs exist which ultimately affect unit capital cost, operating cost, efficiency, parasitic power consumption, complexity, reliability, availability, fuel cell life and operational flexibility. While a detailed discussion of fuel cell optimization and integration is not within the scope of this section, a few of the most common system optimization areas are examined.

From Figure 7-2, it can be seen that the fuel cell itself has many trade-off options. A fundamental trade-off is determing where along the current density voltage curve should the system operate. As the operating point moves up in voltage by moving (left) to a lower current density, the system becomes more efficient but requires a greater fuel cell area to produce the same amount of current. That is, by moving up the voltage current density line, the system will experience lower operating costs at the expense of higher capital costs. Many other parameters can be varied simultaneously to achieve the desired operating point. Some of the significant fuel cell parameters which can be varied are pressure, temperature, fuel composition and utilization, and oxidant composition and utilization. The system design team has a fair amount of freedom to manipulate design parameters until the best combination of variables meeting the design requirements is found.

7.2.1 Pressurization

The issue of fuel cell pressurization is typical of many optimization issues, in that there are many interrelated factors that can complicate the question of whether to pressurize the fuel cell operation. Pressurization increases the performance of the fuel cell at the cost of providing the pressurization. Fundamentally, the question of pressurization is a trade-off between the improved performance (or reduced cell area) and the reduced piping volume, insulation, and heat loss

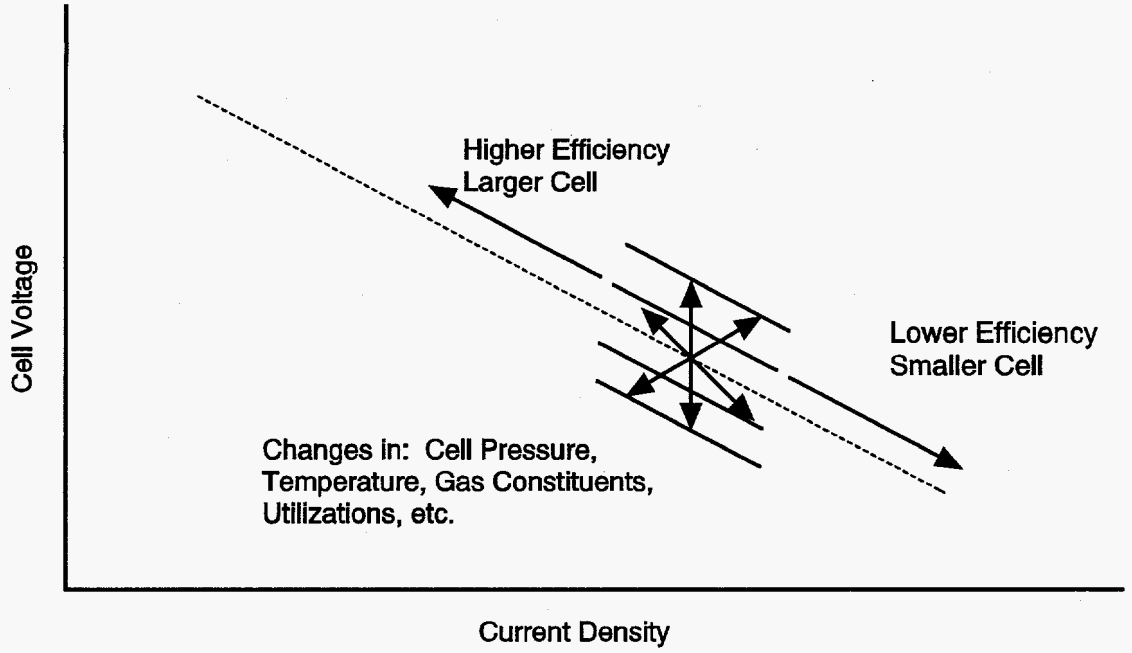

Figure 7-2 Optimization flexibility in a fuel cell power system

compared to the increased parasitic load and capital cost of the compressor and related equipment. However, other factors can further complicate the issue. To examine this issue in more detail, the issue of pressurization for an MCFC system will be examined.

In an MCFC power system, increased pressure can also result in increased cathode corrosion. The cathode corrosion mechanism is related to the acidity of the cell which increases with the partial pressure of CO_2, and therefore with the cell pressure. Such corrosion is typified by cathode dissolution and nickel precipitation, which can ultimately result in a shorted cell, causing cell failure (6). Thus, the chosen pressurization of the MCFC has a direct link to the cell life, economics and commercial viability.

Increasing the pressure in a MCFC system can also increase the likelihood of soot formation reactions and decrease the extent of methane reforming. Both are undesirable. Furthermore, the effect of contaminants on the cell and their removal from a pressurized MCFC system have not been quantified. The increased pressure will also challenge the fuel cell seals (6).

The selection of a specific fuel cell pressure will affect numerous design parameters and considerations such as: the current collector widths, gas flow patterns, pressure vessel size, pipe and insulation size, blower size and design, compressor auxiliary load, and the selection of a bottoming cycle and its operation conditions.

These issues do not eliminate the possibility of a pressurized MCFC system, but they do favor the selection of more moderate pressures.

The performance of an internal reforming MCFC would also benefit from pressurization, but unfortunately, the increase is accompanied by other problems. One such problem that would need to be overcome, is the increased potential for poisoning of the internal reforming catalyst resulting from the increase in sulfur partial pressure.

Pressurization of a SOFC yields a smaller gain in fuel cell performance than either the MCFC or PAFC. For example, based on the pressure relationships presented earlier, changing the pressure from one to ten atmospheres would change the cell voltage by 146, 77, and 59 mV for the PAFC, MCFC and SOFC, respectively. In addition to the cell performance improvement,

pressurization of SOFC systems allows the thermal energy leaving the SOFC to be recovered in a gas turbine, or gas turbine combined cycle, instead of just a steam bottoming cycle. Westinghouse is investigating the possibilities associated with pressurizing the SOFC when scaling to larger plants.

Large plants benefit the most from pressurization, because of the benefit of economy of scale on the additional equipment such as compressors, turbines, and pressure vessels. Pressurizing small systems is not practical, as the cost of the associated equipment outweighs the performance gains.

Pressurization in operating PAFC systems demonstrates the economy of scale at work. The IFC 200 kWe and the Fuji Electric 500 kWe PAFC offerings have been designed for atmospheric operation while larger units operate at pressure. The 11 MWe plant at the Goi Thermal Power Station operates at a pressure of 8.2 atmospheres (7), while a 5 MWe PAFC unit (NEDO / PAFCTRA) scheduled for operation in 1994 will operate at slightly less than 6 atmospheres (8). NEDO has three 1 MWe plants; two of which are pressurized while one is atmospheric (8).

Although it is impossible to generalize at what size a plant would benefit by pressurization, when plants increase in size to approximately 1 MW and larger, the question of pressurization should be addressed.

7.2.2 Temperature

Although the open circuit voltage decreases with increasing temperature, the performance at operating current densities increases with increasing temperature due to reduced mass transfer polarizations and ohmic losses. The increased temperature also yields a higher quality rejected heat stream. The temperatures at which the various fuel cells can operate are however limited by material constraints. The PAFC and MCFC are both limited by life shortening corrosion at higher temperatures. The SOFC is limited by material property limitations. An additional benefit to an increased temperature in the PAFC cell is an increased tolerance to CO levels which poisons the fuel cell catalyst. Again the fuel cell and system designers should evaluate what compromise will work best to meet their particular requirements.

The PAFC is limited to temperatures in the neighborhood of 200° C before corrosion and lifetime loss become significant. The MCFC is limited to a cell average temperature of approximately 650° C for similar reasons. Local temperatures of a MCFC can not exceed 700° C before corrosion becomes significant. With a cell temperature rise on the order of 100° C, an average MCFC temperature of 650° C will provide the longest life, highest performance compromise. In fact one reference (9) cites "the future target of the operating temperature must be 650° C ±30° C."

The high operating temperature of the SOFC puts numerous requirements (phase and conductivity stability, chemical compatibility, and thermal expansion) on the material selection and development (10). Many of these problems could be alleviated with lower operating temperatures. However, a high temperature of approximately 1000° C, i.e., the present operating temperature, is required in order to have sufficiently high ionic conductivities with the existing materials and configurations (10).

7.2.3 Utilizations

Both fuel and oxidant utilizations involve trade-offs with respect to the optimum utilization for a given system. High utilizations are considered desirable (particularly in smaller systems) since they minimize the required fuel and oxidant flow, for a minimum fuel cost and compressor/blower load and size. However, utilizations that are pushed too high result in significant voltage drops.

One study (11) cites that low utilizations can be advantageous in large fuel cell power cycles with efficient bottoming cycles since the low utilization improves the performance of the fuel cell, and makes more heat available to the bottoming cycle. Like almost all design parameters, the selection of the optimum utilizations requires an engineering trade-off that considers the specifics of each case.

Fuel Utilization: High fuel utilizations are desirable in small power systems, since in such systems the fuel cell is usually the sole power source. However, since the complete utilization of the fuel is not practical, and other requirements for fuel exist, the selection of the utilization represents a balance between other fuel requirements, and the impact of utilization on the overall performance.

Natural gas systems with endothermic steam reformers often make use of the residual fuel in a reformer burner. Alternatively, the residual fuel could also be combusted prior to a gas expander to boost performance. In an MCFC system, the residual fuel is often combusted to maximize the supply of CO_2 to the cathode. In a SOFC system, the residual fuel is often combusted to provide the high temperature portion of the required air preheating.

In addition, the designer has the ability to increase the overall utilization of fuel (or the oxidant) by recycling a portion of the spent stream back to the inlet. This increases the overall utilization while maintaining a lower per pass utilization of reactants within the fuel cell to ensure good cell performance. The down side of recycling is the increased auxiliary power and capital cost of the recycle fan or blower.

One study by Minkov et al (11) suggests that low fuel and oxidant utilizations yield the lowest COE in large fuel cell power systems. By varying the fuel cell utilization, the electric power generation split between the fuel cell, steam turbine and gas turbine are changed. The low fuel utilization decreases the percentage of power from the fuel cell while increasing the fuel cell performance. The increased power output from the gas turbine and steam turbine also results in their improved performance and economy of scale. The specific analysis results are, of course, dependent upon the assumed stack costs. The optimal power production split between the fuel cell, and gas and steam turbines is approximately 35%, 47% and 17% for a 575 MW MCFC power plant. The associated fuel utilization is a relatively low 55%.

Oxidant Utilization: In addition to the obvious trade-off between cell performance and compressor or blower auxiliary power, oxidant flows and utilizations in the cell are often determined by other design objectives. For example, in the MCFC and SOFC cells, the oxidant flow is determined by the required cooling. This tends to yield oxidant utilizations that are fairly low (~25%). In a PAFC, the oxidant utilizations based on cell performance and a minimized auxiliary load and capital cost are in the range of 50 to 70%.

7.2.4 Heat Recovery

Although fuel cells are not heat engines, significant quantities of heat are still produced in a fuel cell power system which must be removed. Depending upon the size of the system, the temperature of the available heat, and the requirements of the particular site, this thermal energy can either be rejected, used to produce steam or hot water, or converted to electricity via a gas turbine or steam bottoming cycle or some combination thereof.

Cogeneration: When small quantities of heat and/or low temperatures typify the waste heat, the heat is either rejected or used to produce hot water or low pressure steam. For example, in a PAFC cycle where the fuel cell operates at approximately 205°C (400°F), the highest pressure

steam that could be produced would be something less than 14 atm (205 psia). This is obviously not sufficient for a steam turbine bottoming cycle, regardless of the quantity of heat available. At the other end of the spectrum is the SOFC, which operates at 1000° C (1832° F) and often has a cell exhaust temperature of approximately 815° C (1500° F) after air preheating. Gas temperatures of this level are capable of producing steam temperatures in excess of 540° C (1000° F) which makes it more than suited for a steam bottoming cycle. However, even in a SOFC power system, if the quantity of waste heat is relatively small, the most that would be done with the heat would be to make steam or hot water. In a study performed by Westinghouse of 50 to 2000 kW SOFC systems, the waste heat was simply utilized to generate 8 atm (100 psig) steam (1).

Bottoming Cycle Options: Whenever significant quantities of high temperature waste heat are available, a bottoming cycle can add significantly to the overall electric generation efficiency. Should the heat be contained within a high pressure gas stream, then a gas turbine potentially followed by a heat recovery steam generator and steam turbine should be considered. If the heat stream is at low pressure, then a steam bottoming cycle is logical.

If a steam bottoming cycle is appropriate, many design decisions need to be made and includes the selection of the turbine cycle (reheat or non-reheat) and the operating conditions. Usually steam turbines below 100 MW are non-reheat while turbines above 150 MW are reheat turbines. This generalization is subject to a few exceptions. In fact, a small (83 MW) modern reheat steam turbine went into operation (6/90) as a part of a gas turbine combined cycle repowering (12).

7.2.5 Miscellaneous

Compressor Intercooling: Whether a compressor should be intercooled or not depends on the trade-off between the increased efficiency of the intercooled compressor and its increase capital cost. In general, intercooling is required in large compressors for pressure ratios that exceed approximately 5:1 (13). The designer should also consider whether the heat is advantageous to the process or not. For example, when near the 5:1 pressure ratio, it may not be appropriate to intercool if the compressed stream will subsequently require preheating as it would be in the process air of a MCFC or SOFC system.

Humidification/Dehumidification: Water is often added or removed in fuel cell systems to promote or prevent certain chemical reactions. For some reactions, an excess of water can help to drive the reaction, while too much requires larger equipment and can even reduce the yield of a reaction or decrease the performance of a fuel cell. Excess water is often utilized to increase the yield of reforming reactions and the water gas shift.

In a natural gas fueled PAFC, water is condensed out of the fuel stream going to the fuel cell to increase the partial pressure of hydrogen. In a coal gasification MCFC, water is often added to the fuel before it is introduced to the fuel cell to prevent soot formation. The addition of excess steam not only prevents the soot formation but causes a voltage drop of approximately 2 mV per each percentage point increase in steam content (14). The use of a zinc ferrite hot gas cleanup can aggravate the soot formation problem due to the catalytic effect of the sorbent on the carbon formation, and require even higher moisture levels (15).

7.2.6 Concluding Remarks on System Optimization

System design and optimization encompass many questions, issues, and trade-offs. The engineer should address the selection of the best process to accomplish the task, best possible component arrangement, best set of operating conditions, best combination of fuel cell and bottoming cycle technologies and associated power production split, and the best system integration.

The objective is not to present a detailed review of the subject of optimization, but simply to presents a few select issues of system optimization as they apply to fuel cell power systems.

References

1. W.L. Lundberg, "Solid Oxide Fuel Cell Cogeneration System Conceptual Design," prepared by Westinghouse for Gas Research Institute, Report No. GRI-89-0162, July 1989.
2. R. Shreve and J. Brink, Chemical Process Industries, fourth edition, McGraw-Hill, 1977.
3. J.H. Hirschenhofer, D.B. Stauffer, J.S. White, "Carbon Dioxide Capture in Fuel Cell Power Systems," Gilbert/Commonwealth Report No. 2981, September, 1993, prepared for U.S. Department of Energy, under Contract No. DE-AC01-88FE61684, Task 16, 1993.
4. Coal Gasification Systems: A Guide to Status, Applications and Economics, prepared by Synthetic Fuels Associates, Inc., EPRI AP-3109, Project 2207, Final Report, June 1983.
5. K. Yokota, K. Uehara, J. Caraceni, Y. Shiraiwa, T. Amemiya, "Load Operation Characteristics of TEPCO 11 MW PAFC Power Plant," paper presented at International Fuel Cell Conference, February 3-6, 1992, Makuhari, Japan, p 87, 1992.
6. M.C. Williams, and T.J. George, "Research Issues in Molten Carbonate Fuel Cells: Pressurization," Presented at the 1992 IECEC, Vol 3, pp. 263-267.
7. "Overview of 11 MW Fuel Cell Power Plant," Non-Published information from Tokyo Electric Power Company, September, 1989.
8. T. Koshimizu, et al, "Development of 5000 kW and 1000 kW PAFC Plants," Presented at the JASME-ASME Joint Conference (ICOPE-93), Tokyo, September 1993.
9. T. Okado, et al, "Study of Temperature Control in Indirect Internal Reforming MCFC Stack," Presented at 25th IECEC, pp. 207-212, 1990.
10. N.Q. Minh, "High-Temperature Fuel Cells, Part 2: The Solid Oxide Cell," Chemtech, Vol. 21, February 1991.
11. V. Minkov, et al, "Topping Cycle Fuel Cells Effective Combined With Turbines," Power Engineering, July 1988, pp. 35-39. "Design and Economics of Large Fuel Cell Power Plants," Presented at 1986 Fuel Cell Seminar, Tucson, AZ, p 255.
12. F.G. Baily, "Steam Turbines for Advanced Combined Cycles," Presented at the 35th GE Turbine State-of-the-Art Technology Seminar, 1991.
13. M.S. Peters, and K.D. Timmerhaus, Plant Design and Economics for Chemical Engineers, Third Edition, McGraw-Hill, 1980.
14. M. Farooque, "Development of Internal Reforming Carbonate Fuel Cell Stack Technology," Performed under Contract No. DE-AC21-87MC23274, DOE/MC/23374-2941, October 1990.
15. M. Farooque, et al, "Comparative Assessment of Coal-Fueled Carbonate Fuel Cell and Competing Technologies," Presented at the 25th IECEC, Vol 3, 193-200, 1990.

8. CONCLUDING REMARKS

The types of cells addressed in this Handbook have attained different degrees of advancement towards their commercial use. Common to all is that the technical concepts have been proven by individual cell and stack tests. No technical or economic "showstoppers" have been identified that would prohibit the incorporation of the various cells into early power plants fueled by natural gas (and methanol for the PEFC). Initial applications for the various type cells have been defined and all fuel cell types have programs in place towards demonstrating their use in completed systems. Depending on the cell type, it is now a matter of refining the cell materials and design configurations, scaling the cells to full area and stacks to full height, integrating the fuel cell stack with its system, and improving developed power plants to meet the commercial goals of life, reliability, and cost.

In summary, the PAFC is the type furthest along towards commercialization with numerous demonstrations in the 50 to 200 kW range, Major manufacturers in the U.S. and abroad have as a goal for PAFCs to be commercialized by 1997-1998. Designs, which have the potential to achieve limited commercial penetration ($1,500 to $2,000/kW), are defined and are capable of being built. Tests demonstrate that 475 to 675 kW stacks have a life of 15,000 hours and one 200 kW power plant has operated for 14,000 total hours. Numerous units placed in the field in 1992 and 1993 will provide data on whether life goals of 40,000 hours can be met; predictions indicate this goal can be met. The environmental benefits of PAFC systems have been confirmed (there is nothing to indicate that MCFCs, SOFCs and PEFCs won't exhibit similar low emissions).

Automatic manufacturing facilities for the PAFC power plants have been built. One of the leading manufacturers has the capability to produce two hundred, 200 kW units per year in its facility using robotic manufacturing and assembly techniques. Present capital costs are approximately $3,500/kW, but the new designs should lower this cost by approximately one-half.

Still to be confirmed is the ability of the PAFCs to reach an operating life of 40,000 hours and to exhibit acceptable reliability over power plant life. Reductions in cost, by further improvements in design and increased production, to a goal of $1,000/kW will expand the PAFCs market to widespread usage.

The MCFC has reached a point where cells are being built at commercial size and full height stacks are beginning to be tested. Short stacks with full size cells and full height stacks with smaller cells have demonstrated lifetimes of approximately 9,000 hours. There are projections, based on individual cell component tests, that MCFC stacks can achieve a life goal of 40,000 hours when operated at atmospheric conditions; this has yet to be demonstrated. Systems concepts have been defined, a 100 kW power system has been tested on a limited, non-integrated basis. Efforts have turned towards developing systems which are acceptable on a commercial basis. Studies indicate that the materials used in MCFCs will result in stacks being produced for the goal cost of $400/kW.

The SOFC tubular concept needs scaling to commercial size and a reduction in the cost of fabrication. System concepts for the tubular cell are more integrated and less complex than the MCFC. As a result, several units of 25 kW capacity have been produced and are being tested. Reaching cost goals however, represent a major challenge. Scaling of the tubular cell to longer lengths and development of alternative SOFC concepts are being pursued in hopes of lowering the capital cost. The alternative concepts are at an earlier stage of development than the tubular concept.

Attributes of the PEFC make it well suited to provide motive power for vehicles. Concepts have been demonstrated, but work is still needed in the areas of cell component design, configuration, and system development. It should be acknowledged that one manufacturer is producing and marketing 5 kW stacks and systems operating on hydrogen and air. Early efforts toward producing a fuel processor so that methanol and natural gas can be used as fuels have started and initial results have proven the concept possible.

AFC technology is considered viable for use in space applications since endurance is not required and because special weight and fuel requirements make this application cost effective. However, there is a possibility that the AFC could be replaced by the PEFC as its development progresses.

The intent of this Handbook is to focus on the various types of fuel cells and their current technical status, and only to a lesser extent on their applications. As described in the preceding sections (Sections 3 through 6), the various fuel cells have undergone dramatic changes in the past two decades and research continues to improve the technology. Optimization of parameters such as pressure, temperature, reactant composition, and utilization are important to obtain the maximum performance from fuel cells systems. Since the fuel cell must be integrated with other subsystems involving fuel processing, thermal management and power conditioning, a systems approach to utilizing fuel cells is needed, this is addressed in Section 7. Finally, it is apparent that there are numerous markets where fuel cells can play a prominent role if certain economic and technical issues are resolved. As these issues and the institutional barriers confronting fuel cells are overcome, fuel cell technologies are expected to penetrate the commercial and industrial marketplaces in the mid to late 1990s.

Since the pioneering efforts by Dr. F. T. Bacon in the 1930s, the development of various fuel cell systems has flourished. The published literature describing various aspects of fuel cell technology has also proliferated. Lists of pertinent books, proceedings publications, and bibliographies are included in Appendix 9.7 which supplement the list in the previous Handbook. A list of fuel cell publications from periodicals is not presented because these citations can be found in the bibliographies.

9. APPENDIX

9.1 Heat Capacity Correlation

The thermodynamic data (e.g., ΔG, ΔH, ΔS) required to calculate the efficiency parameters (see Section 2) for fuel cells must be available for temperatures (T) other than standard temperature, usually 298° K. ΔH and ΔS at a given T are obtained by the use of the equations presented in Section 2 and the heat capacity correlation such as the one given in Table 9-1 (1).

Reference

1. H.M. Spencer, *J. Amer. Chem. Soc.*, **67**, 1858, 1945.

9.2 Reactant Gas Utilization in Molten Carbonate Fuel Cells

The electrochemical reactions occurring in a MCFC are:

$$\text{Anode:} \quad H_2 + CO_3^{=} \rightarrow H_2O + CO_2 + 2e^- \tag{9-1}$$

and,

$$\text{Cathode:} \quad \tfrac{1}{2}O_2 + CO_2 + 2e^- \rightarrow CO_3^{=} \tag{9-2}$$

The overall cell reaction is:

$$H_2 + \tfrac{1}{2}O_2 + CO_2\,(\text{cathode}) \rightarrow H_2O + CO_2\,(\text{anode}) \tag{9-3}$$

and the corresponding reversible cell potential is computed from the Nernst equation[a]

$$E = E^\circ + \frac{RT}{2F} \ln [P_{H_2} P_{O_2}^{1/2}/P_{H_2O}] + \frac{RT}{2F} \ln [(P_{CO_2})_c/(P_{CO_2})_a] \tag{9-4}$$

[a] The activity gradient for $CO_3^{=}$ is assumed to be zero through the cell.

Table 9-1 Heat Capacities of Gases (273-1500° K)

$$C_P = a + bT + cT^2 \ (C_P \text{ in cal/mol-deg K})$$

Gas	a	b x 10^3	c x 10^7
H_2	6.9469	-0.1999	4.808
O_2	6.148	3.102	-9.23
N_2	6.524	1.250	-0.01
CO	6.420	1.665	-1.96
H_2O	7.256	2.298	2.83
CO_2	6.214	10.396	-35.45
CH_4	3.381	18.044	-43.00

Source: H.M. Spencer, *J. Amer. Chem. Soc.*, **67**, 1858, 1945.

In an operating fuel cell, the cell voltage changes in response to the utilization of the reactant gases, as well as other processes that result in polarization. The influence of reactant utilization on the MCFC cell voltage can be determined. This calculation is discussed below.

In the following analysis, the fuel gas composition at the anode inlet is assumed to correspond to the equilibrium composition established by the water gas shift reaction. This is a reasonable assumption since the water gas shift reaction reaches equilibrium rapidly in MCFCs. Thus, H_2 that electrochemically reacts at the anode can originate from the H_2 present in the inlet gas stream [moles H_2 (in)] and from H_2 obtained from CO [moles CO (in)] by the water gas shift reaction in the cell. That is, the total H_2 available for electrochemical oxidation is equal to the moles H_2 (in) + moles CO (in).

Fuel Utilization: The utilization of H2 (β) is defined as

$$\beta = \frac{\text{moles } H_2 \text{ consumed}}{\text{moles } H_2 \text{ (in)} + \text{moles CO (in)}} = \frac{f_{in}[X_{H_2} + X_{CO}]_{in} - f_{out}[X_{H_2}]_{out}}{f_{in}[X_{H_2} + X_{CO}]_{in}} \qquad (9\text{-}5)$$

where $[X_{H_2} + X_{CO}]$ corresponds to the sum of the mole fraction of H_2 and CO, and subscripts in and out refer to the inlet and outlet of the cell, respectively. The total gas flow rate at the inlet and outlet is given by f_{in} and f_{out}, respectively. When H_2 electrochemically reacts at the anode, an equivalent amount of CO_2 and H_2O are formed, i.e.,

$$\beta f_{in}[X_{H_2} + X_{CO}]_{in} = CO_2 \text{ (produced)} = H_2O \text{ (produced)} \qquad (9\text{-}6)$$

Thus, there is a net increase in the amount of gas at the outlet,

$$CO_2 \text{ (produced)} + H_2O \text{ (produced)} - H_2 \text{ (consumed)} = \beta f_{in}[X_{H_2} + X_{CO}]_{in} \quad (9\text{-}7)$$

and,

$$\text{Total gas flow (out)} = \text{Total gas flow (in)} + \beta f_{in}[X_{H_2} + X_{CO}]_{in} = f_{in}(1 + \beta[X_{H_2} + X_{CO}]_{in}) \quad (9\text{-}8)$$

The mole fraction of H_2 + CO at the anode outlet $[X_{H_2} + X_{CO}]_{out}$ is obtained from Equations 9-5 and 9-8.

$$[X_{H_2}]_{out} = \frac{(1 - \beta)[X_{H_2} + X_{CO}]_{in}}{1 + \beta[X_{H_2} + X_{CO}]_{in}} \quad (9\text{-}9)$$

A net gain in CO_2 is obtained at the anode outlet,

$$CO_2 \text{ (out)} = CO_2 \text{ (in)} + CO_2 \text{ (produced)} = f_{in}[X_{CO_2}]_{in} + f_{in}\,\beta[X_{H_2} + X_{CO}]_{in} \quad (9\text{-}10)$$

The mole fraction of CO_2 at the anode outlet $[X_{CO_2}]_{out}$ is given by:

$$[X_{CO_2}]_{out} = \frac{[X_{CO_2}]_{in} + \beta[X_{H_2} + X_{CO}]_{in}}{1 + \beta[X_{H_2} + X_{CO}]_{in}} \quad (9\text{-}11)$$

Similarly, the mole fraction of H_2O at the anode outlet $[X_{H_2O}]_{out}$ is given by:

$$[X_{H_2O}]_{out} = \frac{[X_{H_2O}]_{in} + \beta[X_{H_2} + X_{CO}]_{in}}{1 + \beta[X_{H_2} + X_{CO}]_{in}} \quad (9\text{-}12)$$

The mole fraction $[X_{inert}]_{out}$ of inert gases (e.g., N_2), if present, is given by:

$$[X_{inert}]_{out} = \frac{[X_{inert}]_{in}}{1 + \beta[X_{H_2} + X_{CO}]_{in}} \quad (9\text{-}13)$$

The mole fraction of CO at the anode outlet $[X_{CO}]_{out}$ is obtained from the equilibrium gas composition at the anode outlet, taking into account the water gas shift reaction, i.e.,

$$K = \frac{[X_{H_2O}]_{out}[X_{CO}]_{out}}{[X_{H_2}]_{out}[X_{CO_2}]_{out}} \quad (9\text{-}14)$$

Oxidant Utilization: The utilization of oxidant (γ) can be defined in terms of the quantity of CO_2 consumed,

$$\gamma = \frac{\text{moles } CO_2 \text{ consumed}}{\text{moles } CO_2 \text{ (in)}} = \frac{f_{in}[X_{CO_2}]_{in} - f_{out}[X_{CO_2}]_{out}}{f_{in}[X_{CO_2}]_{in}} \tag{9-15}$$

where the terms f and X have been defined above. The cathode reaction involves the consumption of 2 moles of CO_2 for each mole of O_2. Thus,

$$CO_2 \text{ reacted} = \gamma f_{in} [X_{CO_2}]_{in} \tag{9-16}$$

and

$$O_2 \text{ reacted} = \tfrac{1}{2}\gamma f_{in} [X_{CO_2}]_{in} \tag{9-17}$$

At the cathode, the reaction of 0.5 mole of O_2 with 1.0 mole of CO_2 produces a net loss of 1.5 $\gamma f_{in} [X_{CO_2}]_{in}$ moles of oxidant, and therefore,

$$\text{total gas (out)} = \text{total gas (in)} - 1.5\ \gamma f_{in} [CO_2]_{in} \tag{9-18}$$

or

$$f_{out} = f_{in} - 1.5\ \gamma f_{in} [X_{CO_2}]_{in} \tag{9-19}$$

From Equations 9-15 and 9-19, the mole fraction of CO_2 at the outlet is given by,

$$[X_{CO_2}]_{out} = \frac{(1 - \gamma)\ [X_{CO_2}]_{in}}{1 - 1.5\ \gamma[X_{CO_2}]_{in}} \tag{9-20}$$

In the case of O_2, the amount that is present at the cathode outlet is given by,

$$O_2 \text{ (out)} = O_2 \text{ (in)} - 0.5\ \gamma f_{in} [X_{CO_2}]_{in} \tag{9-21}$$

and,

$$[X_{O_2}]_{out} = \frac{[X_{O_2}]_{in} - 0.5\ \gamma[X_{CO_2}]_{in}}{1 - 1.5\ \gamma[X_{CO_2}]_{in}} \tag{9-22}$$

The mole fraction of inert gases $[X_{inert}]_{out}$ is given by,

$$[X_{inert}]_{out} = \frac{[X_{inert}]_{in}}{1 - 1.5\ \gamma[X_{CO_2}]_{in}} \tag{9-23}$$

Nernst Potential: The mole fraction of specie i (X_i) is related to its partial pressure by,

$$X_i = \frac{P_i}{P_T} \tag{9-24}$$

or upon rearrangement,

$$P_i = X_i P_T \tag{9-25}$$

where P_T is the total gas pressure. Substituting for P_i in the Nernst Equation (9-4) yields the reversible potential at the outlet of a MCFC, i.e.,

$$E = E^o + \frac{RT}{2F} \ln \frac{[X_{H_2}][X_{O_2}]^{½} [X_{CO_{2,c}}]P^{½}}{[X_{H_2O}][X_{CO_{2,a}}]} \tag{9-26}$$

where $P_c = P_a = P$ is assumed.

9.3 Equilibrium Constants

The temperature dependence of the equilibrium constants for the water gas shift reaction,

$$CO_2 + H_2 = CO + H_2O \tag{9-27}$$

carbon deposition (Boudouard reaction) reaction,

$$2CO \rightarrow C + CO_2 \tag{9-28}$$

methane decomposition reaction,

$$CH_4 \rightarrow C + 2H_2 \tag{9-29}$$

and methane formation reaction,

$$CO + 3H_2 \rightarrow CH_4 + H_2O \tag{9-30}$$

are presented in Figure 9-1, using data from Rostrup-Nielsen (1).

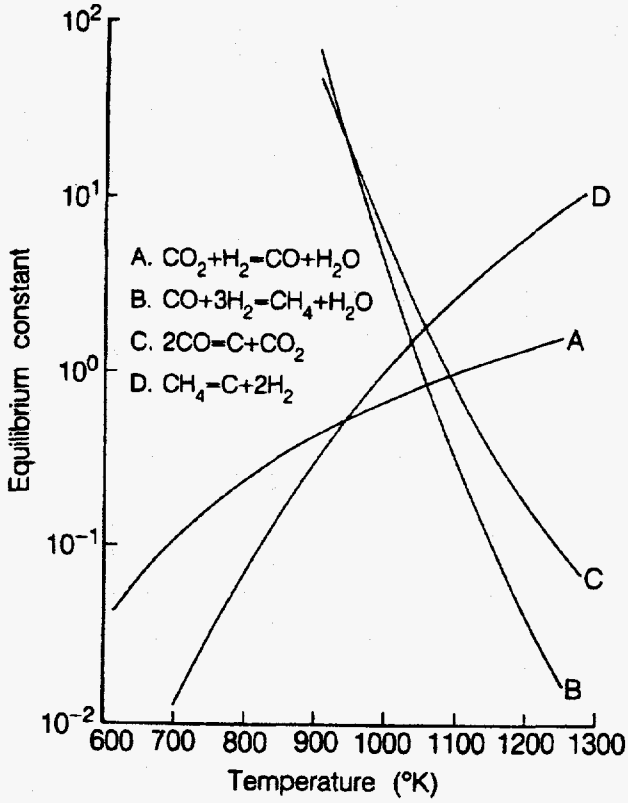

Figure 9-1 Equilibrium constants (partial pressures in MPa) for: (a) water gas shift, (b) methane formation, (c) carbon deposition (Boudouard reaction), and (d) methane decomposition. See Appendix 9.3 for chemical reactions.
Source: J.R. Rostrup-Nielsen, in Catalysis Science and Technology, Edited by J.R. Anderson and M. Boudart, Springer-Verlag, Berlin GDR, p.1, 1984.

Reference

1. J.R. Rostrup-Nielsen, in Catalysis Science and Technology, Volume 5, Edited by J.R. Anderson and M. Boudart, Springer-Verlag, Berlin, German Democratic Republic, p. 1, 1984.

9.4 Contaminants from Coal Gasification

A list of contaminant levels that result from various coal gasification processes are presented in Table 9-2 (1). The contaminant levels obtained after a first stage of hot gas cleanup with zinc ferrite are also listed.

Table 9-2 Typical Contaminant Levels Obtained from Selected Coal Gasification Processes

Parameters	Coal Gasification Process		
	LURGI Fixed Bed	METC (raw gas) Fixed Bed	Cleaned Gas
Max. Product Temp. (°C)	750	1300	<800
Gasification	O_2 blown	Air blown	Regenerative
Pressure (psi)	435	220	150
Product Gas (°C)	600	650	<700
Methane (vol%)	11	3.5	3.5
Coal type	Sub-bitum. Navajo	Sub-bitum. New Mexico	(Humidified Output)
Particulates (g/l)	0.016	0.058	0.01 est.
Sulfur (ppm) (Total H_2S, COS, CS_2, mercaptans)	2,000	5,300	<10
NH_3 (vol%)	0.4	0.44	0.25
Trace metals (ppm)			
As	2	NS[a]	NS
Pb	0.8	2	1.7
Hg	0.4	NS	NS
Zn	0.4	NS	140
Halogens (ppm)	200	700	500
Hydrocarbons (vol%)			
C_2H_6	1	NS	NS
C_2H_4	1	0.3	NS
C_2H_2	1	NS	NS
Oil tar	0.09	NS	NS

[a] Not specified

Source: A. Pigeaud, Progress Report prepared by Energy Research Corporation for U.S. Department of Energy, Morgantown, WV under Contract No. DC-AC21-84MC21154, June 1987.

Reference

1. A. Pigeaud, Progress Report prepared by Energy Research Corporation for U.S. Department of Energy, Morgantown, WV under Contract No. DC-AC21-84MC21154, June 1987.

9.5 Cost of Electricity

Three major contributors are considered in the computation of the cost of electricity (COE) for a fuel cell power plant: 1) capital cost, 2) fuel cost and 3) operation and maintenance costs. The cost of electricity ($/kW-yr) can be calculated using these parameters as follows:

$$COE = 0.125CC + \frac{3413H}{\varepsilon_s}\frac{FC}{10^6} + O\&M \tag{9-31}$$

where 0.125 is a fixed charge rate, CC is the capital cost ($/kW), FC is the fuel cost ($/$10^6$ Btu), 3413 is the theoretical heat rate for 100% efficiency (Btu/kWh), ε_s is the efficiency, H is the h/yr operated, and O&M is the operating and maintenance costs ($/kW-yr fixed cost and $/MW-hr variable cost).

9.6 Entrained Bed Coal Gasifiers

The Texaco coal gasifier is an entrained bed gasifier that produces either a low- or medium-Btu synthesis gas, using either air or oxygen (1, 2). Gasification of coal takes place by the following sequence of reactions. The combustion reaction,

$$C + O_2 \rightarrow CO_2 \tag{9-32}$$

provides the heat energy needed to drive the endothermic reactions involving H_2O/C and CO_2/C:

$$C + H_2O \rightarrow CO + H_2 \tag{9-33}$$

and

$$C + CO_2 \rightarrow 2CO \tag{9-34}$$

Other reactions such as the water gas shift reaction and methanation also occur in the gasifier.

In this process, ground coal of a carefully controlled size (<3.8 cm) is mixed with water, and the slurry (0.24-0.43 steam/carbon weight ratio) is then fed to the gasifier. The gasifier operates in the temperature range of 1260 to 1430°C and at a pressure of about 600 psig (41 atm). Due to the high operating temperatures, no oils, tars, coal fines or ash are present in the gas. Ammonia and hydrogen sulfide are the principal impurities to be removed. The Texaco gasifier functions equally well with air or oxygen, but the product gas composition is considerably higher in nitrogen and lower in hydrogen in an air-blown gasifier than that in an oxygen-blown gasifier. In addition, the presence of nitrogen in the gases from air-blown gasifiers requires the use of larger, more expensive components in the gas cleanup subsystem. A typical composition for Illinois No. 6 coal is listed in Table 9-3 (3), and the typical gas composition obtained from an oxygen-blown Texaco gasifier, using Illinois No. 6 coal in a pilot plant, is listed in Table 9-4 (3).

Table 9-3 Typical Composition of Illinois No. 6 Coal

Proximate Analysis, Wt.%	
Moisture	4.2
Ash	9.6
Fixed carbon	52.0
Volatile matter	34.2
Total	100.0
Ultimate Analysis[a], Wt.%	
Carbon	77.26
Hydrogen	5.92
Oxygen	11.14
Nitrogen	1.39
Sulfur	4.29
Total	100.0
Heating Value[b], Btu/lb	
Higher heating value	12,235
Net heating value	11,709

[a] Dry, ash-free basis
[b] As received

Source: E.C. Mangold, M.A. Muradaz, R.P. Ouellette, O.G. Farah and P.N. Cheremisinoff, *Coal Liquefaction and Gasification Technologies*, Ann Arbor Science, Ann Arbor, MI, p. 213, 1982.

Table 9-4 Typical Gas Composition from Oxygen-Blown Texaco Gasifier with Illinois No. 6 Coal

Gas composition, vol%	
CO	44.62
CO_2	17.97
H_2	35.78
CH_4	0.03
H_2O	1.02
COS	0.05
N_2 + Ar	6.48
HHV of gas, Btu/scf	~320

Source: E.C. Mangold, M.A. Muradaz, R.P. Ouellette, O.G. Farah and P.N. Cheremisinoff, *Coal Liquefaction and Gasification Technologies*, Ann Arbor Science, Ann Arbor, MI, p. 213, 1982.

Shell has produced an entrained bed gasifier which relies on a dry coal feed system. The Shell coal gasifier typically operates with 10 percent less oxygen than the Texaco gasifier because of its dry feed design. It cannot achieve the high pressure which the Texaco gasifier can (400 psia versus up to 1,200 psia), but its pressure level is higher than the expected operating pressure level of any fuel cell system.

References

1. E.C. Mangold, M.A. Muradaz, R.P. Ouellette, O.G. Farah and P.N. Cheremisinoff, *Coal Liquefaction and Gasification Technologies*, Ann Arbor Science, Ann Arbor, MI, p. 209, 1982.
2. *Coal Gasification Processes*, Edited by P. Nowacki, Noyes Data Corporation, Park Ridge, NJ p. 254, 1981.
3. E.C. Mangold, M.A. Muradaz, R.P. Ouellette, O.G. Farah and P.N. Cheremisinoff, *Coal Liquefaction and Gasification Technologies*, Ann Arbor Science, Ann Arbor, MI, p. 213, 1982.

9.7 General Fuel Cell References, 1988 to Present

Books on Fuel Cells:

1. Appleby, A.J., and Foulkes, F.R., *Fuel Cell Handbook*, Van Norstand Reinhold, New York, NY, 1989. Republished by Krieger Publishing Company, Melborne, FL, 1993.

2. Blomen, L.J., Mugerwa, M.N., eds., *Fuel Cell Systems*, ISBN 0-306-44158-6, Plenum Press, New York, NY, 1992.

Bibliographies on Fuel Cells:

1. U.S. Department of Energy, Morgantown Energy Technology Center, *Fuel Cells - A Bibliography*, DOE/METC-88/6091, NTIS/DE88001081, National Technical Information Service, Springfield, VA, 1988.

Proceedings and Abstracts from Fuel Cell Meetings:

1. *Fuel Cell Seminar, Programs and Abstracts*, Fuel Cell Seminars, sponsored by Fuel Cell Seminar Organizing Committee, meetings held every two years in different U.S. cities in the autumn.

   1990 - Phoenix, AZ.

   1992 - Tucson, AZ.

2. *Proceedings of the Annual Fuel Cells Contractors Review Meeting*. Meetings held annually in summer at the U.S. DOE Morgantown Energy Research Center, Morgantown, WV:

   First - DOE/METC-89/6105, May, 1989.

Second - DOE/METC-90/6112, May, 1990.

Third - DOE/METC-91/6120, June, 1991.

Fourth - DOE/METC-92/6127, July, 1993.

3. *An EPRI/GRI Fuel Cell Workshop on Technology Research and Development*, Cosponsored by EPRI and GRI, Proceedings by EPRI, Palo Alto, CA., April, 1993.

4. J.R. Selman, et. al., ed. *Proceedings of the Second Symposium on Molten Carbonate Fuel Cell Technology*, Proceedings Vol. 90-16, The Electrochemical Society, Inc., Pennington, NJ, 1989.

5. D. Shores, et. al., ed. *Carbonate Fuel Cell Technology*, Proceedings Vol. 93-3, The Electrochemical Society, Inc., Pennington, NJ, 1993.

6. Singhal, S.C., ed. *Proceedings of the First International Symposium on Solid Oxide Fuel Cells*, The Electrochemical Society, Inc., Pennington, NJ, 1989.

7. Grosz, F., Zegers, P., Singhal, S., Yamamoto, O., eds. *Proceedings of the Second International Symposium on Solid Oxide Fuel Cells*, EUR 13564 EN, Joule, CEC, 1991.

8. Singhal, S.C., H. Iwahara, *Proceedings at the Third International Symposium on Solid Oxide Fuel Cells*, Proceedings Vol. 93-4, The Electrochemical Society, Inc., Pennington, NJ, 1993.

9. *Proceedings of the Grove Anniversary Fuel Cell Symposium*, Journal of Power Sources, V 29, No. 1-2, Elsevier Sequoia Science, The Netherlands, Jan. 1990.

10. *Proceedings of the Grove Anniversary Fuel Cell Symposium*, Journal of Power Sources, V 37, No. 1-2, Elsevier Sequoia Science, The Netherlands, Jan. 1991.

11. *The International Fuel Cell Conference Proceedings*, NEDO/MITI, Tokyo, Japan, February, 1992.

12. *Proceedings of the Intersociety Energy Conversion Engineering Conference*. Sponsorship of meeting rotates among seven technical societies. Meetings are held annually (usually in August) in different cities of the United States:

24th - Institute of Electrical and Electronics Engineers, Washington, DC, Volume 3, 1989.

25th - American Institute of Chemical Engineers, Reno, NV, Volume 3, 1991.

26th - American Nuclear Society, Boston, MA, Volume 3, 1991.

27th - Society of Automotive Engineers, Inc., San Diego, CA, Volume 3, 1992.

28th - American Chemical Society, Atlanta, GA, Volume 1, 1993.

Other Important Annual Information on Fuel Cells:

1. U.S. DOE, *Fuel Cell Program Plans*, published each Fiscal Year by U.S. Department of Energy, Assistant Secretary of Fossil Energy:

   1989 - DOE/FE-0128

   1990 - DOE/FE-0106P

   1991 - DOE/FE-0238P

   1992 - DOE/FE-0260P

   1993 - DOE/FE-0280

2. *Fuel Cells Technology Status Reports*, Reports published by U.S. Department of Energy, Morgantown Energy Research Center, Morgantown, WV:

   1988 - Berry, D.A., M.J. Mayfield, eds. DOE/METC-89/0266. NTIS/DE89000983, National Technical Information Services, Springfield, VA.

   1989 - George, T.J., Mayfield, M.J., DOE/METC-90/0268, NTOS/DE90009686, National Technical Information Services, Springfield, VA.

3. NEDO, *Research and Development on Fuel Cell Power Generation Technology*, published yearly by the New Energy and Industrial Technology Development Organization, Tokyo, Japan.

4. *Fuel Cell RD&D in Japan*, Published annually by the Fuel Cell Development Information Center c/o The Institute of Applied Energy, Tokyo, Japan, usually in August.

9.8 List of Symbols

Abbreviations:

AFC	alkaline fuel cell
CC	capital cost
COE	cost of electricity
CVD	chemical vapor deposition
DIR	direct internal reforming
DOE	Department of Energy
EVD	electrochemical vapor deposition
FC	fuel cost
FEP	fluoro-ethylene-propylene
HHV	higher heating value
HR	heat rate
IIR	indirect internal reforming
iR	ohmic loss
J-M	Johnson Mathey Technology Center

LHV	lower heating value
MCFC	molten carbonate fuel cell
O&M	operating and maintenance costs
OS/IES	on-site/integrated energy systems
PAFC	phosphoric acid fuel cell
PC	phthalocyanines
PEFC	polymer electrolyte fuel cell
PMSS	pyrolysis of metallic soap slurry
Pt	platinum
PTFE	polytetrafluoroethylene
RDF	refuse-derived-fuels
SOFC	solid oxide fuel cell
TAA	tetraazaannulenes
TBA	tetrabutyl ammonium
TFMSA	trifluoromethane sulfonic acid
THT	tetrahydrothiophene (thiophane)
TMPP	tetramethoxyphenylporphyrins
TPP	tetraphenylporphyrins
TZP	tetragonal phase
YSZ	yittria stabilized zirconia

Roman Letter Symbols:

a	coefficient
a	$(-2.3RT/\alpha nF) \log i_o$
b	coefficient
b	$2.3RT/\alpha nF$
b	Tafel slope
C_B	bulk concentration
C_p	heat capacity
C_S	surface concentration
c	coefficient
D	diffusion coefficient
D	pore diameter
<D>	equilibrium pore size
E^o	standard potential
e^-	electron
E	equilibrium (reversible) potential
ΔE	potential difference
E_a	activation energy
F	Faraday's constant
f	gas flow rate
ΔG	Gibbs free energy
ΔH_c	heat available from combustion of fuel gas
ΔH_r	enthalpy of reaction
I	current
i	current density
i_L	limiting current density

i_o	exchange current density
K	equilibrium constant
k(T)	constant, function of temperature
n	number of electrons participating in a reaction
n_{max}	maximum stoichiometric value
P	pressure
P_i	partial pressure
ppm	parts per million
P_T	total pressure
R	cell resistance
R	universal gas constant
ΔS_r	entropy of reaction
T	temperature
t	electrolyte thickness
U	utilization
V	cell voltage
V	volume
ΔV	voltage difference
V_c	voltage of single cell
v	rate at which reactant species are consumed
W_{el}	maximum electrical work
X	mole fraction

Greek Letter Symbols:

α	transfer coefficient
β	hydrogen utilization
Γ	mole fraction
γ	interfacial surface tension
γ	oxidant utilization
δ	diffusion layer thickness
η_{act}	activation polarization
η_{conc}	concentration polarization
η_{ohm}	ohmic polarization
θ	electrolyte contact angle
θ_{CO}	CO coverage

Subscripts:

a	anode
c	cathode
e	electrolyte
i	species
in	cell inlet
out	cell outlet
p	pressure
T	temperature

☆ U.S. GOVERNMENT PRINTING OFFICE: 1994—509-226